Intrinsic, periodic and tunable metabolic dynamics: a scaffold for cellular coherence

Papagiannakis, Alexandros

Intrinsic, periodic and tunable metabolic dynamics: a scaffold for cellular coherence

Alexandros Papagiannakis

Cover design by Alexandros Papagiannakis

The cover depicts the Canis Major (greater dog), a constellation which contains Sirius, the brightest star in the night sky, also known as the "dog star". In 1844, Friedrich Wilhelm Bessel observed oscillations in the motion of Sirius, inferring the existence of an unseen "dark companion" exerting gravitational forces. In 2003 an image taken by the Hubble Space Telescope clearly demonstrated Sirius A, 2 times bigger and 25 times brighter than our sun, next to its stellar companion, a white dwarf known as Sirius B. Eventually, Sirius is a system of two stars. This is an example of how the collective synchrony within a system of coupled oscillators may be used to infer the existence of individual components and possibly also their interactions.

The work published in this thesis was carried out in the Molecular Systems Biology research group, part of the Groningen Biomolecular Sciences and Biotechnology Insitute (GBB), at the University of Groningen, in The Netherlands. Research was funded by the Marie Curie Innovative Training Network (ITN) ISOLATE (grant agreement nr. 289995).

ISBN 978-94-6299-596-3

university of groningen

Intrinsic, periodic and tunable metabolic dynamics: a scaffold for cellular coherence

PhD Thesis

to obtain the degree of PhD at the
University of Groningen
on the authority of the
Rector Magnificus Prof. E. Sterken
and in accordance with
the decision by the College of Deans

This thesis will be defended in public on
Monday 15 May 2017 at 16.15 hours

By
Alexandros Papagiannakis

born on 4 January 1987
in Thessaloniki, Greece

Supervisor
Prof. M. Heinemann

Assessment Committee
Prof. B. Poolman
Prof. P.J.M. van Haastert
Prof. B. Tu

Contents

Chapter 1

The cell cycle is a higher order function, which emerges from the collective synchrony between metabolic, chromatin remodeling and CDK-activity oscillators

Alexandros Papagiannakis, Matthias Heinemann

Molecular Systems Biology, Groningen Biomolecular Sciences and Biotechnology Institute, University of Groningen, Nijenborgh 4, 9747 AG Groningen, The Netherlands;

Summary

The cell cycle is the periodic process of biomass duplication and segregation. According to the traditional view on cell cycle regulation, waves of cyclins tune the activity of a cyclin dependent kinase, the master regulator of cell cycle transcription and chromosome dynamics. However, the late advent of cyclin dependent kinases in the evolution of eukaryotes, together with the sustained transcriptional and late cell cycle oscillations during cell cycle arrest, support the existence of cyclin/CDK independent cell cycle regulators. In this review we discuss the possibility that an autonomous metabolic oscillator provides periodic triggers for cell cycle initiation and progression. Specifically, we summarize the molecular connections between oscillating metabolites, previously measured in synchronized yeast populations, and the cell cycle machinery, providing a global understanding on the cell cycle operation within a milieu of coupled oscillators. The early cell cycle correlates with enhanced respiro-fermentative metabolism, chromatin activation and biomass formation, oscillating oppositely in phase with the late cell cycle which correlates with energy conservation, chromatin silencing and biomass segregation.

Highlights

- A CDK-independent metabolic oscillator could constitute a primitive cell cycle regulator.
- Oscillating metabolites interact with the cyclin/CDK machinery, either directly, or indirectly via signaling pathways and histone modifications.
- The early cell cycle coincides with anabolism and chromatin activation, whereas the late cell cycle coincides with energy conservation and chromatin silencing.
- Additional control was imposed on a primitive, metabolically driven cell cycle network, in the form of activator/inhibitor pairs, for the robust transition between the cell cycle phases.

Introduction

The cell cycle is the process of biomass duplication and segregation. In eukaryotes it consists of four phases, the G1, S, G2 phase and Mitosis, which occur in strict order. During the G1 phase, the cell prepares for DNA replication. Specifically, the progenitor cell volume steadily increases until it reaches a critical size, when it commits for DNA replication. This point of commitment is commonly referred to as START in yeasts or the restriction point in mammalian cells (Johnson and Skotheim, 2013). During the early cell cycle and DNA replication, cells boost biomass formation further increasing their size (Barnum and O'Connell, 2014; Ferrezuelo et al., 2012; Soifer and Barkai, 2014). In the G2 phase, an additional cell size checkpoint (Barnum and O'Connell, 2014; Soifer and Barkai, 2014) ensures continuation of the cell cycle, and commitment to mitosis and biomass segregation, only when the cells have synthesized sufficient biomass. During Mitosis, the duplicated chromosomes are condensed (Prophase), aligned (Metaphase), separated (Anaphase) and partitioned (Telophase) between the two poles of the cell. After mitosis, cytokinesis takes place, where the grown cell, containing duplicated components (e.g. DNA, protein, organelles, membrane), is split into two identical daughters (symmetric

division (Shahriyari and Komarova, 2013)) or a bigger mother and a smaller daughter cell (asymmetric division (Yang et al., 2015)), each containing equal amounts of genetic information and thus being able to commence a new cell division program. A molecular cell cycle machinery coordinates - in two timely separated steps - the duplication of the biomass in the S phase and the segregation in the M phase. It stands to reason that proper functioning of the cell cycle is necessary for the equal partitioning of biomass components between the progenies, for the maintenance of genomic integrity (ploidy) and survival (Pines, 2011; Tyson and Novak, 2008).

The traditional cell cycle view

The discovery of the molecular engine that coordinates the cell cycle phases was the result of decades of research in yeasts, echinoderms, amphibians and mammalian cells, yielding a Nobel Prize in 2001 (Watts, 2001), jointly awarded to Leland Hartwell, Tim Hunt and Paul Nurse. The cell cycle engine, also known as the Cylin/CDK machinery, consists of one central Cyclin Dependent Kinase (CDK) and its regulators, the cyclins (Figure 1). Timely ordered waves of cyclin abundance control the activity of the CDK, which in turn controls the onset of the next cell cycle phase only when the previous one is complete (Barik et al., 2010).

In budding yeast (*Saccharomyces cerevisiae*) the only CDK is Cdc28. During the G1 phase and prior to START, the Cln3 cyclin is available for coupling with Cdc28. The Cln3/Cdc28 dimers phosphorylate Whi5, a transcriptional repressor. As a result, the phosphorylated Whi5 sequesters into the cytoplasm, signaling the START point and the activation of the SBF and MBF transcriptional factors, which drive the early cell cycle transcription (also known as G1 transcription) (Barik et al., 2010; Tyson and Novak, 2008). It has previously been conjectured that the threshold for START is set by the abundance of the Cln3 and thus the Cln3/Cdc28 heterodimers, as well as the nuclear abundance of Whi5 (Liu et al., 2015; Schmoller et al., 2015). The SBF and MBF transcriptional factors drive the expression of additional cyclins (Cln1,2 and Clb5,6), which initiate the S phase and specifically DNA replication and budding (Bähler, 2005). At this point the irreversibility of START is also

set (Charvin et al., 2010), with Cln1,2/Cdc28 further phosphorylating Whi5 thus hampering its sequestration back in the nucleus.

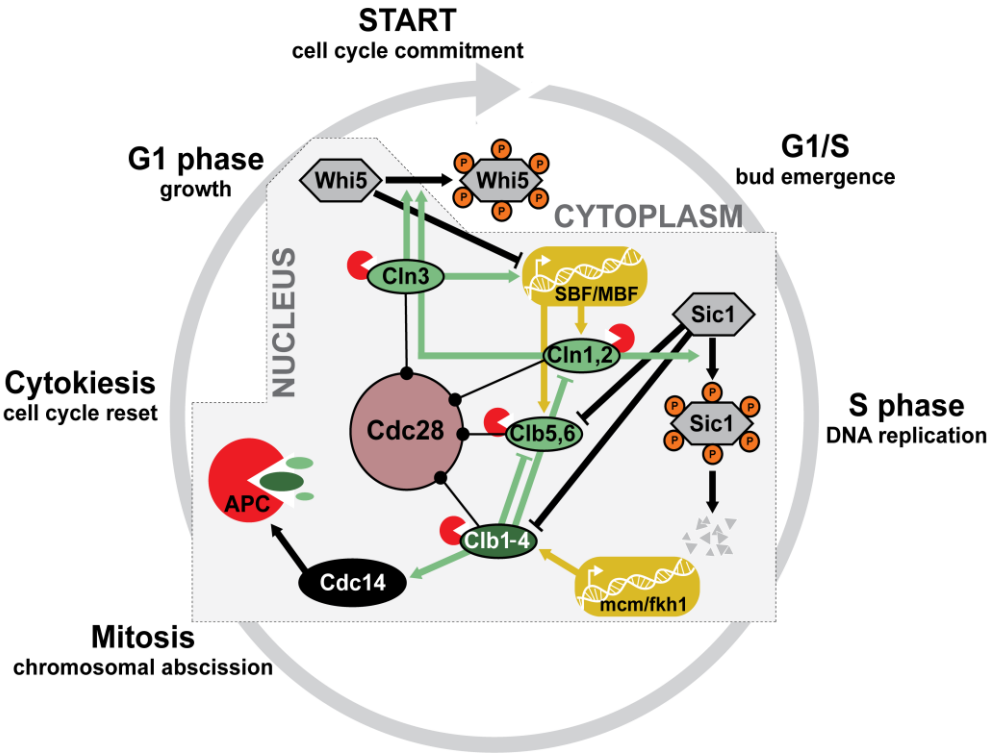

Figure 1: CDK-centric model of cell cycle regulation. The cyclin dependent kinase, the activity of which is driven by the early (Cln1,2,3 and Clb5,6 – light green) and the late (Clb1,2,3,4 – dark green) cyclins, coordinates the transition through the cell cycle phases (Barik et al., 2010). During the G1 phase the cells grow, accumulating Cln3 and possibly also diluting the Whi5 repressor of cell cycle transcription into the nucleus. When sufficient Cln3/Cdc28 complexes are assembled, they phosphorylate Whi5 causing its sequestration in the cytoplasm and the onset of cell cycle transcription via the SBF/MBF transcriptional factors (Liu et al., 2015; Schmoller et al., 2015). At this point, also known as the START, cells commit to cell division. The remaining early cyclins are then transcribed triggering the onset of budding (Cln1,2) and DNA replication (Clb5,6) (Barik et al., 2010; Tyson and Novak, 2008). At this point, the Sic1 inhibitor of the b-type cyclins (Clb1,2,3,4,5,6) is phosphorylated and degraded (Barberis, 2012). The accumulation of the late cyclins is assisted via the mcm/fkh1 dependent transcription (Linke et al., 2013) signaling the transition past the S phase into Mitosis. The late cyclins activate the anaphase promoting complex (APC) via Cdc14. The APC is not only necessary for chromosomal abscission and the separation of the sister chromatids, but also degrades all remaining cyclins, signaling mitotic exit and resetting the cell cycle program (Acquaviva and Pines, 2006; Manchado et al., 2010; Peters, 2006).

The early waves of the G1/S cyclins (Cln1,2,3 and Clb5,6) are succeeded by the late cyclin waves, namely Clb3,4 and Clb1,2, which also regulate the activity of Cdc28 and promote the transition past the G2 phase into Mitosis (Barik et al., 2010; Tyson and Novak, 2008) (Figure 1). The late cyclin waves activate the Anaphase Promoting Complex (APC), a conserved multiprotein complex harboring an E3 ubiquitin ligase, which catalyzes the addition of polyubiquitin chains to proteins targeting them for proteasomal degradation (Acquaviva and Pines, 2006). The APC facilitates the separation of the sister chromatids (duplicated DNA) via releasing separase, a protease that cleaves cohesin, a protein complex that keeps the sister chromatids together (Manchado et al., 2010). At the same time, APC catalyzes the degradation of all remaining cyclins (Figure 1), thus resetting the cell division program back to the G1 phase (Peters, 2006). The APC is also known as the cycleosome due to its central role in resetting the cell cycle.

According to the current view on cell cycle regulation, the cyclin/CDK machinery together with the cycleosome (APC) constitute an autonomous oscillator (Figure 2A), which orchestrates the transitions between the cell cycle phases. Several mathematical models have been developed describing the functioning of the cell cycle (Gérard et al., 2013), leading to the development of a minimal cell cycle model in *Schizosaccharomyces pompe* (Coudreuse and Nurse, 2010), where one CDK together with a B-type cyclin (Clb) and the APC constitute a free-running oscillator driving cell division. Minimal cell cycle models (Coudreuse and Nurse, 2010; Gérard et al., 2013) have gained wide acceptance due to their simple nature. However, there are clues that contradict this notion of cell cycle control. These cues point towards an external, non-Cln/CDK cell cycle regulator, which provides dynamic triggers for biomass duplication and segregation.

Evidence for external cell cycle regulation

In yeast, the initiation of the cell cycle (START) is known to be triggered by Cln3/Cdc28. Cln3, is regulated at a post-transcriptional level: the Whi3 cell cycle inhibitor binds the Cln3 mRNA in the cytoplasm, preventing its translation (Garí et al., 2001). During the G1 phase, the Cln3 mRNA levels increase more than they are inhibited by Whi3, thus resulting in Cln3 translation. The emergent Cln3/Cdc28 complexes phosphorylate and deactivate cell

cycle transcriptional inhibitors (e.g. Whi5 and Rpd3) promoting the G1/S transition (de Bruin et al., 2004; Verzijlbergen et al., 2014). The G1 cyclin has been shown to trigger START only when the cells have reached a critical size (Figure 2A) (Ferrezuelo et al., 2012). This critical threshold for cell cycle initiation is set by the nuclear abundance of cell cycle inhibitors (e.g. Whi5), as well as the cell volume increase rate during G1 and thus the growth conditions, commonly related to the rate of Cln3 expression (Liu et al., 2015; Schmoller et al., 2015). According to the accepted view on cell cycle regulation, *Cln3Δ* mutants should constantly increase in volume and thus fail to start the cell cycle. However, experiments have shown that *Cln3Δ* cells not only successfully manage to initiate and complete cell division, but they also exhibit a growth-dependent critical volume at START (Ferrezuelo et al., 2012), similarly to wild type cells. Furthermore, *Saccharomyces cerevisiae* cells can still divide in the absence of two out of their three early cyclins (Cln1,2,3). When cell cycle inhibitors were deleted (e.g. Sic1) (Schneider et al., 1996; Sherr and Roberts, 2004; Tyers, 1996), cell division was also possible in the absence of all three cyclins. Similarly, *Schizosacharmomyces pompe* cells lacking all early cyclins are also viable (Fisher and Nurse, 1996; Sherr and Roberts, 2004). These findings suggest that an oscillator external to the Cln/CDK machinery, and not the timely ordered cyclin waves, could regulate cell cycle initiation.

Further indication for the existence of a Cln/CDK-independent cell cycle regulator has been discovered: When yeast cells bearing temperature-sensitive B-type cyclins (Clb1,2,3,4,5,6) were subjected to the restrictive temperature, they were found to exhibit periodic transcription in the absence of cell cycle progression (Orlando et al., 2008). Specifically, although the cyclin mutants were unable to complete the S phase or Mitosis, nearly 70% of the periodically transcribed genes in normally dividing cells, continued to oscillate with similar periods and phases, but with different amplitudes. Even the late G1 transcripts (normally activated by SBF) continued to oscillate in the cell cycle arrested cells. This led to the suggestion that a global transcription oscillator could be a CDK-independent cell cycle regulator (Figure 2B).

However, recent findings challenge the existence of a CDK-independent global transcription oscillator: In *Schizosaccharomyces pompe* no periodic G1 or M transcription was observed when the cell cycle was arrested by cyclin B/CDK inhibition, on a minimal

cell cycle background (absence of remaining cyclins or CDKs) (Banyai et al., 2016). Similarly in Saccharomyces cerevisiae when the cell cycle was arrested by depletion of all the early and late cyclins, the SBF/MBF dependent transcription was halted (Rahi et al., 2016). Still, in both studies the existence of periodic transcription was assessed by comparing the amplitudes of the oscillations during cell cycle arrest, to the periodic transcription in normally dividing cells. In fact, if the global transcriptional oscillations persist even in the absence of CDK activity, yet with significantly lower amplitude as previously suggested, their detection largely depends on the arbitrarily set amplitude threshold between significant periodicity and noise in gene expression. Most importantly, in *Saccharomyces cerevisiae*, even during cell cycle arrest and despite the absence of CDK activity, three genes (SIC1, CDC6 and CYK3) from the Swi5 cluster (transcriptional factor activated together with the APC during mitosis) continued to oscillate, lending additional support to the existence of a CDK-independent cell cycle regulator.

Similarly, when cells were arrested in metaphase via the constitutive expression of a stable, non-degradable B-type cyclin (Clb2kd), they exhibited cycles of Cdc14 nucleolar/cytoplasmic localization, even in the absence of cell cycle initiation (START) and budding (early S) (Lu and Cross, 2010) (Figure 2B). The Cdc14 phosphatase is an essential activator of Cdh1, a subunit of the APC, which harbors the substrate for poly-ubiquitination. The persistent localization cycles of Cdc14 indicate a periodic activity of the APC and the late cell cycle even in the absence of cell division. Similarly, when the cell cycle was delayed in *Cdh1Δ Sic1Δ* GAL-SIC1 cells growing on glucose, DNA endo-replication cycles were reported, indicating a periodic activity of the early cell cycle without a new budding event and before the end of Mitosis (Wasch and Cross, 2002). The persistent DNA endo-replication, Cdc14 localization and transcriptional cycles observed in cell cycle arrested or delayed yeast cells suggest the existence of a free-running oscillator, which drives the early and late cell cycle events, and possibly global gene expression, also independently of the Cln/CDK machinery (Figure 2B).

In accordance with the idea that a CDK-independent regulator exerts major cell cycle control, an amino-acid sequence-based reconstruction of the maximum-likelihood phylogeny of cell cycle control kinases, revealed that Cdc28 appeared late in the evolution of eukaryotes (Krylov et al., 2003). The earliest branching cell cycle control kinases have

functions related to metabolism (amino-acid and polyamine transport, TCA cycle), gene expression (elongation of ribosomal gene RNAs), ion homeostasis (regulation of H^+ or K^+ transport) or pheromone response (inhibition of the pheromone response pathway). Consequently, in early eukaryotes, cell division, namely the process of biomass duplication and segregation, might be controlled by an ancient oscillator in the absence of a Cln/CDK machinery (Murray, 2004).

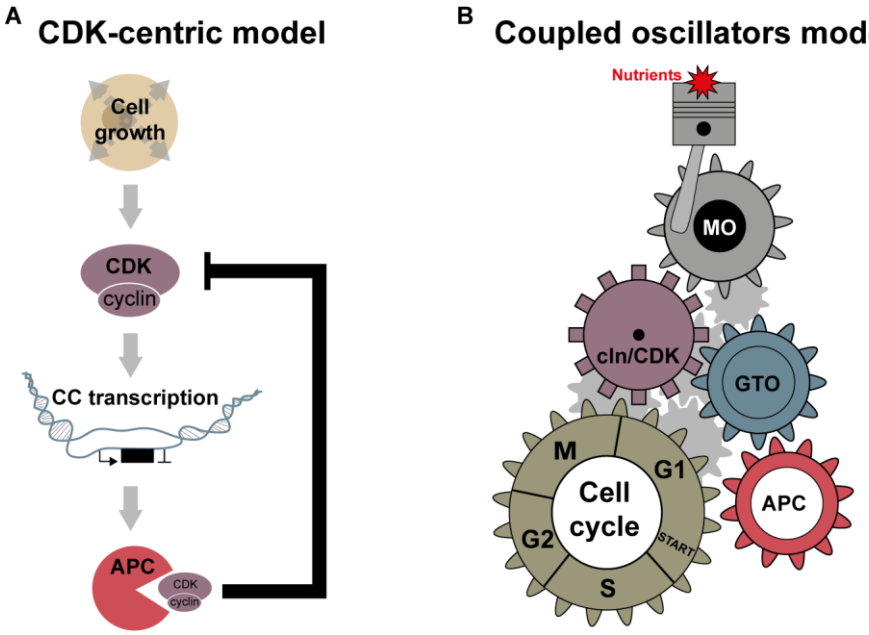

Figure 2: The CDK-centric contrasted to the coupled oscillators model of cell cycle regulation. **(A)** According to the CDK-cetric model, the cell cycle is a phosphorylation cascade (Barik et al., 2010) orchestrated by the cyclin dependent kinase (CDK). When the cells have reached a ctitical size in G1, and the production of the G1 cyclins has increased beyond their inhibition threshold, the CDK is activated. The cyclin/CDK complexes drive the early and late cell cycle transcription, eventually activating the anaphase promoting complex, which separates the duplicated chromosomes and degrades the cyclins, thus establishing a negative feedback to the cyclin/CDK activity, setting the periodicity of the cyclin/CDK machinery. For this reason, the APC is also known as the cycleosome, establishing the periodic activity of the CDK-dependent phosphorylation cascade. **(B)** According to the coupled oscillators model, each of the cell cycle effectors presented in the CDK-centric model constitutes an oscillator. An autonomous metabolic oscillator (MO) drives biomass production in response to the available nutrients, and is coupled to a global transcription oscillator (GTO) (Orlando et al., 2008) and the anaphase promoting complex (APC) (Lu and Cross, 2010). A cyclin/CDK oscillator operates for the robust separation of the cell cycle phases (Talia et al., 2007). Cell cycle

control emerges as a higher order function, from the collective synchrony between the coupled oscillators.

The above experimental and evolutionary clues suggest the existence of a Cln/CDK-independent oscillator as a regulator of cell division. If such a cell cycle regulator is conserved across organisms – which might be deduced from the fact that CDKs evolved late calling for some primitive and thus conserved control – then metabolism is a good candidate. Genome-wide comparisons of genes and their functions among species, have shown that metabolic enzymes and central metabolic pathways (e.g. energy, amino acid, and nucleotide metabolism) stand out for their common representation across all 26 taxa of life (Peregrín-Alvarez et al., 2009). A metabolically driven cell cycle regulator (for instance, in the form of a metabolic oscillator), could constitute the here conjectured ancient regulator of cell division.

Such a metabolic oscillator would allow for the integration of nutrient signals to the cell cycle (Figure 2B), thus determining the cell cycle initiation in a carbon source and growth-rate specific manner, and it could explain the nutrient dependency of the critical size at START, previously described in yeast, both in the presence and absence of Cln3 (Ferrezuelo et al., 2012). An oscillating metabolism would allow for the timely ordered provision of all necessary nutrients and building blocks required for each of the cell cycle processes (e.g. nucleotides for DNA replication). Eventually, the autonomous metabolic oscillator, the global transcription, the cyclin/CDK machinery and the anaphase promoting complex could form a system of coupled oscillators operating in synchrony to robustly gate the cell cycle phases and orchestrate cell division. (Figure 2B).

Yeast metabolic oscillations

The idea of an oscillating metabolism controlling the cell cycle is not new. Already in the late 60s the activity of glucose-6-phosphate dehydrogenase, catalyzing the first step into the pentose phosphate pathway, and lactate dehydrogenase, catalyzing the production of lactate from pyruvate, were shown to oscillate three times during the cell cycle of Chinese hamster

cells (Klevecz, 1969; Klevecz and Ruddle, 1968). These oscillations occurred in phase. High enzyme activity was reported during the early cell cycle (G1 and S phases), and correlated with increased protein synthesis and cell size increase. Ten years later, oscillations in the rate of oxygen consumption and protein production were observed in cell cycle synchronized amoeba cells (Acanthamoeba castellanii) (Lloyd et al., 1982). The respiration and protein production cycles occurred in phase and were temperature compensated. Also in *Schizosaccharomyces pompe* (fission yeast), autonomous oscillations in CO_2 were suggested to set the pace of cell division (Novak and Mitchison, 1987; Novak et al., 1988).

These findings from mammalian, amoeba and yeast cells suggest the existence of a metabolic oscillator in eukaryotes, orbiting in synchrony with and possibly regulating the cell cycle. Still, these oscillatory behaviors could also be due to the temporal cell cycle activity. In any case, the notion of a metabolically driven cell cycle was abandoned after the cyclin/CDK machinery was discovered (Watts, 2001). We conjecture that the potential artifacts of cell cycle synchronization (Aon et al., 2007; Henson, 2004; Laxman et al., 2010; Sohn et al., 2000) combined with the lack of experimental methods to dynamically assess metabolism in unsynchronized single cells, constitute the main reasons for this abandonment. Still, while cell cycle research was focused on the cyclin/CDK machinery, the yeast field continued investigating the existence and the role of an oscillating metabolism. When budding yeast is grown in continuous nutrient-limited cultures, cells spontaneously synchronize their cell cycle and metabolism (Lloyd and Murray, 2005; Slavov and Botstein, 2011; Tu et al., 2005; Xu and Tsurugi, 2006), which allowed to uncover metabolic oscillations in the ultradian domain. Metabolic oscillations were found with period that correlated with the doubling time (Burnetti et al., 2016; Slavov and Botstein, 2011), but also with frequencies that were higher than the frequency of cell division (Burnetti et al., 2016; Machné and Murray, 2012; Murray et al., 2007; Slavov and Botstein, 2011).

In the first case, the metabolic oscillations exhibited periods well above the maximum growth rate of aerobically fermenting yeast (approx. 100 min) (Figure 3A). For instance cells with a growth rate of 0.09 h^{-1} (doubling time: 462 min), would exhibit metabolic oscillations with a period of 250 minutes (Slavov and Botstein, 2011). A significant fraction

of non-dividing yet metabolically oscillating cells could account for the lower doubling times as compared to the periods of the metabolic oscillations. In each metabolic cycle a different group of cells might enter or skip cell division, as previously conjectured (Burnetti et al., 2016). However, we cannot exclude the possibility that a steady fraction of non-dividing quiescent cells would be responsible for lowering the measured growth rate below the metabolic frequency. In either case, the discovery of metabolic oscillations in the absence of cell division (Novak and Mitchison, 1987; Slavov et al., 2011) in synchronized yeast populations, supports the existence of metabolically oscillating yet non-dividing cellular fractions (Figure 3A).

In the second case, the metabolic oscillations orbit faster than the maximum growth rate of yeast (approx. 100 min) (Figure 3B). Metabolic oscillations with periods of approximately 40 min are occasionally reported (Lloyd and Murray, 2005). Impartial synchronization in the chemostat fermenter, with two or more yeast sub-populations oscillating in frequency synchrony yet not in phase, could generate collective synchrony with faster dynamics than the ones reported in single cells or in each sub-population alone. The prolonged G1 phase of the daughter cells, which is prominent in glucose-limited conditions, could account for the emergence of such population fractions. Alternatively, a combination of both models, namely the presence of non-dividing yet metabolically oscillating cell fractions (Figure 3A) and the emergence of oscillating subpopulation in frequency but not phase synchrony (Figure 3B), could explain the reported discrepancy between the metabolic and cell cycle frequencies.

The yeast metabolic cycles are manifested as oscillations in the rates of CO_2, ethanol, acetate or sulfide excretion, in the rate of O_2 uptake, as well as in the intracellular concentration of more than 100 metabolites (Tu et al., 2007). Based on the partial oxygen pressure (pO_2 - dissolved oxygen in the chemostat fermenter) measurements, the metabolic oscillations can be divided into an oxidative and a reductive phase (Tu et al., 2005). Mitochondrial respiration is restricted into the oxidative phase, marked by high oxygen consumption and a fast drop in the pO_2 levels (Klevecz et al., 2004; Lloyd and Murray, 2005; Müller et al., 2003; Tu et al., 2005). However, the fast liquidation of storage carbohydrates, the accumulation of ethanol, together with an increased respiratory quotient (CO_2-production/O_2-consumption > 1), all measured during the oxidative phase (Müller et

al., 2003), show up-regulated fermentation in addition to mitochondrial respiration (Futcher, 2006). Overall, these experiments showed that metabolism in yeast oscillates along the cell cycle. However, certain researchers also stated the these oscillations might just be due to the spontaneous cell cycle synchronization the origin of which still remains elusive (Aon et al., 2007; Henson, 2004; Laxman et al., 2010; Sohn et al., 2000).

Analyses of the transcriptome in glucose-limited continuous yeast cultures (Klevecz et al., 2004; Li and Klevecz, 2006; Lloyd and Murray, 2005; Machné and Murray, 2012; Tu et al., 2005), provide insights on the correlation between cellular processes and the oxidative or the reductive phase of the yeast metabolic oscillations. Amino-acid synthesis and ribosomal biogenesis are timely compartmentalized into the early oxidative phase, indicating a strong correlation between glycolysis and global protein synthesis. Consistently, metabolism has been shown to oscillate in synchrony with the DNA content and the budding index, in glucose-limited chemostat cultures (Burnetti et al., 2016; Slavov and Botstein, 2011; Tu et al., 2005). During the late oxidative phase and until the onset of the reductive phase, DNA replication and mitochondrial biogenesis occurs (Machné and Murray, 2012; Tu et al., 2005). Into the reductive phase cells switch to autophagy and fatty acid oxidation, to generate metabolic precursors and energy, express environmental stress response genes and accumulate storage carbohydrates (trehalose and glycogen), all reporting the lack of available nutrients. Low oxygen consumption, is also accompanied by cytokinesis and cell wall synthesis (Machné and Murray, 2012; Tu et al., 2005).

Overall, metabolic oscillations have been discovered in glucose-limited continuous cultures of budding yeast, possibly in synchrony with the cell cycle. However, given the potential artifacts of synchronization, such as the partial synchrony or the possible periodic entrainment of metabolism by sulfide production and intercellular communication, it remains an open question whether the yeast metabolic oscillations are an intrinsic property of metabolism, or an artifact of the applied methodology.

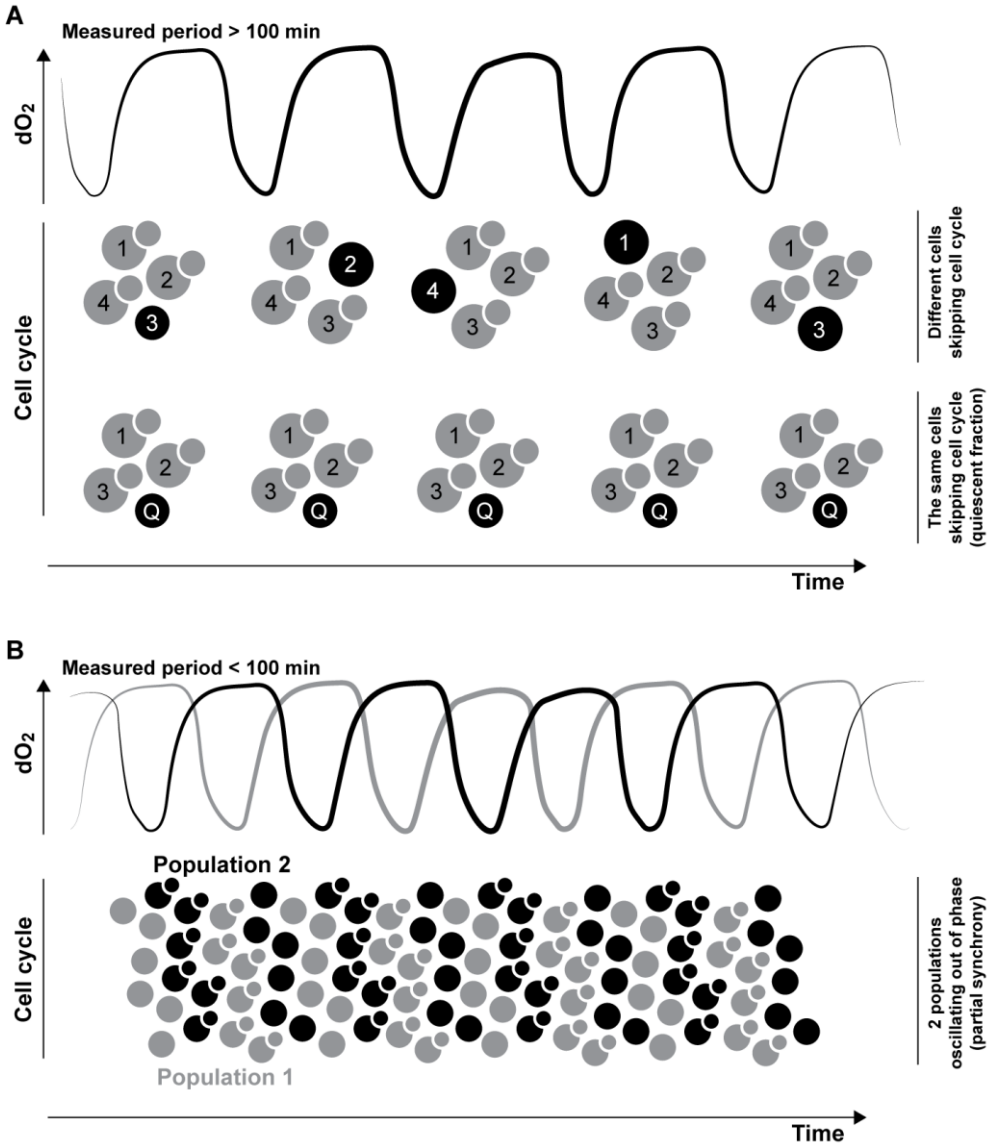

Figure 3: Two possible explanations for the discrepancy between the slower cell division frequencies and the faster metabolic frequencies, measured in glucose-limited continuous yeast cultures. The metabolic oscillations are commonly reported as oscillations in the dissolved oxygen in the chemostat,(dO_2) or oscillations in oxygen consumption and thus respiration. **(A)** For metabolic periods longer than the maximum doubling time of aerobically fermenting yeast (approx. 100 min) non-dividing but metabolically oscillating cellular fractions could explain the faster metabolic in comparison to the cell cycle dynamics, as previously conjectured (Burnetti et al., 2016). In a hypothetical population of four cells (top) numbered accordingly (1, 2, 3 and 4), each of the four cells could occasionally skip cell division, resulting to slower cell division frequencies in the population. Alternatively (bottom), a constant fraction of non-dividing quiescent cells (annotated as Q) could be formed during glucose-limited growth and low dilution rates in the continuous culture. **(B)** For

metabolic periods shorter than the maximum doubling time of aerobically fermenting yeast (approx. 100 min), partial synchrony and specifically the existence of subpopulations (black or grey cells) oscillating and dividing oppositely in phase, may explain the previously measured fast metabolic oscillations in synchrony with the cell cycle.

Additionally, in case there is a metabolic oscillator, it is still unknown if and how the oscillatory metabolite abundances provide dynamic triggers for cell cycle initiation and/or progression. Below we provide an overview of the known molecular interactions between metabolism (metabolites and metabolic enzymes) and the cell cycle (cyclin/CDK machinery components), which could mediate control signals from metabolism to the cell cycle.

A direct connection between metabolism and the CDK-machinery

Signals from the metabolic oscillator to the cell cycle could be transmitted via interactions between oscillating metabolites and cell cycle proteins. Such interactions may be direct, or indirect employing signaling pathways. A direct interaction between fructose-2,6-biphosphate (F2,6PB) and Cdk1 has been suggested in mammalian (HeLa) cells (Yalcin et al., 2009, 2014). F2,6BP is the product of the fructose-6-phosphate (F6P) phosphorylation reaction, catalyzed by the enzyme 6-phosphofructo-2-kinase (PFKFB3). F2,6BP cannot be further metabolized and is known to regulate glycolysis via the allosteric activation of phosphofructokinase (PFK1), the enzyme that catalyzes the phosphorylation of F6P to F1,6BP (Hers et al., 2016). In contrast to F2,6BP, F1,6BP can be further metabolized to pyruvate.

Based on its glycolytic function, one would expect PFKFB to be localized in the cytoplasm. However, one of the four PFKFB1-4 isoenzymes, PFKFB3, localizes to the nucleus (Yalcin et al., 2009, 2014). Ectopic expression of PFKFB3 in the cytoplasm, or the abolishment of its kinase activity significantly reduced proliferation rates as well as the Cdk1-mediated inactivation of the cell cycle inhibitor p27 (Yalcin et al., 2009). Because F2,6BP is known to significantly enhance the p27 phosphorylation and deactivation in vitro, a direct

interaction between F2,6BP and Cdk1 has been conjectured (Yalcin et al., 2009). Consistently, the degradation of the PFKFB3 mRNA via the use of interfering RNAs (siRNAs) has been shown to reduce Cdk1 activity, leading to increased cell cycle arrest in the G1 phase and apoptosis (Yalcin et al., 2014).

Oscillations in the F2,6BP levels could periodically control the cell cycle initiation. One would expect the F2,6BP levels to peak late in the late G1 phase, at the onset of the oxidative phase, directly activating Cdk1 and indirectly minimizing p27 activity, thus promoting the G1/S transition. The F2,6BP would reach a trough in the early G1 phase, when the p27 activity peaks, oppositely in phase. Although there is no direct evidence that F2,6BP levels oscillate, the previously reported F6P and F1,6BP oscillations (Sasidharan et al., 2012) strongly support the existence of F2,6BP oscillations. Especially F6P levels were found to peak early in the oxidative phase, or the late G1 phase of the cell cycle.

The cAMP/PKA pathway wires the metabolic oscillator to the cell cycle machinery.

Most of the known interactions between metabolites and the cell cycle machinery are likely not direct, but instead mediated via signaling pathways. The cAMP/PKA pathway is known to sense intracellular as well as extracellular nutrients and regulate cell division (Thevelein and de Winde, 1999) (Figure 4A-C). The central enzyme of the cAMP/PKA pathway is the adenylate cyclase (Cyr1) (Figure 4B). Cyr1 catalyzes the cyclization of ATP to cAMP, which activates the protein kinase A (PKA). PKA phosphorylates and deactivates its downstream target, the Rim15 kinase (Lee et al., 2013; Reinders et al., 1998), up-regulating glycolysis and fostering growth. Low cAMP/PKA activity triggers the Rim15-dependent transcription of genes containing stress response (STREs) (Smith et al., 1998) and post-diauxic shift (PDS) promoter elements (Pedruzzi et al., 2000), and correlates with a stationary phase metabolism, characterized by accumulation of storage carbohydrates (trehalose and glycogen), down-regulation of ribosomal synthesis, increased resistance to nutrient or heat stress, and quiescence entry (Figure 4B). G proteins anchored to the cytosolic membrane, namely the Ras and Gpa2 GTPases, activate Cyr1 (Wang et al., 2004).

Gpa2 is phosphorylated by the glucose receptor (Gpr1), in response to abrupt changes in the extracellular glucose levels (e.g. addition of glucose to a stationary culture). Ras activity is necessary for the localization of Cyr1 at the cytoplasmic membrane and thus for the Gpr1-Gpa2 mediated PKA activation. Additionally, the G protein Ras has been suggested to modulate the activity of the cAMP signaling, in response to the intracellular pH and potentially ATP levels (Thevelein, 1991) or the glycolytic intermediate glucose-6-phosphate (Conrad et al., 2014).

A few years back, the cAMP/PKA pathway was suggested to drive an oscillating metabolism and the cell cycle. According to the 'finishing kick to START' hypothesis (Futcher, 2006), a periodic cAMP/PKA activity entrains the metabolism of storage carbohydrates and glycolysis, in synchrony with cell division. When the cells have accumulated critical trehalose or glycogen concentrations, a fast increase in cAMP levels and cAMP/PKA activity triggers the liquidation of the stored carbon into glycolysis, promoting protein synthesis (Figure 4C). This PKA-dependent up-regulation of protein synthesis increases the translation of Cln3 in a growth dependent manner (Hall et al., 1998; Polymenis and Schmidt, 1997), and causes the accumulation of the early cyclin beyond its inhibition threshold set by Whi3 at a post-transcriptional level (Garí et al., 2001). At the same time, PKA phosphorylates Whi3 decreasing its binding to the Cln3 mRNA (Mizunuma et al., 2013). cAMP signaling is also known to inhibit the expression of the remaining early cyclins in yeast (Cln1/2) (Baroni et al., 1994) and the transition into the S phase. The activation of Cln3 in combination with the inhibition of Cln1/2 by the cAMP/PKA pathway causes the cells to grow in size, until enough Cln3 is produced to deactivate the cell cycle inhibitor Whi5 and the expression of the next cyclin (Cln1/2) wave, granting a cell-size dependent START. cAMP/PKA signaling not only regulates START, but is also known to phosphorylate and deactivate the mammalian anaphase promoting complex (subunits APC1 and APC3) (Kotani et al., 2016), thus ensuring the inhibition of the late cell cycle machinery at START, for the robust temporal separation of the early and the late cell cycle.

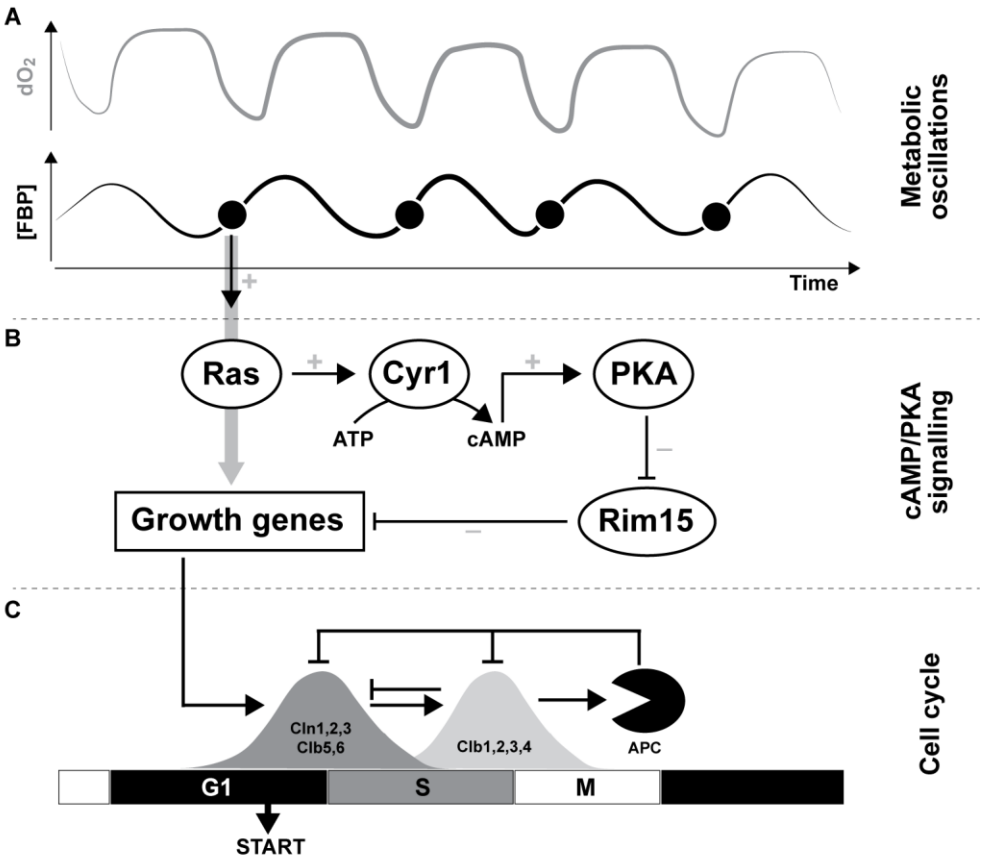

Figure 4: The cAMP/PKA pathway receives periodic input from signaling metabolites and controls the cell cycle. (A) The concentration of the glycolytic flux dependent metabolite FBP is known to oscillate in synchrony with the dissolved oxygen (dO2) oscillations previously measured in glucose-limited continuous yeast cultures (Sasidharan et al., 2012). **(B)** The Ras GTPase and the cAMP/PKA pathway is activated by glycolytic intermediates such as FBP, DHAP and GA3P (Peters, 2013), integrating signals from the metabolic oscillator and regulating the expression of growth related genes (e.g. ribosomal subunits). The Rim15 inhibition (-) and the repression of gene expression (-) result in activation (grey arrow) of global protein expression and growth when the glycolytic flux is elevated and the concentration of FBP increases. **(C)** This up-regulation of global gene expression, results in the synthesis of early cyclins (e.g. Cln3) above their inhibition threshold for START and the G1/S transition.

While the hypothesized periodic cAMP/PKA activity (Futcher, 2006) would cause metabolism to cycle between respiration (storage accumulation) and fermentation (storage liquidation), consistently with the yeast metabolic oscillations, two facts cast doubt on the role of the cAMP/PKA pathway as a prime driver of the metabolic oscillations and the cell

cycle: Although low cAMP/PKA activity causes cell cycle arrest and entry into quiescence (G0), *Rim15Δ* cells are able to grow even in the absence of PKA activity (Reinders et al., 1998). Consequently, entry into quiescence is caused by the constitutively active stress response activators, which would are inhibited via the basal cAMP-dependent Ras signaling. Second, after the deletion of the trehalose and glycogen accumulation/liquidation enzymes, exponentially growing cells on ethanol or glycerol did not exhibit any growth defects, and were morphologically similar to wild type yeast (Zhao et al., 2016).

Another problem with the finishing kick to start hypothesis is that it remains unknown what the origin of the periodic cAMP/PKA activity would be, or how the cAMP/PKA pathway could sense the accumulation of storage carbohydrates. Instead, an autonomous metabolic oscillator could provide dynamic inputs for the cAMP/PKA pathway. In fact, the Ras GTPases, are known to be activated by the glycolytic intermediates fructose-1,6-biphosphate (FBP) (Figure 4A-B), dihydroxy-acetone-phosphate (DHAP) and glyceraldehyde-3-phosphate (GA3P) (Peters, 2013). Metabolomics measurements performed in synchronized glucose-limited chemostat cultures with yeast have shown the intracellular F1,6BP (Sasidharan et al., 2012) levels to oscillate in synchrony with the cell division (Figure 4A). Ras could be dynamically activated by these oscillating metabolite levels, triggering periodic cAMP signaling and regulating storage carbon metabolism. Such a periodic cAMP/PKA activity would be in line with the observed rapid increase of cAMP levels at START (Müller et al., 2003), just prior to DNA replication and budding, followed by the liquidation of storage carbohydrates (trehalose and glycogen), both measured in synchronized chemostat cultures.

Mitochondrial activity controls the cell cycle via the AMPK pathway

The yeast metabolic cycles are commonly described as a periodically alternating balance between oxidative and reductive metabolism (Tu et al., 2005) or cycles of mitochondrial energization (Lloyd et al., 2002). Enhanced mitochondrial respiration is gated in the oxidative phase, accompanied with an up-regulation of glycolysis and protein synthesis, necessary for the G1/S transition and START. The periodic activity of mitochondrial respiration is not only reflected in the oxygen consumption rates (Klevecz et al., 2004;

Lloyd and Murray, 2005; Müller et al., 2003; Tu et al., 2005) but also on the structure of the organelle during cell division (Finkel and Hwang, 2009; Lee and Finkel, 2013). In rat kidney cells, during the G1/S transition, mitochondria are fused to a single tubular network (Mitra et al., 2009) (Figure 5A). This hyperfused mitochondrial network is known to consume more oxygen, generate higher membrane potential and thus produce more ATP, until it is fragmented into smaller low energy mitochondrial structures during the S phase (Figure 5A).

Several findings indicate the importance of the mitochondrial activity for cell cycle progression. Firstly, more than 60% of prominently oscillating transcripts correspond to mitochondrial proteins, such as ribosomal subunits, tRNA synthetases, and elongation factors, all essential components of the mitochondrial protein translation machinery (Tu et al., 2005). Secondly, mutation of the cytochrome oxidase subunit Va (CoVa) in Drosophila cells, caused cell cycle arrest in G1 (Mandal et al., 2005). Thirdly, in rat kidney cells, mitochondrial depolarization led to cell cycle arrest in G1 (Mitra et al., 2009).

In fact, there are connections between cellular energization and the cell cycle: The ADP/ATP and AMP/ATP ratios are reporters of the ATP availability and thus the energy status of cells. Due to the activity of adenylate kinase, the enzyme which catalyzes the reversible production of AMP and one ATP nucleotide from 2 ADP nucleotides (2ADP ↔ AMP + ATP), the AMP/ATP ratio varies as the square of the ADP/ATP ratio (Hardie, 2004), and thus is more sensitive to changes of the intracellular adenine nucleotide consistency. At the same time, the AMP nucleotide is an allosteric activator if the AMPK (AMP-activated kinase), as reported in mammalian (Hardie, 2011; Xiao et al., 2007) and insect cells (Pan and Hardie, 2002). AMPK signaling and its downstream target p53, activate catabolism (ATP production) over anabolic processes (ATP consumption), decreasing the AMP/ATP ratio and re-establishing energy homeostasis (Jones et al., 2005). However, AMPK not only targets metabolism. Increased AMPK in CoVa-depleted Drosophila cells, driven by the decreased mitochondrial energization and ATP production, was found to promote the proteasomal degradation of cyclin E, in a p53 dependent manner (Mandal et al., 2005) (Figure 5B-C). Adversely, in rat kidney cells, induction of mitochondrial hyperfusion increased the cyclin E levels (Mitra et al., 2009). In fact, the cell cycle arrest was bypassed when AMPK or p53 were mutated, although the intracellular

ATP levels remained low. As a result, the AMPK pathway is not necessary for cell division, but operates to ensure adequate energy supply to the cell cycle processes (e.g. DNA and protein synthesis).

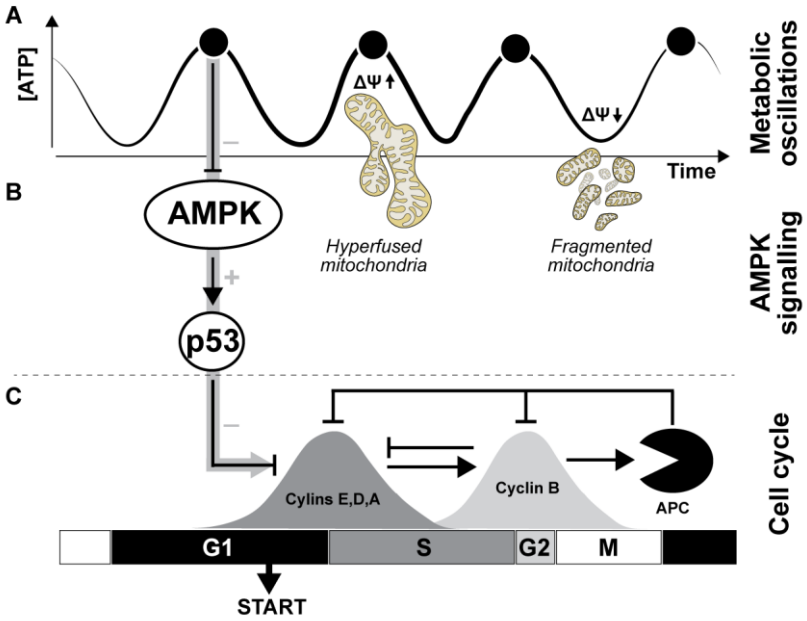

Figure 5: Cycles of mitochondrial morphology and energization regulate the cell cycle via the AMPK signaling. (A) In mammalian and insect cells, mitochondria have been shown to fuse into a tubular hyperpolarized network in the late G1 phase and during the early cell cycle (Finkel and Hwang, 2009; Lee and Finkel, 2013). Mitochondrial fission during the late cell cycle results in fragmented mitochondria with deceased membrane potential (ΔΨ). Thus, oscillations in mitochondrial morphology reflect cycles of mitochondrial energization and potentially intracellular ATP oscillations, in synchrony with cell division. **(B)** Elevated ATP production, or the corresponding decrease in the AMP/ATP ratio, inhibits AMPK. **(C)** The ATP dependent AMPK inhibition releases the p53 mediated inhibition of the early cyclin E, and operates as a metabolic checkpoint (Jones et al., 2016), allowing the G1/S transition only when there is sufficient energy.

Contrary to multicellular organisms cells, in yeast cells the Snf1 (AMPK analog) promotes cell cycle initiation. The Snf1 has been shown to interact with Swi6, an essential component of the MBF and SBF G1-transcriptional activation complexes (Busnelli et al., 2013), facilitating the expression of the early cyclin Clb5 (Pessina et al., 2010). Additionally, although the mammalian AMPK signaling is known to promote histone de-

acetylation and chromatin silencing (Busti et al., 2010; Cantó et al., 2009), Snf1 promotes the opposite process, namely histone acetylation (Abate et al., 2012; Lo et al., 2001), activating the transcription of growth related genes (e.g. ribosomal subunits). Despite the opposite functions of the AMPK and Snf1, similarly to multicellular organisms where low ATP or high AMPK signaling activates catabolic processes, also in yeast cells and during the metabolic oscillations, catabolic gene clusters are expressed in the reductive phase (low ATP levels), whereas the expression of anabolic genes is gated in the oxidative phase (high ATP) (Cornelia Amariei, 2014).

Next to the AMPK mediated cell cycle arrest, elevated reactive oxygen species (ROS), by-products of oxidative phosphorylation, were also found to delay cell cycle entry via the activation of the Dacapo (p27 homolog) inhibitor in Drosophila mutants harboring a disrupted electron transport chain (complex I mutation) (Owusu-Ansah et al., 2008). The Dacapo activation inhibits the Cyclin E/CDK2 complex without affecting the intracellular levels of Cyclin E and is mediated by the JNK (Jun amino-terminal kinase) signaling. In summary, mitochondrial energization signals (ATP and ROS) interact with the cell cycle machinery indirectly via the AMPK and JNK signaling pathways for the coordination of mitochondrial respiration and cell division.

Mitochondria have been shown to undergo reversible structural and energetic transformation in vitro, switching between a condensed (energized) to an orthodox conformation of reduced energy transfer, which indicates that the apparent ATP oscillations could be an intrinsic behavior of the mitochondrion. Because the period of mitochondrial hyper-fusion cycles in vivo, is at least two times slower (longer than 40 min) compared to the mitochondrial cycles reported in vitro (20 min), it was suggested that an external ultradian clock, entrains the mitochondrial dynamics, in synchrony with cell division. Such synchrony between the mitochondrial energization cycles and cell division cycles can be crucial for the temporal separation of incompatible cellular processes. It has previously been suggested that respiration cannot not occur together with DNA synthesis due to the hazards of oxidative DNA damage (Tu et al., 2005). Thus the oxidative phase might be gated prior to the S phase and DNA replication.

Epigenetics provide a link between metabolism and the cell cycle

Dynamic changes between histone acetylation/de-acetylation eventually induced by a cycling metabolism, could also dynamically control transcription and cell cycle progression. Histone acetyl-transferases (HATs) are known to activate gene expression via the transfer of one acetyl group, from acetyl-CoA to the Nε-group of lysine residues in histones (Bannister and Kouzarides, 2011). The acetylated histones lose their positive charge and interact less strongly with the negatively charged nucleosomal DNA, thus decreasing the chromatin condensation and increasing the accessibility of promoters by transcriptional factors. Additionally, acetylated histones attract and bind to proteins via their bromo-domains (Josling et al., 2012). Such proteins are HATs, chromatin remodeling (e.g. Snf2 in yeast) proteins as well as transcriptional activators (e.g. BdfI/II in yeast).

Opposite to acetylation, histone de-acetylation correlates with a condensed chromatin state. Histone de-acetylases (HDACs) not only reverse the effect of HATs, but also regulate the availability of histone lysine residues for additional post-translational epigenetic modifications, such as methylation which is linked with the formation of heterochromatin (Yamada et al., 2005). Here, the possibility of a metabolic oscillator dynamically regulating the balance between histone acetylation/de-acetylation and in extent cell cycle is investigated.

In two independent studies (Klevecz et al., 2004; Tu et al., 2005), approximately 3500 or 5300 transcripts were found to oscillate in synchrony with the yeast metabolic cycle, comprising 62-95% of the protein encoding genes in the yeast genome. Similar global changes in gene expression have been reported in cancer cells (Park et al., 2011), where they have been attributed to histone and chromatin modifications. In yeast, it was found that the acetylation of the histones is periodic and in synchrony with the yeast metabolic oscillations (Kuang et al., 2014). Specifically, the acetylation of histones H3 and H4 was significantly increased during the oxidative phase of the metabolic oscillation, coinciding with a peak in the also oscillating intracellular acetyl-CoA concentration (Figure 6A-B), at the START point of the cell cycle.

These histone acetylation cycles were found to be driven by the SAGA transcriptional co-activator (Spt-Ada-Gcn5-Acetyltransferase) and the Gcn5 acetyl-transferase, in response to

the intracellular acetyl-CoA concentrations (Cai et al., 2011) (Figure 6A-B). According to the proposed mechanism, the Gcn5 acetyl-transferase first catalyzes the acetylation of the Spt7p, Ada3p and Sgf73p proteins, also components of the SAGA complex. Especially the acetylation of Sgf73p subunit, harboring many acetylation sites, was found to be sensitive to the addition of acetyl-CoA in vitro, potentially acting as an integrator of the acetyl-CoA signal. The acetylated SAGA complex is then recruited to growth related genes, where it activates their transcription via the acetylation of the H3 and H4 histones. Together with the growth related genes, the SAGA complex was also found to acetylate histones at the promoter region of the Cln3 gene (Shi and Tu, 2013), thus providing a link between the acetyl-CoA oscillations and the Cln/CDK machinery (Figure 6B-C). Consistently, attenuated activity of the acetyl-CoA carboxylase (Acc1), the enzyme that catalyzes the carboxylation of acetyl-CoA for the production of malonyl-CoA, was found to increase histone acetylation and gene expression, via affecting the availability of acetyl-CoA in yeast (Galdieri and Vancura, 2012).

The Sirtuins (Sir2) constitute another family of chromatin modifying enzymes which can sense and mediate metabolic signals. The Sirtuins are histone de-acetylases dependent on NAD^+ availability (Figure 6A-B), but not NADH, $NADP^+$ or NADPH (North and Verdin, 2004). The NAD^+ and NADH intracellular abundance have been found to oscillate opposite in phase (Sasidharan et al., 2012), maintaining a constant pool of nicotinamide adenine dinucleotides (Xu and Tsurugi, 2006). As a result, the intracellular concentration of either NAD+ or NADH signals the redox status inside the cells. Strikingly, the Sirtuin activity peaks during mitosis or the early G1 phase (Dryden et al., 2003; Fox and Weinreich, 2008), and thus coincides with the peak of the oscillating NAD^+ levels, as previously measured in yeast synchronized populations (Sasidharan et al., 2012; Xu and Tsurugi, 2006) (Figure 6A). The Sir2 HDAC could provide a link between periodic redox signal (NAD^+) and the cell cycle (Figure 6A-C). In yeast cells, the deletion of two Sir2 homologs (Hst3/4) was found to arrest cells in Mitosis (Brachmann et al., 1995). Sir2 is recruited to the Clb2 (Linke et al., 2013) and possibly also the Swi5 (Cipak et al., 2009) promoters by the Fkh1/2 transcriptional factors, where it suppresses transcription and controls the M/G1 transition.

Overall, the periodic intracellular abundances of acetyl-CoA and NAD^+ have the potential to dynamically regulate histone acetylation and gene expression (Figure 6A-C). These two

metabolites oscillate out-of phase (Sasidharan et al., 2012; Tu et al., 2007; Xu and Tsurugi, 2006) (Figure 6A) and thus could be responsible for timely separated transcriptional events of the early and the late cell cycle, which are evident in continuous yeast cultures (Klevecz et al., 2004; Tu et al., 2005). The elevated acetyl-CoA levels at the G1/S transition might be responsible for the activation of growth related genes (e.g. ribosomal subunits) and the early cell cycle via the Gcn5 acetyl-transferase. The oscillation of NAD^+ could periodically activate Sir2, in turn mediating silencing of the late cell cycle genes (e.g. Clb2) and the M/G1 transition. A similar temporal compartmentalization of the early and late cell cycle transcription has also been reported in non-dividing yeast populations (Slavov et al., 2011), pointing towards a free-running metabolic oscillator as the driver of cell cycle transcription. Because the Gcn5-related-N-acetyl-transferases (GNATs) and Sirtuins are widely represented across prokaryotes and eukaryotes (Pandey et al., 2002), they could constitute together with the metabolic oscillator a primitive mechanism for periodic transcription, growth and division.

Next to the histone acetylation, another category of chromatin modification complexes use the energy provided by ATP hydrolysis (Gangaraju and Bartholomew, 2007) to shift the relative conformation between the DNA and the nucleosome, thus generating DNA bulges or waves which are accessible to transcriptional activators or repressors. It has previously been conjectured that the ATP oscillations measured in glucose-limited synchronized yeast populations could periodically modify DNA occupancy and gate the expression of the anabolic or the catabolic gene clusters oppositely in phase and in specific metabolic phases (Cornelia Amariei, 2014; Machné and Murray, 2012). Because the ATP-dependent chromatin structure remodeling (RSC) complex is essential for yeast growth (Hsu et al., 2003), and because it has also been shown to be involved in the cohesion of sister chromatids (Huang and Laurent, 2004), we conjecture that it may be part of a previously described ancestral non-CDK DNA replication and segregation controller.

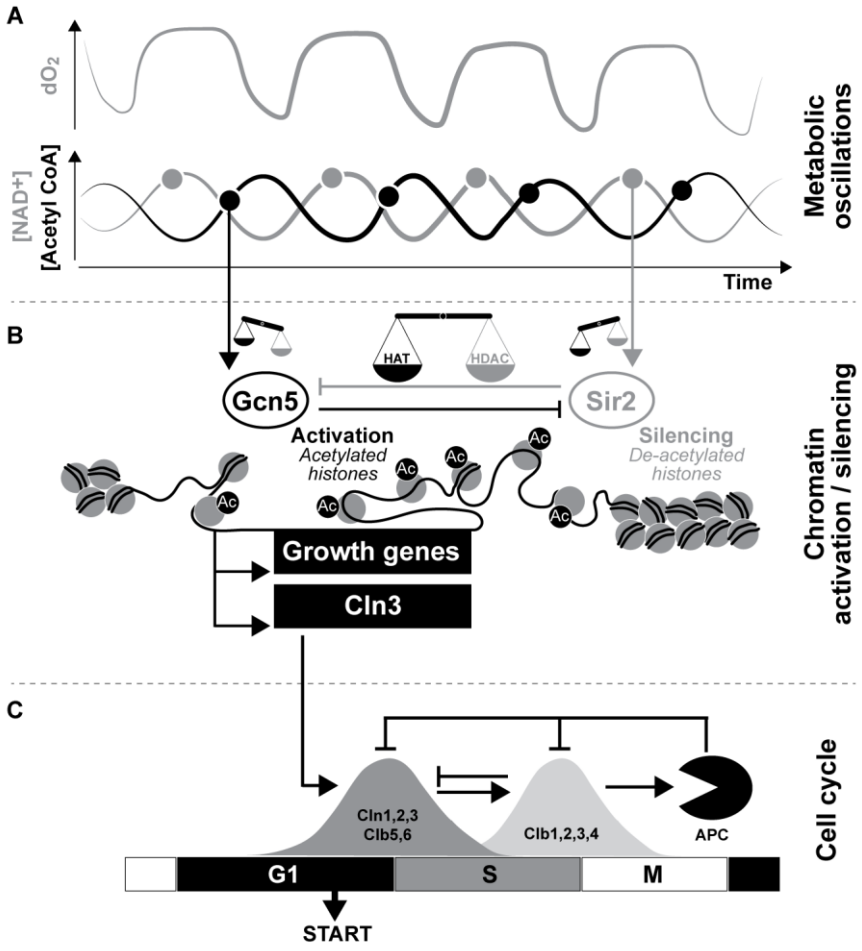

Figure 6: Oscillating metabolites control the expression of the early cyclins on the epigenetic level. (A) In glucose-limited chemostat yeast cultures, the acetyl-CoA and NAD^+ concentrations have been shown to oscillate oppositely in phase (Sasidharan et al., 2012; Xu and Tsurugi, 2006), and in synchrony with the dissolved oxygen (dO2) oscillations and the cell cycle. **(B)** Acetyl-CoA activates the Gcn5 histone acetyl-transferase (HAT), which acetylates histones and activates the chromatin around growth related genes and Cln3 (Cai et al., 2011; Shi and Tu, 2013). Adversely, NAD^+ activates the histone de-acetylase (HDAC) Sir2 and chromatin silencing (North and Verdin, 2004). The yeast metabolic oscillations could set a fine balance between histone acetylation and de-acetylation, **(C)** gating chromatin activation during the early cell cycle, and chromatin silencing during the late cell cycle.

The cyclin/CDK machinery entrains metabolism

So far we have summarized how the oscillating concentration of metabolites could regulate cell growth and division. However, connections in the opposite have also been described. The cyclin/CDK machinery has been shown to entrain the metabolic operation and specifically storage carbon metabolism and mitochondrial respiration, during the course of the cell cycl.

First, in two independent studies (Ewald et al., 2016; Zhao et al., 2016) it was shown that the Cdc28 (budding yeast CDK) together with PKA, activate the neutral trehalase (Nth1) at START, promoting the liquidation of trehalose into glycolysis. Second, in human and mouse cells it was shown that the cyclinB1/CDK1 complex translocates into the mitochondrial matrix where it phosphorylates components of the respiratory complex I, enhancing mitochondrial respiration (Wang et al., 2014). The mitochondrial activity of cyclinB1/CDK1 was found to be enhanced in the late G2 phase, accelerating the G2/M transition and robustly coordinating the mitochondrial activity with the cell cycle. Third, the glycolytic enzyme PFKFB3, previously conjectured to activate Cdk1 in mammalian cells, is a substrate of the S phase ubiquitin ligase SCF-β-TrCP (Tudzarova et al., 2011) as well as the anaphase-promoting complex (Almeida et al., 2010). Both ubiquitin ligase complexes target the glycolytic effector PFKFB3, gating its activity and high glycolysis during the late G1 phase, for the G1/S transition.

Discussion

Here we provide a systems view on cell cycle regulation, including a metabolic oscillator and its metabolite dynamics, signaling pathways, epigenetic modifications and the cyclin/CDK machinery, altogether converging at the point of cell cycle transcription to drive cell growth and division (Figure 7). Despite the complexity and the evident redundancy in this intertwined network, we can derive global higher order operations robustly emerging from the collective synchrony between the individual components. The cell division cycle can be summarized as a periodic switch between catabolic and anabolic processes. During the early cell cycle or the oxidative phase of the metabolic oscillations,

cells consume energy to produce biomass (anabolism), whereas during the late cell cycle, or the reductive phase of the metabolic oscillations, the cells enter an energy conservation program, oxidizing proteins and lipids (catabolism) and segregating their duplicated biomass.

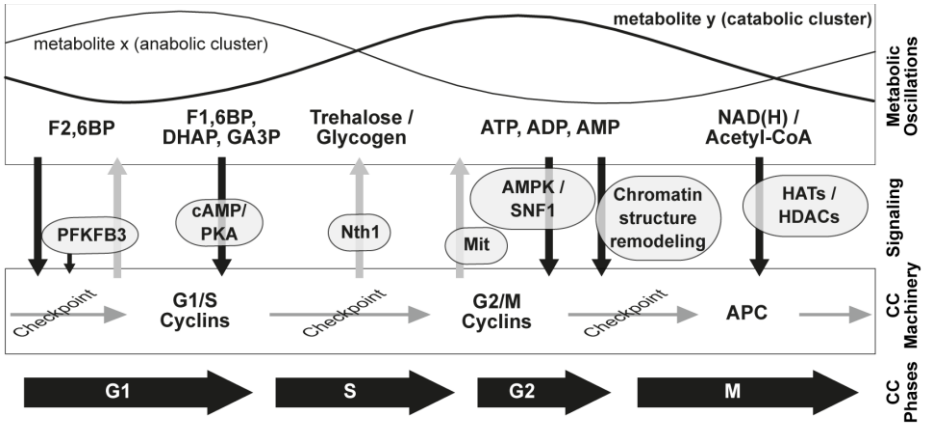

Figure 7: An overview of the direct and the indirect connections between the yeast metabolic oscillations and the cell cycle. From left to right: the glycolytic end-point metabolite F2,6BP has been suggested to directly interact and activate Cdk1 in mammalian cells (Yalcin et al., 2009, 2014). The synthesis of F2,6BP is catalyzed by PFKFB3, a glycolytic enzyme which also translocates into the nucleus facilitating the G1/S transition (Yalcin et al., 2009, 2014). The PFBFB3 is targeted by the anaphase promoting complex for proteasomal degradation during the late cell cycle (Almeida et al., 2010; Tudzarova et al., 2011). The cAMP/PKA pathway is activated by oscillating metabolites (FBP, DHAP, GA3P) (Peters, 2013) and in turn activates global protein synthesis, growth and START (Futcher, 2006). The yeast CDK has been shown to activate the neutral trehalase and trehalose liquidation into glycolysis at START (Ewald et al., 2016; Zhao et al., 2016). Together with the cAMP/PKA pathway, the cyclin/CDK have been suggested to drive the oscillations in the intracellular concentration of carbon storage (trehalose and glycogen), previously measured in glucose-limited continuous yeast cultures (Müller et al., 2003). In mammalian cells, the cyclin B1/CDK1 complex is sequestered into the mitochondrial matrix where it phosphorylates components of the respiratory complex I, enhancing mitochondrial respiration and facilitating the G2/M transition (Wang et al., 2014). The ATP oscillations, previously measured in glucose-limited chemostat yeast cultures (Sasidharan et al., 2012), and conjectured in mammalian cells (Finkel and Hwang, 2009; Lee and Finkel, 2013), could provide periodic signals for the G1/S transition via the activation of the Snf1 pathway in yeast (Busnelli et al., 2013) or the deactivation of the AMPK signaling pathway (Jones et al., 2005) in mammals. The Snf1 pathway activates the early cell cycle transcription, whereas the AMPK pathway induces cell cycle arrest in G1, mediated by p53. The ATP oscillations could regulate gene expression and the cell cycle also on the epigenetic level, via the ATP dependent

chromatin remodeling complexes. The acetyl-CoA metabolite induces histone acetylation via the SAGA complex, and epigenetic activation of growth related genes and Cln3, triggering START (Cai et al., 2011; Shi and Tu, 2013). Adversely, the NAD^+ metabolite activates the Sir2 histone de-acetylates and chromatin silencing (North and Verdin, 2004).

This periodic switch between anabolism and catabolism, or energy consumption and energy conservation, or chromatin activation and chromatin silencing, may constitute a primitive function of cell division, conserved among eukaryotes and possibly also prokaryotes. It was previously shown that the bacterial enzyme gyrase has an ATP-dependent negative supercoiling activity (Machné and Murray, 2012; Wijker et al., 1995). Thus, when ATP is abundant the enzyme relaxes the supercoiled chromosome, and renders it accessible to the transcription and replication machineries. Thus, the activity of gyrase alone can couple and synchronize the metabolic activity and ATP abundance, with biomass formation, namely global protein synthesis and DNA replication in bacteria. Still, it remains unknown whether autonomous ATP oscillations drive cell division in bacteria.

Similarly to bacteria, the ATP dependent chromatin remodeling complexes (e.g. RSC) provide a direct link between the metabolic oscillator, biomass formation and segregation in eukaryotes (Saha et al., 2002). The cyclin/CDK machinery and signaling pathways (e.g. cAMP/PKA, AMPK) were possibly grafted onto this primitive periodic operation for the robust separation of the cell cycle phases and coordination between metabolism and the cell cycle. Consistently, it has been shown that yeast can still grow and divide in the absence of the early cyclins Cln3 and/or Cln2, however exhibiting slower growth rates on average and higher noise in the duration of the G1 phase (Talia et al., 2007). This noise could stem from stochasticity in the metabolic or gene expression dynamcis.

In order to identify the minimal constituents of a primitive CDK-independent cell cycle engine it is necessary to unravel the redundancy in the studied network including the metabolic oscillator, signaling pathways, chromatin remodeling complexes and the cyclin/CDK machinery. It has previously been shown that the deletion of adenylate cyclase, the central enzyme of the cAMP/PKA machinery, can be synthetically rescued by the deletion of its downstream effector and metabolic inhibitor Rim15 (Reinders et al., 1998) (Figure 8A). Similarly, budding yeast cells lacking all early cyclins can be synthetically

rescued when Sic1, an inhibitor of DNA replication, is deleted (Tyers, 1996) (Figure 8B). We conclude that additional regulation was imposed to the primitive cell cycle engine in pairs of activators (e.g. Cyr1 or Cln1,2,3) and inhibitors (e.g. Rim15 or Sic1). The deletion of the activator modules causes growth arrest and is lethal. However, deletion of the entire activator/inhibitor pair restores cell division, yet making it prone to noise. Similarly, the acetyl-CoA dependent activity of histone acetyl-transferases (HATs) is competed by the NAD^+ dependent activity of histone de-acetylases (HDACs), with the two metabolites oscillating opposite in phase (Sasidharan et al., 2012; Tu et al., 2007). In fact, it has been shown that the deletion of the Gcn5 acetyl-transferase causes a phenotype sensitive to stress (Johnsson et al., 2006), which is reversed by the additional deletion of the Sir2 or Clr3 de-acetylases (Johnsson and Wright, 2010) (Figure 8C).

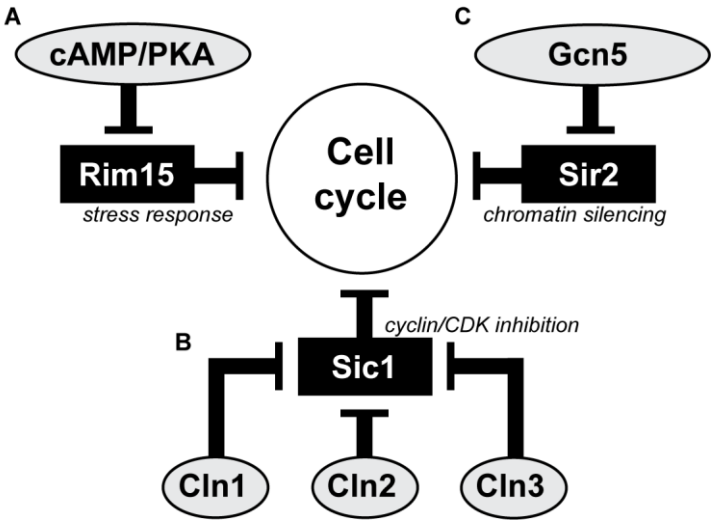

Figure 8: Three yeast examples of redundant pairs of cell cycle inhibitors (black boxes) and activators (grey boxes). (A) In the absence of cAMP-signaling the Rim15 kinase activates the stress response and entry into quiescence. However, deletion of the cAMP/PKA pathway together with its downstream target (Rim15) restores cell division (Reinders et al., 1998). **(B)** The presence of only one of the three G1 cyclins (Cln1, 2 or 3) is enough to inhibit the Sic1 CDK inhibitor and promote the G1/S transition. When all three cyclins were deleted together with Sic1, cells can enter cell division (Tyers, 1996). **(C)** The Sir2 histone de-acetylase, and the Gcn5 histone acetyl-transferase compete the opposite reacrinos and compete for chromatin silencing or activation respectively. The stress sensitive phenotype of Gcn5 deletion, can be reversed when the Sir2 is also deleted (Johnsson and Wright, 2010).

The yeast metabolic oscillations, and the corresponding oscillations of intracellular signaling metabolites provide a framework for a metabolically driven cell cycle. However, it remains unclear if the yeast metabolic oscillations constitute an intrinsic operation of metabolism, or an artifact of cell cycle synchronization and intercellular communication (Aon et al., 2007; Henson, 2004; Laxman et al., 2010; Sohn et al., 2000). Sulfide, a diffusible gas, product of cysteine metabolism, and an inhibitor of the respiratory chain, has been suggested to periodically inhibit respiration, causing metabolic oscillations and synchrony on the population level (Henson, 2004; Sohn et al., 2000). The notion of a gaseous agent inducing metabolic synchrony, is further supported by the fact that yeast metabolic oscillations were only measured at low dilution rates (below 0.2 h^{-1}) (Sheppard and Dawson, 1999), under a critical range of aeration (0.1 – 0.5 VVM) and pH (3.4 – 4.0) (Keulers et al., 1996). As a result, in order to establish the metabolic oscillator as a primitive cell cycle regulator it is necessary to show that metabolism oscillates also in unsynchronized yeast cells. Recently developed single cell technologies, including microfluidic devices for the long-term (over multiple cell divisions) observation of yeast cells, and single cell metabolite sensors, can optimally be used for this purpose. The establishment of an autonomous metabolic oscillator as a dynamic component within the cell cycle engine network, is going to provide new means for cell cycle control, against proliferative disorders, targeted to metabolic enzymes or pathways.

Aim of the thesis

The purpose of this thesis is to investigate the existence of an autonomous metabolic oscillator as a crucial component of cell cycle control. Microfluidics and single cell metabolite reporters will be used to dynamically measure the metabolic dynamics in dividing or cell cycle arrested cells, in the absence of synchronization and cell-to-cell communication, during steady growth or perturbed conditions. Nutrient switches will provide the means for metabolic perturbations, whereas the conditional and orthogonal depletion of targeted proteins, together with constitutive gene deletions, will serve as tools for the perturbation of the cyclin/CDK machinery or signaling pathways (e.g. cAMP/PKA pathway), and altogether will be used to investigate the interactions between an oscillating

metabolism and the cell cycle. The cell cycle could emerge as a higher order function from the collective synchrony between metabolism and the cyclin/CDK machinery.

References

Abate, G., Bastonini, E., Braun, K.A., Verdone, L., Young, E.T., and Caserta, M. (2012). Snf1/AMPK regulates Gcn5 occupancy, H3 acetylation and chromatin remodelling at S. cerevisiae ADY2 promoter. Biochim. Biophys. Acta 1819, 419–427.

Acquaviva, C., and Pines, J. (2006). The anaphase-promoting complex/cyclosome: APC/C. J. Cell Sci. 119, 2401 LP-2404.

Almeida, A., Bolaños, J.P., and Moncada, S. (2010). E3 ubiquitin ligase APC/C-Cdh1 accounts for the Warburg effect by linking glycolysis to cell proliferation. Proc. Natl. Acad. Sci. 107, 738–741.

Aon, M.A., Cortassa, S., Lemar, K.M., Hayes, A.J., and Lloyd, D. (2007). Single and cell population respiratory oscillations in yeast: A 2-photon scanning laser microscopy study. FEBS Lett. 581, 8–14.

Bähler, J. (2005). Cell-cycle control of gene expression in budding and fission yeast. Annu. Rev. Genet. 39, 69–94.

Bannister, A.J., and Kouzarides, T. (2011). Regulation of chromatin by histone modifications. Cell Res. 21, 381–395.

Banyai, G., Baidi, F., Coudreuse, D., and Szilagyi, Z. (2016). Cdk1 activity acts as a quantitative platform for coordinating cell cycle progression with periodic transcription. Nat Commun 7.

Barberis, M. (2012). Molecular Systems Biology of Sic1 in Yeast Cell Cycle Regulation Through Multiscale Modeling BT - Advances in Systems Biology. I.I. Goryanin, and A.B. Goryachev, eds. (New York, NY: Springer New York), pp. 135–167.

Barik, D., Baumann, W.T., Paul, M.R., Novak, B., and Tyson, J.J. (2010). A model of yeast cell-cycle regulation based on multisite phosphorylation. Mol. Syst. Biol. 6, 405.

Barnum, K.J., and O'Connell, M.J. (2014). Cell Cycle Regulation by Checkpoints. Methods Mol. Biol. 1170, 29–40.

Baroni, M.D., Monti, P., and Alberghina, L. (1994). Repression of growth-regulated Gl cyclin expression by cyclic AMP in budding yeast. Nature 371, 339–342.

Brachmann, C.B., Sherman, J.M., Devine, S.E., Cameron, E.E., Pillus, L., and Boeke, J.D. (1995). The SIR2 gene family, conserved from bacteria to humans, functions in silencing, cell cycle progression, and chromosome stability. Genes Dev. 9, 2888–2902.

de Bruin, R.A.M., McDonald, W.H., Kalashnikova, T.I., Yates III, J., and Wittenberg, C. (2004). Cln3 Activates G1-Specific Transcription via Phosphorylation of the SBF Bound Repressor Whi5. Cell 117, 887–898.

Burnetti, A.J., Aydin, M., and Buchler, N.E. (2016). Cell cycle Start is coupled to entry into the yeast metabolic cycle across diverse strains and growth rates. Mol. Biol. Cell 27, 64–74.

Busnelli, S., Tripodi, F., Nicastro, R., Cirulli, C., Tedeschi, G., Pagliarin, R., Alberghina, L., and Coccetti, P. (2013). Snf1/AMPK promotes SBF and MBF-dependent transcription in budding yeast. Biochim. Biophys. Acta - Mol. Cell Res. 1833, 3254–3264.

Busti, S., Coccetti, P., Alberghina, L., and Vanoni, M. (2010). Glucose Signaling-Mediated Coordination of Cell Growth and Cell Cycle in *Saccharomyces Cerevisiae*. Sensors (Basel). 10, 6195–6240.

Cai, L., Sutter, B.M., Li, B., and Tu, B.P. (2011). Acetyl-CoA Induces Cell Growth and Proliferation by Promoting the Acetylation of Histones at Growth Genes. Mol. Cell 42, 426–437.

Cantó, C., Gerhart-Hines, Z., Feige, J.N., Lagouge, M., Noriega, L., Milne, J.C., Elliott, P.J., Puigserver, P., and Auwerx, J. (2009). AMPK regulates energy expenditure by modulating NAD(+) metabolism and SIRT1 activity. Nature 458, 1056–1060.

Charvin, G., Oikonomou, C., Siggia, E.D., and Cross, F.R. (2010). Origin of irreversibility of cell cycle start in budding yeast. PLoS Biol. 8, e1000284.

Cipak, L., Spirek, M., Novatchkova, M., Chen, Z., Rumpf, C., Lugmayr, W., Mechtler, K., Ammerer, G., Csaszar, E., and Gregan, J. (2009). An improved strategy for tandem affinity purification-tagging of Schizosaccharomyces pombe genes. Proteomics 9, 4825–4828.

Conrad, M., Schothorst, J., Kankipati, H.N., Van Zeebroeck, G., Rubio-Texeira, M., and Thevelein, J.M. (2014). Nutrient sensing and signaling in the yeast *Saccharomyces cerevisiae*. FEMS Microbiol. Rev. 38, 254 LP-299.

Cornelia Amariei, R.M.V.S.T.S.M.T. and D.B.M. (2014). Time resolved DNA occupancy dynamics during the respiratory oscillation uncover a global reset point in the yeast growth program. Microb. Cell 1, 279–288.

Coudreuse, D., and Nurse, P. (2010). Driving the cell cycle with a minimal CDK control network. Nature 468, 1074–1079.

Dryden, S.C., Nahhas, F.A., Nowak, J.E., Goustin, A.-S., and Tainsky, M.A. (2003). Role for Human SIRT2 NAD-Dependent Deacetylase Activity in Control of Mitotic Exit in the Cell Cycle. Mol. Cell. Biol. 23, 3173–3185.

Ewald, J.C., Kuehne, A., Zamboni, N., and Skotheim, J.M. (2016). The Yeast Cyclin-Dependent Kinase Routes Carbon Fluxes to Fuel Cell Cycle Progression. Mol. Cell 62, 532–545.

Ferrezuelo, F., Colomina, N., Palmisano, A., Garí, E., Gallego, C., Csikász-Nagy, A., and Aldea, M. (2012). The critical size is set at a single-cell level by growth rate to attain homeostasis and adaptation. Nat. Commun. 3, 1–11.

Finkel, T., and Hwang, P.M. (2009). The Krebs cycle meets the cell cycle: Mitochondria and the G1–S transition. Proc. Natl. Acad. Sci. 106, 11825–11826.

Fisher, D.L., and Nurse, P. (1996). A single fission yeast mitotic cyclin B p34cdc2 kinase promotes both S-phase and mitosis in the absence of G1 cyclins. EMBO J. 15, 850–860.

Fox, C.A., and Weinreich, M. (2008). Beyond heterochromatin: SIR2 inhibits the initiation of DNA replication. Cell Cycle 7, 3330–3334.

Futcher, B. (2006). Metabolic cycle, cell cycle, and the finishing kick to Start. Genome Biol. 7, 107.

Galdieri, L., and Vancura, A. (2012). Acetyl-CoA Carboxylase Regulates Global Histone Acetylation. J. Biol. Chem. 287, 23865–23876.

Gangaraju, V.K., and Bartholomew, B. (2007). Mechanisms of ATP Dependent Chromatin Remodeling. Mutat. Res. 618, 3–17.

Garí, E., Volpe, T., Wang, H., Gallego, C., Futcher, B., and Aldea, M. (2001). Whi3 binds the mRNA of the G(1) cyclin CLN3 to modulate cell fate in budding yeast. Genes Dev. 15, 2803–2808.

Gérard, C., Tyson, J.J.J., and Novák, B. (2013). Minimal Models for Cell-Cycle Control Based on Competitive Inhibition and Multisite Phosphorylations of Cdk Substrates. Biophys. J. 104, 1367–1379.

Hall, D.D., Markwardt, D.D., Parviz, F., and Heideman, W. (1998). Regulation of the Cln3-Cdc28 kinase by cAMP in *Saccharomyces cerevisiae*. EMBO J. 17, 4370–4378.

Hardie, D.G. (2004). The AMP-activated protein kinase pathway – new players upstream and downstream. J. Cell Sci. 117, 5479 LP-5487.

Hardie, D.G. (2011). Sensing of energy and nutrients by AMP-activated protein kinase. Am. J. Clin. Nutr. 93, 891S–896S.

Henson, M. a (2004). Modeling the synchronization of yeast respiratory oscillations. J. Theor. Biol. 231, 443–458.

Hers, H.-G., Hue, L., and Van Schaftingen, E. (2016). Fructose 2,6-bisphosphate. Trends Biochem. Sci. 7, 329–331.

Hsu, J., Huang, J., Meluh, P.B., and Laurent, B.C. (2003). The Yeast RSC Chromatin-Remodeling Complex Is Required for Kinetochore Function in Chromosome Segregation. Mol. Cell. Biol. 23, 3202–3215.

Huang, J., and Laurent, B.C. (2004). A Role for the RSC chromatin remodeler in regulating cohesion of sister chromatid arms. Cell Cycle 3, 973–975.

Johnson, A., and Skotheim, J.M. (2013). Start and the Restriction Point. Curr. Opin. Cell Biol. 25, 10.1016/j.ceb.2013.07.010.

Johnsson, A.E., and Wright, A.P.H. (2010). The role of specific HAT-HDAC interactions in transcriptional elongation. Cell Cycle 9, 467–471.

Johnsson, A., Xue-Franzén, Y., Lundin, M., and Wright, A.P.H. (2006). Stress-Specific Role of Fission Yeast Gcn5 Histone Acetyltransferase in Programming a Subset of Stress Response Genes . Eukaryot. Cell 5, 1337–1346.

Jones, R.G., Plas, D.R., Kubek, S., Buzzai, M., Mu, J., Xu, Y., Birnbaum, M.J., and Thompson, C.B. (2005). AMP-activated protein kinase induces a p53-dependent metabolic checkpoint. Mol. Cell 18, 283–293.

Jones, R.G., Plas, D.R., Kubek, S., Buzzai, M., Mu, J., Xu, Y., Birnbaum, M.J., and Thompson, C.B. (2016). AMP-Activated Protein Kinase Induces a p53-Dependent Metabolic Checkpoint. Mol. Cell 18, 283–293.

Josling, G.A., Selvarajah, S.A., Petter, M., and Duffy, M.F. (2012). The Role of Bromodomain Proteins in Regulating Gene Expression. Genes (Basel). 3.

Keulers, M., Suzuki, T., Satroutdinov, A.D., and Kuriyama, H. (1996). Autonomous metabolic oscillation in continuous culture of *Saccharomyces cerevisiae* grown on ethanol. FEMS Microbiol. Lett. 142, 253 LP-258.

Klevecz, R.R. (1969). TEMPORAL ORDER IN MAMMALIAN CELLS : I. The Periodic Synthesis of Lactate Dehydrogenase in the Cell Cycle. J. Cell Biol. 43, 207–219.

Klevecz, R.R., and Ruddle, F.H. (1968). Cyclic Changes in Enzyme Activity in Synchronized Mammalian Cell Cultures. Science (80-.). 159, 634–636.

Klevecz, R.R., Bolen, J., Forrest, G., and Murray, D.B. (2004). A genomewide oscillation in transcription gates DNA replication and cell cycle. Proc. Natl. Acad. Sci. U. S. A. 101, 1200–1205.

Kotani, S., Tugendreich, S., Fujii, M., Jorgensen, P.-M., Watanabe, N., Hoog, C., Hieter, P., and Todokoro, K. (2016). PKA and MPF-Activated Polo-like Kinase Regulate Anaphase-Promoting Complex Activity and Mitosis Progression. Mol. Cell 1, 371–380.

Krylov, D.M., Nasmyth, K., and Koonin, E. V. (2003). Evolution of eukaryotic cell cycle regulation: stepwise addition of regulatory kinases and late advent of the CDKs. Curr. Biol. 13, 173–177.

Kuang, Z., Cai, L., Zhang, X., Ji, H., Tu, B.P., and Boeke, J.D. (2014). High-temporal-resolution view of transcription and chromatin states across distinct metabolic states in budding yeast. Nat Struct Mol Biol 21, 854–863.

Laxman, S., Sutter, B.M., and Tu, B.P. (2010). Behavior of a metabolic cycling population at the single cell level as visualized by fluorescent gene expression reporters. PLoS One 5, e12595.

Lee, I.H., and Finkel, T. (2013). Metabolic regulation of the cell cycle. Curr. Opin. Cell Biol. 25, 724–729.

Lee, P., Kim, M.S., Paik, S.-M., Choi, S.-H., Cho, B.-R., and Hahn, J.-S. (2013). Rim15-dependent activation of Hsf1 and Msn2/4 transcription factors by direct phosphorylation in *Saccharomyces cerevisiae*. FEBS Lett. 587, 3648–3655.

Li, C.M., and Klevecz, R.R. (2006). A rapid genome-scale response of the transcriptional oscillator to perturbation reveals a period-doubling path to phenotypic change. Proc. Natl. Acad. Sci. U. S. A. 103, 16254–16259.

Linke, C., Klipp, E., Lehrach, H., Barberis, M., and Krobitsch, S. (2013). Fkh1 and Fkh2 associate with Sir2 to control CLB2 transcription under normal and oxidative stress conditions. Front. Physiol. 4, 173.

Liu, X., Wang, X., Yang, X., Liu, S., Jiang, L., Qu, Y., Hu, L., Ouyang, Q., and Tang, C. (2015). Reliable cell cycle commitment in budding yeast is ensured by signal integration. Elife 4.

Lloyd, D., and Murray, D.B. (2005). Ultradian metronome: timekeeper for orchestration of cellular coherence. Trends Biochem. Sci. 30, 373–377.

Lloyd, D., Edwards, S.W., and Fry, J.C. (1982). Temperature-compensated oscillations in respiration and cellular protein content in synchronous cultures of Acanthamoeba castellanii. Proc. Natl. Acad. Sci. U. S. A. 79, 3785–3788.

Lloyd, D., Salgado, L.E.J., Turner, M.P., Suller, M.T.E., and Murray, D. (2002). Cycles of mitochondrial energization driven by the ultradian clock in a continuous culture of *Saccharomyces cerevisiae*. Microbiology 148, 3715–3724.

Lo, W.-S., Duggan, L., Tolga, N.C., Emre, Belotserkovskya, R., Lane, W.S., Shiekhattar, R., and Berger, S.L. (2001). Snf1--a Histone Kinase That Works in Concert with the Histone Acetyltransferase Gcn5 to Regulate Transcription. Science (80-.). 293, 1142 LP-1146.

Lu, Y., and Cross, F.R. (2010). Periodic cyclin-Cdk activity entrains an autonomous Cdc14 release oscillator. Cell 141, 268–279.

Machné, R., and Murray, D.B. (2012). The yin and yang of yeast transcription: elements of a global feedback system between metabolism and chromatin. PLoS One 7, e37906.

Manchado, E., Eguren, M., and Malumbres, M. (2010). The anaphase-promoting complex/cyclosome (APC/C): cell-cycle-dependent and -independent functions. Biochem. Soc. Trans. 38, 65 LP-71.

Mandal, S., Guptan, P., Owusu-Ansah, E., and Banerjee, U. (2005). Mitochondrial Regulation of Cell Cycle Progression during Development as Revealed by the tenured Mutation in Drosophila. Dev. Cell 9, 843–854.

Mitra, K., Wunder, C., Roysam, B., Lin, G., and Lippincott-Schwartz, J. (2009). A hyperfused mitochondrial state achieved at G(1)–S regulates cyclin E buildup and entry into S phase. Proc. Natl. Acad. Sci. U. S. A. 106, 11960–11965.

Mizunuma, M., Tsubakiyama, R., Ogawa, T., Shitamukai, A., Kobayashi, Y., Inai, T., Kume, K., and Hirata, D. (2013). Ras/cAMP-dependent Protein Kinase (PKA) Regulates Multiple Aspects of Cellular Events by Phosphorylating the Whi3 Cell Cycle Regulator in Budding Yeast. J. Biol. Chem. 288, 10558–10566.

Müller, D., Exler, S., Aguilera-Vázquez, L., Guerrero-Martín, E., and Reuss, M. (2003). Cyclic AMP mediates the cell cycle dynamics of energy metabolism in *Saccharomyces cerevisiae*. Yeast 20, 351–367.

Murray, A.W. (2004). Recycling the Cell Cycle: Cyclins Revisited. Cell 116, 221–234.

Murray, D.B., Beckmann, M., and Kitano, H. (2007). Regulation of yeast oscillatory dynamics. Proc. Natl. Acad. Sci. U. S. A. 104, 2241–2246.

North, B.J., and Verdin, E. (2004). Sirtuins: Sir2-related NAD-dependent protein deacetylases. Genome Biol. 5, 224.

Novak, B., and Mitchison, J.M. (1987). Periodic cell cycle changes in the rate of CO_2 production in the fission yeast Schizosaccharomyces pombe persist after a block to protein synthesis. J. Cell Sci. 87, 323–325.

Novak, B., Halbauer, J., and Laszlo, E. (1988). The effect of CO_2 on the timing of cell cycle events in fission yeast Schizosaccharomyces pombe. J. Cell Sci. 89, 433–439.

Orlando, D.A., Lin, C.Y., Bernard, A., Wang, J.Y., Socolar, J.E.S., Iversen, E.S., Hartemink, A.J., and Haase, S.B. (2008). Global control of cell-cycle transcription by coupled CDK and network oscillators. Nature 453, 944–947.

Owusu-Ansah, E., Yavari, A., Mandal, S., and Banerjee, U. (2008). Distinct mitochondrial retrograde signals control the G1-S cell cycle checkpoint. Nat Genet 40, 356–361.

Pan, D.A., and Hardie, D.G. (2002). A homologue of AMP-activated protein kinase in Drosophila melanogaster is sensitive to AMP and is activated by ATP depletion. Biochem. J. 367, 179–186.

Pandey, R., Müller, A., Napoli, C.A., Selinger, D.A., Pikaard, C.S., Richards, E.J., Bender, J., Mount, D.W., and Jorgensen, R.A. (2002). Analysis of histone acetyltransferase and histone deacetylase families of Arabidopsis thaliana suggests functional diversification of chromatin modification among multicellular eukaryotes. Nucleic Acids Res. 30, 5036–5055.

Park, Y.J., Claus, R., Weichenhan, D., and Plass, C. (2011). Genome-wide epigenetic modifications in cancer. Prog. Drug Res. 67, 25–49.

Pedruzzi, I., Bürckert, N., Egger, P., and De Virgilio, C. (2000). *Saccharomyces cerevisiae* Ras/cAMP pathway controls post-diauxic shift element-dependent transcription through the zinc finger protein Gis1. EMBO J. 19, 2569–2579.

Peregrín-Alvarez, J.M., Sanford, C., and Parkinson, J. (2009). The conservation and evolutionary modularity of metabolism. Genome Biol. 10, R63–R63.

Pessina, S., Tsiarentsyeva, V., Busnelli, S., Vanoni, M., Alberghina, L., and Coccetti, P. (2010). Snf1/AMPK promotes S-phase entrance by controlling CLB5 transcription in budding yeast. Cell Cycle 9, 2189–2200.

Peters, J.-M. (2006). The anaphase promoting complex/cyclosome: a machine designed to destroy. Nat Rev Mol Cell Biol 7, 644–656.

Peters, K. (2013). Molecular mechanisms involved in activation of the Ras proteins by glycolytic flux. Katholieke Universiteit Leuven.

Pines, J. (2011). Cubism and the cell cycle: the many faces of the APC/C. Nat. Rev. Mol. Cell Biol. 12, 427–438.

Polymenis, M., and Schmidt, E. V (1997). Coupling of cell division to cell growth by translational control of the G(1) cyclin CLN3 in yeast. Genes Dev. 11, 2522–2531.

Rahi, S.J., Pecani, K., Ondracka, A., Oikonomou, C., and Cross, F.R. (2016). The CDK-APC/C Oscillator Predominantly Entrains Periodic Cell-Cycle Transcription. Cell 165, 475–487.

Reinders, A., Bürckert, N., Boller, T., Wiemken, A., and De Virgilio, C. (1998). *Saccharomyces cerevisiae* cAMP-dependent protein kinase controls entry into stationary phase through the Rim15p protein kinase. Genes Dev. 12, 2943–2955.

Saha, A., Wittmeyer, J., and Cairns, B.R. (2002). Chromatin remodeling by RSC involves ATP-dependent DNA translocation. Genes Dev. 16, 2120–2134.

Sasidharan, K., Soga, T., Tomita, M., and Murray, D.B. (2012). A yeast metabolite extraction protocol optimised for time-series analyses. PLoS One 7, e44283.

Schmoller, K.M., Turner, J.J., Koivomagi, M., and Skotheim, J.M. (2015). Dilution of the cell cycle inhibitor Whi5 controls budding-yeast cell size. Nature 526, 268–272.

Schneider, B.L., Yang, Q.-H., and Futcher, A.B. (1996). Linkage of Replication to Start by the Cdk Inhibitor Sic1. Science (80-.). 272, 560–562.

Shahriyari, L., and Komarova, N.L. (2013). Symmetric vs. Asymmetric Stem Cell Divisions: An Adaptation against Cancer? PLoS One 8, e76195.

Sheppard, J.D., and Dawson, P.S.S. (1999). Cell synchrony and periodic behaviour in yeast populations. Can. J. Chem. Eng. 77, 893–902.

Sherr, C.J., and Roberts, J.M. (2004). Living with or without cyclins and cyclin-dependent kinases. Genes Dev. 18, 2699–2711.

Shi, L., and Tu, B.P. (2013). Acetyl-CoA induces transcription of the key G1 cyclin CLN3 to promote entry into the cell division cycle in *Saccharomyces cerevisiae*. Proc. Natl. Acad. Sci. 110, 7318–7323.

Slavov, N., and Botstein, D. (2011). Coupling among growth rate response, metabolic cycle, and cell division cycle in yeast. Mol. Biol. Cell 22, 1997–2009.

Slavov, N., Macinskas, J., Caudy, A., and Botstein, D. (2011). Metabolic cycling without cell division cycling in respiring yeast. Proc. Natl. Acad. Sci. 108, 19090–19095.

Smith, A., Ward, M.P., and Garrett, S. (1998). Yeast PKA represses Msn2p/Msn4p-dependent gene expression to regulate growth, stress response and glycogen accumulation. EMBO J. 17, 3556–3564.

Sohn, H.Y., Murray, D.B., and Kuriyama, H. (2000). Ultradian oscillation of Saccharomyces cerevisiae during aerobic continuous culture: hydrogen sulphide mediates population synchrony. Yeast 16, 1185–1190.

Soifer, I., and Barkai, N. (2014). Systematic identification of cell size regulators in budding yeast. Mol. Syst. Biol. 10, 761.

Talia, S. Di, Skotheim, J.M., Bean, J.M., Siggia, E.D., and Cross, F.R. (2007). The effects of molecular noise and size control on variability in the budding yeast cell cycle. Nature 448, 947–951.

Thevelein, J.M. (1991). Fermentable sugars and intracellular acidification as specific activators of the RAS-adenylate cyclase signalling pathway in yeast: the relationship to nutrient-induced cell cycle control. Mol. Microbiol. 5, 1301–1307.

Thevelein, J.M., and de Winde, J.H. (1999). Novel sensing mechanisms and targets for the cAMP-protein kinase A pathway in the yeast *Saccharomyces cerevisiae*. Mol. Microbiol. 33, 904–918.

Tu, B.P., Kudlicki, A., Rowicka, M., and McKnight, S.L. (2005). Logic of the yeast metabolic cycle: temporal compartmentalization of cellular processes. Science 310, 1152–1158.

Tu, B.P., Mohler, R.E., Liu, J.C., Dombek, K.M., Young, E.T., Synovec, R.E., and Mcknight, S.L. (2007). Cyclic changes in metabolic state during the life of a yeast cell. Proc. Natl. Acad. Sci. 104, 16886–16891.

Tudzarova, S., Colombo, S.L., Stoeber, K., Carcamo, S., Williams, G.H., and Moncada, S. (2011). Two ubiquitin ligases, APC/C-Cdh1 and SKP1-CUL1-F (SCF)-β-TrCP, sequentially regulate glycolysis during the cell cycle. Proc. Natl. Acad. Sci. 108, 5278–5283.

Tyers, M. (1996). The cyclin-dependent kinase inhibitor p40SIC1 imposes the requirement for Cln G1 cyclin function at Start. Proc. Natl. Acad. Sci. U. S. A. 93, 7772–7776.

Tyson, J.J., and Novak, B. (2008). Temporal organization of the cell cycle. Curr. Biol. 18, R759–R768.

Verzijlbergen, K.F., Nerusheva, O.O., Kelly, D., Kerr, A., Clift, D., de Lima Alves, F., Rappsilber, J., and Marston, A.L. (2014). Shugoshin biases chromosomes for biorientation through condensin recruitment to the pericentromere. Elife 3, e01374.

Wang, Y., Pierce, M., Schneper, L., Güldal, C.G., Zhang, X., Tavazoie, S., and Broach, J.R. (2004). Ras and Gpa2 Mediate One Branch of a Redundant Glucose Signaling Pathway in Yeast. PLoS Biol. 2, e128.

Wang, Z., Fan, M., Candas, D., Zhang, T.-Q., Eldridge, A., Wachsmann-Hogiu, S., Ahmed, K.M., Chromy, B.A., Nantajit, D., Duru, N., et al. (2014). CyclinB1/Cdk1 Coordinates Mitochondrial Respiration for Cell Cycle G2/M Progression. Dev. Cell 29, 217–232.

Wasch, R., and Cross, F.R. (2002). APC-dependent proteolysis of the mitotic cyclin Clb2 is essential for mitotic exit. Nature 418, 556–562.

Watts, G. (2001). Three cell cycle scientists win Nobel prize. BMJ Br. Med. J. 323, 823.

Wijker, J.E., Jensen, P.R., Snoep, J.L., Vaz Gomes, A., Guiral, M., Jongsma, A.P.M., de Waal, A., Hoving, S., van Dooren, S., van der Weijden, C.C., et al. (1995). Energy, control and DNA structure in the living cell. Biophys. Chem. 55, 153–165.

Xiao, B., Heath, R., Saiu, P., Leiper, F.C., Leone, P., Jing, C., Walker, P.A., Haire, L., Eccleston, J.F., Davis, C.T., et al. (2007). Structural basis for AMP binding to mammalian AMP-activated protein kinase. Nature 449, 496–500.

Xu, Z., and Tsurugi, K. (2006). A potential mechanism of energy-metabolism oscillation in an aerobic chemostat culture of the yeast *Saccharomyces cerevisiae*. FEBS J. 273, 1696–1709.

Yalcin, A., Clem, B.F., Simmons, A., Lane, A., Nelson, K., Clem, A.L., Brock, E., Siow, D., Wattenberg, B., Telang, S., et al. (2009). Nuclear targeting of 6-phosphofructo-2-kinase (PFKFB3) increases proliferation via cyclin-dependent kinases. J. Biol. Chem. 284, 24223–24232.

Yalcin, A., Clem, B.F., Imbert-Fernandez, Y., Ozcan, S.C., Peker, S., O'Neal, J., Klarer, A.C., Clem, A.L., Telang, S., and Chesney, J. (2014). 6-Phosphofructo-2-kinase (PFKFB3) promotes cell cycle progression and suppresses apoptosis via Cdk1-mediated phosphorylation of p27. Cell Death Dis 5, e1337.

Yamada, T., Fischle, W., Sugiyama, T., Allis, C.D., and Grewal, S.I.S. (2005). The Nucleation and Maintenance of Heterochromatin by a Histone Deacetylase in Fission Yeast. Mol. Cell 20, 173–185.

Yang, J., McCormick, M.A., Zheng, J., Xie, Z., Tsuchiya, M., Tsuchiyama, S., El-Samad, H., Ouyang, Q., Kaeberlein, M., Kennedy, B.K., et al. (2015). Systematic analysis of asymmetric partitioning of yeast proteome between mother and daughter cells reveals "aging factors" and mechanism of lifespan asymmetry. Proc. Natl. Acad. Sci. U. S. A. 112, 11977–11982.

Zhao, G., Chen, Y., Carey, L., and Futcher, B. (2016). Cyclin-Dependent Kinase Co-Ordinates Carbohydrate Metabolism and Cell Cycle in S. cerevisiae. Mol. Cell 62, 546–557.

Chapter 2

Published in Molecular Cell, Volume 65, January 2017
DOI http://dx.doi.org/10.1016/j.molcel.2016.11.018

Autonomous metabolic oscillations robustly gate the early and the late cell cycle

Alexandros Papagiannakis[1], Bastian Niebel[1], Ernst Wit[2], Matthias Heinemann[1]

[1] Molecular Systems Biology, Groningen Biomolecular Sciences and Biotechnology Institute, University of Groningen, Nijenborgh 4, 9747 AG Groningen, The Netherlands;
[2] Probability and Statistics, Johann Bernoulli Institute of Mathematics and Computer Science, University of Groningen, Nijenborgh 9, 9747 AG Groningen, The Netherlands

Summary

Eukaryotic cell division is known to be controlled by the cyclin/CDK machinery. However, eukaryotes have evolved prior to CDKs, and cells can divide in the absence of major cyclin/CDK components. We hypothesized that an autonomous metabolic oscillator provides dynamic triggers for cell cycle initiation and progression. Using microfluidics, cell cycle reporters, and single-cell metabolite measurements, we found that metabolism of budding yeast is a CDK-independent oscillator that oscillates across different growth conditions, both in synchrony with and also in the absence of the cell cycle. Using environmental perturbations and dynamic single-protein depletion experiments, we found that the metabolic oscillator and the cell cycle form a system of coupled oscillators, with the metabolic oscillator separately gating and maintaining synchrony with the early and late cell cycle. Establishing metabolism as a dynamic component within the cell cycle network opens new avenues for cell cycle research and therapeutic interventions for proliferative disorders.

Highlights

- Metabolic cycles are an intrinsic, growth-condition independent behavior of single cells.
- The metabolic oscillations are not the result of the cell cycle, and thus are autonomous.
- The metabolic oscillator and the cyclin/CDK machinery form a system of coupled oscillators.
- Both the early and late cell cycle operate in coordination with the metabolic oscillator.

Introduction

Initiation and progression of the cell cycle are considered to occur in response to the timely ordered transcriptional, post-transcriptional, and post-translational regulation of the cell cycle (cyclin/CDK) machinery components (Barik et al., 2010; Coudreuse and Nurse, 2010; Tyson and Novak, 2008). However, there is evidence that a cell cycle regulator external to the cyclin/CDK machinery provides triggers for cell cycle initiation or progression. First, cell cycle entry can occur even in the absence of major cell cycle machinery components (e.g., the early cyclins) (Sherr and Roberts, 2004). Second, late cell cycle proteins (e.g. cdc14 and sic1) (Lu and Cross, 2010; Rahi et al., 2016), and possibly also global transcription (Haase and Reed, 1999; Orlando et al., 2008), continue to oscillate in cell cycle–arrested cells. Third, the eukaryotic cell cycle evolved before CDKs and thus the early eukaryotes must have employed non-CDK cell cycle regulators (Krylov et al., 2003).

Because metabolism oscillates in synchrony with (Futcher, 2006; Klevecz et al., 2004; Müller et al., 2003; Silverman et al., 2010; Tu et al., 2005, 2007; Xu and Tsurugi, 2006) and – as suggested – also without the cell cycle (Novak et al., 1988; Slavov et al., 2011), and because metabolic checkpoints exist in the cell cycle program (Jones et al., 2005; Saqcena et al., 2013; Takubo et al., 2013), we conjectured that metabolism operates as an autonomous, cell cycle–independent oscillator, which together with the cell cycle might form a system of coupled oscillators. In response to nutrients, the metabolic oscillator could orbit with different frequencies and provide periodic triggers for cell cycle initiation and

progression. Interactions between metabolites and cell cycle proteins (Buchakjian and Kornbluth, 2010; Lee and Finkel, 2013; Shi and Tu, 2013; Yalcin et al., 2014) could convey those triggers, and in reverse, the cell cycle could entrain metabolism via the regulation of enzyme activity (Ewald et al., 2016; Lee et al., 2014; Tudzarova et al., 2011; Wang et al., 2014; Zhao et al., 2016).

Here, using novel methods for the dynamic quantification of metabolites in single cells, in combination with microfluidics and time-lapse microscopy, we demonstrate that the metabolism of budding yeast is an oscillator, which orbits autonomously of the cell cycle. Perturbation experiments, including dynamic nutrient shifts as well as conditional and targeted depletion of cell cycle proteins, revealed that the metabolic oscillator together with the cell cycle forms a system of coupled oscillators. The metabolic and the cell cycle oscillators accomplish frequency synchrony - required for the activation and progression of the cell division program - only within a certain window of metabolic frequencies - whereas the robust gating of the cell cycle phases by the metabolic dynamics ensures the temporal separation of biomass production (early cell cycle) and segregation (late cell cycle). Our findings demonstrate that the metabolic oscillator is an indispensable component of cell cycle regulation, open new research avenues into cell cycle control, and suggest the metabolic oscillator as a novel and global therapeutic target against proliferative disorders.

Results

Metabolic cycles are an intrinsic, growth-condition independent behavior of single cells

To test our hypothesis, after which metabolism is an oscillator that is coupled to the cell cycle, we used *Saccharomyces cerevisiae* as a model. First, we asked whether a metabolic oscillator exists. Because it has been conjectured that population-level cell-cycle synchronization and cell-to-cell communication artificially induce metabolic oscillations (Aon et al., 2007; Laxman et al., 2010; Sohn et al., 2000), we investigated metabolic and cell cycle dynamics on the single cell level. We used a microfluidic device for the long-term microscopic observation of single budding yeast cells (Huberts et al., 2013), the auto-

fluorescence of the reduced nicotinamide nucleotide NAD(P)H to assess its intracellular levels (Gustavsson et al., 2012; Lloyd et al., 2002), and a protein-based Förster resonance energy transfer (FRET) sensor to measure ATP (Imamura et al., 2009). Optimization of the sensor expression and imaging settings led to adequate signal intensities with marginal cellular photo-damage and -toxicity during the long-term (>12 hours) imaging (Figure S1A-B).

Using these tools, we first investigated whether periodic NAD(P)H and ATP fluctuations occur in single cells, grown on high (10 gL^{-1}) glucose without cell-to-cell communication or cell-cycle synchronization (Figure S1C). These fluctuations, subsequently identified (Figure 1A-B, Movie S1) and confirmed by autocorrelation analysis (Figure S2A-B), occurred with an average period of approximately 2 hours, which corresponds to the average doubling time under this condition. Through comparative analyses, we validated that the measured single-cell FRET signals reflect intracellular ATP concentrations (Text S1, Figure S1D-H), and that the measured metabolite dynamics are not due to a correlated variability (such as periodic volume chances) (Text S2). Given the absence of cell cycle synchronization (Figure S1C), our findings demonstrate that, contrary to previous reports (Aon et al., 2007; Laxman et al., 2010; Sohn et al., 2000), metabolic cycles with periods in the hour range are an intrinsic behavior of single cells.

To test whether metabolic cycles also occur at other growth conditions, we subjected yeast to different nutrients and metabolic operations (aerobic fermentation, respiration, gluconeogenesis), which varied the doubling time in single cells from 1.4 to 11 h. Despite these different metabolic operations, we consistently identified oscillations in the NAD(P)H and ATP levels (Figure S3A–F), demonstrating that the metabolic cycles occur regardless of growth conditions.

To investigate whether the metabolic cycles occur in synchrony with the cell cycle, we correlated the frequencies of budding with the frequencies of the NAD(P)H or ATP oscillations. Despite the wide range of doubling times across nutrient conditions, the budding frequencies always matched the frequencies of the corresponding NAD(P)H or ATP oscillations (Figure 1C). Thus, the metabolic oscillations and the cell cycle operate in frequency synchrony over the range of growth conditions tested, which suggests a coupling between the two periodic processes.

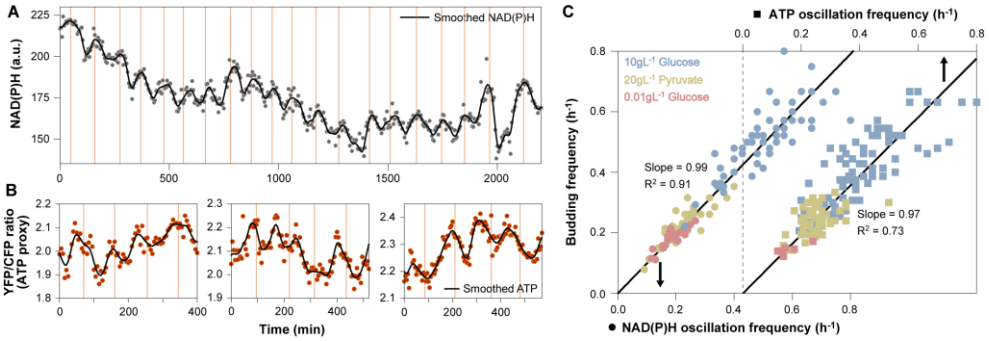

Figure 1. Metabolism oscillates in single cells, across nutrients and in frequency synchrony with the cell cycle. (A) Oscillating NAD(P)H levels in a single cell. **(B)** Oscillating ATP levels (three single cells), dynamically measured using the ATeam 1.03 FRET sensor (Imamura et al., 2009). Cells were grown on high glucose (10 gL^{-1}), in the absence of synchronization (Figure S1C). Black lines indicate smoothing splines used for visualization. Vertical orange lines indicate budding. **(C)** Budding and the frequency of NAD(P)H and ATP oscillations correlate across growth conditions; n = 38 cells with 137 NAD(P)H oscillations (solid circles) and 38 cells with 136 ATP oscillations (solid squares). Time periods between consecutive buddings, or consecutive peaks of NAD(P)H and ATP oscillations, were used to determine budding and oscillation frequency data, respectively. Linear regressions (black diagonals) illustrate the correlations. The greater noise in the ATP oscillation frequency estimation (Figure S2A-B) is reflected in the different R2 values for NAD(P)H and ATP.

The metabolic oscillations are not the result of the cell cycle, and thus are autonomous

To determine if the metabolic oscillations are a mere consequence of the cell cycle operation or if they occur in a cell cycle-independent manner and thus are autonomous, we searched in our single cell data for metabolic oscillations that were unaccompanied by cell cycle progression. Such events occurred for all growth conditions (Figure 2A, Figures S4A-B), with an approximate incidence of 1/50 metabolic oscillations on 10 gL^{-1} glucose. On 0.01 gL^{-1} glucose, we also found many cells with consecutive metabolic oscillations without cell cycle progression (Figure 2A, Figure S4C-D, Movie S2).

To determine the cell cycle status of the non-dividing cells, we used a strain with fluorescently tagged Whi5, a transcriptional repressor of early cyclins and target of CDK phosphorylation. Whi5 sequesters into the nucleus at late mitosis (hereafter denoted as ‘M

exit'), and exits upon phosphorylation at late G1 (denoted as 'START'), reporting an active CDK (Bloom and Cross, 2007; Costanzo et al., 2004; Ferrezuelo et al., 2012) (Figure S5A–C). Using this reporter, we found that cells with metabolic oscillations but without an accompanying cell cycle were either arrested at G1 (i.e. Whi5 in the nucleus, Figure 2B, Movie S3) or occasionally after budding in a non-G1 phase (i.e. Whi5 in the cytoplasm, Movie S4).

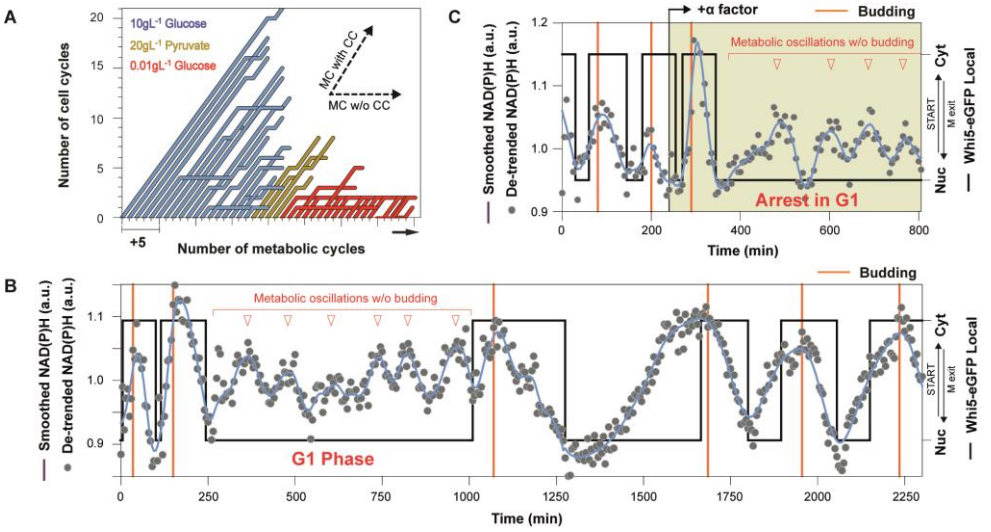

Figure 2. Metabolic oscillations are independent of the cell cycle. (A) Metabolic oscillations without cell cycle initiation occur spontaneously under all growth conditions. Each line corresponds to a single cell. Diagonal trajectories indicate metabolic cycles (MC) in synchrony with budding and the cell cycle (CC); horizontal trajectories show "uncoupled" MCs without budding. **(B)** After two coupled MC/CC event, spontaneous G1 arrest occurred at 245 minutes in a single cell (grown on 10 gL^{-1} glucose), and the metabolic oscillations continued (also see Movie S3). Arrest persisted for 765 minutes, before resumption of MC/CC synchrony. NAD(P)H oscillations are indicated by grey lines, Whi5-eGFP localization by black lines, and the budding events by orange lines. Red triangles indicate peaks of metabolic oscillations without budding. **(C)** Mating pheromone alpha factor (added at 240 min) caused cell cycle arrest in G1 and the metabolic oscillations continued (data for a single cell grown on 10 gL^{-1} glucose).

To substantiate the finding that metabolic oscillations are not the consequence of the cell cycle operation, we added the mating pheromone (alpha factor), which induces G1 arrest

(Bardwell, 2004), to cells growing in the microfluidic device. Also after the pheromone-induced cell cycle arrest, the NAD(P)H levels continued to oscillate (Figure 2C, Figure S6). Together, these findings demonstrate that the metabolic oscillations are not the result of the cell cycle operation and CDK activity, but constitute an autonomous behavior of metabolism, occurring across growth conditions. The autonomy of the metabolic oscillator, and its frequency synchrony with the cell cycle (Figure 1C) in normally dividing cells, suggest metabolism as a separate component in the cell cycle control engine.

The metabolic oscillator and the cell cycle form a system of coupled oscillators

We conjectured that the metabolic and the cell cycle oscillator form a system of coupled oscillators, similar to other instances of synchrony in biology, including the rhythmic flashes of fireflies, or the synchronized discharge of the cardiac pacemaker cells (Strogatz, 2001). Analogously to the fact that an effective contraction of the heart muscle requires a strict synchrony between the cells in the sinoatrial node, also here, cell cycle control could emerge from the coupling and mutual entrainment between the metabolic and the cell cycle oscillator.

To investigate whether the metabolic oscillator and the cell cycle indeed form a coupled oscillator system, we searched for signature features of such systems, by means of steady-state and dynamic perturbations. A common characteristic of coupled oscillators is that their natural frequencies (i.e. the frequency of each individual oscillator when uncoupled) converge to a common compromise frequency (i.e. the common frequency of the oscillators when they are coupled) proportional to the strength of their coupling (Strogatz, 2014). We determined the frequency of the metabolic oscillator in the presence of cell cycle (compromise frequency) in normally dividing cells and in the absence of cell cycle progression (natural frequency of the metabolic oscillator), the latter in cells where the cell cycle was arrested with the alpha factor (Figures S6). In line with the theory of coupled oscillators (Strogatz, 2014), we found a linear correlation between the natural metabolic and compromise frequencies under different conditions (Figure 3A). The compromise frequency was routinely 16% lower than its corresponding natural metabolic frequency

(Figure 3A) - a reduction that could be interpreted as a load imposed on the metabolic oscillator by the cell cycle upon coupling.

Another distinctive feature of coupled oscillator systems is that coupling and synchrony are only accomplished when the natural frequencies of the individual oscillators are proximal (Nolte, 2015; Strogatz, 2014). With different nutrient conditions resulting in different natural frequencies for the metabolic oscillator (Figure 3A), we investigated at which natural metabolic frequencies coupling with the cell cycle occurs. Here, we found that at very low metabolic frequencies and at very high ones no coupling occurred. Given the standardized reduction of the compromise frequency (16%) (Figure 3A), we identified the range of natural metabolic frequencies from 0.15 h^{-1} to 0.96 h^{-1} to enable coupling (Figure 3B). On 0.01 gL^{-1} glucose, 75% of the metabolic oscillations without cell cycle (Figure S4C-D) had a natural metabolic frequency below the estimated threshold for coupling and thus cell cycle initiation (Figure 3B), resulting in a substantial fraction of non-dividing cells. A statistical analysis (hazard function analysis – Supplemental Experimental Procedures) of the dynamic NAD(P)H signals and START occurrence further demonstrates the importance of the metabolic frequency for coupling and cell cycle initiation (Figure 3C). These findings reveal a second characteristic of coupled oscillators: coupling between the metabolic oscillator and the cell cycle is only achieved within a window of natural metabolic frequencies; lower or higher metabolic frequencies are not sufficient for coupling and thus for cell cycle initiation.

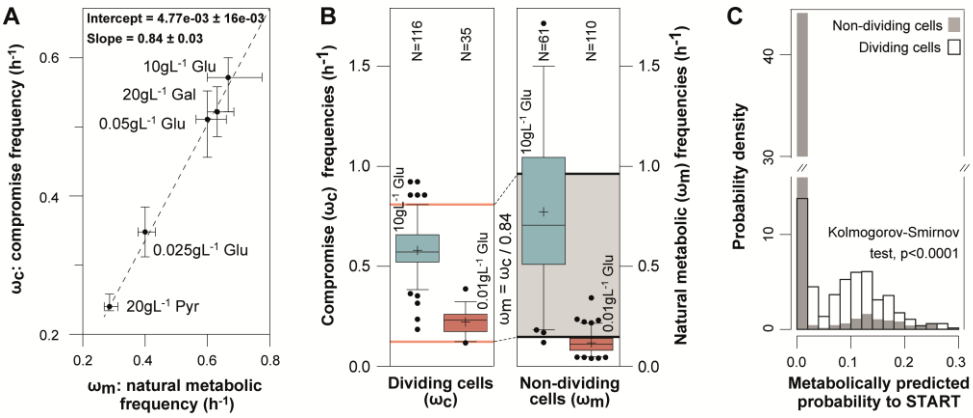

Figure 3 Coupling slows down the metabolic oscillator, and occurs only within a window of natural metabolic frequencies. (A) Median compromise frequencies measured in dividing cells versus median natural metabolic frequencies measured in alpha factor–arrested cells, under different growth conditions. Both frequencies were estimated from consecutive trough intervals in single cell NAD(P)H oscillations. Median frequencies and their 95% confidence intervals (error bars) were estimated using non-parametric bootstrapping. The slope and intercept of the fitted line with standard errors are indicated. **(B)** The frequencies of metabolic oscillations with or without cell cycle, measured during growth on high (10 gL^{-1}) and low (0.01 gL^{-1}) glucose. Natural metabolic frequencies were measured in cells spontaneously skipping ≥1 cell cycles (e.g. Figure 2B, Figures S4A&C). Crosses indicate distribution means. Natural metabolic frequencies necessary for cell cycle initiation (grey shaded area) were estimated by dividing the fastest (95th percentile – 10gL^{-1} glucose) and slowest compromise frequencies (5th percentile – 0.01gL^{-1} glucose) by 0.84 (estimated slope in Figure 3A). **(C)** The probabilities for cell cycle START based on the dynamics of the NAD(P)H signal are significantly different for dividing (white bars) versus non-dividing cells (grey bars) on low glucose. Probabilities were computed using predictive densities based on a Cox proportional hazards analysis (Cox, 1972) and reflect the hazard of a START event with NAD(P)H dynamics as a time-dependent covariate (hazard function analysis – Supplementary Experimental Procedures). The accuracy of prediction is approximately 70% (Receiver Operating Characteristic - ROC analysis).

Another characteristic of coupled oscillators is phase gating, i.e. the maintenance of a relative phase between oscillators in synchrony (Feillet et al., 2014; Mori et al., 1996). Initially focusing on cells grown on high (10 gL^{-1}) glucose, we found strict phase gating of the cell cycle events at specific metabolic phases: START and budding (i.e. early S phase; Figure S5D-F) consistently occurred at the ascending part of the oscillating NAD(P)H signal. Mitotic exit always occurred at the signal trough (Figure 4A, Figure S7A–F). ATP oscillations were shifted by approximately 180°, with budding occurring at the descending part of the ATP signals (Figure S8A-B).

Next, we examined whether this pattern of phase gating is maintained under other nutrient conditions. We found that at decreased compromise frequencies START and the early S phase shifted to later NAD(P)H phases (Figure 4B-C). In contrast, M exit always occurred at the troughs of the NAD(P)H oscillations, thus exhibiting a strict, condition-independent phase synchrony with metabolism (Figure 4B-C). The condition-independent gating of the late cell cycle (M exit) indicates its strong coupling to the metabolic oscillator. Adversely, the frequency-dependent phase gating of the early cell cycle elements (START/early S) indicates a weaker coupling.

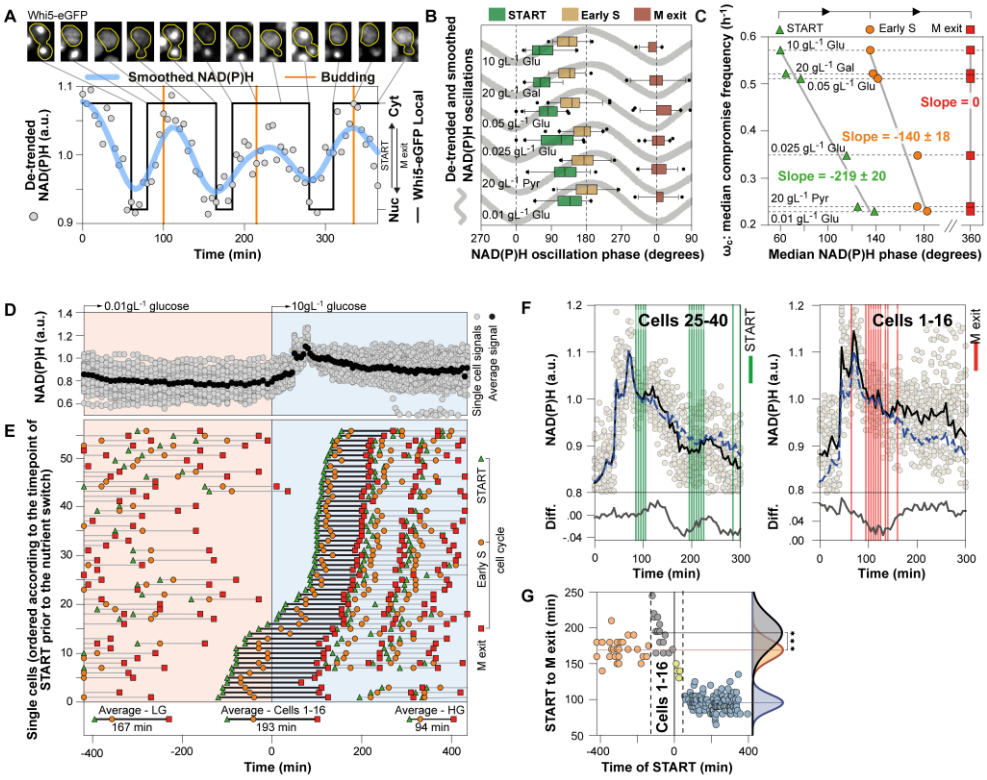

Figure 4: Cell cycle events are robustly gated to distinct metabolic phases. (A) Whi5-eGFP translocations (cytosolic (cyt) and nuclear (nuc); black lines), together with the NAD(P)H signals in a single cell growing on high glucose. Orange lines denote budding. **(B)** The distributions of START, budding and M exit on the NAD(P)H oscillations at different growth conditions; error bars 5-95 percentiles. The same data as in Figure S7A–F were used. **(C)** Median NAD(P)H phase at START, budding, and M exit with median compromise frequencies under different nutrient conditions. **(D)** Metabolic response to glucose upshift (from 0.01 gL^{-1} to 10 gL^{-1}) at 0 min. NAD(P)H signals from 56 cells normalized to the 100 min signal. **(E)** Timing of START (triangle), budding (circle), and M exit (square), for 56 cells ordered by the START time closest to the nutrient switch. The average cell cycle durations according to glucose concentration (LG, 0.01 gL^{-1}; HG, 10 gL^{-1}) and when interrupted by the nutrient switch (Cells 1-16) are indicated. **(F)** START (green lines) is confined to the ascending part of the NAD(P)H oscillation following the metabolic response (cells 25–40); M exit (red lines) is restricted to the trough (cells 1–16). Single cell (grey symbols) and averaged (black line) NAD(P)H signals are shown. The average NAD(P)H signal of the whole population (blue dashed line) was subtracted from subgroup (cells 25–40 or cells 1–16) averages (black line) to reveal the subgroup-specific NAD(P)H dynamics (labeled as Diff.). **(G)** The single cell timing of START relative to its cell cycle length (START to M exit), demonstrating the significant prolongation (*** two-tailed t-test p-value < 0.001, Shapiro-Wilk normality test, Welch's correction for unequal variances) of the cell cycle as a result of the M exit confinement to the trough of the metabolic response. Normal distributions were fitted to data for low (red) and high (blue) glucose, and for cells that were interrupted by the nutrient switch (grey).

Next, to test the robustness of the phase gating, we dynamically perturbed metabolism by switching cells from low (0.01 gL^{-1}) to high (10 gL^{-1}) glucose and recorded their cell cycle events. Upon the nutrient upshift, all cells responded with a strong, synchronously occurring peak in the NAD(P)H levels (Figure 4D), independently of their stage in the cell cycle (Figure 4E). Thereafter, the NAD(P)H oscillations continued with periods (START to M exit) matching those on high glucose (Figure 4E). Remarkably, those cells that had completed M exit before the nutrient shift (Figure 4E, cells 25–40), consistent with the phase gating under steady-state conditions (Figure 4B), would START only at the ascending part of the NAD(P)H oscillation following the metabolic response (Figure 4F, left panel), regardless of the timing of their prior M exit (Figure 4E, cells 25–40). Cells interrupted by the nutrient switch after START (Figure 4E, cells 1–16) showed significantly longer (two-tailed t-test, p-value <0.001) cell cycle duration, even compared to those cultured on low glucose (Figure 4G, grey symbols). Consistent with the observed steady-state and frequency-independent phase gating of M exit (Figure 4C), cells would only exit mitosis at the trough of their NAD(P)H oscillation following the metabolic response (Figure 4F, right panel), which prolonged their cell cycle (Figure 4G). Our results show that the gating of the cell cycle phases by the metabolic oscillator is also maintained during dynamic metabolic perturbations and thus is robust. As a result, cell cycle events are delayed even during nutrient upshifts, waiting for the 'right' metabolic phase to occur after the metabolic perturbation, in order to maintain synchrony with the metabolic oscillator.

Together, the proportionality between the natural metabolic and compromise frequencies, the critical bandwidth of natural metabolic frequencies required for coupling and cell cycle initiation, and the phase gating of the cell cycle phases on the metabolic oscillator indicate that the metabolic and the cell cycle oscillator form a system of coupled oscillators. Further, the autonomous nature of the metabolic oscillator, the robust phase gating of the cell cycle events even during dynamic metabolic perturbations, and the dependency of cell cycle initiation on the metabolic frequency suggest that the oscillating metabolism is an indispensable component in the cell cycle regulation machinery, determining the timing of the cell cycle phases and setting the pace of cell division.

The early and the late cell cycle are separately coupled and in coordination with the metabolic oscillator

On the basis of our data, we derived an interaction topology for the system of coupled oscillators, where the metabolic oscillator is coupled to, and gates the phase the early cell cycle (biomass duplication) and the late cell cycle (biomass segregation) (Figure 5A), operating in addition to the classic CDK-centric connections (Figure 5B). Because we observed the phase gating of M exit to be condition-independent (Figure 4C) and to be maintained even during dynamic perturbations (Figure 4F – right panel), we postulate that a strong connection exists between the autonomous metabolic oscillator and the late cell cycle. Consequently, if indeed strongly connected to the metabolic oscillator, the late cell cycle should also oscillate when the early cell cycle is halted. This notion is supported by the observations of Lu and Cross, who found periodic nucleolar/cytoplasmic localization of the Cdc14 phosphatase (an essential activator of the Anaphase Promoting Complex and mitotic exit) in metaphase-arrested cells (i.e. in cells with fixed cyclin/CDK activity accomplished through stable non-degradable Clb2kd) (Lu and Cross, 2010). These findings demonstrate that the late cell cycle can oscillate even in the absence of the early cell cycle oscillations, supporting its strong coupling to the autonomous metabolic oscillator.

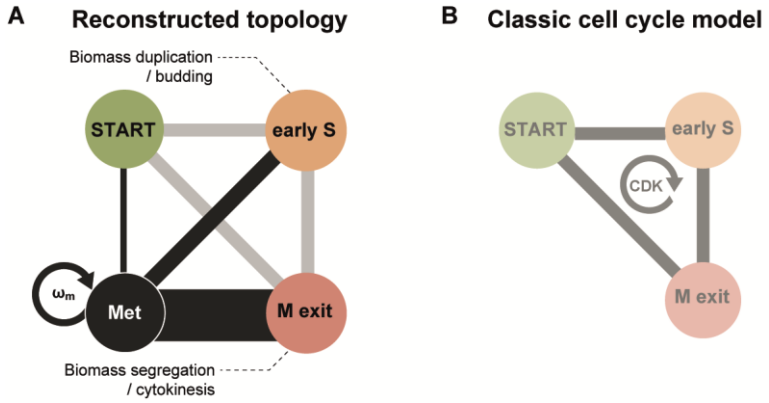

Figure 5 Interaction topology between the metabolic oscillator and the cell cycle elements. (A) The reconstructed topology of cell cycle regulation. The black lines indicate couplings between the metabolic oscillator ('MET') and the cell cycle elements (START, early S and M exit), scaled to their phase-difference (Figure 4C). The grey lines indicate the classical connections between the cell cycle

phases. ω_m denotes the frequency of the metabolic oscillator. This model extends the classic, CDK-centric view **(B)** of cell cycle regulation.

Further, according to the inferred interaction topology between the metabolic oscillator and the cell cycle elements (Figure 5A), the metabolic oscillator should also be connected to the early cell cycle. If this is indeed true, the early cell cycle should continue to oscillate when the late cell cycle is halted. To test this, we halted the late cell cycle by dynamic depletion of Cdc14 (Movie S5) using the yeast-adapted auxin-based degron system (Nishimura et al., 2009), an orthogonal system for the conditional and targeted protein degradation. First, following the dynamics of NAD(P)H, we found that the metabolic oscillations persisted after the arrest of the late cell cycle (Figures 6A-B, Movie S6, arrest of the late cell cycle confirmed by the absence of cytokinesis: cf. Figure 6C, Movie S5), also here witnessing the cell-cycle autonomous nature of the metabolic oscillator. Second, analyzing the dynamics of the cell size, we found that during the late cell cycle arrest biomass synthesis continued to occur in waves. Each wave was accompanied by one metabolic oscillation (cf. Figure 6B-C, Movie S6). The clockwise phase correlation between the oscillating NAD(P)H rates and the oscillating cell volume increase rates in Cdc14-depleted cells (Figures 6D & S9) similarly to dividing cells (Figure 6E & S9) confirm the coordination between the metabolic oscillator and early S also in the Cdc14-depleted cells. Remarkably, biomass synthesis waves ceased once the metabolic cycling stopped, or its amplitude was low (Figure 6B-C).

To substantiate the connection between the metabolic oscillator and the early cell cycle, we tested whether DNA replication, an S phase reporter, also persists in the Cdc14-depleted cells. As a dynamic single-cell measure of DNA replication we used the histone H2A, tagged with mRFP1, previously (Rattray and Müller, 2012) and here (Figure 6F-G) shown to correlate with the DNA content. After the auxin-induced Cdc14-depletion and late cell cycle arrest we found that the DNA amount continued to increase (Figure 6F-H). The identified chromosomal bridges (Figure 6I), indicating spindle defects, absence of chromosomal abscission and nuclear division (Amaral et al., 2016), additionally confirm late cell cycle arrest. Each metabolic oscillation, also during late cell cycle arrest, resulted in one additional genome (Figure 6G-H). Together, the sustained metabolic oscillations in

the absence of late cell cycle activity, and the maintenance of their synchrony with the cell size (biomass synthesis) and DNA content dynamics evidence the direct coupling of the metabolic oscillator to the early cell cycle.

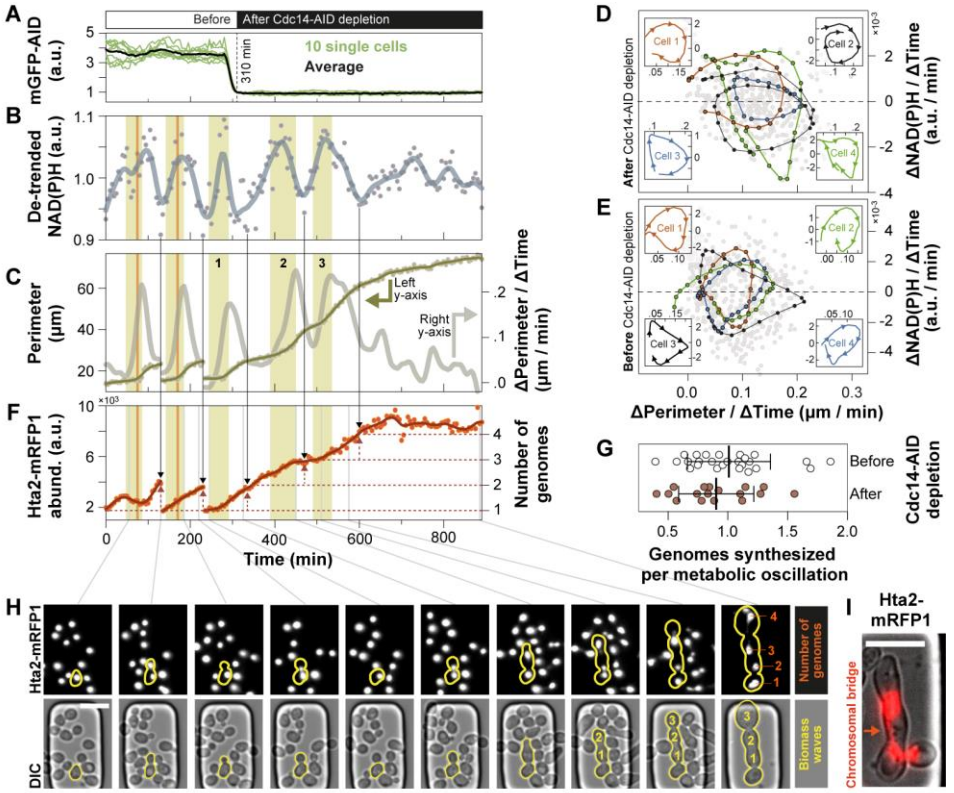

Figure 6. The metabolic oscillator is directly coupled to the early cell cycle. In this experiment, we arrested the late cell cycle (M exit) by dynamic depletion of Cdc14-AID at 310 min. **(A)** mGFP-AID expressing cells, present in the same microfluidic chip, were used to determine the timing of Cdc14-AID depletion upon the addition of auxin (as in Movie S5). **(B)** Single cell NAD(P)H levels continued to oscillate after the depletion of Cdc14 (grey line, smoothing spline for visualization). **(C)** The rate of perimeter increase (right y-axis), estimated from the smoothed cell perimeter (left y-axis), used as a proxy of the biomass synthesis rate. Yellow areas indicate periods with rapid biomass synthesis where budding (vertical orange lines for first two cycles) occurs or would occur (in the cycles after Cdc14 depletion) (see also Movie S6). Three consecutive biomass synthesis waves occur after the last cytokinesis (last bud release before Cdc14 depletion) at 235 min, each in synchrony with the oscillating metabolism (cf. Figure 6B). The oscillating NAD(P)H and perimeter increase rates are coordinated in **(D)** late cell cycle arrested cells similarly to **(E)** dividing cells (see also Figure S9). The respective single cell signals are plotted against each other for each time-point (grey markers). Exemplary trajectories from four single cells are presented for each condition (colored lines and markers). **(F)** The histone Hta2-mRFP1 abundance, a reporter for the DNA content, was measured in

the same cell (as in Figure 6B-C) prior and after the late cell cycle arrest. After every metabolic oscillation (from trough to trough of the NAD(P)H signal) the DNA content (Hta2-mRFP1 abundance – left y-axis) increased by the same amount, before and also after Cdc14 depletion. The number of genomes were determined by dividing the Hta2 abundance at any given time point by the value at 240 min (just after cytokinesis), when cells have exactly one copy of their genome. Vertical black arrows extending from Figure 6B mark the troughs of each metabolic oscillation. **(G)** Per metabolic oscillation, the Hta2-mRFP1 abundance increases by an amount corresponding to approximately one genome in dividing cells (before Cdc14-depletion – 26 oscillations from 15 single cells) and in Cdc14 depleted cells (17 oscillations from 11 single cells). Data from the metabolic oscillations, which were interrupted by the Cdc14-AID depletion (at 310 min) were not included in the analysis. Means and the standard deviation are presented. Both distributions passed the Shapiro-Wilk normality test. **(H)** Microscopy images for certain time points (as indicated by grey lines) in the Hta2-mRFP1 and DIC channels show the increase in the DNA content and cell volume in the same single cell as in Figure 6B-C&F (scale, 10 μm). After Cdc14 depletion, in the absence of cytokinesis, each of the three consecutive metabolic oscillations occurs in synchrony with one biomass production cycles (yellow numbers) and one DNA replication cycle. **(I)** Chromosomal bridges, found in Cdc14-depleted cells using 100x magnification, confirm the late cell cycle arrest (scale, 10 μm).

Discussion

Through dynamic monitoring of NAD(P)H and ATP levels as well as cell cycle events in single cells, we found that metabolism is a cell cycle–independent, nutrient-responsive oscillator, which together with the cell cycle forms a system of coupled oscillators. By means of steady-state and dynamic perturbations, we revealed that the metabolic oscillator is separately coupled to the early and the late cell cycle, globally orchestrating biomass formation and segregation. Our findings demonstrate the biological significance of the metabolic oscillator. The cells are unable to progress through the cell cycle in the absence of an oscillating metabolism, and the oscillating metabolism dynamically gates the occurrence of the cell cycle events (e.g. START and M exit) in response to nutrient changes.

The idea of endogenous oscillations in respiration or global protein synthesis setting the pace of the cell cycle was already suggested in the 1980s (Klevecz, 1969; Klevecz and Ruddle, 1968; Lloyd et al., 1982; Novak and Mitchison, 1987; Novak et al., 1988), but was abandoned soon after the discovery of the cyclin/CDK machinery (Watts, 2001), likely because the respective analyses of synchronized cultures did not generate broadly convincing data. Here, through exploiting latest advances in single cell technology (Huberts

et al., 2013) and single cell metabolite measurements to circumvent cell cycle synchronization, in combination with targeted protein depletion (Morawska and Ulrich, 2013; Nishimura et al., 2009) to replace the classic temperature-sensitive mutants (Hartwell et al., 1974), we could for the first time demonstrate that metabolism is an autonomous oscillator, which together with the cell cycle forms a system of coupled oscillators. With these tools, not only we avoided potential synchronization (Aon et al., 2007; Laxman et al., 2010; Sohn et al., 2000) or temperature-related (Murray et al., 2001) artifacts, but also used the inherent cell-to-cell variability to unravel the interactions between metabolism and the cell cycle.

Accordingly, cell cycle control is not just the result of the cyclin/CDK machinery, but emerges from the collective synchrony between coupled and mutually entrained oscillators. While it has been suggested that the CDK oscillator locks the phase of 'peripheral oscillators', namely the Cdc14-release, the global transcription and centrosome duplication oscillators (Cross et al., 1989; Oikonomou and Cross, 2010), our work establishes the metabolic oscillator as an additional, key component within the cell cycle control network. The metabolic oscillator and the cyclin/CDK machinery independently are not sufficient for cells to divide. Only the ensemble of the metabolic oscillator and cell cycle oscillators (and eventually also the cell cycle transcription program (Banyai et al., 2016; Hillenbrand et al., 2016; Rahi et al., 2016)) exerts the higher order function of cell cycle control. Thus, our discovery does not undermine the importance of the cyclin/CDK machinery, but expands the current view on cell cycle regulation.

The role of the metabolic oscillator in cell cycle control is supported by evolutionary findings. An amino acid sequence-based reconstruction of the maximum-likelihood phylogeny of cell cycle regulating kinases has shown that the CDKs emerged late in the evolution of eukaryotes (Krylov et al., 2003). The metabolic oscillator could constitute the previously conjectured ancestral non-CDK controller driving DNA replication and segregation (Murray, 2004). We envisage that during evolution, the CDK oscillator was grafted onto the metabolic oscillator to finely-tune the coordination between biomass formation and segregation (Pines, 2011; Tyson and Novak, 2008), to reduce noise in the duration of the cell cycle phases (Talia et al., 2007) and to robustly order the cell cycle phases.

Through our work we open a new avenue for the investigation of cell cycle control. Future research will need to unravel the nature of the metabolic oscillator, which we found to oscillate on all nutrient conditions. Such research efforts require the development of novel methods to dynamically assess the activity of metabolic pathways in single cells. Only when the nature of the metabolic oscillator is discovered, it will be possible to unravel the precise molecular functioning of the proposed system of coupled oscillators, incorporating the recently identified connections from the cyclin/CDK machinery towards metabolic enzymes (Ewald et al., 2016; Zhao et al., 2016), or in the opposite direction (Shi and Tu, 2013) and the cyclic expression of metabolic enzymes (Silverman et al., 2010; Wyart et al., 2010).

Once fully unraveled, the metabolic oscillator and its connections to the CDK-machinery could serve as targets for the manipulation of cell fate (dormancy or proliferation) (Vander Heiden et al., 2009; Pearce et al., 2009; Wang and Green, 2012) or therapeutic targets against proliferative disorders (Galluzzi et al., 2013).

Experimental Procedures

Strains

All strains (Table S1) were constructed on the background of the prototrophic YSBN6 (Kümmel et al., 2010) and its HIS^- auxotrophic version (YSBN16). The construction of all stains is described in the Supplemental Experimental Procedures. Primer sequences are included (Table S2).

Cultivation

Cells were grown in minimal medium (Verduyn et al., 1992) supplemented with the appropriate carbon source (glucose, galactose or pyruvate). Exponentially growing cells were loaded in the microfluidic dissection platform as described (Huberts et al., 2013; Lee

et al., 2012). A detailed description of the pre-culturing and culturing schemes is provided in the Supplemental Experimental Procedures.

Microscopy

We used Nikon-Ti inverted microscopes with either an Andor 897 Ultra EX2 EM-CCD camera, or 2x Andor LucaR EM-CCD cameras (dual camera system for FRET measurements), together with the CooLED pE2 excitation system. For NAD(P)H measurements, cells were excited at 365 nm (15 % LED intensity / 200 msec exposure), using a 350/50 nm bandpass filter, a 409 nm beam-splitter and a 435/40 nm emission filter. For GFP measurements, cells were excited at 470 nm (15 % / 200 msec), using a 470/40 nm bandpass filter, a 495 nm beam-splitter and a 525/50 nm emission filter. For RFP measurements, cells were excited at 565 nm (15 % / 200 msec for mRFP1, 50 % / 600 msec for mCherry), using a 560/40 nm bandpass filter, a 585 nm beam-splitter and a 630/75 nm emission filter. For FRET measurements, the donor (CFP) was excited at 440 nm (5 % / 50 msec) using a 438/24 nm bandpass filter. Donor emission was recorded using a 458 nm beam-splitter and a 483/32 nm emission filter. Acceptor (YFP) emission was recorded using a 535/30 emission filter. Only for FRET imaging, 2x2 pixel binning and 3x EM-gain (within the linear amplification range) were applied during image acquisition. In the DIC channel, the light of a halogen lamp was passed through a 420 nm beam-splitter, to exclude UV light and minimize cell damage during long-term acquisition. For the FRET measurements 60x Nikon Plan Apochromat objective was used. For the rest of the measurements a 40x Nikon Super Fluor Apochromat was used. Images were taken every 5 min for fast growth conditions, 10 min during slow growth or 20 min during growth on 0.01 gL^{-1} glucose. The NIS elements software was used to control the microscope.

Image Analysis

The BudJ plug-in (Ferrezuelo et al., 2012) for ImageJ (Schneider et al., 2012) was used to segment, track single cells, and measure the NAD(P)H, Cln2-eGFP, mGFP-AID, Cdc14-mCherry-AID fluorescence. The Whi5-eGFP localization was manually determined for

each single cell. The FRET donor and acceptor signals were manually determined, separately in each fluorescent channel. For the determination of the cellular perimeter and Hta2-mRFP1 abundance before and after Cdc14-AID depletion, cells were manually segmented using the DIC channel (as in Figure 6H) and imageJ (Schneider et al., 2012). A detailed description of image analysis, including background estimation and clustered fluorescence quantification is provided in the Supplemental Experimental Procedures.

Signal analysis

All single cell fluorescent signals (NAD(P)H, ATP-FRET, Cln2-eGFP) presented in Figures 2B-C, 4A, S4C, S5D and S6, were de-trended by dividing with a fitted smoothing spline in order to remove low frequency variations. In Figures 1A-B, 2B-C, 4A, S4A-B&E and S6, a spline functions (fitted to the raw, or de-trended NAD(P)H or ATP signals) were added only for the visualization of the metabolic dynamics and were not used in further analysis. In the Cdc14-depletion experiments, spline functions (parameter value 5e-4) were used to de-noise the perimeter and the NAD(P)H oscillations, and estimate the rate of perimeter increase and NAD(P)H in single cells (Figure S9). Smoothing splines were fitted using the MATLAB Curve Fitting Toolbox™.

Author contributions

AP designed the study, developed all reporters, performed all experiments, and analyzed all data. BN contributed to the development of the study and performed the autocorrelation function analysis. EW performed the hazard function and the autocorrelation function analysis. MH conceived, designed and supervised the study. AP and MH wrote the manuscript.

Acknowledgements

Financial support is acknowledged from the EU ITN project ISOLATE. The authors thank Jakub Leszek Radzikowski and the Molecular Systems Biology group for helpful discussion, Andrew Millar, Marcel van Vugt, Peter van Haastert, Maarten Linskens, and Bayu Jayawardhana for discussion and critical comments on the manuscript, and Marti Aldea for useful advice and support on image analysis (BudJ toolbox).

References

Amaral, N., Vendrell, A., Funaya, C., Idrissi, F.-Z., Maier, M., Kumar, A., Neurohr, G., Colomina, N., Torres-Rosell, J., Geli, M.-I., et al. (2016). The Aurora-B-dependent NoCut checkpoint prevents damage of anaphase bridges after DNA replication stress. Nat Cell Biol 18, 516–526.

Aon, M.A., Cortassa, S., Lemar, K.M., Hayes, A.J., and Lloyd, D. (2007). Single and cell population respiratory oscillations in yeast: A 2-photon scanning laser microscopy study. FEBS Lett. 581, 8–14.

Banyai, G., Baidi, F., Coudreuse, D., and Szilagyi, Z. (2016). Cdk1 activity acts as a quantitative platform for coordinating cell cycle progression with periodic transcription. Nat Commun 7.

Bardwell, L. (2004). A walk-through of the yeast mating pheromone response pathway. Peptides 25, 1465–1476.

Barik, D., Baumann, W.T., Paul, M.R., Novak, B., and Tyson, J.J. (2010). A model of yeast cell-cycle regulation based on multisite phosphorylation. Mol. Syst. Biol. 6, 405.

Bloom, J., and Cross, F.R. (2007). Multiple levels of cyclin specificity in cell-cycle control. Nat Rev Mol Cell Biol 8, 149–160.

Buchakjian, M.R., and Kornbluth, S. (2010). The engine driving the ship: metabolic steering of cell proliferation and death. Nat. Rev. Mol. Cell Biol. 11, 715–727.

Costanzo, M., Nishikawa, J.L., Tang, X., Millman, J.S., Schub, O., Breitkreuz, K., Dewar, D., Rupes, I., Andrews, B., and Tyers, M. (2004). CDK activity antagonizes Whi5, an inhibitor of G1/S transcription in yeast. Cell 117, 899–913.

Coudreuse, D., and Nurse, P. (2010). Driving the cell cycle with a minimal CDK control network. Nature 468, 1074–1079.

Cox, D.R. (1972). Regression Models and Life-Tables. J. R. Stat. Soc. Ser. B 34, 187–220.

Cross, F., Roberts, J., and Weintraub, H. (1989). Simple and Complex Cell Cycles. Annu. Rev. Cell Biol. 5, 341–396.

Ewald, J.C., Kuehne, A., Zamboni, N., and Skotheim, J.M. (2016). The Yeast Cyclin-Dependent Kinase Routes Carbon Fluxes to Fuel Cell Cycle Progression. Mol. Cell 62, 532–545.

Feillet, C., Krusche, P., Tamanini, F., Janssens, R.C., Downey, M.J., Martin, P., Teboul, M., Saito, S., Lévi, F.A., Bretschneider, T., et al. (2014). Phase locking and multiple oscillating attractors for the coupled mammalian clock and cell cycle. Proc. Natl. Acad. Sci. 111, 9828–9833.

Ferrezuelo, F., Colomina, N., Palmisano, A., Garí, E., Gallego, C., Csikász-Nagy, A., and Aldea, M. (2012). The critical size is set at a single-cell level by growth rate to attain homeostasis and adaptation. Nat. Commun. 3, 1–11.

Futcher, B. (2006). Metabolic cycle, cell cycle, and the finishing kick to Start. Genome Biol. 7, 107.

Galluzzi, L., Kepp, O., Heiden, M.G. Vander, and Kroemer, G. (2013). Metabolic targets for cancer therapy. Nat Rev Drug Discov 12, 829–846.

Gustavsson, A.-K., van Niekerk, D.D., Adiels, C.B., du Preez, F.B., Goksör, M., and Snoep, J.L. (2012). Sustained glycolytic oscillations in individual isolated yeast cells. FEBS J. 279, 2837–2847.

Haase, S.B., and Reed, S.I. (1999). Evidence that a free-running oscillator drives G1 events in the budding yeast cell cycle. Nature 401, 394–397.

Hartwell, L.H., Culotti, J., Pringle, J.R., and Reid, B.J. (1974). Genetic Control of the Cell Division Cycle in Yeast. Science (80-.). 183, 46–51.

Vander Heiden, M.G., Cantley, L.C., and Thompson, C.B. (2009). Understanding the Warburg Effect: The Metabolic Requirements of Cell Proliferation. Science 324, 1029–1033.

Hillenbrand, P., Maier, K.C., Cramer, P., and Gerland, U. (2016). Inference of gene regulation functions from dynamic transcriptome data. Elife 5, e12188.

Huberts, D.H.E.W., Lee, S.S., González, J., Janssens, G.E., Vizcarra, I.A., and Heinemann, M. (2013). Construction and use of a microfluidic dissection platform for long-term imaging of cellular processes in budding yeast. Nat. Protoc. 8, 1019–1027.

Imamura, H., Huynh, K.P., Togawa, H., Saito, K., Iino, R., Kato-yamada, Y., Nagai, T., and Noji, H. (2009). Visualization of ATP levels inside single living cells with fluorescence resonance energy transfer-based genetically encoded indicators. Proc. Natl. Acad. Sci. 106, 15651–15656.

Jones, R.G., Plas, D.R., Kubek, S., Buzzai, M., Mu, J., Xu, Y., Birnbaum, M.J., and Thompson, C.B. (2005). AMP-activated protein kinase induces a p53-dependent metabolic checkpoint. Mol. Cell 18, 283–293.

Klevecz, R.R. (1969). TEMPORAL ORDER IN MAMMALIAN CELLS: I. The Periodic Synthesis of Lactate Dehydrogenase in the Cell Cycle. J. Cell Biol. 43, 207–219.

Klevecz, R.R., and Ruddle, F.H. (1968). Cyclic Changes in Enzyme Activity in Synchronized Mammalian Cell Cultures. Science (80-.). 159, 634–636.

Klevecz, R.R., Bolen, J., Forrest, G., and Murray, D.B. (2004). A genomewide oscillation in transcription gates DNA replication and cell cycle. Proc. Natl. Acad. Sci. U. S. A. 101, 1200–1205.

Krylov, D.M., Nasmyth, K., and Koonin, E. V. (2003). Evolution of eukaryotic cell cycle regulation: stepwise addition of regulatory kinases and late advent of the CDKs. Curr. Biol. 13, 173–177.

Kümmel, A., Ewald, J.C., Fendt, S.-M., Jol, S.J., Picotti, P., Aebersold, R., Sauer, U., Zamboni, N., and Heinemann, M. (2010). Differential glucose repression in common yeast strains in response to HXK2 deletion. FEMS Yeast Res. 10, 322–332.

Laxman, S., Sutter, B.M., and Tu, B.P. (2010). Behavior of a metabolic cycling population at the single cell level as visualized by fluorescent gene expression reporters. PLoS One 5, e12595.

Lee, I.H., and Finkel, T. (2013). Metabolic regulation of the cell cycle. Curr. Opin. Cell Biol. 25, 724–729.

Lee, S.S., Avalos, I., Huberts, D.H.E.W., Lee, L.P., and Heinemann, M. (2012). Whole lifespan microscopic observation of budding yeast aging through a microfluidic dissection platform. Proc. Natl. Acad. Sci. 109, 4916–4920.

Lee, Y., Dominy, J.E., Choi, Y.J., Jurczak, M., Tolliday, N., Camporez, J.P., Chim, H., Lim, J.-H., Ruan, H.-B., Yang, X., et al. (2014). Cyclin D1-Cdk4 controls glucose metabolism independently of cell cycle progression. Nature 510, 547–551.

Lloyd, D., Edwards, S.W., and Fry, J.C. (1982). Temperature-compensated oscillations in respiration and cellular protein content in synchronous cultures of Acanthamoeba castellanii. Proc. Natl. Acad. Sci. U. S. A. 79, 3785–3788.

Lloyd, D., Salgado, L.E.J., Turner, M.P., Suller, M.T.E., and Murray, D. (2002). Cycles of mitochondrial energization driven by the ultradian clock in a continuous culture of *Saccharomyces cerevisiae*. Microbiology 148, 3715–3724.

Lu, Y., and Cross, F.R. (2010). Periodic cyclin-Cdk activity entrains an autonomous Cdc14 release oscillator. Cell 141, 268–279.

Morawska, M., and Ulrich, H.D. (2013). An expanded tool kit for the auxin-inducible degron system in budding yeast. Yeast 30, 341–351.

Mori, T., Binder, B., and Johnson, C.H. (1996). Circadian gating of cell division in cyanobacteria growing with average doubling times of less than 24 hours. Proc. Natl. Acad. Sci. U. S. A. 93, 10183–10188.

Müller, D., Exler, S., Aguilera-Vázquez, L., Guerrero-Martín, E., and Reuss, M. (2003). Cyclic AMP mediates the cell cycle dynamics of energy metabolism in *Saccharomyces cerevisiae*. Yeast 20, 351–367.

Murray, A.W. (2004). Recycling the Cell Cycle: Cyclins Revisited. Cell 116, 221–234.

Murray, D.B., Roller, S., Kuriyama, H., and Lloyd, D. (2001). Clock control of ultradian respiratory oscillation found during yeast continuous culture. J. Bacteriol. 183, 7253–7259.

Nishimura, K., Fukagawa, T., Takisawa, H., Kakimoto, T., and Kanemaki, M. (2009). An auxin-based degron system for the rapid depletion of proteins in nonplant cells. Nat. Methods 6, 917–922.

Nolte, D, D. (2015). Introduction to Modern Dynamics - Chaos, Networks, Space and Time (OXFORD UNIVERSITY PRESS).

Novak, B., and Mitchison, J.M. (1987). Periodic cell cycle changes in the rate of CO_2 production in the fission yeast Schizosaccharomyces pombe persist after a block to protein synthesis. J. Cell Sci. 87, 323–325.

Novak, B., Halbauer, J., and Laszlo, E. (1988). The effect of CO_2 on the timing of cell cycle events in fission yeast Schizosaccharomyces pombe. J. Cell Sci. 89, 433–439.

Oikonomou, C., and Cross, F.R. (2010). FREQUENCY CONTROL OF CELL CYCLE OSCILLATORS. Curr. Opin. Genet. Dev. 20, 605–612.

Orlando, D.A., Lin, C.Y., Bernard, A., Wang, J.Y., Socolar, J.E.S., Iversen, E.S., Hartemink, A.J., and Haase, S.B. (2008). Global control of cell-cycle transcription by coupled CDK and network oscillators. Nature 453, 944–947.

Pearce, E.L., Walsh, M.C., Cejas, P.J., Harms, G.M., Shen, H., Wang, L.-S., Jones, R.G., and Choi, Y. (2009). Enhancing CD8 T Cell Memory by Modulating Fatty Acid Metabolism. Nature 460, 103–107.

Pines, J. (2011). Cubism and the cell cycle: the many faces of the APC/C. Nat. Rev. Mol. Cell Biol. 12, 427–438.

Rahi, S.J., Pecani, K., Ondracka, A., Oikonomou, C., and Cross, F.R. (2016). The CDK-APC/C Oscillator Predominantly Entrains Periodic Cell-Cycle Transcription. Cell 165, 475–487.

Rattray, A.M.J., and Müller, B. (2012). The control of histone gene expression. Biochem. Soc. Trans. 40, 880–885.

Saqcena, M., Menon, D., Patel, D., Mukhopadhyay, S., Chow, V., and Foster, D.A. (2013). Amino Acids and mTOR Mediate Distinct Metabolic Checkpoints in Mammalian G1 Cell Cycle. PLoS One 8, e74157.

Schneider, C.A., Rasband, W.S., and Eliceiri, K.W. (2012). NIH Image to ImageJ: 25 years of image analysis. Nat Meth 9, 671–675.

Sherr, C.J., and Roberts, J.M. (2004). Living with or without cyclins and cyclin-dependent kinases. Genes Dev. 18, 2699–2711.

Shi, L., and Tu, B.P. (2013). Acetyl-CoA induces transcription of the key G1 cyclin CLN3 to promote entry into the cell division cycle in *Saccharomyces cerevisiae*. Proc. Natl. Acad. Sci. 110, 7318–7323.

Silverman, S.J., Petti, A. a, Slavov, N., Parsons, L., Briehof, R., Thiberge, S.Y., Zenklusen, D., Gandhi, S.J., Larson, D.R., Singer, R.H., et al. (2010). Metabolic cycling in single yeast cells from unsynchronized steady-state populations limited on glucose or phosphate. Proc. Natl. Acad. Sci. U. S. A. 107, 6946–6951.

Slavov, N., Macinskas, J., Caudy, A., and Botstein, D. (2011). Metabolic cycling without cell division cycling in respiring yeast. Proc. Natl. Acad. Sci. 108, 19090–19095.

Sohn, H.Y., Murray, D.B., and Kuriyama, H. (2000). Ultradian oscillation of *Saccharomyces cerevisiae* during aerobic continuous culture: hydrogen sulphide mediates population synchrony. Yeast 16, 1185–1190.

Strogatz, S.H. (2001). Exploring complex networks. Nature 410, 268–276.

Strogatz, S.H. (2014). Nonlinear Dynamics and Chaos (WESTVIEW PRESS).

Takubo, K., Nagamatsu, G., Kobayashi, C.I., Nakamura-Ishizu, A., Kobayashi, H., Ikeda, E., Goda, N., Rahimi, Y., Johnson, R.S., Soga, T., et al. (2013). Regulation of glycolysis by Pdk functions

as a metabolic checkpoint for cell cycle quiescence in hematopoietic stem cells. Cell Stem Cell 12, 49–61.

Talia, S. Di, Skotheim, J.M., Bean, J.M., Siggia, E.D., and Cross, F.R. (2007). The effects of molecular noise and size control on variability in the budding yeast cell cycle. Nature 448, 947–951.

Tu, B.P., Kudlicki, A., Rowicka, M., and McKnight, S.L. (2005). Logic of the yeast metabolic cycle: temporal compartmentalization of cellular processes. Science 310, 1152–1158.

Tu, B.P., Mohler, R.E., Liu, J.C., Dombek, K.M., Young, E.T., Synovec, R.E., and Mcknight, S.L. (2007). Cyclic changes in metabolic state during the life of a yeast cell. Proc. Natl. Acad. Sci. 104, 16886–16891.

Tudzarova, S., Colombo, S.L., Stoeber, K., Carcamo, S., Williams, G.H., and Moncada, S. (2011). Two ubiquitin ligases, APC/C-Cdh1 and SKP1-CUL1-F (SCF)-β-TrCP, sequentially regulate glycolysis during the cell cycle. Proc. Natl. Acad. Sci. 108, 5278–5283.

Tyson, J.J., and Novak, B. (2008). Temporal organization of the cell cycle. Curr. Biol. 18, R759–R768.

Verduyn, C., Postma, E., Scheffers, A.W., and van Dijken, J. (1992). Effect of Benzoic Acid on Metabolic Fluxes in Yeasts: A Continuous-Culture Study on the Regulation of Respiration and Alcoholic Fermentation. Yeast 8, 501–517.

Wang, R., and Green, D.R. (2012). Metabolic checkpoints in activated T cells. Nat Immunol 13, 907–915.

Wang, Z., Fan, M., Candas, D., Zhang, T.-Q., Qin, L., Eldridge, A., Wachsmann-Hogiu, S., Ahmed, K.M., Chromy, B.A., Nantajit, D., et al. (2014). Cyclin B1/Cdk1 coordinates mitochondrial respiration for cell-cycle G2/M progression. Dev. Cell 29, 217–232.

Watts, G. (2001). Three cell cycle scientists win Nobel prize. BMJ Br. Med. J. 323, 823.

Wyart, M., Botstein, D., and Wingreen, N.S. (2010). Evaluating gene expression dynamics using pairwise RNA FISH data. PLoS Comput. Biol. 6, e1000979.

Xu, Z., and Tsurugi, K. (2006). A potential mechanism of energy-metabolism oscillation in an aerobic chemostat culture of the yeast *Saccharomyces cerevisiae*. FEBS J. 273, 1696–170.

Yalcin, A., Clem, B.F., Imbert-Fernandez, Y., Ozcan, S.C., Peker, S., O'Neal, J., Klarer, A.C., Clem, A.L., Telang, S., and Chesney, J. (2014). 6-Phosphofructo-2-kinase (PFKFB3) promotes cell cycle progression and suppresses apoptosis via Cdk1-mediated phosphorylation of p27. Cell Death Dis 5, e1337.

Zhao, G., Chen, Y., Carey, L., and Futcher, B. (2016). Cyclin-Dependent Kinase Co-Ordinates Carbohydrate Metabolism and Cell Cycle in S. cerevisiae. Mol. Cell 62, 546–557.

Supplemental Information for

Autonomous metabolic oscillations robustly gate the early and the late cell cycle

Alexandros Papagiannakis[1], Bastian Niebel[1], Ernst Wit[2], Matthias Heinemann[1]¶

[1] Molecular Systems Biology, Groningen Biomolecular Sciences and Biotechnology Institute, University of Groningen, Nijenborgh 4, 9747 AG Groningen, The Netherlands

[2] Probability and Statistics, Johann Bernoulli Institute of Mathematics and Computer Science, University of Groningen, Nijenborgh 9, 9747 AG Groningen, The Netherlands

Supplemental Experimental Procedures

Chemicals

All regular chemicals were purchased from Sigma-Aldrich, Acros-Organics, Formedium or Merck-Millipore. Anhydrotetracycline hydrochloride, α_1-mating factor acetate salt, potassium phthalate monobasic and 3-indoleacetic acid sodium salt (auxin) were purchased from Sigma-Aldrich.

Strains and strain construction

The prototrophic, S288c-derived strain of *Saccharomyces cerevisiae* YSBN6 (Kümmel et al., 2010) and the corresponding HIS$^-$ strain (YSBN16) were used. For an overview on strains, refer to Table S1. ATP levels in single cells were measured using the Ateam 1.03 ATP FRET sensor (Imamura et al., 2009), codon-optimized version for yeast (Geneart). Two expression cassettes were constructed and tested for the expression of the ATeam 1.03 FRET sensor: (i) the PFY1p based inverter device (Blount et al., 2012) and (ii) a constitutive expression cassette via the strong TEF1p promoter. For the development of the first construct, the whole tetracycline inducible system (i.e. the tetracycline repressor expression cassette, the yEGFP coding sequence, the iPFY1p-tetO promoter) was amplified from the pINV plasmid (Blount et al., 2012) and incorporated into the HO-poly-KanMX-HO plasmid (Voth et al., 2001) using circular polymerase extension cloning (CPEC) (Quan and Tian, 2009, 2011) DNA assembly method and the primer pairs HO and HO-TetEX (Table S2), resulting in the vector pC6B. Next, we used Gibson DNA assembly (Gibson et al., 2009, 2010) and the primer pairs TetEX and ATP (Table S2) to incorporate the ATP FRET sensor coding sequence into the pC6B vector, replacing the yEGFP coding sequence to yield the plasmid pG5A. The pC6B and pG5A plasmids were amplified in *Escherichia coli*, and checked using restriction digestion and sequencing (primers Seq1-3 – Table S2). After linearization of the vector pG5A using the primer pair Seq4, we transformed YSBN6 cells, using an established protocol (Gietz and Schiestl, 2007), with the resistance to the G418 antibiotic as a selection marker. Correct homologous recombination in the HO region

located in chromosome IV was tested with PCR (primers Seq6Fwd-Seq6Rev and seq5Fwd-seq5Rev, see Table S2).

For the development of the second construct, the pG5A plasmid was linearized using the primer pair TEFATP (Table S2). The linearized plasmid was then self-ligated in a single step phosphorylation-ligation reaction to generate the pTEF:ATP plasmid with the TEF1p constitutive yeast promoter upstream the ATP FRET sensor coding sequence. The pTEF:ATP recombinant plasmids was amplified in *Escherichia coli*, and checked using restriction digestion and sequencing (primers Seq1Fwd, Seq2Rev & Seq4Rev – Table S2). The pTEF:ATP plasmid was then linearized using the Seq4 (Table S2) primer pair and was used to transform YSBN6 cells, using an established protocol (Gietz and Schiestl, 2007), with the resistance to the G418 antibiotic as a selection marker. Correct homologous recombination in the HO region was tested with PCR (primers Seq6Fwd-Seq6Rev and seq5Fwd-seq5Rev, see Table S2). We checked for functional Förster energy transfer between the donor (CFP) and acceptor (YFP) modules in the ATeam 1.03 FRET sensor by measuring the emission spectrum from 465 to 599 nm in cells expressing the ATP sensor and excited at 420 nm.

To generate cell cycle reporter strains, we PCR-amplified the eGFP-tagged Whi5 and Cln2 gene from the yeast GFP collection (Invitrogen) (Huh et al., 2003) including the HIS3MX6 auxotrophic selection marker and sequences upstream and downstream the STOP codon of the respective genes, necessary for homologous recombination (primers Whi5 and Cln2, see Table S2). The PCR products were then transformed into the YSBN16 HIS^- strain, using an established protocol (Gietz and Schiestl, 2007), for the generation of the YSBN16 Whi5-eGFP and YSBN6 Cln2-eGFP prototrophic yeast strains. Correct integration was checked with PCR (primers Whi5Ver, CLn2Ver, see Table S2).

To dynamically deplete the Cdc14 phosphatase, an essential activator of the Anaphase Promoting Complex (APC) and late mitosis, we used the auxin-based degron system adapted for yeast (Morawska and Ulrich, 2013). First, we implemented the auxin-based degron system in our yeast strains. Therefore, we generated the pG1J plasmid, which contained a gene for mGFP (monomeric GFP) tagged at the C terminus with the AID^{71-114} auxin-induced sequence (Morawska and Ulrich, 2013). Specifically, the backbone of the pC6B plasmid, including the pTEF1 promoter and CYC1 transcriptional terminator, was

amplified (primer pair C6B – Table S2). The degron tag (S3-5GA-AID$^{71-114}$) was amplified from the #2189 plasmid (Morawska and Ulrich, 2013) (primer pair AID Fwd/5GA Rev – Table S2), and the mGFP coding sequence from the pHIPZ-mGFP-fusionator plasmid (Saraya et al., 2010) (primer pair mGFP – Table S2). The three amplified pieces were assembled using Gibson DNA assembly for the construction of the pG1J plasmid (Table S1), which was validated by restriction digestion and sequencing (primers Seq1Fwd, Seq9Rev, Seq7Rev & Seq8Rev). Next, the *Oryza sativa* TIR1 (Os-TIR1) coding sequence, together with its regulatory elements (ADH1p) were amplified from the BY25598 yeast strain (Table S1) provided by the NBRP, Japan (Nishimura et al., 2009) (primers pADH1Fwd/AtTIR1Rev – Table S2), and inserted into the amplified backbone of the pG1J plasmid (primer pair G1JBkbn), together with the transcriptional terminator ADH1tt, which was amplified from the pInverter plasmid (Blount et al., 2012) (primers ADH1TTFwd / AtTIRADH1TT Rev – Table S2). The three amplicons were assembled using Gibson DNA assembly, yielding the pG2J plasmid. The pG2J plasmid was amplified in *Escherichia coli* and validated by restriction digestion and sequencing (primers Seq1Fwd, Seq1Rev, Seq9Rev, Seq7Rev & Seq8Rev – Table S2). The recombinant pG2J plasmid was linearized (primer pair Seq4 – Table S2) and transformed into YSBN6 wild type yeast cells for integration into the HO locus (Chromosome IV), with the resistance to the G418 antibiotic as a selection marker, thus resulting in the YSBN6.G2J strain, which contained the S3-5GA-AID71-114 tagged version of mGFP. Correct homologous recombination into the HO locus was tested with PCR (primers Seq5Fwd / Seq6Rev – Table S2). In our single cell time-lapse microscopy measurements, we used this an internal control to monitor the protein depletion dynamics as a result of auxin (IAA) addition. Finally, to generate a plasmid encoding only for the OsTIR1 expression cassette for future use with any fluorescently labeled protein, we removed the mGFP expression cassette from the G2J plasmid using a phosphorylation ligation protocol. Specifically, the pG2J plasmid was linearized (primer Prim1Fwd/Prim2Rev – Table S2). Then, the linearized plasmid was self-ligated in a single step phosphorylation-ligation reaction to generate the pOsTIR1w/oGFP plasmid encoding for the OsTIR1 module but no fluorescence reporters. The pOsTIR1w/oGFP recombinant plasmid was amplified in *Escherichia coli*, and checked using restriction digestion and sequencing (primers Seq1Fwd, Seq1Rev, Seq9Rev, Seq7Rev & Seq8Rev – Table S2). The pOsTIR1w/oGFP plasmid was then linearized using the Seq4 primer pair (Table S2) and was used to transform YSBN6 cells, using an established

protocol (Gietz and Schiestl, 2007), with the resistance to the G418 antibiotic as a selection marker, for the construction of the YSBN6.OsTIR1w/oGFP strain. Correct homologous recombination in the HO region was tested with PCR (primers Seq5Fwd, Seq6Rev – Table S2). The YSBN6.OsTIR1w/oGFP strain was then used as a scaffold for the dynamic depletion of fluorescently labeled proteins tagged with the degron sequence (S3-5GA-AID$^{71-114}$).

To tag Cdc14 (phosphatase and essential activator of M exit) with the AID* degron sequence into the YSBN6.OsTIR1w/oGFP strain, we constructed the pG23A plasmid. We first, amplified the S3-5GA-AID$^{71-114}$ degron sequence from the #2189 plasmid (Morawska and Ulrich, 2013) (primer pair IAA – Table S2), the mCherry coding sequence from the pBS35 plasmid ((Hailey et al., 2002) – Yeast Resource Center, University of Washington) (primer pair mCherry – Table S2), the natMX expression cassette offering resistance to clonNAT from the pAG36 vector ((Goldstein and McCusker, 1999) – AddGene) (primer pair Nat – Table S2), the flanking sequences upstream and downstream the STOP codon of the Cdc14 ORF from the wild type YSBN6 genome (primer pairs Cdc14CDS & Cdc14DOWN respectively – Table S2) and the backbone of the pG2J plasmid (primer pair Amp – Table S2). The seven amplicons with complementary overhangs were used in a Gibson DNA assembly reaction for the construction of the pG23A plasmid. The pG23A plasmid was amplified in *Escherichia coli*, and checked using restriction digestion. The pG23A plasmid was then used to transform the YSBN6.OsTIR1w/oGFP strain using clonNAT and G418 antibiotics as selection markers, for the construction of YSBN6.OsTIRw/oGFP.G23A. Correct homologous recombination in the Cdc14 region was tested with PCR (primers Cdc14CDSFwd / Cdc14DOWNRev – Table S2). The YSBN6.OsTIRw/oGFP.G23A strain expresses Cdc14 fused with mCherry and tagged with the AID$^{71-114}$ sequence. Using this strain, we could dynamically deplete Cdc14 by the addition of indole-3-acetic acid (IAA) into the culture medium.

In order to combine conditional Cdc14 depletion and late cell cycle arrest experiments with RFP labeled cell cycle reporters, we constructed a strain which expressed the degron-tagged Cdc14 (Cdc14-AID$^{71-114}$) without any fluorescent label. First, we linearized the pG23A plasmid (primer pair Cdc14LinRFPex – see Table S2) excluding the coding sequence of mCherry. The linearized plasmid was then self-ligated in a single step phosphorylation-

ligation reaction to generate the pG23ARFPex plasmid. The pG23ARFPex recombinant plasmid was amplified in *Escherichia coli*, and checked using restriction digestion and sequencing (primers Seq1Rev & Seq101 – Table S2). The pG23ARFPex plasmid was then linearized using the G23Lin (Table S2) primer pair and used to transform YSBN16.Whi5-eGFP (Table S1) cells, applying an established protocol (Gietz and Schiestl, 2007), with the resistance to the clonNAT antibiotic as a selection marker, to generate the YSBN16.Whi5-eGFP.G23ARFPex strain (Table S1). Correct homologous recombination in the Cdc14 region was tested with PCR (primers Cdc14CDSFwd / Cdc14DOWNRev - see Table S2). Next, the Os-TIR1 module was incorporated to assemble the auxin inducible protein degradation machinery. Specifically, the linearized pOsTIR1w/oGFP plasmid (primer pair Seq4 - Table S2) was transformed in the YSBN16.Whi5-eGFP.G23ARFPex strain (Table S1) (Gietz and Schiestl, 2007) with the resistance to the G418 and ClonNAT antibiotics as selection markers, for the construction of the YSBN16.Whi5-eGFP.OsTIR1w/oGFP.G23ARFPex strain (Table S1). Correct homologous recombination in the HO region was tested with PCR (primers Seq5Fwd, Seq6Rev – Table S2). Complete integration of the constructs was also confirmed by the absence of cytokinesis upon the addition of auxin, as the physiological effect of Cdc14 depletion.

In order to quantify the DNA content during late cell cycle arrest (after Cdc14-AID$^{71\text{-}114}$ depletion), we labeled histone H2A with mRFP1 (Hta2-mRFP1). Specifically, the Hta2-mRFP1 cassette and the phleomycin resistance cassette (Ble) were amplified in one piece from the KOY.TM6*P hxk2-GFP hta2-mRFP1 strain (Schmidt, 2014) (Table S1) using the primer pair Hta2Lin. The linearized cassette was transformed in the YSBN16.Whi5-eGFP.OsTIR1w/oGFP.G23ARFPex strain (Table S1), using an established protocol (Gietz and Schiestl, 2007), with the resistance to the G418, ClonNAT and Phleomycin antibiotics as selection markers, for the construction of the YSBN16.Whi5-eGFP.Hta2-mRFP1.OsTIR1w/oGFP.G23ARFPex strain (Table S1). Correct homologous recombination in the Hta2 region was verified with PCR (primer pair Hta2Lin – Table S2) and the fluorescence in the RFP channel clearly corresponding to chromatin structures.

Cultivation

Single yeast colonies growing on YPD 20 gL^{-1} glucose agar plates were used to inoculate 10 mL minimal 10 gL^{-1} glucose medium (pH was adjusted with 10mM K-Phthalate-KOH to pH 5) (Verduyn et al., 1992) in 100 mL shake flasks, and grown (at 30°C, 300 rpm) overnight past the diauxic shift (to OD between 5 and 10). The overnight culture was used to inoculate fresh 10 gL^{-1} glucose medium to an OD of 0.1, which was grown to an OD between 1 and 1.5 (still exponential growth on 10 gL^{-1} glucose). For the expression of the ATeam 1.03 sensor via the tetracycline inducible the iPFY1p promoter, 300 ng mL^{-1} of anhydrous tetracycline were applied (also in the pre-culture).

For microscopy experiments on 10 gL^{-1} glucose, the exponentially growing cells were again diluted to an OD of 0.1 in fresh 10 gL^{-1} glucose medium, and then used to load the microfluidic chip as described (Huberts et al., 2013; Lee et al., 2012). For microscopy experiments on pyruvate or galactose, the exponentially growing cells on high glucose (10 gL^{-1}) were diluted in 20 gL^{-1} pyruvate or galactose medium to an OD of 0.1. The cells were grown to an OD of 1 to 1.5 (still exponential growth on pyruvate or galactose), diluted to an OD of 0.1 in pyruvate or galactose medium, and loaded onto the microfluidic chip. For microscopy experiments on 0.05, 0.025 or 0.01 gL^{-1} glucose, the exponentially growing cells on 10 gL^{-1} glucose were used to inoculate a 0.05, 0.025 or 0.01 gL^{-1} glucose medium to an OD of 0.05, and grown to an OD of 0.2 to 0.8. This exponentially growing culture was used to inoculate a fresh 0.05, 0.025 or 0.01 gL^{-1} glucose medium to an OD of 0.05, where the cells were grown for 2 hours and then used to load the microfluidic chip. In the Cdc14 depletion experiments, the Cdc14-AID or Cdc14-AID-mCherry expressing cells were always mixed with cells expressing mGFP-AID (YSBN6.G2J - Table S1) to determine the timing of Cdc14 depletion (Movie S5).

For cell culturing in the microfluidic chip, cells were fed at 4.8 µL min^{-1} with the same media as in the culture just before loading. The provided media were pre-warmed to 30°C and saturated with atmospheric air by shaking at 300 rpm for at least two hours prior to be used. For the metabolic perturbation experiment (switch from 0.01 gL^{-1} to 10 gL^{-1} glucose), the carbon source was switched 12-15 h hours after cell loading on the chip. In alpha factor perturbation experiments, the medium was switched to a medium supplemented with 5 µg mL^{-1} alpha factor (Futcher, 1999) after 4 h of growth. After a 12 h arrest, we switched back

to the medium without pheromone. In the cell cycle perturbation experiments, we depleted the Cdc14 phosphatase by adding 0.1 mM of indole-3-acetic acid (IAA) to the medium after 4-7 h of normal growth on minimal 10 gL^{-1} glucose medium.

Image Analysis

For segmentation and tracking of single yeast cells, the BudJ plug-in (Ferrezuelo et al., 2012) for ImageJ (Schneider et al., 2012) was used. The plug-in was used to determine the background-corrected average cytoplasmic pixel fluorescence intensity from single cells, for the GFP and NAD(P)H channels. Specifically, cells to be tracked over time were selected by clicking at the center of the desired cell and its boundaries were estimated by BudJ based on the pixel intensity change at the perimeter of the cell, as visualized in the DIC image. The average fluorescence intensity of the pixels contained within the specified cell boundaries was determined for each cell by BudJ for the NAD(P)H channel, and the GFP channel (Cln2-eGFP, mGFP-AID^{71-114}). The modal grey value of the whole image area in each fluorescent channel determined for each time-point was subtracted from the fluorescence of each monitored cell. A comparison of the automated background estimation (i.e. the modal grey value) with a manual background acquisition (average intensity of the pixels around the cell covering the pad area) showed no significant differences between the two methods. Cells with large vacuoles (occasionally occurring) were manually excluded from the data set. The Whi5 nuclear or cytoplasmic localization was manually determined for each single cell. The time point of budding was also manually determined as the moment of first bud appearance on the cell surface, which we monitored in the DIC channel. The perimeter of cells (in μm) was manually measured in each single cell and each individual frame, using the white cellular borderline in the DIC channel (as in Figure 6H).

The ATP FRET images were manually analyzed using ImageJ (Schneider et al., 2012). Specifically, the average pixels intensity within the area of a cell was determined, separately for the YFP and CFP channels. The average pixel intensity of the area around the monitored single cell was measured at each time point and subtracted from the cellular fluorescence for each of the fluorescent channels. The FRET signals were determined by dividing the background-corrected YFP by the background-corrected CFP fluorescence.

For the quantification of the Cdc14-mCherry-AID nuclear localization and intracellular abundance, we used the BudJ plug-in (Ferrezuelo et al., 2012) for ImageJ (Schneider et al., 2012) and specifically the Cluster Index function, setting the cluster threshold at 1 standard deviation (brightest pixels by 1 standard deviation at the foci), the minimum fluorescence change at foci at 5%, the minimum foci size at 2 pixels, and the maximum foci size at 10 pixels. The background corrected average fluorescence intensity of Cdc14 at the foci was used as a marker of Cdc14 localization in and out of the nucleus, as well as its dynamic depletion as a result of the indole-3-acetic acid (IAA) addition.

For the quantification of the intracellular Hta2-mRFP1 abundance, cells in the DIC images were manually segmented using ImageJ (Schneider et al., 2012) (as in Figure 6H). The whole cell median fluorescence was used as the cellular background fluorescence, and subtracted from the fluorescence images. The DNA specific fluorescence abundance was then quantified by multiplying the segmented whole cell area in μm2 (number of scaled pixels: 0.4 μm per pixel – 40x objective), by the mean fluorescence intensity.

Hazard function analysis

To investigate the importance of the metabolic oscillation frequency for cell cycle initiation, we investigated whether we can predict START in cells solely on the basis of their NAD(P)H dynamics. First, we separated the recorded NAD(P)H oscillations into those with and without cell cycle progression, based on a computational algorithm that segments each NAD(P)H oscillation in six discrete segments. Segment 1 started at the NAD(P)H trough and extended over the first 25% of the ascending part, segment 2 covered 50% of the ascending part, whereas segment 3 covered the final 25% of the ascending part to the peak of the de-trended NAD(P)H signal. The same pattern was used to segment the descending part from the peak to the next trough of the NAD(P)H oscillation. To identify these six segments, we applied the computational algorithm in R on the de-trended NAD(P)H signals. The background-corrected NAD(P)H signals were de-trended by subtracting an adaptive smoothing function, fitted using a window smoother (runmed) in the computing environment R. We used the segmented NAD(P)H signals to automatically identify those metabolic oscillations, where no cell cycle progression takes place. Specifically, in case six

segments past the last cell cycle event (START, budding or M exit) occurred without any progression to the next cell cycle event, then this metabolic cycle was flagged as a metabolic oscillation without cell cycle. The NAD(P)H signals from the beginning of each experiment until the first mitotic exit were omitted.

Using a Cox proportional hazard model, we identified on the basis of the NAD(P)H signals and the associated cell cycle progressions, which frequency-related and time-dependent NAD(P)H characteristics would be most predictive for START. We tested the (i) NAD(P)H levels: amplitude of the de-trended signal, (ii) NAD(P)H slope: segment-specific derivative of the de-trended signal, (iii) NAD(P)H rate: derivative of the de-trended and smoothed NAD(P)H signal, and (iv) the NAD(P)H integral: area under the dynamic de-trended NAD(P)H curve. Specifically, we defined a Cox proportional hazard model (Cox, 1972) for START by means of its hazard function, $\lambda(t|Z) = \lambda_0(t)e^{\beta Z(t)}$, where Z(t) is the relevant characteristic of the time-dependent signal and λ0 is the baseline hazard function. This model described the instantaneous cell cycle transition probability as a combination of an underlying baseline event probability across time and a covariate dependent hazard multiplier. The analysis was performed in R, using the coxph function in the survival package. The correlation and thus predictive power of the estimated metabolic NAD(P)H characteristics on cell cycle progression was statistically evaluated, using the Akaike Information Criterion (AIC), R2 and the likelihood ratio test. Here, we found the NAD(P)H integral to have the highest predictive power for START. Next, we estimated the probability for START as a function of the time-dependent metabolic integral of the NAD(P)H signal from the last M exit, separately in the dividing and the non-dividing cells. The sensitivity of our model predictions was validated using a ROC (receiver operating characteristic) analysis (Pepe, 2007).

Supplemental Tables

Table S1: Yeast strains developed and/or used in this study.

Strain	Genotype	Source
YSBN6	YSBN6 wild type	Steve Oliver lab, Cambridge
YSBN16	YSBN6 his3Δ1	(Kümmel et al., 2010)
YSBN6.6CB.2B	ho::yEGFP-TetR-KanMX4	This study
YSBN6.G5A.2B	ho::ATeam1.03-TetR-KanMX4	This study
YSBN6.TEFATP.1B	ho::TEF1p-ATeam1.03-KanMX4	This study
YSBN16 Whi5-GFP	YSBN16 Whi5::eGFP-HIS3MX6	This study
YSBN16 Cln2-GFP	YSBN16 Cln2:: eGFP-HIS3MX6	This study
YSBN6.G2J	YSBN6 ho::ADH1p-OsTIR1-mGFP-KanMX4	This study
BY25598	W303-1a Ura3-1::ADH1-OsTIR1-9Myc(URA3)	(Nishimura et al., 2009) NBRP, Japan
YSBN6.OsTIR1w/oGFP	YSBN6 ho::ADH1p-OsTIR1-KanMX4	This study
YSBN6.OsTIR1w/oGFP.G23A	YSBN6 ho::ADH1p-OsTIR1-KanMX4 Cdc14::mCherry-AID$^{71-114}$-natMX	This study
KOY.TM6*P hxk2-GFP hta2-mRFP1	KOY.TM6 Hta2::mRFP1-Ble Hxk2::eGFP-KanMX4	(Schmidt, 2014)

YSBN16.Whi5-eGFP.Hta2-mRFP1.OsTIR1w/oGFP.G23ARFPex	YSBN16 ho::ADH1p-OsTIR1-KanMX4 Whi5::eGFP-HIS3MX6 Hta2::mRFP1-Ble Cdc14::mCherry-AID$^{71-114}$-natMX	This study

Table S2: Primer sequences used for the development of all recombinant strains.

The underlined sequences correspond to the overhangs designed for CPEC and/or Gibson assembly. The term "gDNA" stands for purified genomic DNA.

Primer	Fwd/Rev	Sequence (5´ to 3´)	Templates
HO	Fwd	CGGGTTAATTAAGGCGCGCCAG	HO-poly-KanMX-HO plasmid (Voth et al., 2001)
	Rev	CAGCGTACGACGCCATTTTAAGTCC	
HO-TetEX	Fwd	GGACTTAAAATGGCGTCGTACGCTGAGCTGGATCTTCGAGCGTCC	pINV plasmid (Blount et al., 2012)
	Rev	GATCTGGCGCGCCTTAATTAACCCGCAGCTGGAATTCCACACCATAGC	
TetEX	Fwd	CATTTTAATAACTAGTAGTTGGGTTCTCTATC	pC6B plasmid (This study)
	Rev	CTCGAGTAAGCTTGGTACCG	
ATP	Fwd	CGCGGTACCAAGCTTACTCGAGTCATTCAATGTTATGTCTAATTTTGAAGTTGG	pMK-RQ (KanR) – ATeam 1.03 (Imamura et al., 2009) (yeast codon opt)
	Rev	GTGATAGAGAACCCAACTACTAGTTATTAAAATGGTTTCTAAGGGTGAAGAATTATTCAC	
TEFATP	Fwd	CTAGGAAACTTAGATTAGATTGCTATGC	pG5A plasmid (This study)
	Rev	GTTATTAAAATGGTTTCTAAGGGTGAAG	

Seq4	Fwd	AATTATCCTGGGCACGAG	pC6B plasmid pG5A plasmid pTEFATP plasmid (This study) (linearization / verification)
	Rev	ACTGTAAGATTCCGCCAC	
Whi5	Fwd	CACGTCGCTATCACAACAG	H10 clone -GFP collection genomic DNA (Huh et al., 2003)
	Rev	CAAGGTTAAGCCTAGTGGCA	
Cln2	Fwd	AAATCACGGGTCCTAACAGC	G3 clone-GFP collection genomic DNA (Huh et al., 2003)
	Rev	ATGTCGTCGCTTCTTATCCC	
Seq1	Fwd	GGAGTATTGTGTCATGTTCG	pC6B plasmid pG5A plasmid pG1J plasmid pG2J plasmid pOsTIR1w/oGFP plasmid YSBN6.6CB.2B gDNA YSBN6.G5A.2B gDNA YSBN6.TEFATP.1 B gDNA (This study) (verification)
Seq1	Rev	CGAGTAAGCTTGGTACCG	
Seq2	Fwd	TTGAAGCTATGGTGTGG	
Seq2	Rev	GACAGTCACATCATGCC	
Seq3	Rev	GAGGTCGCTCCAATTCC	
Seq5	Fwd	GGGTCCAGCAATACTTTGA	YSBN6.6CB.2B gDNA YSBN6.G5A.2B gDNA YSBN6.TEFATP.1 B gDNA YSBN6.G2J gDNA YSBN6.OsTIR1w/ oGFP gDNA
	Rev	CCTGAAGTCTAGGTCCCTAT	
Seq6	Fwd	GACATCATCTGCCCAGA	
	Rev	CCGGTAACGCTTTTTGTATC	

			(This study) (verification)
Whi5Ver	Fwd	CTTCTGGTGCTAAAGGGAAG	YSBN16 Whi5-GFP gDNA (This study) (verification)
	Rev	GACGACAATAGCATCAGTGT	
Cln2Ver	Fwd	AACATCTACTTTACTTCATCGTCA	YSBN16 Cln2-GFP gDNA (This study) (verification)
	Rev	CGTCTACAGTGGCATCACTA	
C6B	Fwd	CTCGCCCTTGCTCACCATTTTAATAACCTAGGAAACTTAGATTAG	pC6B plasmid (This study)
	Rev	AAGGTATCACCCGGGTAACTCGAGTAAGCTTGGTACC	
AID	Fwd	AGCTTACTCGAGTTACCCGGGTGATACCTTC	#2189 plasmid (Morawska and Ulrich, 2013)
5GA	Rev	GACGAGCTGTACAAGGTCGACGGTGCAGG	
mGFP	Fwd	GCCTGCACCGTCGACCTTGTACAGCTCGTCCATG	pHIPZ-mGFP-fusionator plasmid (Saraya et al., 2010)
	Rev	TAGGTTATTAAAATGGTGAGCAAGGGCGAG	
ADH1	Fwd	CCTTTGGACTTAAAATGGCGGGGTGTACAATATGGACTTCC	BY25598 gDNA (Nishimura et al., 2009)
AtTIR1	Rev	AAGATCCAGCTCAGCGTACGAGCGACCTCATGCTATACC	
G1JBkbn	Fwd	AGGTATAGCATGAGGTCGCTCGTACGCTGAGCTGGATC	pG1J plasmid (This study)
	Rev	GAAGTCCATATTGTACACCCCGCCATTTTAAGTCCAAAGGC	
ADH1TT	For	AAGATCCAGCTCAGCGTACGAGCGACCTCATGCTATACC	pC6B (This study)

ADH1TT	Rev	ACTTCGTCAAGATTTTATGAAACAATTC TTCGCCAGAGG	
Prim1	For	AGATCTGTTTAGCTTGCCTC	pG2J plasmid (This study)
Prim2	Rev	CGTACGAGCGACCTCAT	
Seq7	Rev	ACAAGCTGGAGTACAACTAC	pG1J plasmid pG2J plasmid pOsTIR1w/oGFP plasmid (This study) (verification)
Seq8	Rev	GATCCACTAGTTCTAGAGCG	
Seq9	Rev	TCTAGGGTGTCGTTAATTACC	
IAA	Fwd	GCATGGACGAGCTGTACAAGGTCGACG GTGCAGG	#2189 plasmid (Morawska and Ulrich, 2013)
	Rev	ACGCCGCCATCCAGTGTCGACGTACGCT GAGCTGGA	
mCherry	Fwd	TCGACACTGGATGGC	pBS35 plasmid (Hailey et al., 2002)
	Rev	AGCTTGCCTTGTCCC	
Nat	Fwd	ATGGTGAGCAAGGGCGA	pAG36 plasmid (Goldstein and McCusker, 1999)
	Rev	CTTGTACAGCTCGTCCATGC	
Cdc14CDS	Fwd	TTATGCTTCCGCGGCTCGTATGTTGTGTG GAATTAAGAGATTTAACCATGACGCCG	YSBN6 wt gDNA YSBN6.OsTIR1w/ oGFP.G23A gDNA (This study)
	Rev	CATGTTATCCTCCTCGCCCTTGCTCACCA TTTTCTTGATGGAGCCACTTATTTTTCT	
Cdc14 DOWN	Fwd	CCGGGTGACCCGGCGGGGACAAGGCAA GCTCAGTGTCCCTTCTCGCTG	
	Rev	GTTCCAGTTTGGAACAAGAGTCCACTAT TACCATGACGGAGATAATGACACTA	
Amp	Fwd	TAATAGTGGACTCTTGTTCC	pG2J plasmid (This study)
	Rev	CCACACAACATACGAGC	

Cdc14LinRFPex	Fwd	GTCGACGGTGCAGG	pG23A plasmid (This study)
	Rev	TTTCTTGATGGAGCCACTT	
Seq101	Fwd	ATGACGAATCCATGCAGG	pG23ARFPex (This study) (verification)
Hta2Lin	Fwd	CAATTTCGACTGCATGATGC	KOY.TM6*P hxk2-GFP hta2-mRFP1 gDNA (Schmidt, 2014)
	Rev	GGAAGAACTACGCACTCTTTC	

Supplemental Text

Text S1: Validation of FRET-based dynamic ATP measurements in single, unsynchronized yeast cells.

So far, the ATeam 1.03 FRET sensor has only been applied for the short-term (approx. 17 min) measurement of the intracellular ATP levels in single yeast cells (Bermejo et al., 2010). Here, we used a yeast codon-optimized version of the ATeam 1.03 FRET sensor to investigate if ATP levels oscillate. Because there could be numerous issues with FRET sensors (for instance sensitivity to redox or pH), we checked whether the FRET signals that we measured indeed reported intracellular ATP levels.

First, we estimated the intracellular ATP concentration range in our cells using the measured FRET ratios and a calibration curve from the literature (Imamura et al., 2009) (cf. Figure S1D). Here, we found that the thereby estimated intracellular concentrations of ATP (between 3.5 mM and 6 mM; Figure S1E) matched those determined in metabolomics experiments (Canelas et al., 2009; Walther et al., 2010). Second, we compared our measured ATP dynamics with the enzymatically determined ATP oscillations observed in synchronized chemostat cultures (Müller, 2006) (Figure S1F). For the comparison, we used the budding indexes as reported in these chemostat experiments (Figure S1G), which we converted into budding rates (Figure S1H). In the chemostat culture the budding rate was highest when the ATP levels dropped (Figure S1F-H). This behavior is consistent with our single-cell ATP measurements where budding occurred at the descending part of the ATP oscillators, after the peak (Figures S1E and S8B). These comparative analyses demonstrate that our single-cell ATP FRET measurements indeed reflect intracellular ATP levels.

Text S2: The metabolic oscillations are not caused by the process of budding.

One could speculate that the observed NAD(P)H and ATP oscillations that we found in frequency synchrony with budding might just be a consequence of volume variations during the cell cycle (e.g. budding and cytokinesis). Here, we demonstrate that the metabolite oscillations are not caused by volume oscillations, but constitute an intrinsic cyclic metabolic behavior: Firstly, the NAD(P)H and ATP oscillations occur also in the absence of budding and cell division, when no periodic changes in cell morphology or volume occur (Figure S4A-C, Movie S2). Secondly, the NAD(P)H and ATP oscillations occur oppositely in phase (Figure S8A-B). If the metabolic oscillations were the result of volume variations and budding, rather than an intrinsic cyclic metabolic behavior, all measured metabolites would have shown oscillations that are in phase.

Supplemental Figures

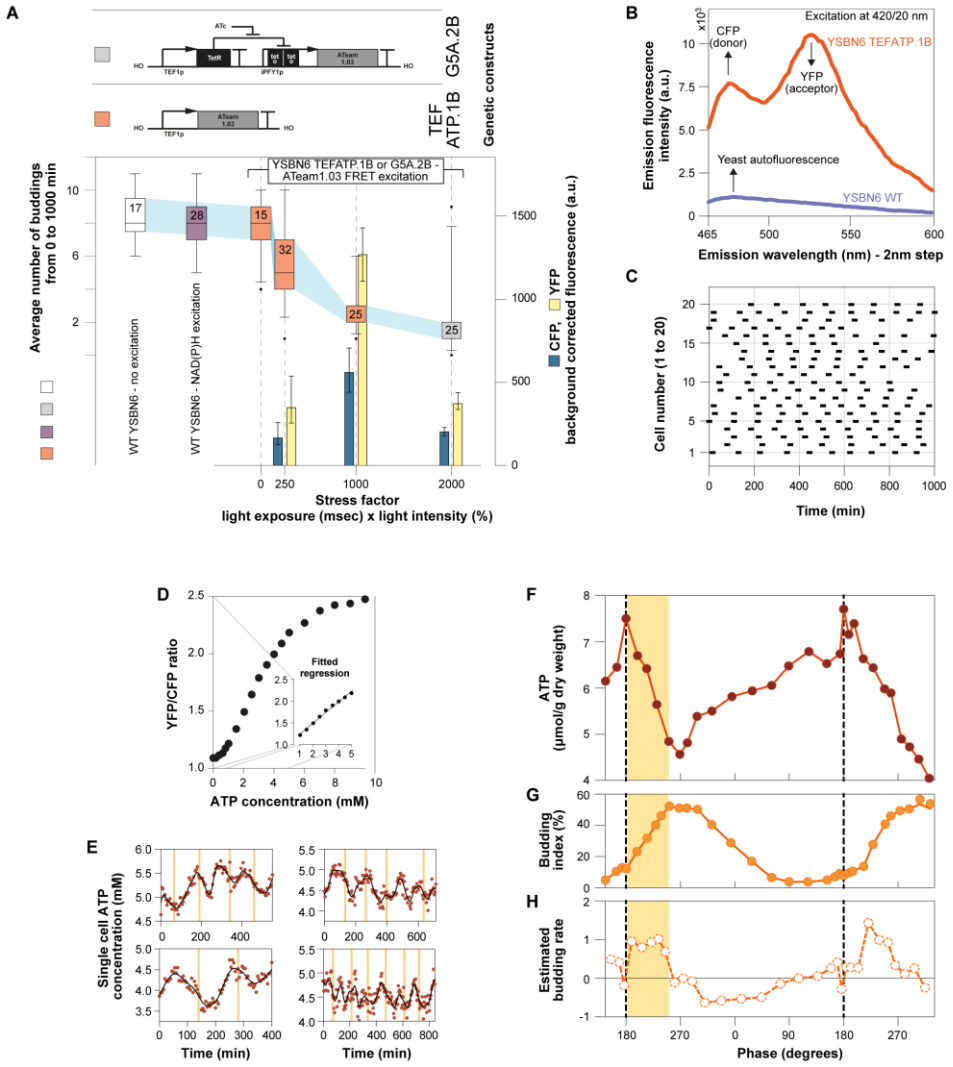

Figure S1: Establishing and validating the FRET-based, dynamic ATP measurements in single, unsynchronized yeast cells. This supplementary figure demonstrates that with optimized expression and light exposure ATP FRET signals can be obtained from single cells with limited negative effects on cell growth **(A)**, shows the fluorescence spectra of the cells expressing the FRET sensor compared to the cellular background fluorescence **(B)**, demonstrates that in the microfluidic chip cells are not synchronized **(C)**, shows the linear range used for the ATP FRET signal calibration **(D)**, and finally shows the estimated ATP concentration range and the related budding occurrence in our single cell measurements **(E)** in comparison to previously reported ATP **(F)** and budding **(G, H)** time series measured in synchronized yeast populations. Specifically: **(A)** Optimization of imaging settings to measure NAD(P)H and ATP levels in single cells. The NAD(P)H excitation does not have any

significant effect on the viability of single yeast cells as shown by a comparison of the average number of buddings during the first 1000 min of growth in the microfluidics device, estimated from 28 YSBN6 wild type cells subjected to NAD(P)H and brightfield imaging every 5 min (purple box), and 17 YSBN6 wild type cells imaged only in the brightfield channel every 5 min (white bar). The error bars represent the 5% to 95% percentiles and the numbers in each box correspond the number of cells used for the respective analysis. Towards optimizing imaging of ATP levels, we developed two expression cassettes for the ATeam 1.03 ATP FRET sensor (Imamura et al., 2009) (G5A.2B and TEF ATP.1B – Table S1, see panel) and integrated them into the yeast genome. The construct with the tetracycline inducible moderate promoter iPFY1 (Blount et al., 2012) (grey box in panel) allowed for tuning the expression levels of the sensor by changing the tetracycline concentration in the medium. In the other genetic construct (red boxes), the sensor's expression was driven by the strong constitutive TEF1 promoter, thus allowing for a strong expression of the sensor. As a quantitative measure of the phototoxic effect of CFP excitation, we defined a 'stress factor', estimated as the product of the percent light intensity of the excitation light source and the exposure time in milliseconds for a fixed image acquisition frequency of 1 image per 5 minutes. We found the 'stress factor' to have a significant effect on viability which was defined as the average number of buds produced during 1000 min of image acquisition. However, by expressing the ATP sensor via the strong constitutive promoter (TEF1p), we achieved sufficient signal intensities with marginal effects on growth (number of buddings per 1000 minutes). Thus, through a combination of excitation light intensities and exposure times, and optimized expression of the ATeam 1.03 ATP sensor, we managed to identify imaging conditions (5%, 50msec, pTEF1-ATeam1.03) for the long-term ATP measurements in single yeast cells. **(B)** The emission spectrum of YSBN6.ATPTEF.1B cells (Table S1) (red) was measured using a plate reader (TECAN Spark 10M) to confirm the excitation of the acceptor (YFP) by the donor (CFP) module in the ATeam1.03 FRET sensor, and thus its functionality in vivo. **(C)** The random distribution of the budding events between cells, over the time course of 1000 min, demonstrates the absence of cell cycle synchronization in our microfluidic device. Budding occurrence was measured in 20 cells, all grown in the same microfluidic device on high glucose (10 gL^{-1}). Each marker (black line) corresponds to a budding event and each row to a monitored single cell. **(D)** The previously published (Imamura et al., 2009) calibration curve of the ATeam 1.03 ATP sensor, and fitted a linear regression in the YFP/CFP ratio range from 1.2 to 2.2, with which we estimated the ATP levels in our cells. **(E)** The calibration curve was used to estimate the oscillating ATP levels, as shown here in six single cells growing on 10 gL^{-1} glucose in the microfluidics device. **(F)** Published ATP data from synchronized yeast populations in glucose-limited chemostat cultures determined enzymatically (Müller, 2006). Here, the ATP levels oscillate in synchrony with the **(G)** budding index, namely the percentage of the budding cells. We converted the time in phase, by defining 360 phase degrees between two consecutive peaks of the reported oscillating ATP signal and budding index. **(H)** Using the first derivative of the budding index as a proxy of the budding frequency in the synchronized population, we found the highest budding frequencies (yellow shaded region) to coincide with decreasing part of the ATP oscillations, similar to what we found with the ATP FRET sensor in single cells, cf. **(E)**.

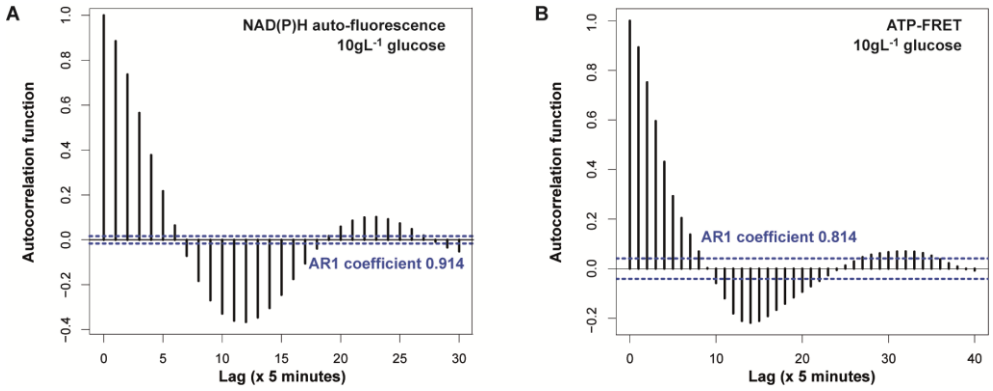

Figure S2: An autocorrelation function analysis confirmed that NAD(P)H and ATP signals oscillate in single cells. We performed the autocorrelation function analysis on **(A)** NAD(P)H (137 metabolic oscillations from 29 single cells) and **(B)** ATP (66 metabolic oscillations from 12 cells) signals from cells growing in high ($10gL^{-1}$) glucose, using the R software and the acf function. Here, we found a period of approximately 125 min for NAD(P)H and 165 min for ATP (time lag required for the correlogram to complete a full oscillation). The longer estimated periodicity for the ATP compared to the NAD(P)H signals is the result of the stress caused by the CFP (ATP-FRET donor) excitation (Figure S1A – stress factor 250). The black vertical lines correspond the sampled autocorrelations for each time lag. The blue dashed lines indicate the 95% significance bounds, outside of which the null hypothesis that there is no auto-correlation is rejected. Consequently, only results above or below the blue dashed lines indicate a significant periodicity, and all results within the blue dashed lines are due to noise. The autocorrelation coefficient (AR1) corresponds to the correlation of the first order auto-regression of our time series, and was estimated by regressing the observation at time t-1 onto the observation at time t. The AR1 coefficient shows the amount of self-similarity of one signal to the next, from which the amount of noise in the signal can be deduced. From the AR1 coefficients, it can be seen that the noise levels of the NAD(P)H signals (AR1=0.914) are lower compared to the ATP signals (AR1 = 0.814). As a result, the estimation of the periodicity in the ATP compared to the NAD(P)H signals is more noisy (blue dashed lines in Figure S2A-B). This can be explained by the fact that the NAD(P)H levels are directly estimated on the basis of the metabolite's auto-fluorescence, whereas the ATP levels are determined indirectly using a radiometric optical sensor and involves the ratio of two noisy measurements (acceptor/donor fluorescence). The higher noise in the estimation of ATP compared to NAD(P)H oscillation periods is responsible for the lower R2 value in the ATP-budding correlation compared to the NAD(P)H budding correlation as shown in Figure 1C.

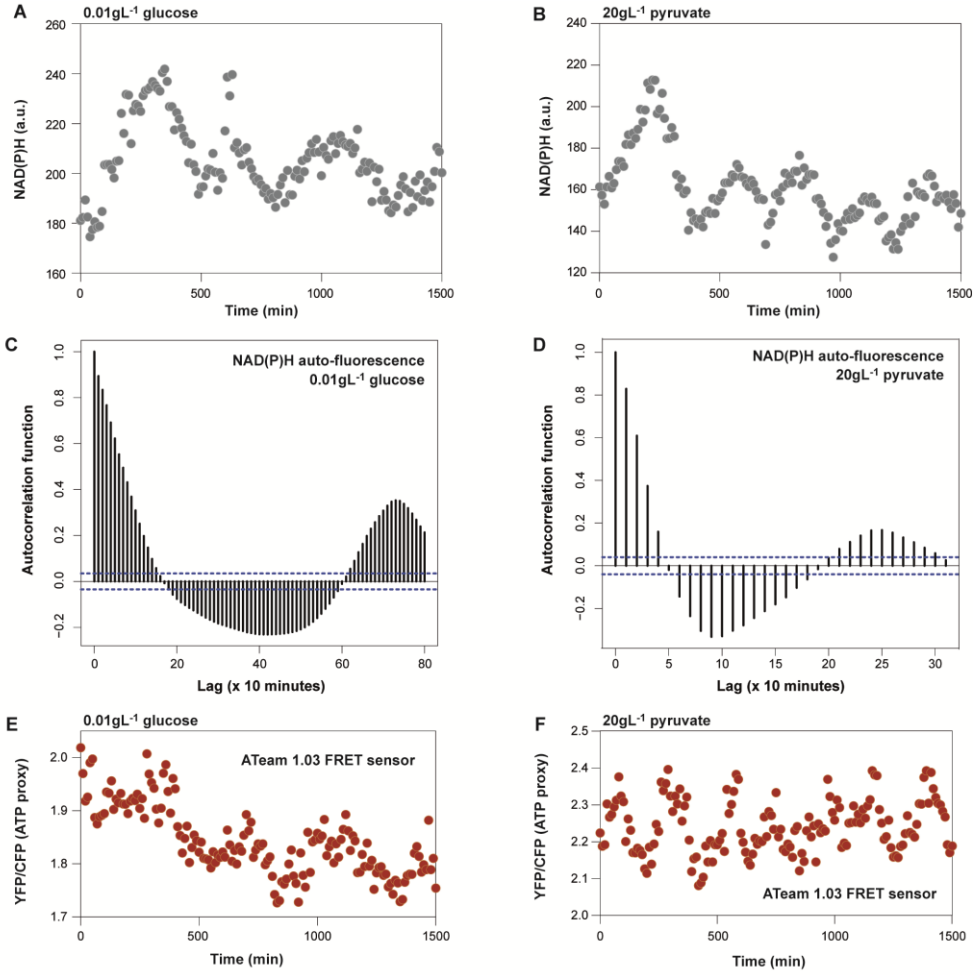

Figure S3: Metabolic oscillations occur also under respiratory growth on glucose and gluconeogenic growth on pyruvate. Single-cell background corrected NAD(P)H oscillations during **(A)** respiratory growth on low glucose and **(B)** gluconeogenic growth on pyruvate. Autocorrelation function analyses demonstrated the existence of metabolic oscillations with an average period of **(C)** 700 min on low glucose (94 cells) and **(D)** 270 min on pyruvate (12 cells) (time lag required for the correlogram to complete a full oscillation). Single-cell ATP oscillations measured using the ATP FRET sensor **(E)** during respiratory growth on low glucose, or **(F)** gluconeogenic growth on pyruvate.

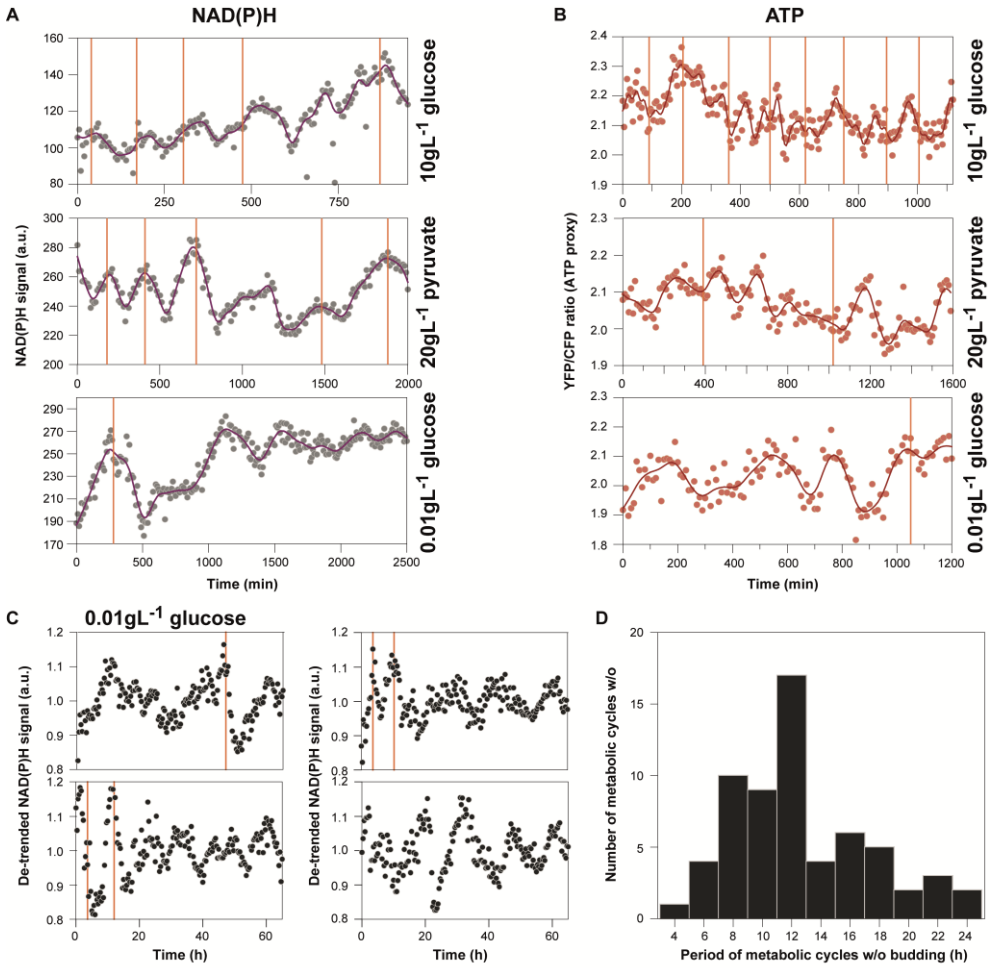

Figure S4: Metabolic oscillations in the absence of budding occur in all tested growth conditions, but most frequently on 0.01 gL^{-1} glucose. (A) Oscillatory NAD(P)H signals from three single cells growing on high glucose (10 gL^{-1} glucose - top), pyruvate (20 gL^{-1} pyruvate – middle) or low glucose (0.01 gL^{-1} glucose – bottom), and the related budding events (vertical orange lines), where at certain metabolic oscillations no budding occurred. **(B)** Oscillatory ATP signals from single cells growing on high glucose (10 gL^{-1} glucose - top), pyruvate (20 gL^{-1} pyruvate – middle), or low glucose (0.01 gL^{-1} glucose – bottom), and the related budding events (vertical orange lines), where at certain metabolic oscillations no budding occurred. **(C)** A collection of four cells with sustained metabolic oscillations without budding during growth on low glucose (0.01 gL^{-1}) (see also Movie S2). The NAD(P)H signals were de-trended by dividing by a fitted smoothing spline. **(D)** Histogram of the frequency distribution of the periods of 63 metabolic oscillations without budding from 14 cells growing on low glucose and exhibiting multiple subsequent oscillations without budding. The period of each oscillation was estimated from the time between two consecutive troughs. This data shows that the autonomous metabolic oscillator can cycle at broadly different periods ranging from 3 to 25 hours with periods of 12 hours occurring most frequently in cells without cell cycle on low glucose.

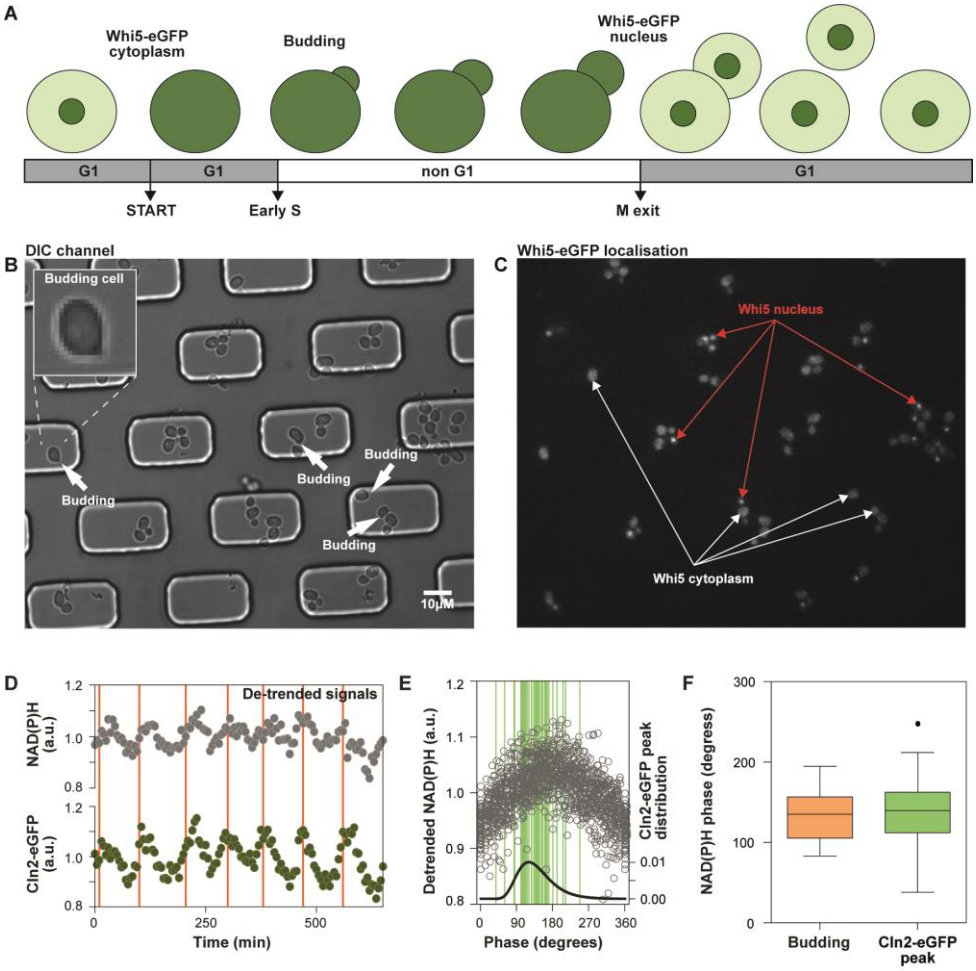

Figure S5: Illustration and validation of single cell reporters used to resolve the three cell cycle events START, early S and Mitotic exit. (A) Whi5-eGFP transfer to the cytoplasm and transfer to the nucleus is used to indicate START of the cell cycle in the late G1 phase and mitotic exit (Ball et al., 2011; Costanzo et al., 2004; Ferrezuelo et al., 2012), respectively. Budding has been shown to correlate with the early S phase (Ball et al., 2011; Fatima and Kim, 1993). **(B)** Illustration of how DIC images were used to determine the time-points were budding occurred (white arrows) and thus the early S phase. In the top left corner, a magnified image of a budding cell is shown. **(C)** Exemplary image of the GFP channel used to capture the Whi5-eGFP localization in the nucleus (red arrows) or the cytoplasm (white arrows). **(D)** NAD(P)H and Cln2-eGFP oscillations in a single yeast cell. The orange vertical lines indicate budding. **(E)** Comparison of the distribution of the Cln2-eGFP peaks with the NAD(P)H phase. 50 NAD(P)H oscillations from 4 single cells were de-trended by dividing over a fitted smoothing spline to remove the low frequency noise. The de-trended signals were aligned by converting time into phase and superimposed. The green vertical lines indicate the peaks of the Cln2-eGFP oscillations on the respective NAD(P)H phases. A lognormal distribution (black solid line) describes the density distribution of the Cln2-eGFP peaks. **(F)** A Tukey box plot indicating

the NAD(P)H phase, at which budding and the Cln2-eGFP peak occurred on high glucose. 31 buddings are included from 5 single cells, and 50 Cln2-eGFP oscillation peaks from 4 single cells. With the levels of the Cln2 reaching a maximum in the early S phase (Ball et al., 2011; Fatima and Kim, 1993), and budding occurring at the same moment as Cln2 peaks, these observations suggest that budding is a good indicator of the early S phase. Because the Cln2-eGFP signals are noisy and peak identification is thus difficult, and recording of Cln2-eGFP signals also requires additional light exposure of the cells, we used the easy-to-identify bud appearance as reporter for the early S phase.

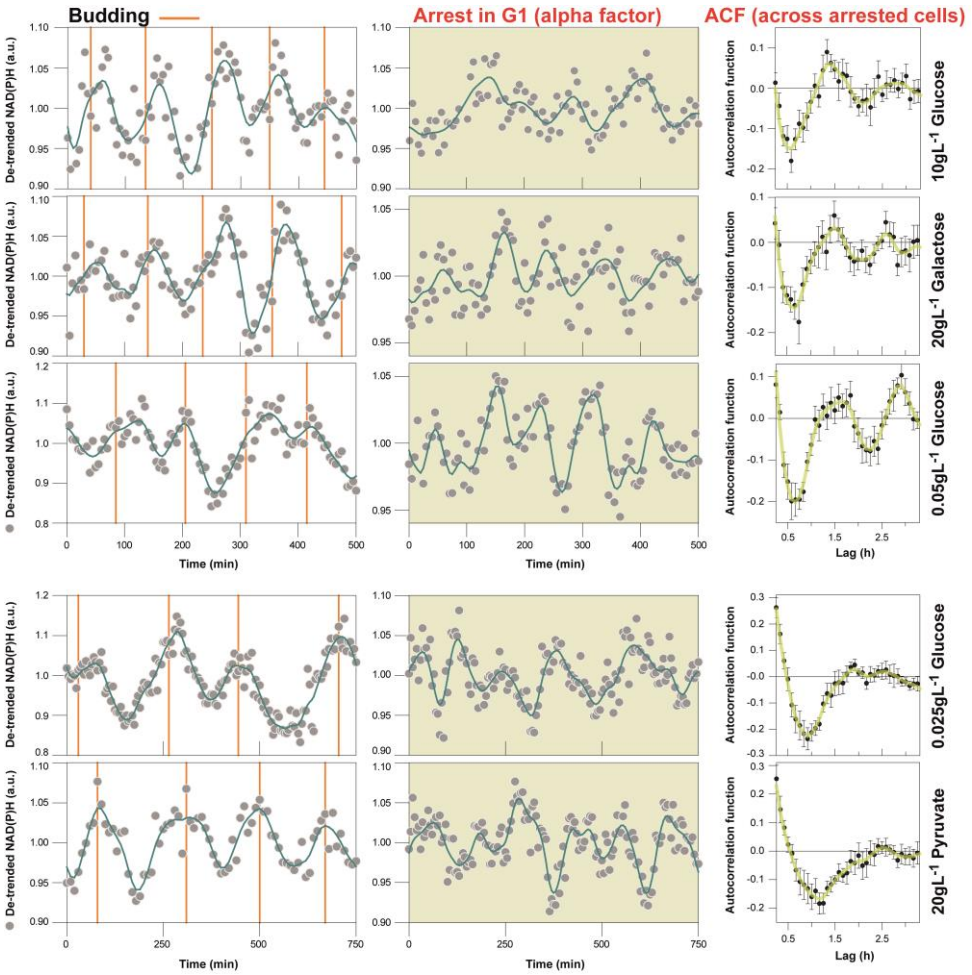

Figure S6: Metabolism continues to oscillate in alpha factor arrested cells, across nutrient conditions. Single cell NAD(P)H signals in dividing (left column) and cell cycle arrested cells (alpha factor, middle column), on 10 gL^{-1} glucose, 20 gL^{-1} galactose, 0.05 gL^{-1} glucose, 0.025 gL^{-1} glucose and 20 gL^{-1} pyruvate (top to bottom). Autocorrelation function analyses was performed to confirm periodicity in the cell cycle-arrested cells at each condition (right column). The autocorrelation function analysis was first applied for each single cell, and then the average correlogram was plotted (error bars: standard error of the mean).

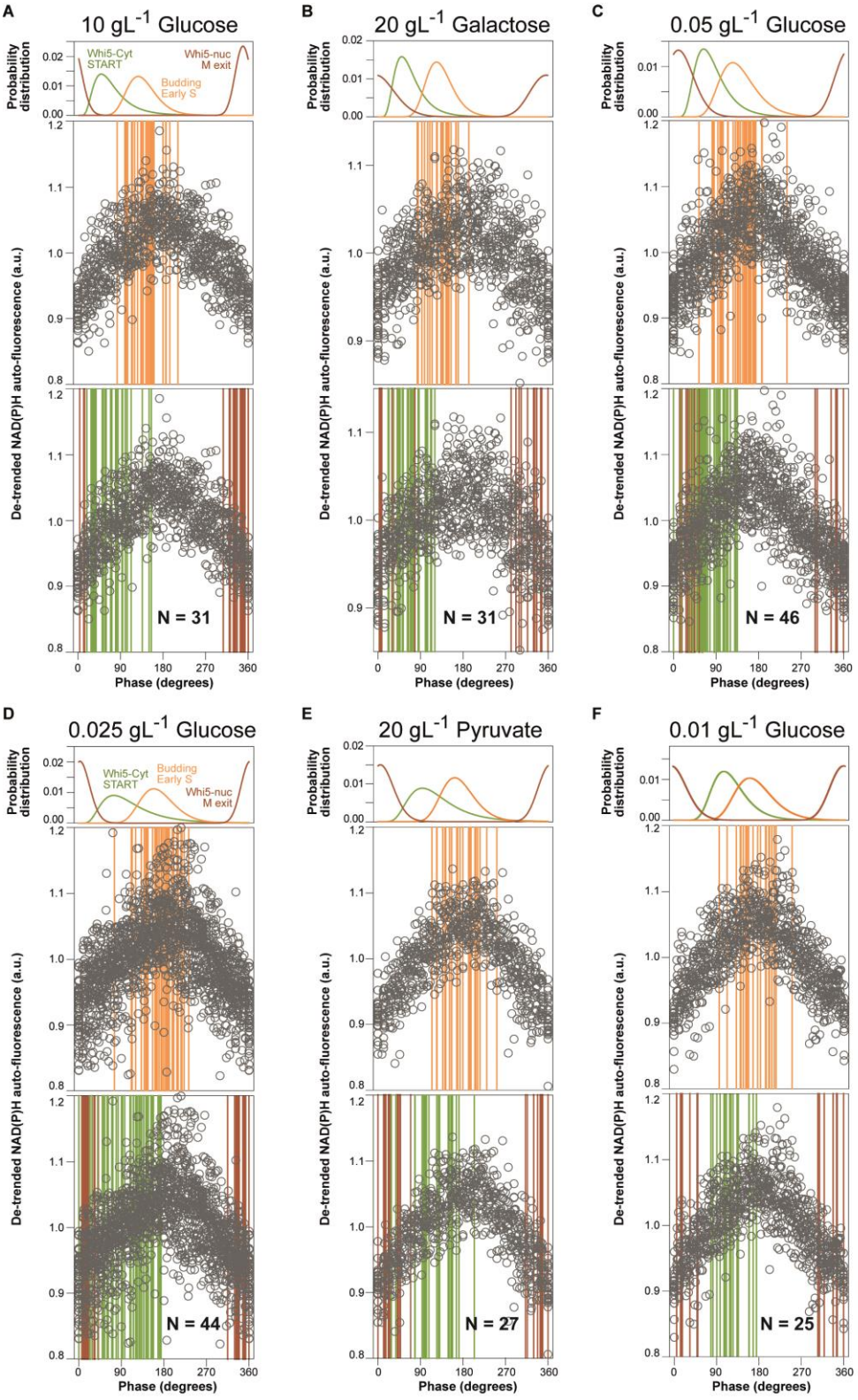
A
10 gL-1 Glucose
B
20 gL-1 Galactose
C
0.05 gL-1 Glucose
D
0.025 gL-1 Glucose
E
20 gL-1 Pyruvate
F
0.01 gL-1 Glucose
Probability distribution
Whi5-Cyt START
Budding Early S
Whi5-nuc M exit
De-trended NAD(P)H auto-fluorescence (a.u.)
Phase (degrees)
N = 31
N = 31
N = 46
N = 44
N = 27
N = 25

Figure S7: The measured cell cycle events are in synchrony with the NAD(P)H oscillations, and occupy specific NAD(P)H phase regions, partly varying with nutrient condition. **(A)** Occurrence of the cell cycle phases (START, Early S, M exit) determined through Whi5-eGFP transfer and budding with respect to the NAD(P)H oscillations on high glucose conditions (10 gL^{-1}). 31 de-trended NAD(P)H oscillations from 5 different cells expressing Whi-eGFP were superimposed by converting the time into phase. Lognormal distributions describe the occurrence of Whi5 location change (red, into the nucleus; green, out of the nucleus) and budding events (orange). **(B)** The same as for cells grown on galactose (20 gL^{-1}) with 31 NAD(P)H oscillations from 8 cells, **(C)** on 0.05 gL^{-1} glucose with 46 NAD(P)H oscillations from 16 cells, **(D)** on 0.025 gL^{-1} glucose with 44 NAD(P)H oscillations from 4 cells, **(E)** on pyruvate (20 gL^{-1}) with 27 NAD(P)H oscillations originating from 26 single cells and **(F)** on low glucose conditions (0.01 gL^{-1}) with 20 NAD(P)H oscillations originating from 13 single cells.

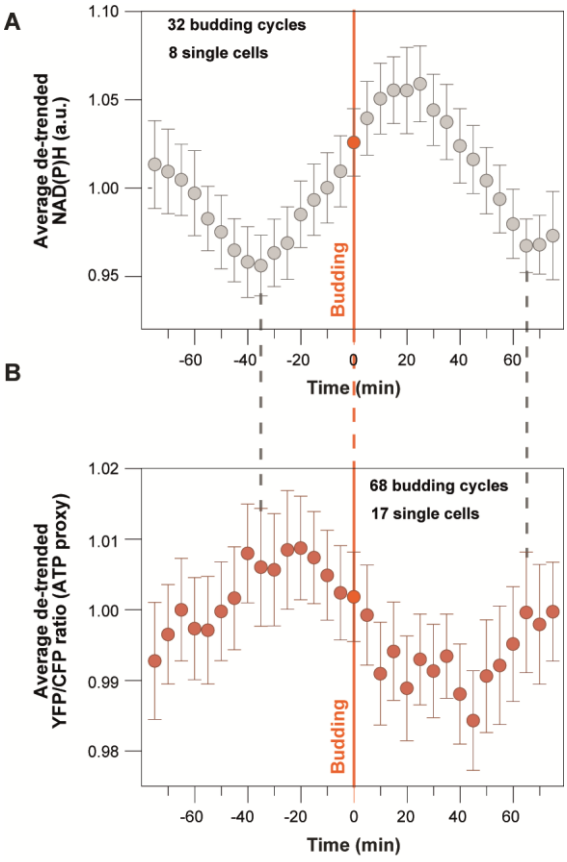

Figure S8: The NAD(P)H and ATP oscillations are opposite in phase. **(A)** Averaged and de-trended NAD(P)H signals from 8 cells (each with 4 oscillations) growing on 10 gL^{-1} glucose, aligned with budding (at 0 min). Error bars represent the 95% confidence intervals of the mean. **(B)** Averaged and de-trended ATP signals from 17 cells (each with 4 oscillations) growing on 10 gL^{-1} glucose, aligned with budding (at 0 min). Error bars represent the 95% confidence intervals of the mean. The grey dashed lines allow for a comparison between the phases of the NAD(P)H and ATP signals. These data showed that the ATP oscillations are opposite in phase to the NAD(P)H oscillations and as such demonstrated that the observed oscillations in the metabolite levels are not the mere result of volume variation and cell division.

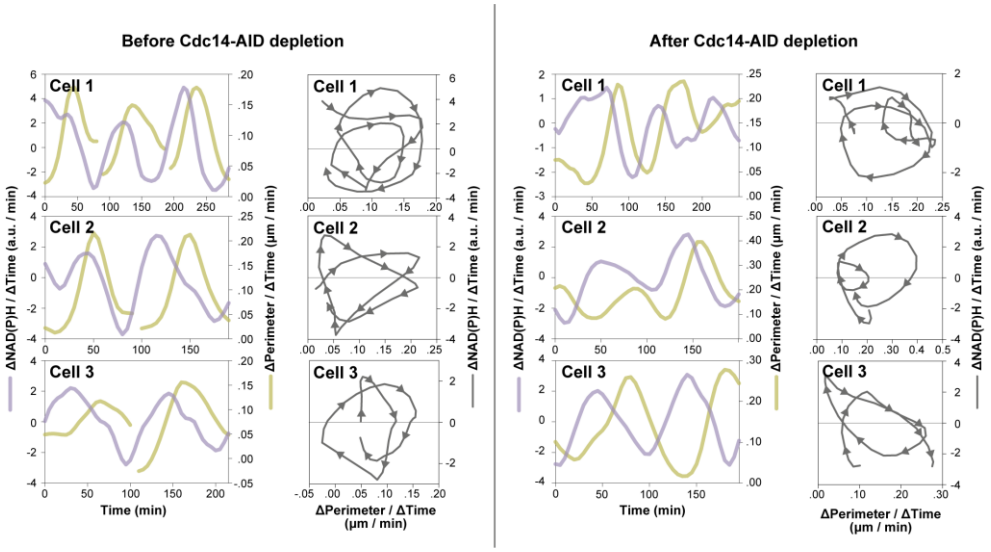

Figure S9: The rate of NAD(P)H oscillates in synchrony with the perimeter increase rate, in normally dividing and late cell cycle arrested cells. Dynamic time derivates of NAD(P)H and perimeter from 6 single cells: 3 normally dividing cells (before Cdc14-AID depletion - left) and 3 late cell cycle arrested cells (after Cdc14-AID depletion – right). The NAD(P)H rates correspond to the first derivative of the detrended and smoothed NAD(P)H signals. The perimeter derivatives were estimated on the basis of the smoothed single cell perimeter data. The NAD(P)H rates oscillate in synchrony with the waves of perimeter increase. The corresponding phase plots (clockwise trajectories) demonstrate the condition-independent (before and after Cdc14-AID depletion) phase correlation between the two signals.

Supplemental Movies

Movie S1: NAD(P)H oscillations in synchrony with cell division in a single yeast cell. The NAD(P)H auto-fluorescence (left – NAD(P)H channel) of a single yeast growing on 20g L^{-1} pyruvate is presented in synchrony with budding (right – DIC channel). The background corrected NAD(P)H signal of the same cell is also plotted at the bottom. Orange vertical lines indicate budding occurrence.

Movie S2: NAD(P)H oscillations measured in non-dividing, quiescent cells on 0.01 gL^{-1} glucose – the metabolic oscillations are not the result of budding or cell volume fluctuations. Four cells supplemented with 0.01g L^{-1} glucose minimal medium. The cells exhibit metabolic oscillations in the absence of periodic volume fluctuations (e.g. budding – vertical orange lines). The same metabolic signals are presented in Figure S4C.

Movie S3: NAD(P)H oscillations in the absence of budding during the G1 phase. Microscopy time-lapse movies of a single cell, expressing the eGFP tagged transcriptional repressor Whi5, in the DIC (left movie) and GFP (right movie) channels. In the GFP channel, the cycles of Whi5 localization in and out of the nucleus indicative of the G1 and non-G1 phases of the cell cycle, respectively, can be seen; below the NAD(P)H signal of the same single cell. Between 500 and 1250 min, and while Whi5 is localized in the nucleus indicating the G1 phase, NAD(P)H oscillations persist in the absence of budding and thus cell cycle (see also Figure S2B).

Movie S4: NAD(P)H oscillations in the absence of budding during the non-G1 phase. Microscopy time-lapse movies of a single cell, expressing the eGFP tagged transcriptional repressor Whi5, in the DIC (left movie) and GFP (right movie) channels. In the GFP channel, the cycles of Whi5 localization in and out of the nucleus indicative of the G1 and non-G1 phases of the cell cycle, respectively, are shown; below the NAD(P)H signal of the same single cell. After 1200 minutes, the cell continues with NAD(P)H oscillations in the absence of budding in the non-G1 (Whi5-eGFP in the cytoplasm) as well as G1 (Whi5-eGFP in the nucleus) cell cycle phases.

Movie S5: Demonstration of dynamic Cdc14 depletion. 2 populations of single yeast cells are grown and monitored in the microfluidic device. The green cells (YSBN6.G2J) constitutively expressed mGFP tagged with the $AID^{71\text{-}114}$ degron sequence. They were used as a marker of protein depletion due to the addition of 0.1 mM of auxin at 04:00 (hh:mm). The rest of the cells (YSBN6.OsTIR1w/oGFP.G23A – Table S1) expressed Cdc14 fused with mCherry and tagged with the $AID^{71\text{-}114}$ degron sequence. The localization of Cdc14 in the nucleolus (red signal) is evident. Cdc14-mCherry-AID and mGFP-AID are depleted at the same time (at 05:30 hh:mm) as a result of auxin addition. After the depletion of Cdc14-mCherry-AID, M exit is not activated in the respective strain, meaning that they cannot complete mitosis and cytokinesis, thus exhibiting filamentous growth. The cells that had mGFP tagged with the degron sequence, continued to grow normally.

Movie S6: When M exit is halted (Cdc14 depletion) cycles of biomass synthesis continue in synchrony with the metabolic oscillations. A single cell expressing Cdc14 tagged with mCherry and the degron sequence AID^{71-114}. The auxin (0.1 mM IAA) induced Cdc14 depletion, as monitored in the indicated (white arrow) single cell, is plotted (top left). Despite the Cdc14 depletion and halting of the late cell cycle (M exit), metabolic oscillations persisted (middle left). At the same time the cellular perimeter increased in waves (bottom left), indicating cycles of biomass synthesis even in the absence of M exit. Each wave of biomass synthesis was accompanied by one metabolic oscillation. The yellow shaded regions across all three plots mark the increasing rate of cellular perimeter, the same region where budding occurs in normally dividing cells (Figure 6C). The time stamp (top right corner) corresponds to the time axis of the depicted plots in minutes.

Supplemental References

Ball, D.A., Marchand, J., Poulet, M., Baumann, W.T., Chen, K.C., Tyson, J.J., and Peccoud, J. (2011). Oscillatory dynamics of cell cycle proteins in single yeast cells analyzed by imaging cytometry. PLoS One 6, e26272.

Bermejo, C., Haerizadeh, F., Takanaga, H., Chermak, D., and Frommer, W.B. (2010). DYNAMIC ANALYSIS OF CYTOSOLIC GLUCOSE AND ATP LEVELS IN YEAST WITH OPTICAL SENSORS. Biochem. J. 432, 399–406.

Blount, B. a, Weenink, T., Vasylechko, S., and Ellis, T. (2012). Rational diversification of a promoter providing fine-tuned expression and orthogonal regulation for synthetic biology. PLoS One 7, e33279.

Canelas, A.B., ten Pierick, A., Ras, C., Seifar, R.M., van Dam, J.C., van Gulik, W.M., and Heijnen, J.J. (2009). Quantitative Evaluation of Intracellular Metabolite Extraction Techniques for Yeast Metabolomics. Anal. Chem. 81, 7379–7389.

Costanzo, M., Nishikawa, J.L., Tang, X., Millman, J.S., Schub, O., Breitkreuz, K., Dewar, D., Rupes, I., Andrews, B., and Tyers, M. (2004). CDK activity antagonizes Whi5, an inhibitor of G1/S transcription in yeast. Cell 117, 899–913.

Cox, D.R. (1972). Regression Models and Life-Tables. J. R. Stat. Soc. Ser. B 34, 187–220.

Fatima, C., and Kim, N. (1993). Yeast G1 cyclins CLN1 and CLN2 and a GAP-like protein have a role in bud formation Fatima. EMBO J. 12, 5277–5286.

Ferrezuelo, F., Colomina, N., Palmisano, A., Garí, E., Gallego, C., Csikász-Nagy, A., and Aldea, M. (2012). The critical size is set at a single-cell level by growth rate to attain homeostasis and adaptation. Nat. Commun. 3, 1–11.

Futcher, B. (1999). Cell cycle synchronization. Methods Cell Sci. 21, 79–86.

Gibson, D.G., Young, L., Chuang, R.-Y., Venter, J.C., Hutchison, C.A., and Smith, H.O. (2009). Enzymatic assembly of DNA molecules up to several hundred kilobases. Nat Meth 6, 343–345.

Gibson, D.G., Smith, H.O., Hutchison, C.A., Venter, J.C., and Merryman, C. (2010). Chemical synthesis of the mouse mitochondrial genome. Nat Meth 7, 901–903.

Gietz, R.D., and Schiestl, R.H. (2007). High-efficiency yeast transformation using the LiAc/SS carrier DNA/PEG method. Nat. Protoc. 2, 31–34.

Goldstein, A.L., and McCusker, J.H. (1999). Three new dominant drug resistance cassettes for gene disruption in *Saccharomyces cerevisiae*. Yeast 15, 1541–1553.

Hailey, D.W., Davis, T.N., and Muller, E.G. (2002). Fluorescence resonance energy transfer using color variants of green fluorescent protein. Methods Enzymol. 351, 34–49.

Huberts, D.H.E.W., Lee, S.S., González, J., Janssens, G.E., Vizcarra, I.A., and Heinemann, M. (2013). Construction and use of a microfluidic dissection platform for long-term imaging of cellular processes in budding yeast. Nat. Protoc. 8, 1019–1027.

Huh, W.-K., Falvo, J. V, Gerke, L.C., Carroll, A.S., Howson, R.W., Weissman, J.S., and O'Shea, E.K. (2003). Global analysis of protein localization in budding yeast. Nature 425, 686–691.

Imamura, H., Huynh, K.P., Togawa, H., Saito, K., Iino, R., Kato-yamada, Y., Nagai, T., and Noji, H. (2009). Visualization of ATP levels inside single living cells with fluorescence resonance energy transfer-based genetically encoded indicators. Proc. Natl. Acad. Sci. 106, 15651–15656.

Kümmel, A., Ewald, J.C., Fendt, S.-M., Jol, S.J., Picotti, P., Aebersold, R., Sauer, U., Zamboni, N., and Heinemann, M. (2010). Differential glucose repression in common yeast strains in response to HXK2 deletion. FEMS Yeast Res. 10, 322–332.

Lee, S.S., Avalos, I., Huberts, D.H.E.W., Lee, L.P., and Heinemann, M. (2012). Whole lifespan microscopic observation of budding yeast aging through a microfluidic dissection platform. Proc. Natl. Acad. Sci. 109, 4916–4920.

Morawska, M., and Ulrich, H.D. (2013). An expanded tool kit for the auxin-inducible degron system in budding yeast. Yeast 30, 341–351.

Müller, D. (2006). Model-Assisted Analysis of Cyclic AMP Signal Transduction in *Saccharomyces cerevisiae* – cAMP as Dynamic Coordinator of Energy Metabolism and Cell Cycle Progression Modellgestützte Analyse der Signaltransduktion durch zyklisches AMP in Saccharomyces cerevi. PhD Thesis, Univ. Stuttgart.

Nishimura, K., Fukagawa, T., Takisawa, H., Kakimoto, T., and Kanemaki, M. (2009). An auxin-based degron system for the rapid depletion of proteins in nonplant cells. Nat. Methods 6, 917–922.

Pepe, M.S. (2007). The Statistical Evaluation of Medical Tests for Classification and Prediction (OXFORD UNIVERSITY PRESS).

Quan, J., and Tian, J. (2009). Circular polymerase extension cloning of complex gene libraries and pathways. PLoS One 4, e6441.

Quan, J., and Tian, J. (2011). Circular polymerase extension cloning for high-throughput cloning of complex and combinatorial DNA libraries. Nat. Protoc. 6, 242–251.

Saraya, R., Cepińska, M.N., Kiel, J.A.K.W., Veenhuis, M., and van der Klei, I.J. (2010). A conserved function for Inp2 in peroxisome inheritance. Biochim. Biophys. Acta 1803, 617–622.

Schmidt, A.M. (2014). Flux-Signaling and Flux-Dependent Regulation in *Saccharomyces cerevisae*. PhD Thesis, ETH Zurich 1–154.

Schneider, C.A., Rasband, W.S., and Eliceiri, K.W. (2012). NIH Image to ImageJ: 25 years of image analysis. Nat Meth 9, 671–675.

Verduyn, C., Postma, E., Scheffers, A.W., and van Dijken, J. (1992). Effect of Benzoic Acid on Metabolic Fluxes in Yeasts: A Continuous-Culture Study on the Regulation of Respiration and Alcoholic Fermentation. Yeast 8, 501–517.

Voth, W.P., Richards, J.D., Shaw, J.M., and Stillman, D.J. (2001). Yeast vectors for integration at the HO locus. Nucleic Acids Res. 29, E59-9.

Walther, T., Novo, M., Rössger, K., Létisse, F., Loret, M.O., Portais, J.C., and François, J.M. (2010). Control of ATP homeostasis during the respiro-fermentative transition in yeast. Mol. Syst. Biol. 6, 344.

Chapter 3

Under revision in Scientific Reports, April 2017

Quantitative characterization of the auxin-inducible degron: a guide for dynamic protein depletion in single yeast cells

Alexandros Papagiannakis, Janeska J de Jonge, Zheng Zhang, Matthias Heinemann

Molecular Systems Biology, Groningen Biomolecular Sciences and Biotechnology Institute, University of Groningen, Nijenborgh 4, 9747 AG Groningen, The Netherlands

Summary

Perturbations are essential for the interrogation of biological systems. The auxin-inducible degron harbors great potential for dynamic protein depletion in yeast. Here, we thoroughly and quantitatively characterize the auxin-inducible degron in single yeast cells. We show that an auxin concentration of 0.25 mM is necessary for fast and uniform protein depletion between single cells, and that in mother cells proteins are depleted faster than their daughters. Although, protein recovery starts immediately after removal of auxin, it takes several generations before equilibrium is reached between protein synthesis and dilution, which is when the original protein levels are restored. Further, we found that blue light, used for GFP excitation, together with auxin results in growth defects, caused by photo-destruction of auxin to its toxic derivatives, which can be avoided if indole-free auxin substitutes are used. Our work provides guidelines for the successful combination of microscopy, microfluidics and the auxin-inducible degron, offering the yeast community an unprecedented tool for dynamic perturbations on the single cell level.

Highlights

- The rate and uniformity of protein depletion positively correlates with the applied auxin concentration and is significantly slower in daughters as compared to yeast mothers.
- The photo-destruction of auxin to cytotoxic indole derivatives, induced by blue light, causes growth defects which can be avoided by the use of indole-free auxin subsitutes.
- After auxin removal, it takes several generations for cells to reach an equilibrium between protein synthesis and dilution, which is when the targeted protein recovers to its original levels.
- The auxin inducible degradation is optimally applied to deplete essential proteins, but may also be used for the generation of milder growth-related phenotypes in combination with growth controls.

Introduction

Perturbations are necessary tools for the investigation of biological systems (Molinelli et al., 2013). Next to static gene deletions, dynamic and reversible perturbations of protein levels are necessary to investigate pathways and their temporal dynamics, resulting either from cell cycle activity, stochasticity in gene expression, or responses to environmental stimuli. While the dynamic down-regulation of protein synthesis can be accomplished on the transcriptional or posttranscriptional level, both perturbations have only an effect on newly expressed proteins. Due to the typically slow protein turnover and growth-related dilution rates (Christiano et al., 2016), these perturbations are severely limited in terms of their dynamics. Perturbations directly on the protein level are thus desirable.

In yeast, temperature-sensitive mutants (Hartwell et al., 1974) have traditionally been used to deplete proteins, and were followed up by the heat-inducible degron (Dohmen et al., 1994). Although both methods result in targeted protein inactivation or depletion, they require a change in temperature, which could cause global effects on cellular physiology (Morano et al., 2012). Novel perturbation methods use different means of induction. A

photo-sensitive degron, activated by blue light, was developed by fusing the cODC C-terminal degron to the light oxygen voltage 2 (LOV2) photoreceptor domain from Arabidopsis thaliana (Renicke et al., 2013; Usherenko et al., 2014), exhibiting fast protein depletion dynamics (i.e. 12 minutes). However, this light inducible degron requires constant blue light illumination, which is known to induce cellular photo-toxicity (Boudreau et al., 2016), thus significantly reducing cell viability and prohibiting its combination with the most widely used fluorescent protein, in dynamic protein depletion experiments.

Alternatively, the auxin-inducible degron (AID), originating from plants, was successfully assembled in yeast and mammalian cells (Nishimura et al., 2009), where it was used for the rapid (< 1 hour) and targeted depletion of proteins tagged with the degron domain. The plant hormone auxin (indole-3-acetic acid; IAA) mediates the interaction between the tagged protein and the plant F-box protein TIR1, which forms an active complex with the conserved E3 ubiquitin ligase components, resulting in the poly-ubiquitylation of the degron domain and the proteasomal degradation of the tagged protein (Nishimura et al., 2009). Truncated versions of the degron sequence (Kubota et al., 2013), combined with various selection markers, epitope tags (i.e. c-myc, HA, FLAG, GFP) (Morawska and Ulrich, 2013) and flanking motifs (Moss et al., 2015) have increased the versatility of the AID system and its applicability in yeast.

While the system has been used in several yeast studies, for instance to study chromosomal structure and dynamics (Farr et al., 2014; Krefman et al., 2015; Orgil et al., 2015; Renshaw et al., 2010; Robellet et al., 2015), DNA replication, cytokinesis (Devrekanli et al., 2013), autophagy (Shirahama-Noda et al., 2013; Tanaka et al., 2014), gametogenesis (Weidberg et al., 2016), ribosomal synthesis (Barrio-Garcia et al., 2016) and exocytosis (Heider et al., 2016), it turns out that the potential off-target effects of the AID system and of the plant hormone auxin in yeast have only been tested qualitatively with spot assays (Kanke et al., 2011; Morawska and Ulrich, 2013; Nishimura et al., 2009; Nishimura and Kanemaki, 2014). Furthermore, until today, the AID system has only been characterized on the yeast population level. In principle, the AID system should be a great tool for single cell studies, especially combined with the recently developed microfluidics devices (Bisaria et al., 2014; Crane et al., 2014; Hansen et al., 2015; Huberts et al., 2013; Jo et al., 2015; Lee et al., 2012; Zhang et al., 2012), where yeast cells are grown under the constant perfusion of nutrients.

In microfluidics, protein degradation signals (e.g. auxin) can be added or removed from the system simply by a switch of the perfused medium. No additional cell manipulation, including centrifugation or washing, is required, thus avoiding potential stresses or technically induced phenotypic variability. Despite the apparent advantages of single cell technologies in perturbation experiments, the potential of the AID system in combination with microfluidics remains unexplored.

Here, we performed an in-depth characterization of the AID system in single yeast cells. We show that the auxin-inducible degradation can be successfully applied in microfluidics for fast and targeted protein depletion. Higher auxin concentrations result in faster protein depletion with lower cell-to-cell variability. The AID system has no effect on growth rate when auxin concentrations up to 0.1 mM are applied. However, blue light, used for GFP excitation, in combination with auxin (indole acetic acid) causes growth defects, which can be avoided by using naphthalene-acetic acid (NAA, a synthetic auxin substitute), which also induces protein degradation. Upon removal of the plant hormone, it takes several generations until the equilibrium between protein synthesis and dilution is reached again, meaning that the recovery of the original protein levels is slow. In two case studies, we show the strengths and limitations of the AID system. With microfluidics technology becoming widely accessible, we anticipate that our thorough characterization of the AID system and establishment of its use on the single cell level will be of significant value for the yeast community, seeking for tools to perturb of proteins and pathways in a targeted manner.

Results

Protein depletion dynamics upon the addition of different auxin concentrations

To investigate the auxin inducible protein degradation dynamics, across a wide range of auxin concentrations (from 0.5 μM to 0.5 mM) in single *Saccharomyces cerevisiae* cells, we used a monomeric GFP variant tagged with the truncated degron sequence $AID^{71\text{-}114}$ (mGFP-AID), in cells expressing the TIR1 F-box protein from *Oryza sativa* (Os-TIR1) (Table S1). Cells were grown in minimal medium (Verduyn et al., 1992) with 10 gL^{-1}

glucose. First, mimicking population-level depletion experiments, we used flow-cytometry and continuously followed the cellular fluorescence upon the addition of 0.5 mM auxin. Here, in agreement with previous immunoblotting experiments (Nishimura et al., 2009), which reported a time of 15 to 45 minutes for complete protein depletion upon the addition of the same auxin concentration, we found the protein to be fully depleted 25 minutes after the addition of auxin (Figure 1A).

To measure the protein depletion dynamics in single cells, we used microfluidics combined with fluorescence time-lapse microscopy (Figure S1A). Yeast cells were cultivated in the microfluidic dissection platform (Huberts et al., 2013; Lee et al., 2012) and their mGFP-AID fluorescence intensities were recorded every 5 minutes, before and after the addition of auxin (Figure 1B-C, upper panels). The average rate of protein depletion was determined from the single cell mGFP-AID trajectories and their first derivatives, at different auxin concentrations (Figure 1B-C, lower panels). Focusing on the lowest negative derivative, corresponding to the highest rate of mGFP-AID depletion (e.g. lowest point in Figure 1B-C, lower panels), we found that the rate of protein depletion correlated with the applied auxin concentration (Figure 1D). The maximum depletion rate was achieved for auxin concentrations equal or higher than 0.25 mM. For the same concentration of auxin (0.1 mM), growth medium with increased pH (from pH 5.1 to 6.8) lead to lower mGFP-AID depletion rates (Figure 1D), possibly caused by the de-protonation of auxin (Michniewicz et al., 2007), and thus its reduced uptake by yeast cells (Saparov et al., 2006). Consistent with the very low rates of protein depletion at auxin concentrations below 0.005 mM (Figure 1D), we observed incomplete degradation of the protein (Figure 1E).

Next, we assessed the intercellular variability in the auxin-induced protein degradation. Inspection of single-cell mGFP-AID trajectories showed that high auxin concentrations (e.g. 0.5 mM – Figure 1B) result in uniform protein depletion dynamics as compared to lower auxin concentrations, where cells respond at different times (e.g. 0.025 mM – Figure 1C). As a quantitative measure for the intercellular variability we used the standard deviation of the average mGFP-AID signal at each time point, determined for each auxin concentration. An increase in the standard deviation (positive derivative) signifies a variability increase upon the addition of auxin (as in Figure 1C). Adversely, a decrease (negative derivative) reports decreased variability and thus a uniform response to the plant

hormone (as in Figure 1B). Here, we found that the addition of 0.25 mM auxin or higher reduces the intercellular variability in a dose-dependent manner, whereas lower auxin concentrations (≤ 0.1 mM) lead to increased variability (Figure 1F). In our single-cell experiments, we also found that the daughter cells, born just prior to the auxin appearance in the medium, show significantly slower (approx. 20 min later) mGFP-AID depletion when compared to their mothers (Figure 1G, Movie S1).

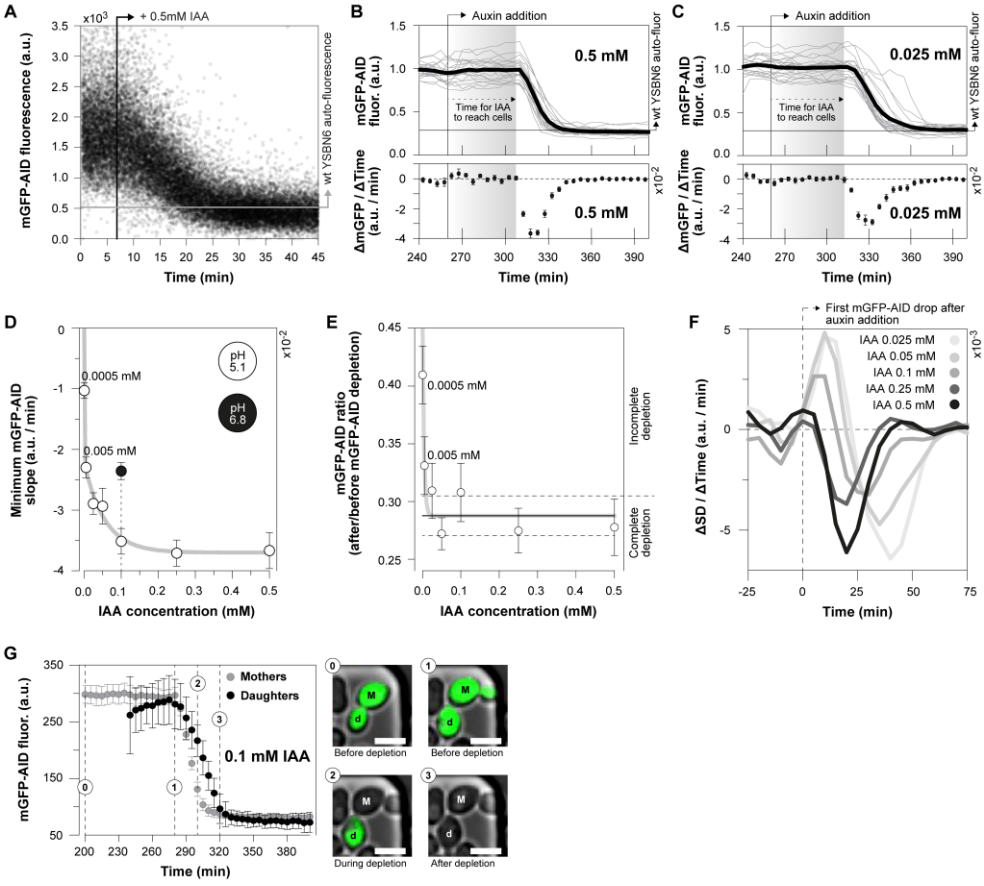

Figure 1: Auxin concentration-dependent dynamics of targeted protein depletion. (A) The mGFP-AID fluorescence continuously measured using flow cytometry. 0.5 mM of auxin were added at 06:50 mm:ss. Each data point corresponds to a single cell. **(B-C)** The average mGFP-AID depletion dynamics upon the addition of **(B)** 0.5 mM (20 cells) and **(C)** 0.025 mM (22 cells) auxin in the microfluidic device. Top figures: single cell (grey lines) and their average (black line) mGFP-AID trajectories. Each single cell trajectory was normalized by dividing over the mean mGFP-AID signal

from 0 to 240 minutes. Bottom figures: average rate (ΔmGFP/ΔTime) of mGFP-AID depletion (error bars: SEM). The levels of yeast auto-fluorescence were divided over the mGFP-IAA levels prior the addition of auxin to indicate the point of complete protein depletion. When we use the syringe pump for the perfusion of medium through the chip, it takes 50±5 minutes for auxin to reach the cells after the switch. This lag time is indicated. **(D)** The minimum mGFP-AID slope (as in Figure 1B-C, or the maximum rate of mGFP-AID depletion, plotted against the auxin concentration (error bars: SEM). For an auxin concentration of 0.1 mM the rate of protein depletion was measured at pH 5.1 (white marker) and pH 6.8 (black marker). A two-phase exponential decay function was fitted to the white markers (y-intercept set to zero). Raw data including the numbers of analyzed cells are presented in Figure S2A-B. **(E)** The completeness of protein depletion: the average mGFP-AID signal after the addition of auxin (500–740 min – as in Figure 1B-C) was divided by the same signal before the addition of auxin (0–240 min – as in Figure 1B-C) for each single cell and auxin concentration. The average ratios are presented and their 95% CI (error bars) reflect cell-to-cell variability. The horizontal lines correspond to the range of complete protein depletion (mean: solid line, 95% CI: dashed lines), estimated non-parametrically (bootstrapping, 100 iterations) by dividing the auto-fluorescence of wild type yeast (13 non-fluorescent cells) by the average mGFP-AID fluorescence (15 cells prior to depletion). A log(dose) response curve with a variable slope was fitted to the data (y-intercept was set to 1, base set to 0.288 – average ratio for complete depletion). **(F)** The change of the standard deviation of the mGFP-AID signal per time interval and auxin concentration reports the uniformity of the response to auxin. Positive slopes denote an increasing standard deviation and a variable response. Negative slopes denote a decrease in cell-to-cell mGFP-AID variability. **(G)** Comparison of the average mGFP-AID depletion dynamics (error bars: 95% CI) between yeast mothers (21 cells) and daughters (7 cells). Microscopy images display their different mGFP-AID depletion (scale 5 μm, same contrast applied in all images). See also Movie S1.

These experiments reveal the effective range of the AID system: High auxin concentrations (≥ 0.25 mM) result in maximal depletion rate, and a uniform response, whereas low auxin concentrations (< 0.25 mM) result in slower concentration-dependent rates of depletion with increased cell-to-cell variability. Furthermore, with the extracellular pH influencing the protonation of auxin, the pH of the medium has an effect on the cellular auxin uptake and thus the protein depletion dynamics.

Auxin causes growth defects when combined with blue light used for GFP excitation

Next to the dynamic nature, orthogonality is an equally important characteristic of perturbation systems. With the most distinguishable and easily observable manifestation of lack of orthogonality being growth defects, here, we investigated whether and if yes, in how

far, the different elements of the AID system affect growth, both in yeast populations (batch cultures) and in single cells grown in the microfluidic device.

First, we found that the expression of the plant F-box protein (TIR1) alone, in the absence of auxin, did not affect the growth of yeast (Figure 2A), indicating that neither the expression of the OsTIR1, nor an eventual degradation of untargeted (non-tagged) proteins, causes a growth rate effect. However, in the microfluidic setup, upon the addition of auxin we found a strong growth defect (Figure 2A) with concentrations as low as 0.5 μM already causing a 35% reduction in growth rate (Figure 2B). By removing the auxin from the microfluidic device, the growth rate recovered within 12 hours (Figure 2C-D). Thus, while the OsTIR1 complex has no effect on growth, we found that auxin – in microfluidic experiments with microscopic observation – slows down the growth of yeast cells. Notably, we found the growth defects to be less pronounced in batch cultures, where only auxin concentrations higher than 0.1 mM lead to slower growth (Figure S3).

In an attempt to explain the cause of this growth rate defect, we focused on the technical differences between experiments performed in microfluidics (Figure 2A-B) and those performed in batch cultures (Figure S3). First, in exponentially growing batch cultures the daughter cells constitute a significant fraction (approx. 50%) of the measured population and thus contribute significantly to the averaged population characteristics (e.g. growth rate). In contrast, in the microfluidic device we only focus on mother cells, because the daughters are constantly washed away. If auxin affects the growth of mothers differently to daughter cells, similarly to what holds for the protein depletion dynamics (Figure 1G, Movie S1), such difference could account for the observed discrepancy between our population and single cell measurements. However, when we analyzed the doubling times of mothers in comparison to the few daughters, which were retained in the microfluidics device, we found them to be equally affected (Figure S4).

Second, in the microfluidic device we regularly (every 5 min) exposed the cells to blue light for the excitation of GFP, which was not the case in the batch culture. In order to test if the blue light causes the pronounced growth rate reduction when auxin is present in microfluidics, we measured the effect of each factor (GFP excitation and auxin) on growth separately and in combination. We found that blue light or 0.1 mM auxin alone caused no significant growth rate reduction (Figure 2E), similarly to our population level

measurements (Figure S3). However, the combination of the plant hormone with blue light causes a pronounced growth rate reduction, even at low auxin concentrations (e.g. 0.5 µM) (Figure 2B&E).

Indole-3-acetic acid (auxin) is known to be sensitive to blue light. Blue light accelerates the oxidative de-carboxylation of indole-3-acetic acid to methylene-oxindole and (Srivastava, 2002) which was previously shown to cause cytotoxicity (Folkes and Wardman, 2001), and we hypothesized that this causes the growth rate reduction in our microscopy experiments. Indeed, when we used naphthalene-acetic acid (0.1 mM), a synthetic, indole-free substitute of auxin, to deplete the targeted protein (mGFP-AID) under frequent (i.e. every 5 min) GFP excitation, we did not observe any significant effect on growth (Figure 2E). Because we found the dynamics of protein depletion with NAA to be similar to the one with IAA (Figure S5), we recommend the use of NAA for the protein depletion in microscopy experiments with GFP excitation.

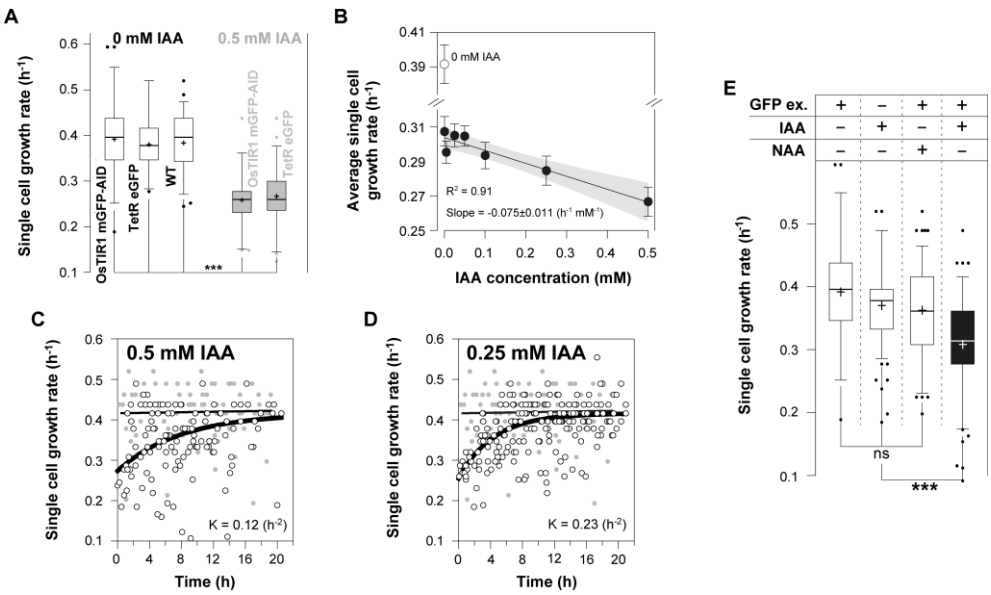

Figure 2: Auxin causes concentration-dependent and reversible growth defects, especially when combined with blue light for GFP excitation. (A) In order to measure potential effects of OsTIR1 or GFP expression on growth, we performed single cell experiments with cells expressing the plant F-box protein (YSBN6.G2J – Table S1), or eGFP via a tetracycline inducible system (YSBN6.C6B –

Table S1), and measured their growth rates in the presence (grey boxes) and absence (white boxes) of auxin (error bars: 5-95 percentile, cross: mean). From left to right: 51 budding cycles from 37 single cells, 31 from 30, 50 from 9, 43 from 26 and 50 budding cycles from 19 single cells. The single cell growth rates (GR_{sc}) were estimated on the basis of the single cell doubling time (DT_{sc}), or the time between two consecutive budding events ($GR_{sc} = \frac{ln(2)}{DT_{sc}}$). The addition of 0.5 mM of auxin in the microfluidics device significantly slows down growth independently of the OsTIR1 expression (Kruskal-Wallis test, Dunns post-test to compare all pairs of data, $p<0.001$ ***). **(B)** The average growth rate of yeast was estimated in the presence of auxin at different concentrations, as well as in the absence of auxin on the single-cell level (error bars: SEM). From left to right: 54 budding cycles from 20 single cells, 57 from 27, 51 from 14, 50 from 16, 41 from 14, 51 from 19 and 50 budding cycles from 19 single cells. **(C-D)** Growth rate recovery after the removal of auxin (at 0 hours). One-phase exponential association functions were fitted to the recovering growth rates (K: rate constant). The plateau was set to the average growth rate of unperturbed wild type cells, grown for the same time in the microfluidic device (grey markers). A linear regression was fitted to the control data to illustrate unperturbed and steady state growth on high (10 gL^{-1}) glucose, in the microfluidic device. Data from **(C)** 195 budding cycles and 24 single cells, or **(D)** 126 budding cycles from 20 single cells are included. **(E)** The single cell growth rates of OsTIR1 expressing cells (error bars: 5-95 percentile, cross: mean), grown and monitored in the microfluidics, together (+) or without (-) GFP excitation, IAA (0.1 mM) or NAA (0.1 mM). From left to right: 51 budding cycles from 37 single cells, 117 from 39, 157 from 30 and 50 budding cycles from 16 single cells. IAA significantly reduces growth only in combination with GFP excitation (Kruskal-Wallis test, Dunns post-test to compare all pairs of data, $p<0.001$ ***).

Protein recovery dynamics upon the removal of auxin

Next, we assessed the reversibility of the AID system. After the removal of auxin from the environment, protein degradation is expected to stop, and the concentration of the protein should recover to its normal levels due to re-synthesis. To assess this, we made use of the medium-switch possibility provided by the microfluidic device in combination with a finely controlled perfusion system (Figure S1B), capable of achieving a complete switch between media compositions within 3-4 minutes (Figure S1C), well below our sampling period (5 minutes). We performed three experiments, where we exposed cells for 10, 20 and 120 minutes to auxin. First, we found that an auxin pulse of at least 20 minutes is required for complete protein depletion (Figure 3A). Second, in all three experiments, the fully or partially depleted mGFP-IAA started recovering almost immediately after switching back to medium without auxin (Figure 3A). These results demonstrate the reversibility of the auxin-inducible degron. Still, we were surprised to find that it took at least 300 minutes for mGFP-AID to reach the levels prior to depletion.

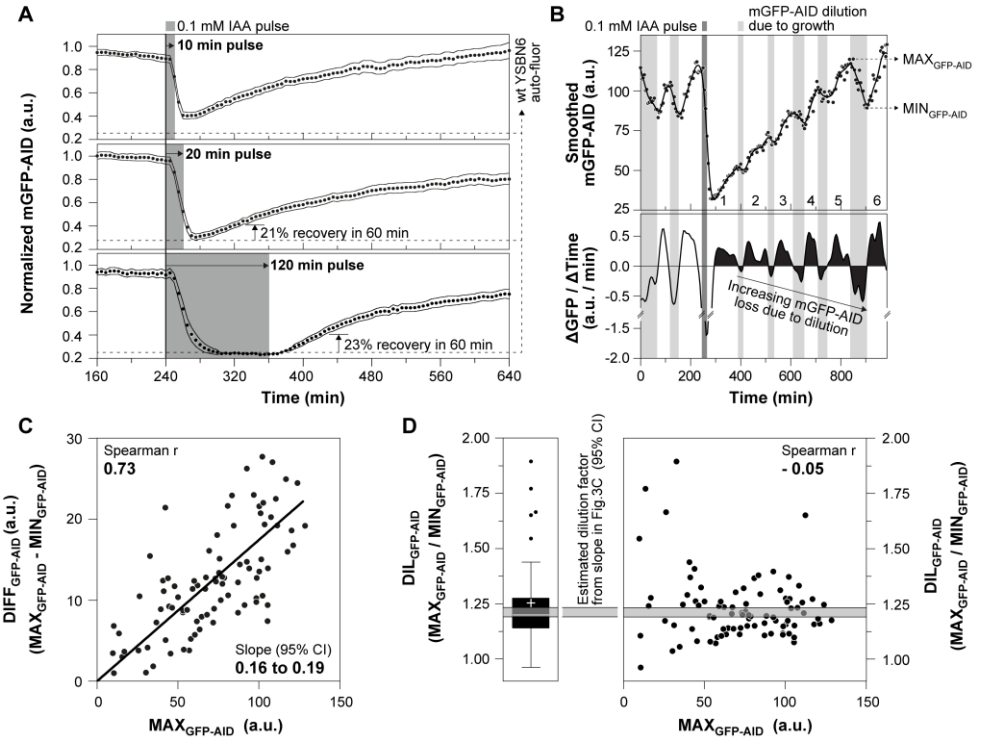

Figure 3: After auxin removal, protein recovery is complete when protein synthesis and dilution reach a new equilibrium, and thus takes several generations. (A) Auxin pulses of 10 min (top figure – 36 single cells), 20 min (middle figure – 36 single cells) and 120 min (bottom figure – 38 single cells) were provided to estimate the protein recovery dynamics after complete or partial protein depletion, in three separate experiments (black markers: averages, error bands: 95% CI). Each single cell trajectory was normalized by dividing over the mean mGFP-AID signal from 0 to 240 minutes, as in Figure 1B-C. The levels of yeast auto-fluorescence, corresponding to complete protein depletion, were estimated by multiplying the mGFP-AID signal at the time of auxin addition (240 min) by the complete depletion factor (folds of fluorescence drop during complete depletion), estimated in Figure 1E. The percentage of protein recovery at 60 min after auxin removal is presented for the 20 min and 120 min pulse experiments. **(B)** Raw single cell mGFP-AID measurements before, during and after the addition of 20 min auxin pulse (single cell from Figure 3A – middle plot). A smoothing spline was fitted to the data and was used to estimate the first derivative of the mGFP-AID dynamics (ΔGFP / ΔTime). The integral of the positive or negative derivatives during protein recovery (after auxin removal), indicating the total amount of protein synthesized or diluted in the yeast mother cell per division cycle, are shaded black. Each number (from 1 to 5) corresponds to one budding and thus division cycle after auxin removal, as observed under the microscope, in the DIC channel. **(C)** The maximum mGFP-AID levels just prior to dilution ($MAX_{GFP\text{-}AID}$), corresponding to the peaks of the oscillating mGFP-AID signal after auxin removal (as in Figure 3B – top), strongly and positively correlate with the drop in the mGFP-AID fluorescence ($DIFF_{GFP\text{-}AID}$), corresponding to the signal at the peak ($MAX_{GFP\text{-}AID}$) minus the signal at the next trough ($MIN_{GFP\text{-}AID}$). A linear regression was fitted to the data and the 95% CI of its slope (SLOPE) were estimated non-parametrically using

bootstrapping. Data from 91 mGFP-AID oscillations, from 19 single cells are presented. **(D)** The slope if the fitted linear regression in Figure 3C was used to estimate the factor of protein dilution (DILGFP-AID) per cell cycle. Specifically we know: $DIL_{GFP-AID} = \frac{MAX_{GFP-AID}}{MIN_{GFP-AID}}$. We also know: $SLOPE = \frac{DIFF_{GFP-AID}}{MAX_{GFP-AID}} = \frac{MAX_{GFP-AID} - MIN_{GFP-AID}}{MAX_{GFP-AID}} = 1 - \frac{MIN_{GFP-AID}}{MAX_{GFP-AID}}$. Thus: $DIL_{GFP-AID} = \frac{1}{1-SLOPE}$. The estimated dilution factor (grey shaded area – 95% CI) is consistent with the experimentally determined dilution factor (Tukey box plot, cross: mean) for each mGFP-AID oscillation during recovery. We found no correlation between the $MAX_{GFP-AID}$ levels and the dilution factor, which confirms a constant mGFP-AID factor of dilution across cell divisions. Data from 91 mGFP-AID oscillations, from 19 single cells are presented, as in Figure 3C.

In order to better understand the mGFP-AID recovery dynamics and explain the long time required for complete protein recovery, we zoomed into single cells. Here, we found that the protein recovery occurs in waves of protein concentration increase and protein dilution with each cell cycle (Figure 3B). We found a strong positive linear correlation (Figure 3C) between the mGFP intensity ($MAX_{GFP-AID}$, as in Figure 3B) and the mGFP intensity drop ($MAX_{GFP-AID}$ - $MIN_{GFP-AID}$, as in Figure 3B), which suggested a constant dilution factor due to cell growth and division, which - using the slope of the correlation (Figure 3C) - we estimated to be 1.2 (Figure 3D – grey band, $DIL_{GFP-AID}$). As we found this factor to be in agreement with the experimentally estimated dilution in single cells (Figure 3D – box-plot and scatter-plot), we concluded that the drops in GFP intensity are because of dilution due to growth.

Thus, while the AID system is fully reversible, as indicated by the almost immediate protein increase after the auxin removal, it takes several divisions until the original protein levels are reached. After removal of auxin, the protein concentration increases (due to protein synthesis), and so does the amount of protein diluted due to cell growth per cell cycle, until these two processes reach an equilibrium. At this point, the original protein level is achieved. The slow protein recovery might represent a limitation of the AID system, especially when studying fast processes where complete protein recovery is required to reverse the conditional depletion phenotype. However, 20% of original protein levels are recovered within one hour after the removal of the plant hormone (Figure 3A – 20 min and 120 min pulse). If such a partial recovery is enough to reverse the conditional depletion phenotype, then the AID may also be used to reversibly perturb processes within

a single cell generation. In all cases, the interesting dynamics of protein recovery might also harbor information on the processes of protein synthesis and dilution during cell division.

Using the AID system to generate growth-related depletion phenotypes

Next, we set to test the AID system in two single-cell case studies. In the first one, we depleted a non-essential protein, the Gcn5 acetyltransferase. Gcn5 is an N-acetyltransferase, activator and catalytic subunit of the SAGA (Spt-Ada-Gcn5-Acetyltrasnderase) transcriptional co-activator (Grant et al., 1997). Gcn5 transfers acetyl groups from acetyl-CoA to the core of H3 and H4 histones, activating the expression of growth related genes in an acetyl-CoA concentration-dependent manner (Cai et al., 2011; Shi and Tu, 2013). Deletion of the Gcn5 acetyltransferase has been shown to reduce the growth rate of yeast by approximately 60% (Cai et al., 2011; Petty et al., 2016).

Here, we used the AID system to dynamically deplete Gcn5. In the microfluidics device, we simultaneously loaded cells expressing a version of Gcn5 that was tagged with mCherry and the degron sequence $AID^{71\text{-}114}$ (Gcn5-mCherry-AID), and control cells expressing mGFP-AID. The two strains were easy to distinguish due to their distinct fluorescent tags (nuclear mCherry, and cytoplasmic mGFP, respectively – Figure 4A-B).

First, we tested if we could use the control strain, to indicate the Gcn5 depletion dynamics. After the addition of auxin (0.1 mM), we found that the cytoplasmic mGFP-AID and the nuclear Gcn5-mCherry-AID fluorescence disappeared simultaneously (Figure 4A-B). Thus, the depletion dynamics of the two proteins are identical. Our results demonstrate that once established, it is possible to use a control strain (e.g. mGFP-AID) in parallel to indicate the depletion dynamics of a targeted protein that is not fluorescently labeled. This increases the availability of fluorescent proteins, which can be used to monitor other than the targeted proteins during conditional depletion, and thus increases the versatility of the AID system on the single cell level.

Next, also using the control strain (mGFP-AID), we tested if we could discriminate between off-target growth defects and those specific to the conditional depletion of the N-acetyltransferase. Before the addition of auxin, we found the Gcn5-mCherry-AID cells to

exhibit significantly (Kruskal-Wallis test, Dunns post-test, p<0.01 **) slower growth, when compared to the control mGFP-AID cells (Figure 4C – 0 mM), indicating either a basal level of Gcn5 depletion or an effect of the degron tag on the activity of the protein. Immediately after the auxin addition, the Gcn5-mCherry-AID depleted cells exhibited a growth rate similar to the Gcn5 deletion strain (Kruskal-Wallis test, Dunns post-test, p>0.05 ns) and significantly lower when compared to the control cells (Kruskal-Wallis test, Dunns post-test, p<0.05 *), reflecting the unspecific growth defects of auxin when combined with GFP measurements. These results demonstrate that with the parallel use of a control strain (e.g. mGFP-AID) it is possible to decipher between specific and unspecific growth defects (Figure 4C-D). After removal of auxin, the growth rate recovered (Figure 4D) and the depleted proteins slowly re-appeared in their subcellular compartments (Figure 4A-B).

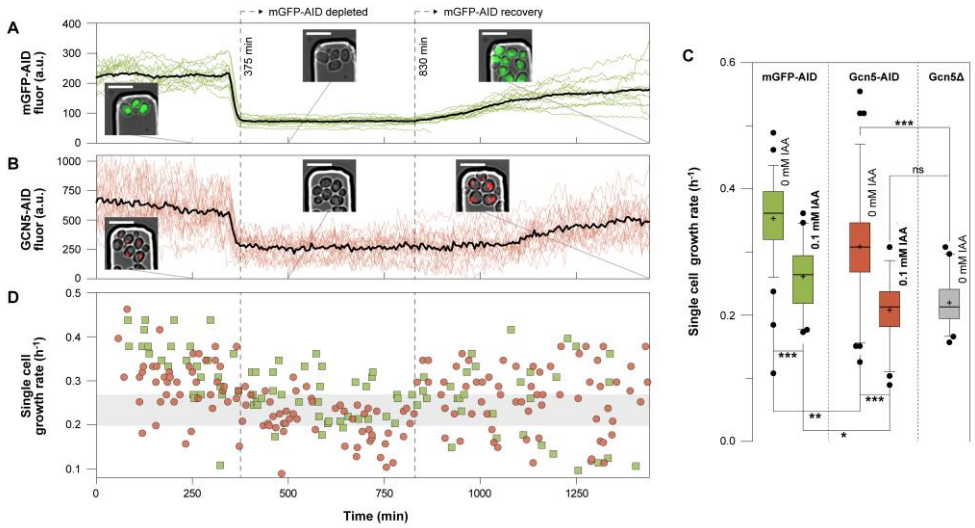

Figure 4: The auxin-induced growth defects have an additive effect on the growth-related Gcn5 depletion phenotype. (A) Control cells expressing mGFP-AID were mixed with **(B)** cells expressing Gcn5-mCherry-AID and grown in the same microfluidic device on 10gL^{-1} glucose. Upon the addition of auxin (0.1 mM), mGFP-AID and the nuclear Gcn5-mCherry-AID were depleted at the same time (375 min). The recovery dynamics of the two proteins after auxin removal (at 830 min) are also visible. The black trajectories correspond to the average mGFP-AID (14 cells) and Gcn5-mCherry-AID (23 cells) signals. The colored trajectories correspond to the single cell signals. Microscopy images confirm the localization and levels of the fluorescent proteins (scale 10 µm) **(C)** The single

cell growth rates in the absence (0 mM IAA) and after the addition (0.1 mM IAA) of auxin, of mGFP-AID (green boxes), Gcn5-mCherry-AID (red boxes) and *Gcn5Δ* cells (grey boxes) growin in minimal medium with high (10 gL^{-1}) glucose (error bars: 5–95 percentile, cross: mean). From left to right: 79 budding cycles from 34 cells, 40 from 14, 76 from 41, 52 from 23, 40 from 17 single cells. (Kruskal-Wallis test, Dunns post-test to compare all pairs of data, $p < 0.001$ ***, $p < 0.01$ **, $p < 0.05$ *, $p > 0.05$ ns). **(D)** The single cell growth rates at different time points are plotted for each yeast strain (green squares: mGFP-AID, red circles: Gcn5-mCherry-AID).

Using the AID system to deplete essential proteins and generate lethal phenotypes

In a second case study, we used the AID system to dynamically deplete the essential cell cycle proteins Cdc28 and Cdc14. Cdc28 is the cyclin dependent kinase (CDK) of yeast controlling the G1/S transition (Mendenhall and Hodge, 1998), the periodic cell cycle transcription and chromosome dynamics in response to periodic waves of early and late cyclins, as well as filamentous growth in response to nutrients and storage carbon metabolism (Tobe et al., 2009). Cdc14 is a phosphatase and essential activator of the anaphase promoting complex (APC) (Bloom et al., 2011). It is necessary for the proteasomal degradation of late cyclins and the de-phosphorylation of the CDK targets for the completion of the cell cycle program and the entry into G1 phase. Conditional depletion of Cdc28 is expected to arrest the cell cycle at any given cell cycle phase. Adversely, conditional depletion of the Cdc14 is expected to stop the cell cycle at late mitosis, maintaining an active CDK.

Prior to the addition of auxin and protein depletion, the Cdc14-AID cells had normal morphology (Figure 5A), in contrast to the Cdc28-AID cells, which exhibited constitutive filamentation (Figure 5B). Because tagging of Cdc28 induced the filamentous phenotype in OsTIR1 expressing cells as well as wild type cells (Figure S6), we conclude that the filamentation is not the result of basal Cdc28 depletion in the absence of auxin. Our results suggest that the degron tag disrupts the interaction of Cdc28 with its Cks1 regulatory domain, an interaction, which reverses the Ras/PKA and Swe1 dependent filamentation (Tobe et al., 2009). Following the Cdc28-AID and Cdc14-AID cells after the depletion of their protein targets and cell cycle arrest, we found their size to increase (Figure 5C). The Cdc14 depleted cells, increased in volume faster than the Cdc28 depleted cells, indicating early cell cycle activity and biomass synthesis even when the anaphase promoting complex

and the late cell cycle are arrested. Consistently, through monitoring the abundance of histone Hta2, previously shown to correlate with DNA content (Papagiannakis et al., 2017; Rattray and Müller, 2012), we found that Cdc14 cells also continued to replicate their DNA, with an approximate rate of one copy per 100 minutes (Figure 5D). Adversely, DNA replication stalled in the absence of CDK activity (Cdc28 depletion).

Consistently with the CDK-centric model of cell cycle regulation (Barik et al., 2010), our results confirm the sustained activity of the early cell cycle in cells lacking Cdc14: In the absence of APC activity, the late cyclins are not degraded and remain in the nucleus resulting in a sustained CDK activity, also reported by the cytosolic localization of Whi5 (Bloom and Cross, 2007; Costanzo et al., 2004; Ferrezuelo et al., 2012), an inhibitor of cell cycle transcription and phosphorylation target of Cdc28 (Figure 5E). This sustained CDK-activity triggers biomass formation via the constitutive activation of the cell cycle transcription program, and DNA endo-replication cycles via the constitutive deactivation of the Sic1, an inhibitor of DNA replication (Bloom and Cross, 2007; Mendenhall and Hodge, 1998). Adversely, in the absence of CDK activity (after Cdc28-AID depletion), reported by the immediate sequestration of Whi5-eGFP into the nucleus (Figure 5F), cells cannot replicate their DNA.

The auxin-inducible protein depletion, exhibiting fast dynamics (approx. 25 min) well below the doubling time of yeast cells growing on glucose (approx. 100 min), was used successfully for to generate depletion phenotypes within a single generation or cell cycle phase. Thus, the AID system provides an alternative to the temperature-sensitive mutants, traditionally used to decipher the cell cycle machinery components (Hartwell et al., 1973), but without their temperature-related effects on cellular physiology (Morano et al., 2012).

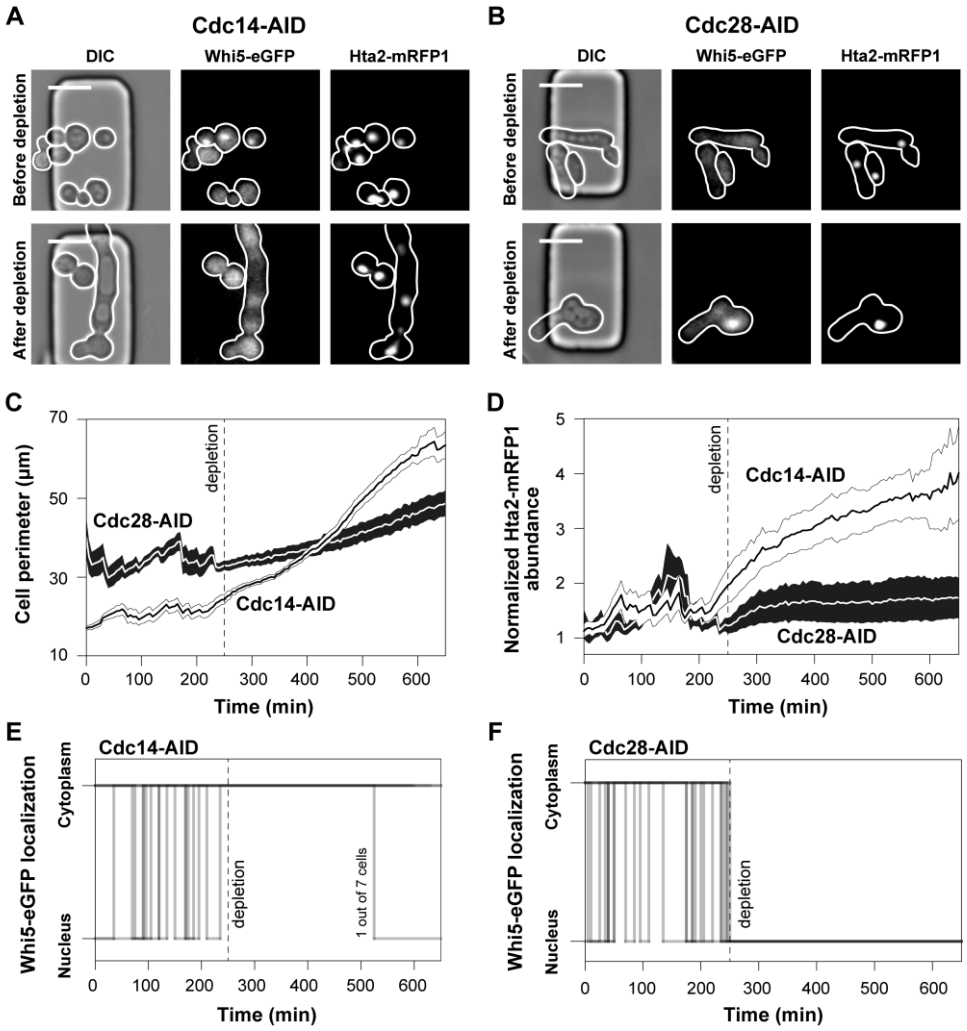

Figure 5: The auxin inducible protein degradation is efficiently used to deplete the Cdc14 and Cdc28 essential cell cycle regulators, and arrest the cell cycle at different phases. Microscopy images illustrate the phenotype of **(A)** Cdc14-AID and **(B)** Cdc28-AID cells prior and after protein depletion, including the cellular morphology, Whi5 localization and Hta2 abundance (scale 10 µm). In the RFP channel the number of genome copies is also visible. **(C)** The average perimeter of Cdc14-AID (white) and Cdc28-AID (black) cells (shaded area: SEM), manually measured in each single cell (7 cells for each strain), and each individual frame, using the white cellular borderline in the DIC channel (as in Figure 5A-B), prior and after protein depletion (at 250 min). **(D)** The average intracellular histone abundance (shaded area: SEM) is plotted over time (before and after protein depletion) for the Cdc14-AID (white) and Cdc28-AID (black) strains (7 single cells each). The histone abundance of each single cell, was divided over the histone abundance just after the first cytokinesis in the G1 phase, which corresponds to one copy of the genome, to estimate the number of genomes per cell. The generated polyploidy after Cdc14-AID depletion is also visible in microscopy

images and the number of Hta2-mRFP1 foci (Figure 6A – Hta2-mRFP1). (E-F) The single cell Whi5 localization dynamics upon the depletion of **(E)** Cdc14-AID or **(F)** Cdc28-AID. Black lines indicate the Whi5 localization trajectories. When the trajectory becomes vertical there is Whi5 translocation from the nucleus to the cytoplasm (bottom to top) or from the cytoplasm to the nucleus (top to bottom). When the lines are horizontal, Whi5 remains in the cytoplasm (top) or the nucleus (bottom). Whi5 is a cell cycle inhibitor and reporter of CDK activity (Bloom and Cross, 2007; Costanzo et al., 2004; Ferrezuelo et al., 2012). In the G1 phase it is localized in the nucleus. At START, Whi5 is phosphorylated by the active Cln3/CDK complex and is being sequestered into the cytoplasm signaling cell cycle initiation and the G1/S transition. Whi5 re-enters the nucleus at late mitosis. **(E)** After Cdc14-AID depletion and halting of the late cell cycle, the anaphase promoting complex is not activated to degrade the remaining cyclins. Thus, the Cdc14-AID depleted single cells maintain a constitutive CDK activity (Whi5 in the cytoplasm). Spontaneous degradation of cyclins occasionally leads to cell cycle completion (1 out of 7 cells). **(F)** Adversely, depletion of Cdc28-AID depletion immediately causes Whi5 sequestration into the nucleus, reporting absence of CDK activity.

Discussion

Here, we comprehensively characterized the auxin-dependent degron system and its capabilities in single yeast cells. By providing optimal experimental parameters for the AID system and by revealing its advantages and potential off-target effects, our work adds value to a powerful tool for yeast researchers. The AID system allows for fast (25 min) protein depletion with minimal cell-to-cell variability. Exposing cells to 0.1 mM auxin for 20 min results in complete protein depletion. We found that the AID is reversible: after removal of the plant hormone, the recovery of the targeted protein starts immediately. However, to reach the equilibrium between protein synthesis and dilution, and thus restore the original protein levels, several generations or growth cycles are necessary. To avoid the photo-destruction of IAA during GFP excitation, leading to the production of toxic indole derivatives and growth defects, NAA should be used in microscopy experiments. As shown here, NAA at 0.1 mM has no effect on growth rate, while it induces protein depletion, similarly to IAA. Although the auxin inducible degron performs optimally when used to deplete essential proteins, or to generate binary phenotypes, it may also serve for the generation of quantitative growth phenotypes when the appropriate controls are used to discriminate between potential off-target effects and those specific to the depletion of the target protein.

Possibly the biggest advantage from combining microfluidics and single cell technologies with the auxin inducible degron is the capacity to assess intercellular variability. For instance, in cell cycle studies, the fact that cells are present at different cell cycle stages in a microfluidics device can be exploited for the generation of highly informative datasets: auxin reaches the cells at different cell cycle phases. As a result, the function of a targeted protein can be studied across the entire cell cycle in a single experiment. Similarly, the protein depletion phenotype may be assessed in young and aged cells, all growing in the same microfluidic device, under the exact same conditions, yielding information on age related biological processes. For instance, our finding that protein depletion is slower in newborn daughters as compared to their mother yeast cells (Figure 1G and Movie S1), provides indication that either protein synthesis rates are enhanced in daughter cells, or their ubiquitination and protein degradation machineries are not fully active as compared to mother cells.

Overall, the AID system is a simple and highly versatile system, providing excellent means to dynamically perturb biological systems. The characterization, insights and solutions provided in this work will allow yeast researchers to adapt this powerful tool for single cell perturbation experiments. We expect that - fueled by recent developments in microfluidics setups (Bisaria et al., 2014; Crane et al., 2014; Huberts et al., 2013; Jo et al., 2015; Lee et al., 2012; Zhang et al., 2012) and in novel single cell reporters (Bermejo et al., 2011; Peroza et al., 2015; Wosika and Pelet, 2017), as well as the need to zoom into the single cell level – these types of experiments will gain importance.

Experimental Procedures

Strains and strain construction

The prototrophic YSBN6 strain, derived from S288c, and its HIS- variant (YSBN16) were used. For an overview on strains refer to Table S1.

In order to dynamically deplete Gcn5 we tagged the protein with a truncated version of the degron tag (AID^{71-114}), previously tested and successfully applied in yeast (Morawska and

Ulrich, 2013). Flanking sequences adjacent the stop codon of the Gcn5 coding sequence were amplified from the YSBN6 wild type genomic DNA (primer pairs GCN5-CDS and GCN5-DOWN – Table S2). The truncated degron tag (AID^{71-114}) was amplified from the pNAT-AID*-9myc plasmid (Morawska and Ulrich, 2013) (Gcn5-IAA primer pair – Table S2). The NatMX expression cassette, offering resistance to clonNAT was amplified from the pAG36 plasmid (Goldstein and McCusker, 1999) (primer pair Gcn5-NatMX – Table S2). The fluorescent protein mCherry was amplified from the pBS35 plasmid (Hailey et al., 2002) (Gcn5-mCherry primer pair – Table S2). The ampicillin resistance cassette and the ColE1 origin of replication, used for selection and amplification into *Escherichia coli*, were amplified in one piece from the pC6B plasmid (Papagiannakis et al., 2017) (Gcn5-Amp primer pair – Table S2). All six pieces were assembled into the pG4J plasmid using Gibson assembly. The pG4J plasmid, encoding for the Gcn5-AID tagging cassette, was verified using sequencing (primers Seq12, Seq24, Seq25, Seq26 – Table S2). The pG4J plasmid, was linearized (Gcn5-Lin primer pair – Table S2) and used to transform YSBN6.OsTIR1w/oGFP cells, under the selection of ClonNAT, for the construction of the YSBN6.OsTIR1w/oGFP.G4J strain (Table S1). We used lithium acetate high efficiency transformation protocol for all yeast transformations performed in this study. Correct integration of the Gcn5-AID cassette was confirmed using PCR (primer pairs Gcn5-Ver1 and Gcn5-Ver2 – Table S2).

To verify the Gcn5-AID conditional phenotype we constructed a Gcn5 deletion strain (YSBN6.*Gcn5Δ* – Table S1). The Gcn5 deletion cassette was amplified (primer pair GCN5-Del – Table S2) from the yeast deletion collection and the clone E21 (Winzeler et al., 1999) and was used to transform YSBN6 wild type cells, under the selection of G418. Correct integration was verified using PCR (GCN5-Del primers – Table S2).

The YSBN16.Whi5-eGFP.Hta2-mRFP1.OsTIR1w/oGFP.G23ARFPex strain (Table S1) was constructed in the following manner: The coding sequence of the OsTIR1 F-box protein was amplified from the pOsTIRw/oGFP plasmid (Papagiannakis et al., 2017) (primers Seq 4 – Table S2), the Hta2-mRFP1 tagging cassette was amplified from the KOY.TM6*P hxk2-GFP hta2-mRFP1 strain (Schmidt, 2014) (primers Hta2Lin – Table S2), and the Cdc14-AID tagging cassette was amplified from the pG23ARFPex plasmid (Papagiannakis et al., 2017) (primers pG23ALinRFPex – Table S2). The three amplicons

were used to transform YSBN16.Whi5-eGFP yeast cells (Papagiannakis et al., 2017) (Table S1) under the selection of G418, phleomycin and ClonNAT respectively, in three separate genomic integration steps.

For the C-terminal tagging of Cdc28 with the degron sequence (AID^{71-114}) (Morawska and Ulrich, 2013), the pG25 plasmid was constructed. The Cdc28 flanking sequences adjacent the stop codon were amplified (primer pairs Cdc28-CDS and Cdc28-DOWN – Table S2). The degron tag together with the NatMX antibiotic resistance cassette were amplified in one piece from the pG23ARFPex plasmid (Papagiannakis et al., 2017), (IAA-NatMX primer pair – Table S2). The ampicillin resistance cassette and the ColE1 origin of replication, used for selection and amplification into *Escherichia coli*, were amplified in a single piece from the pC6B plasmid (Papagiannakis et al., 2017) (primer pair Amp – Table S2). The four pieces were assembled into the pG25 plasmid, using Gibson assembly. Correct assembly was verified using sequencing (primers Seq103 and Seq104 – Table S2). The pG25 plasmid was linearized (Cdc28-Lin primer pair – Table S2) and was used to transform YSBN16.Whi5-eGFP.Hta2-mRFP1.OsTIRw/oGFP cells (Table S1), under the selection of ClonNAT for the construction of the YSBN16.Whi5-eGFP.Hta2-mRFP1.OsTIRw/oGFP.Cdc28-AID strain (Table S1). Correct integration was verified using PCR (Cdc28-Lin primers – Table S2).

Cultivation

All experiments were performed on minimal medium (Verduyn et al., 1992) with 10 gL^{-1} glucose. The pH of the minimal medium was adjusted with 10 mM K-Phthalate-KOH (pH 5) at a final pH of 5.1 or with 100 mM KH2PO4-KOH (pH 7) at a final pH of 6.8, as specified in the text. The medium adjusted to pH 6.8 was prepared before every experiment to avoid salt precipitation. Single yeast colonies growing on YPD 20 gL^{-1} glucose agar plates were used to inoculate 10 mL of minimal 10 gL^{-1} glucose medium in 100 mL shake flasks, and grown (at 30°C, 300 rpm) overnight. The overnight culture was diluted in fresh medium to an OD of 0.1, and grown to an OD between 1 and 1.5 (exponential growth on 10 gL^{-1} glucose).

The exponentially growing cells were diluted to an OD of 0.05 and loaded into the microfluidic chip as described (Huberts et al., 2013; Lee et al., 2012). Cells were fed with minimal 10 gL^{-1} glucose medium. The provided medium was pre-warmed to 30°C and saturated with atmospheric air by shaking at 300 rpm for at least two hours prior to use. Our microfluidic experimental set-ups are described in detail in Figure S1A-B.

In the microfluidic device the Gcn5-AID, Cdc14-AID and Cdc28-AID strains (Table S1) were mixed with control cells expressing mGFP-AID (YSBN6.G2J – Table S1 (Papagiannakis et al., 2017)), to monitor the time when auxin reaches the cells, and to compare their depletion and recovery dynamics. For the flow-cytometry experiments with batch cultures, exponentially growing cells were diluted in fresh, pre-warmed and air saturated minimal medium containing 10 gL^{-1} glucose, at an initial OD of 0.1.

Microscopy

Image acquisition (Nikon Ti-E inverted microscope with an Andor 897 Ultra EX2 EM-CCD camera; CoolLed pE2 excitation system; Nikon PFS dynamic focusing system) took place every 5 min, in the DIC and fluorescence channels using a 40x Nikon Super Fluor Apochromat objective. For GFP measurements (mGFP-AID and Whi5-eGFP), cells were excited at 470 nm with 15% light intensity using a 470/40 nm bandpass filter. The GFP emission was recorded using a 495 nm beamsplitter and a 525/50 nm emission filter. For the RFP measurements (Hta2-mRFP1 and Gcn5-mCherry-AID), cells were excited at 565 nm using a 560/40 nm bandpass filter. The mCherry emission was recorded using a 585 nm beamsplitter and a 630/75 nm emission filter. 20% LED power was used for the excitation of mRFP1 (fused with Hta2) and 50% for the excitation of mCherry (fused with Gcn5). No binning or EM gain was applied. 200 msec exposure time was applied for recording the mGFP and mRFP1 fluorescence, as well as during DIC imaging. 600 msec exposure time was applied for mCherry imaging. In the DIC channel, a halogen lamp was used as a light source, the light of which was filtered through an ultraviolet light filter (420 nm beamsplitter) to minimize cell damage during the long image acquisition. The NIS elements software (LIM) was used to control the microscope and for image acquisition.

Image Analysis

For segmentation and tracking of single yeast cells, the BudJ plug-in (Ferrezuelo et al., 2012) for ImageJ (Schneider et al., 2012) was used. Specifically, cells were selected by clicking in the center, and they were automatically segmented and tracked based on the pixel intensity change at the perimeter of the cell in the DIC images. The average fluorescence intensity of the pixels contained within the specified cell boundaries was determined for each cell and fluorescence channel (GFP and/or RFP). The modal grey value corresponding to the background fluorescence of the whole field of view in each fluorescent channel was subtracted from the fluorescence of each monitored cell, at each time point.

For the quantification of the nuclear concentration of Gcn5-mCherry-AID and its dynamic depletion upon the addition of auxin, we used the BudJ plug-in (Ferrezuelo et al., 2012) for ImageJ (Schneider et al., 2012) and specifically the Cluster Index function. We set the cluster threshold at 1 standard deviation (brightest pixels by 1 standard deviation at the foci), the minimum fluorescence change at foci at 5%, the minimum foci size at 2 pixels, and the maximum foci size at 10 pixels. The average cytoplasmic RFP auto-fluorescence, measured in the control cells (mGFP-AID), which did not express RFP, was subtracted from the nuclear Gcn5-mCherry-AID fluorescence.

The conditionally or constitutively filamentous Cdc14-AID and Cdc28-AID cells, were manually segmented on the basis of the cellular borderline in the DIC channel, using ImageJ (Schneider et al., 2012). For the quantification of the intracellular Hta2-mRFP1 abundance, the whole cell median fluorescence was used as the cellular background fluorescence, and subtracted from the fluorescence images. The total fluorescence, corresponding to the DNA abundance, was quantified by multiplying the segmented whole cell area in μm2 (number of scaled pixels: 0.4 μm per pixel – 40x objective), by the mean fluorescence intensity. The nuclear or cytoplasmic localization of Whi5 was manually determined for each single cell.

Flow cytometry

A BD Accuri flow-cytometer was used to record the dynamics of mGFP-AID depletion upon the addition of 0.5 mM of auxin. Exponentially growing cells on 10 gL^{-1} glucose, were diluted using the same medium at an OD of 0.2 and a final volume of 1.8 mL, and sampled continuously using 10 µl/min flow-rate, and 8 µm core size (diameter of sample flow in between the sheath laminar flow). The plant hormone was added to a concentration of 0.5 mM to the sample without stopping flow and gently mixed by pipetting.

The same instrument was used to measure the cell count of exponentially growing cells with mGFP-AID, Cdc14-AID and Cdc28-AID upon the addition of auxin. Appropriate dilutions were applied to maintain the cell count below 200000 cells / 25 µl.

References

Barik, D., Baumann, W.T., Paul, M.R., Novak, B., Tyson, J.J., 2010. A model of yeast cell-cycle regulation based on multisite phosphorylation. Mol. Syst. Biol. 6, 405.

Barrio-Garcia, C., Thoms, M., Flemming, D., Kater, L., Berninghausen, O., Baszler, J., Beckmann, R., Hurt, E., 2016. Architecture of the Rix1-Rea1 checkpoint machinery during pre-60S-ribosome remodeling. Nat Struct Mol Biol 23, 37–44.

Bermejo, C., Haerizadeh, F., Takanaga, H., Chermak, D., Frommer, W.B., 2011. Optical sensors for measuring dynamic changes of cytosolic metabolite levels in yeast. Nat. Protoc. 6, 1806–1817.

Bisaria, A., Hersen, P., McClean, M.N., 2014. Microfluidic Platforms for Generating Dynamic Environmental Perturbations to Study the Responses of Single Yeast Cells, in: Smith, J.S., Burke, D.J. (Eds.), Yeast Genetics: Methods and Protocols. Springer New York, New York, NY, pp. 111–129.

Bloom, J., Cristea, I.M., Procko, A.L., Lubkov, V., Chait, B.T., Snyder, M., Cross, F.R., 2011. Global Analysis of Cdc14 Phosphatase Reveals Diverse Roles in Mitotic Processes. J. Biol. Chem. 286, 5434–5445.

Bloom, J., Cross, F.R., 2007. Multiple levels of cyclin specificity in cell-cycle control. Nat Rev Mol Cell Biol 8, 149–160.

Boudreau, C., Wee, T.-L. (Erika), Duh, Y.-R. (Silvia), Couto, M.P., Ardakani, K.H., Brown, C.M., 2016. Excitation Light Dose Engineering to Reduce Photo-bleaching and Photo-toxicity. Sci. Rep. 6, 30892.

Cai, L., Sutter, B.M., Li, B., Tu, B.P., 2011. Acetyl-CoA Induces Cell Growth and Proliferation by Promoting the Acetylation of Histones at Growth Genes. Mol. Cell 42, 426–437.

Christiano, R., Nagaraj, N., Fröhlich, F., Walther, T.C.C., 2016. Global Proteome Turnover Analyses of the Yeasts *S. cerevisiae* and *S.pombe*. Cell Rep. 9, 1959–1965.

Costanzo, M., Nishikawa, J.L., Tang, X., Millman, J.S., Schub, O., Breitkreuz, K., Dewar, D., Rupes, I., Andrews, B., Tyers, M., 2004. CDK activity antagonizes Whi5, an inhibitor of G1/S transcription in yeast. Cell 117, 899–913.

Crane, M.M., Clark, I.B.N., Bakker, E., Smith, S., Swain, P.S., 2014. A Microfluidic System for Studying Ageing and Dynamic Single-Cell Responses in Budding Yeast. PLoS One 9, e100042.

Devrekanli, A., Foltman, M., Roncero, C., Sanchez-Diaz, A., Labib, K., 2013. Inn1 and Cyk3 regulate chitin synthase during cytokinesis in budding yeasts. J. Cell Sci. 125, 5453 LP-5466.

Dohmen, R.J., Wu, P., Varshavsky, A., 1994. Heat-inducible degron: a method for constructing temperature-sensitive mutants. Science (80-.). 263, 1273–1276.

Farr, C.J., Antoniou-Kourounioti, M., Mimmack, M.L., Volkov, A., Porter, A.C.G., 2014. The α isoform of topoisomerase II is required for hypercompaction of mitotic chromosomes in human cells. Nucleic Acids Res. 42, 4414–4426.

Ferrezuelo, F., Colomina, N., Palmisano, A., Garí, E., Gallego, C., Csikász-Nagy, A., Aldea, M., 2012. The critical size is set at a single-cell level by growth rate to attain homeostasis and adaptation. Nat. Commun. 3, 1–11.

Folkes, L.K., Wardman, P., 2001. Oxidative activation of indole-3-acetic acids to cytotoxic species—a potential new role for plant auxins in cancer therapy1. Biochem. Pharmacol. 61, 129–136.

Goldstein, A.L., McCusker, J.H., 1999. Three new dominant drug resistance cassettes for gene disruption in *Saccharomyces cerevisiae*. Yeast 15, 1541–53.

Grant, P.A., Duggan, L., Côté, J., Roberts, S.M., Brownell, J.E., Candau, R., Ohba, R., Owen-Hughes, T., Allis, C.D., Winston, F., Berger, S.L., Workman, J.L., 1997. Yeast Gcn5 functions in two multisubunit complexes to acetylate nucleosomal histones: characterization of an Ada complex and the SAGA (Spt/Ada) complex. Genes Dev. 11, 1640–1650.

Hailey, D.W., Davis, T.N., Muller, E.G., 2002. Fluorescence resonance energy transfer using color variants of green fluorescent protein. Methods Enzymol. 351, 34–49.

Hansen, A.S., Hao, N., O'Shea, E.K., 2015. High-throughput microfluidics to control and measure signaling dynamics in single yeast cells. Nat. Protoc. 10, 1181–1197.

Hartwell, L.H., Culotti, J., Pringle, J.R., Reid, B.J., 1974. Genetic Control of the Cell Division Cycle in Yeast. Science (80-.). 183, 46–51.

Hartwell, L.H., Mortimer, R.K., Culotti, J., Culotti, M., 1973. Genetic Control of the Cell Division Cycle in Yeast: V. Genetic Analysis of cdc Mutants. Genetics 74.

Heider, M.R., Gu, M., Duffy, C.M., Mirza, A.M., Marcotte, L.L., Walls, A.C., Farrall, N., Hakhverdyan, Z., Field, M.C., Rout, M.P., Frost, A., Munson, M., 2016. Subunit connectivity, assembly determinants and architecture of the yeast exocyst complex. Nat Struct Mol Biol 23, 59–66.

Huberts, D.H.E.W., Lee, S.S., González, J., Janssens, G.E., Vizcarra, I.A., Heinemann, M., 2013. Construction and use of a microfluidic dissection platform for long-term imaging of cellular processes in budding yeast. Nat. Protoc. 8, 1019–1027.

Jo, M.C., Liu, W., Gu, L., Dang, W., Qin, L., 2015. High-throughput analysis of yeast replicative aging using a microfluidic system. Proc. Natl. Acad. Sci. U. S. A. 112, 9364–9369.

Kanke, M., Nishimura, K., Kanemaki, M., Kakimoto, T., Takahashi, T.S., Nakagawa, T., Masukata, H., 2011. Auxin-inducible protein depletion system in fission yeast. BMC Cell Biol. 12, 1–16.

Krefman, N.I., Drubin, D.G., Barnes, G., 2015. Control of the spindle checkpoint by lateral kinetochore attachment and limited Mad1 recruitment. Mol. Biol. Cell 26, 2620–2639.

Kubota, T., Nishimura, K., Kanemaki, M.T., Donaldson, A.D., 2013. The Elg1 Replication Factor C-like Complex Functions in PCNA Unloading during DNA Replication. Mol. Cell 50, 273–280.

Lee, S.S., Avalos, I., Huberts, D.H.E.W., Lee, L.P., Heinemann, M., 2012. Whole lifespan microscopic observation of budding yeast aging through a microfluidic dissection platform. Proc. Natl. Acad. Sci. 109, 4916–4920.

Mendenhall, M.D., Hodge, A.E., 1998. Regulation of Cdc28 Cyclin-Dependent Protein Kinase Activity during the Cell Cycle of the Yeast *Saccharomyces cerevisiae*. Microbiol. Mol. Biol. Rev. 62, 1191–1243.

Michniewicz, M., Brewer, P.B., Friml, J., 2007. Polar Auxin Transport and Asymmetric Auxin Distribution. Arabidopsis Book 5, e0108.

Molinelli, E.J., Korkut, A., Wang, W., Miller, M.L., Gauthier, N.P., Jing, X., Kaushik, P., He, Q., Mills, G., Solit, D.B., Pratilas, C.A., Weigt, M., Braunstein, A., Pagnani, A., Zecchina, R., Sander, C., 2013. Perturbation Biology: Inferring Signaling Networks in Cellular Systems. PLoS Comput Biol 9, e1003290.

Morano, K.A., Grant, C.M., Moye-Rowley, W.S., 2012. The Response to Heat Shock and Oxidative Stress in *Saccharomyces cerevisiae*. Genetics 190, 1157–1195.

Morawska, M., Ulrich, H.D., 2013. An expanded tool kit for the auxin-inducible degron system in budding yeast. Yeast 30, 341–51.

Moss, B.L., Mao, H., Guseman, J.M., Hinds, T.R., Hellmuth, A., Kovenock, M., Noorassa, A., Lanctot, A., Villalobos, L.I.A.C., Zheng, N., Nemhauser, J.L., 2015. Rate Motifs Tune Auxin/Indole-3-Acetic Acid Degradation Dynamics. Plant Physiol. 169, 803–813.

Nishimura, K., Fukagawa, T., Takisawa, H., Kakimoto, T., Kanemaki, M., 2009. An auxin-based degron system for the rapid depletion of proteins in nonplant cells. Nat. Methods 6, 917–922.

Nishimura, K., Kanemaki, M.T., 2014. Rapid Depletion of Budding Yeast Proteins via the Fusion of an Auxin-Inducible Degron (AID), in: Current Protocols in Cell Biology. John Wiley & Sons, Inc.

Orgil, O., Matityahu, A., Eng, T., Guacci, V., Koshland, D., Onn, I., 2015. A Conserved Domain in the Scc3 Subunit of Cohesin Mediates the Interaction with Both Mcd1 and the Cohesin Loader Complex. PLoS Genet 11, e1005036.

Papagiannakis, A., Niebel, B., Wit, E.C., Heinemann, M., 2017. Autonomous metabolic oscillations robustly gate the early and the late cell cycle. Mol. Cell 65, 285–295.

Peroza, E.A., Ewald, J.C., Parakkal, G., Skotheim, J.M., Zamboni, N., 2015. A genetically encoded Förster resonance energy transfer sensor for monitoring in vivo trehalose-6-phosphate dynamics. Anal. Biochem. 474, 1–7.

Petty, E.L., Lafon, A., Tomlinson, S.L., Mendelsohn, B.A., Pillus, L., 2016. Promotion of Cell Viability and Histone Gene Expression by the Acetyltransferase Gcn5 and the Protein Phosphatase PP2A in Saccharomyces cerevisiae. Genetics 203, 1693 LP-1707.

Rattray, A.M.J., Müller, B., 2012. The control of histone gene expression. Biochem. Soc. Trans. 40, 880–885.

Renicke, C., Schuster, D., Usherenko, S., Essen, L.-O., Taxis, C., 2013. A LOV2 Domain-Based Optogenetic Tool to Control Protein Degradation and Cellular Function. Chem. Biol. 20, 619–626.

Renshaw, M.J., Ward, J.J., Kanemaki, M., Natsume, K., Nédélec, F.J., Tanaka, T.U., 2010. Condensins Promote Chromosome Recoiling during Early Anaphase to Complete Sister Chromatid Separation. Dev. Cell 19, 232–244.

Robellet, X., Thattikota, Y., Wang, F., Wee, T.-L., Pascariu, M., Shankar, S., Bonneil, É., Brown, C.M., D'Amours, D., 2015. A high-sensitivity phospho-switch triggered by Cdk1 governs chromosome morphogenesis during cell division. Genes Dev. 29, 426–439.

Saparov, S.M., Antonenko, Y.N., Pohl, P., 2006. A New Model of Weak Acid Permeation through Membranes Revisited: Does Overton Still Rule? Biophys. J. 90, L86–L88.

Schmidt, A.M., 2014. Flux-Signaling and Flux-Dependent Regulation in Saccharomyces Cerevisae. PhD thesis, ETH Zurich 1–154.

Schneider, C.A., Rasband, W.S., Eliceiri, K.W., 2012. NIH Image to ImageJ: 25 years of image analysis. Nat Meth 9, 671–675.

Shi, L., Tu, B.P., 2013. Acetyl-CoA induces transcription of the key G1 cyclin CLN3 to promote entry into the cell division cycle in *Saccharomyces cerevisiae*. Proc. Natl. Acad. Sci. 110, 7318–7323.

Shirahama-Noda, K., Kira, S., Yoshimori, T., Noda, T., 2013. TRAPPIII is responsible for vesicular transport from early endosomes to Golgi, facilitating Atg9 cycling in autophagy. J. Cell Sci. 126, 4963 LP-4973.

Srivastava, L.M., 2002. CHAPTER 6 - Auxins BT - Plant Growth and Development. Academic Press, San Diego, pp. 155–169.

Tanaka, C., Tan, L.-J., Mochida, K., Kirisako, H., Koizumi, M., Asai, E., Sakoh-Nakatogawa, M., Ohsumi, Y., Nakatogawa, H., 2014. Hrr25 triggers selective autophagy-related pathways by phosphorylating receptor proteins. J. Cell Biol. 207, 91–105.

Tobe, B.T.D., Kitazono, A.A., Garcia, J.S., Gerber, R.A., Bevis, B.J., Choy, J.S., Chasman, D., Kron, S.J., 2009. Morphogenesis signaling components influence cell cycle regulation by cyclin dependent kinase. Cell Div. 4, 12.

Usherenko, S., Stibbe, H., Muscó, M., Essen, L.-O., Kostina, E.A., Taxis, C., 2014. Photo-sensitive degron variants for tuning protein stability by light. BMC Syst. Biol. 8, 128.

Verduyn, C., Postma, E., Scheffers, A.W., van Dijken, J., 1992. Effect of Benzoic Acid on Metabolic Fluxes in Yeasts: A Continuous-Culture Study on the Regulation of Respiration and Alcoholic Fermentation. Yeast 8, 501–517.

Weidberg, H., Moretto, F., Spedale, G., Amon, A., van Werven, F.J., 2016. Nutrient Control of Yeast Gametogenesis Is Mediated by TORC1, PKA and Energy Availability. PLoS Genet. 12.

Winzeler, E.A., Shoemaker, D.D., Astromoff, A., Liang, H., Anderson, K., Andre, B., Bangham, R., Benito, R., Boeke, J.D., Bussey, H., Chu, A.M., Connelly, C., Davis, K., Dietrich, F., Dow, S.W., El Bakkoury, M., Foury, F., Friend, S.H., Gentalen, E., Giaever, G., Hegemann, J.H., Jones, T., Laub, M., Liao, H., Liebundguth, N., Lockhart, D.J., Lucau-Danila, A., Lussier, M., M'Rabet, N., Menard, P., Mittmann, M., Pai, C., Rebischung, C., Revuelta, J.L., Riles, L., Roberts, C.J., Ross-MacDonald, P., Scherens, B., Snyder, M., Sookhai-Mahadeo, S., Storms, R.K., Véronneau, S., Voet, M., Volckaert, G., Ward, T.R., Wysocki, R., Yen, G.S., Yu, K., Zimmermann, K., Philippsen, P., Johnston, M., Davis, R.W., 1999. Functional Characterization of the S. cerevisiae Genome by Gene Deletion and Parallel Analysis. Science (80-.). 285, 901–906.

Wosika, V., Pelet, S., 2017. Relocation sensors to quantify signaling dynamics in live single cells. Curr. Opin. Biotechnol. 45, 51–58.

Zhang, Y., Luo, C., Zou, K., Xie, Z., Brandman, O., Ouyang, Q., Li, H., 2012. Single Cell Analysis of Yeast Replicative Aging Using a New Generation of Microfluidic Device. PLoS One 7, e48275.

Acknowledgements

The authors thank the Molecular Systems Biology group for helpful discussion, and Kevin Knoops and Ida van der Klei for the provision of plasmids and strains. Also, we would like to thank three anonymous reviewers for their excellent comments, which allowed us to further improve this manuscript.

Author contributions

AP designed the study, developed all strains, performed all experiments, and analyzed all data. JJ developed the Gcn5-AID strain and performed the mGFP-AID flow cytometry experiments. ZZ performed the auxin pulse experiments. MH conceived, designed and supervised the study. AP and MH wrote the manuscript. All authors reviewed the manuscript.

Additional information

Financial support is acknowledged from the EU ITN project ISOLATE. The authors declare no competing financial interests. The data generated during and/or analyzed during the current study are available from the corresponding author on reasonable request.

Supplemental Information for

Quantitative characterization of the auxin-inducible degron: a guide for dynamic protein depletion in single yeast cells

Alexandros Papagiannakis, Janeska J de Jonge, Zheng Zhang, Matthias Heinemann

Molecular Systems Biology, Groningen Biomolecular Sciences and Biotechnology Institute, University of Groningen, Nijenborgh 4, 9747 AG Groningen, The Netherlands;

Supplemental Figures

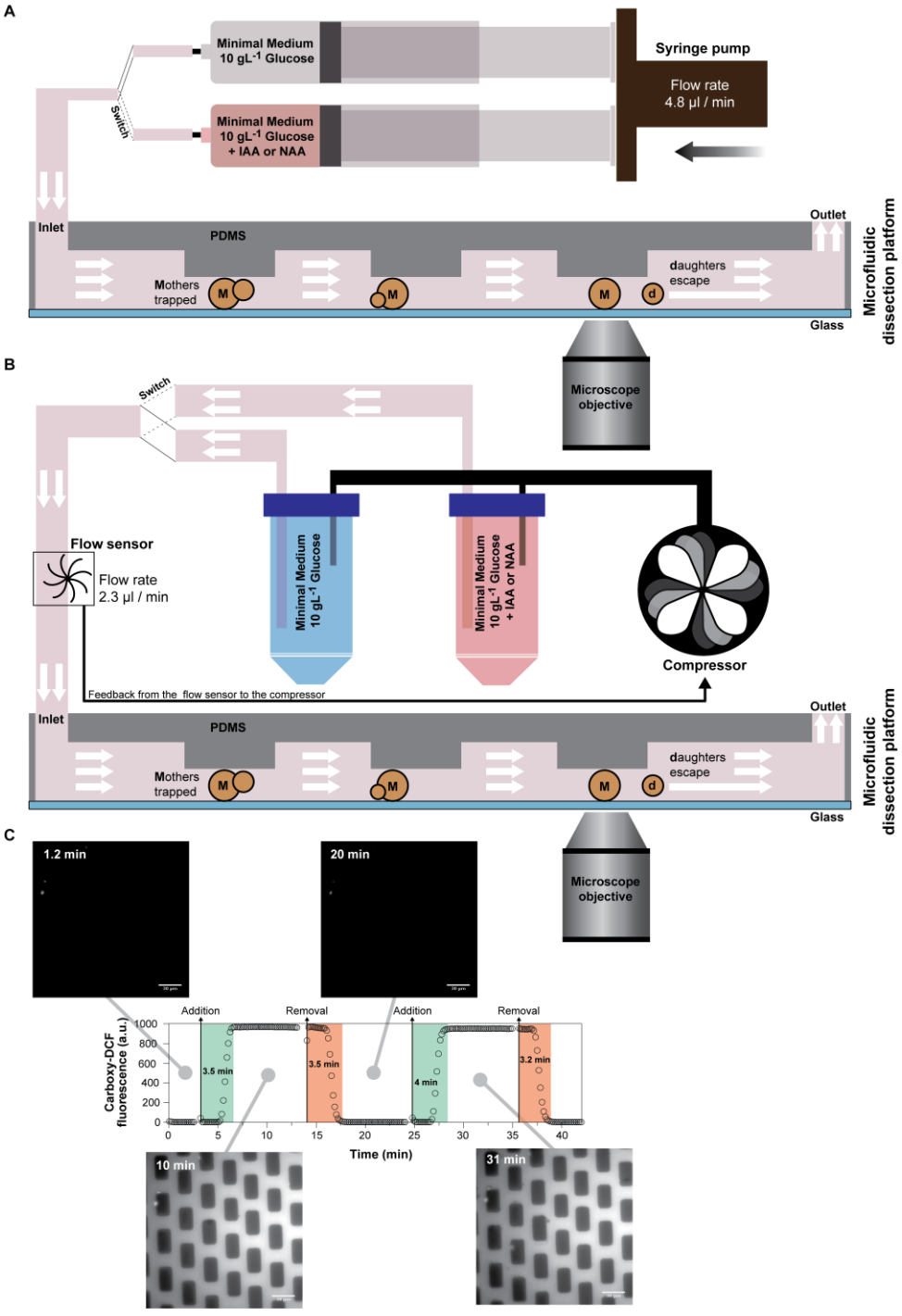

Figure S1: Single cell experimental set-ups used in this study. Single yeast mothers are trapped in a PDMS (Polydimethylsiloxaan) based microfluidics dissection platform. The smaller daughter cells are washed away by constant medium flow, allowing for the microscopic observation of single yeast mothers over multiple generations. Information about the construction and use of the microfluidic device is available (Huberts et al., 2013). Medium is perfused through the microfluidics dissection platform **(A)** either using a programmable syringe pump (Harvard Apparatus – Standard Infuse/Withdraw 11 Elite) or **(B)** air-pressurized flow control (Everflow – OB1) together with flow sensors (Everflow – MFS2). **(C)** The dynamics of pressurized air-driven flow allowed for rapid medium switches (3 to 4 minutes) as shown in a control experiment, where we switched to minimal medium (10gL^{-1} glucose) containing 5-(and -6)-Carboxy-2,7-Dichlorofluorescein (Carboxy-DCF) and back to minimal medium (10gL^{-1} glucose) without the dye, in the microfluidic dissection platform. The fluorescence was monitored every 10 seconds in the GFP channel. The pressurized air-driven flow was exclusively used in the auxin-pulse experiments (Figure 3).

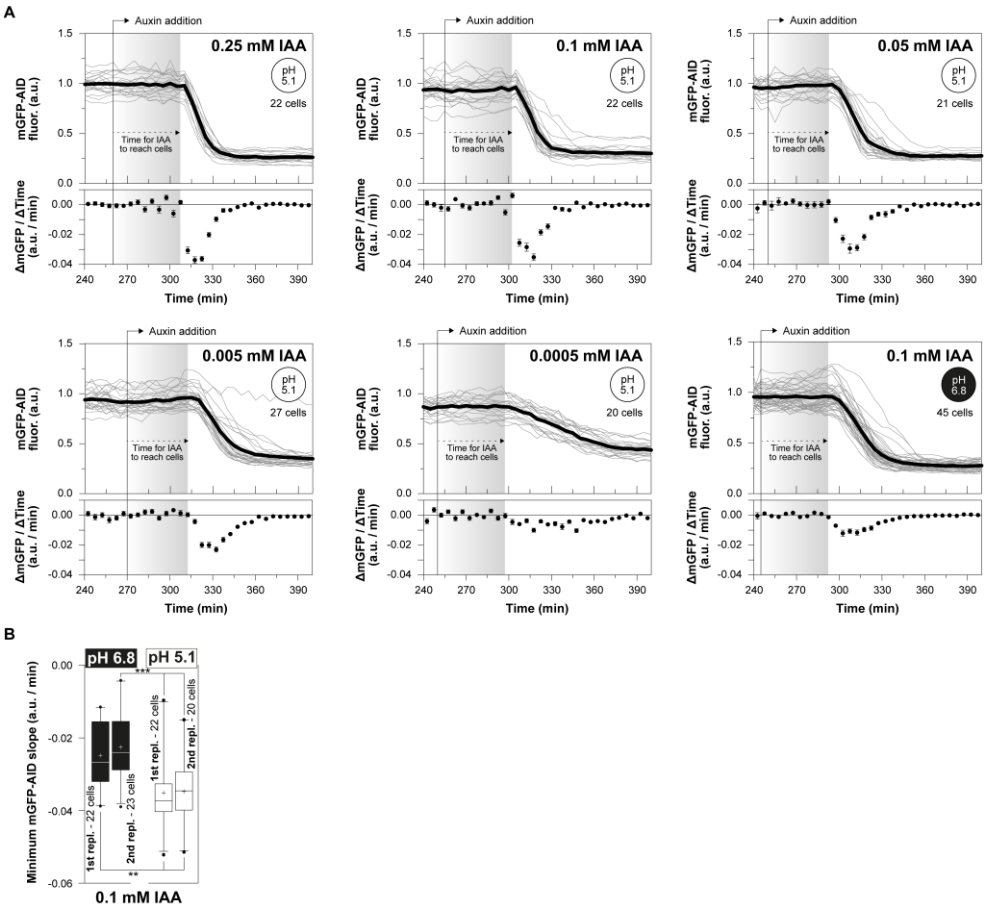

Figure S2: The dynamics of targeted protein depletion across different auxin concentrations and environmental pH values. (A) Top figures: the average (black lines) and single cell (grey lines) mGFP-IAA trajectories are presented for each auxin concentration and environmental pH value (5.1

or 6.8), as in Figure 1B-C. Each single cell trajectory was normalized by dividing over the mean mGFP-AID signal from 0 to 240 minutes. Bottom figures: average rate (ΔmGFP/ΔTime) of mGFP-AID depletion (error bars: SEM). The minimal ΔmGFP/ΔTime values (bottom figures), or maximum rates of mGFP-AID depletion, across auxin concentrations and extracellular pH valiues are also presented in Figure 1D. A comparison between the single cell mGFP-AID levels before and after auxin addition (top figures), was applied to estimated the completeness of mGFP-AID depletion in Figure 1E. The deviation between the single cell mGFP-AID trajectories for each given auxin concentration (top figures) was used to estimate the uniformity of protein depletion in Figure 3F. **(B)** The minimum mGFP-AID slope, or the maximum rate of mGFP-AID depletion, was estimated (as in Figure 1D), for the same auxin concentration (0.1 mM), at pH 6.8 (grey boxes) or pH 5.1 (white boxes) (error bars: 5–95 percentiles, cross: mean). Lower pH significantly increases the rate of mGFP-AID depletion (Kruskal-Wallis test, Dunns post-test for selected pairs of data, $p < 0.0001$ ***, $p < 0.001$ **).

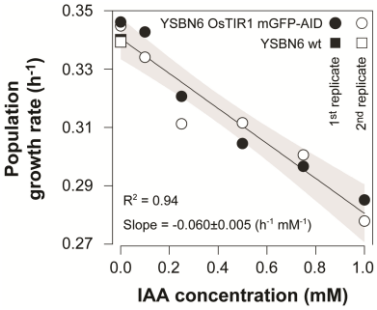

Figure S3: Auxin concentration-dependent effects on the growth rate of yeast populations. The growth rate was measured on the population level using flow cytometry (logarithmic increase of cell count over time), on different concentrations of the plant hormone (0 to 1 mM).

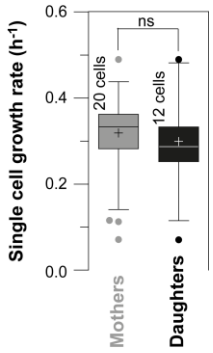

Figure S4: The growth of yeast mothers and their newborn daughters are equally affected by auxin. The single cell growth rate distributions for yeast mothers (grey box) and newborn daughter (black box) after the addition of 0.1 mM auxin (Error bars: 5–95 percentiles, cross: mean) are not significantly different (Mann-Whitney test, $p > 0.05$ ns).

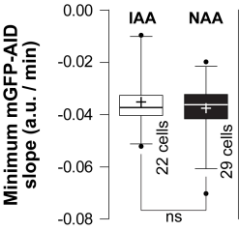

Figure S5: The dynamics of protein depletion with NAA and IAA are identical. 0.1 mM of IAA and NAA were applied in both experiments (error bars: 5–95 percentiles, cross: mean, Mann-Whitney test, $p > 0.05$ ns).

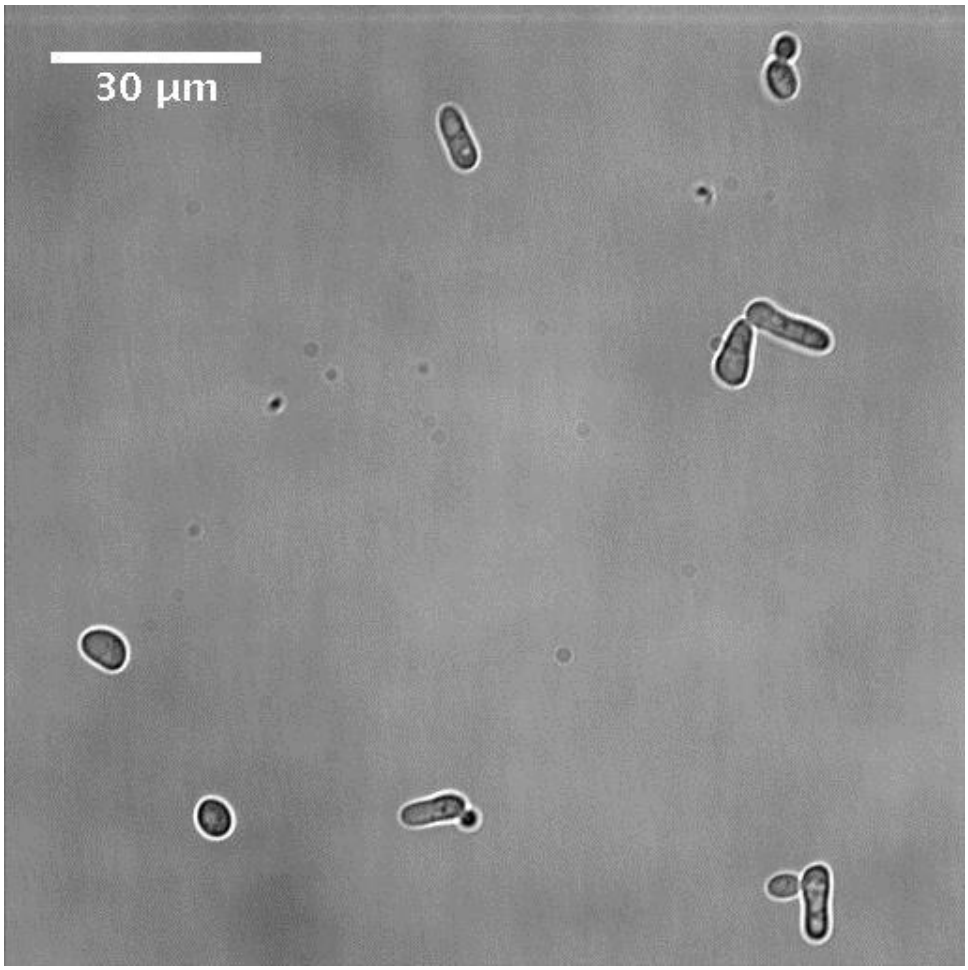

Figure S6: Tagging of Cdc28 with the degron sequence (IAA^{71-114}) causes constitutive filamentation even in the absence of OsTIR1. Exponentially growing YSBN6 Cdc28-AID cells (YSBN6.G25ARFPex – Table S1) in minimal medium supplemented with $10gL^{-1}$ glucose, in the absence of auxin.

Supplemental Movie

Movie S1: The auxin induced protein depletion is slower for the yeast daughters, as compared to their mothers. Yeast cells expressing mGFP-AID, and trapped in the microfluidic device are presented (scale 10 μm). The DIC and GFP channels have been merged. 2 daughter cells are born at 04:00 hh:mm and 04:40 hh:mm just prior the auxin inducible protein degradation (starting at 05:00 hh:mm), exhibit slower protein depletion dynamics. At 05:30 hh:mm there are no traces of the mGFP-AID protein in the mother cells. However, it takes 30 to 40 minites longer for the two newborn daughters to fully deplete their mGFP-AID fluorescence signal (at 06:00 and 06:10 hh:mm respectively).

Supplemental Tables

Table S1: Yeast strains developed and/or used in this study.

Strain	Genotype	Source
YSBN6	YSBN6 wild type	Steve Oliver lab, Cambridge
YSBN16	YSBN6 his3Δ1	(Kümmel et al., 2010)
YSBN16 Whi5-GFP	YSBN16 Whi5::eGFP-HIS3MX6	(Papagiannakis et al., 2017)
YSBN6.C6B	YSBN6 HO::TEF1p-TetR-iPFY1p-eGFP-KanMX4	(Papagiannakis et al., 2017)
YSBN6.G2J	YSBN6 ho::ADH1p-OsTIR1-TEF1p-mGFP-AID-KanMX4	(Papagiannakis et al., 2017)
YSBN6.OsTIR1w/oGFP	YSBN6 ho::ADH1p-OsTIR1-KanMX4	(Papagiannakis et al., 2017)
YSBN6.OsTIR1w/oGFP.G4J	YSBN16 ho::ADH1p-OsTIR1-KanMX4 Gcn5::mCherry-AID$^{71-114}$-NatMX	This study
YSBN6.Gcn5Δ	YSBN6 Gcn5::KanMX4	This study

KOY.TM6*P hxk2-GFP hta2-mRFP1	KOY.TM6 Hta2::mRFP1-Ble Hxk2::eGFP-KanMX4	(Schmidt, 2014)
YSBN16.Whi5-eGFP.Hta2-mRFP1.OsTIR1w/oGFP.G23ARFPex	YSBN16 ho::ADH1p-OsTIR1-KanMX4 Whi5::eGFP-HIS3MX6 Hta2::mRFP1-Ble Cdc14::mCherry-AID$^{71-114}$-NatMX	This study
YSBN16.Whi5-eGFP.Hta2-mRFP1.OsTIR1w/oGFP.G25ARFPex	YSBN16 ho::ADH1p-OsTIR1-KanMX4 Whi5::eGFP-HIS3MX6 Hta2::mRFP1-Ble Cdc28::AID$^{71-114}$-NatMX (C-terminal tagging)	This study
YSBN6 G25ARFPex	YSBN6 Cdc28::AID$^{71-114}$-NatMX (C-terminal tagging)	This study

Table S2: Primer sequences used for the development of all recombinant strains.

The underlined sequences correspond to the overhangs designed for Gibson assembly. The term "gDNA" stands for purified genomic DNA.

Primer	Fwd/Rev	Sequence (5´ to 3´)	Templates
GCN5 CDS	Fwd	GCGGCTCGTATGTTGTGTGGCGAAATCGCATATTGTAAGG	YSBN6 wild type gDNA
	Rev	TCCTCGCCCTTGCTCACCATATCAATAAGGTGAGAATATTCAGG	
GCN5 DOWN	Fwd	CGGCGGGGACAAGGCAAGCTTGCGTAGAAGAAGCTTTTCC	YSBN6 wild type gDNA
	Rev	GGAACAAGAGTCCACTATTATTAACTTTGAAAGAAGCTGAGC	
Gcn5 mCherry	Fwd	AATATTCTCACCTTATTGATATGGTGAGCAAGGGCGA	pBS35
	Rev	CCGGCGCCTGCACCGTCGACCTTGTACAGCTCGTCCATGC	

Gcn5 IAA	Fwd	GCATGGACGAGCTGTACAAGGTCG ACGGTGCAGG	#2189 plasmid (Morawska and Ulrich, 2013)
	Rev	ACGCCGCCATCCAGTGTCGACGTAC GCTGAGCTGGA	
Gcn5 NatMX	Fwd	AAGATCCAGCTCAGCGTACGTCGAC ACTGGATGGC	pAG36 plasmid (Goldstein and McCusker, 1999)
	Rev	GGAAAAGCTTCTTCTACGCAAGCTT GCCTTGTCCC	
Gcn5 Amp	Fwd	TCAGCTTCTTTCAAAGTTAATAATA GTGGACTCTTGTTCC	pC6B plasmid (Papagiannakis et al., 2017)
	Rev	CCTTACAATATGCGATTTCGCCACA CAACATACGAGC	
Gcn5 Lin	Fwd	CGAAATCGCATATTGTAAGG	pG4J (This study)
	Rev	TTAACTTTGAAAGAAGCTGAG	
Cdc28 CDS Cdc28 CDS	Fwd	TTATGCTTCCGCGGCTCGTATGTTGT GTGGGGTATTGCATACTGCCACTC	YSBN6 wild type gDNA
	Rev	AGCACCAGCCCCGGCGCCTGCACC GTCGACTGATTCTTGGAAGTAGGGG T	
Cdc28 DOWN	Fwd	CCGGGTGACCCGGCGGGGACAAGG CAAGCTCAAATGCTACTGCACTGTC	
	Rev	GTTCCAGTTTGGAACAAGAGTCCAC TATTACGGTGACAATGAAACTCTTC	
IAA-NatMX	Fwd	GTCGACGGTGCAGG	pG23A (Papagiannakis et al., 2017)
	Rev	AGCTTGCCTTGTCCC	
Amp	Fwd	CCACACAACATACGAGC	
	Rev	TAATAGTGGACTCTTGTTCC	
NatMX	Fwd	ACAGTGGAAAATAGCTCGACACTG GATGGC	pG23A (Papagiannakis et al., 2017)
	Rev	GGAGTAGAAACATTTTGAAGCTATG GTGTGAGCTTGCCTTGTCCC	
Cdc28 Lin	Fwd	GGTATTGCATACTGCCACTC	pG25

	Rev	CGGTGACAATGAAACTCTTC	(This study)
Amp	Fwd	TAATAGTGGACTCTTGTTCC	pG2J plasmid (This study)
	Rev	CCACACAACATACGAGC	
Hta2Lin	Fwd	CAATTTCGACTGCATGATGC	KOY.TM6*P hxk2-GFP hta2-mRFP1 gDNA (Schmidt, 2014)
	Rev	GGAAGAACTACGCACTCTTTC	
GCN5 Del	Fwd	AATGAGATGTAGCAATGCAG	E21 clone – Yeast Deletion Project (Winzeler et al., 1999)
	Rev	TGCGGATGATGGTTATCAAC	
GCN5 Ver1	Fwd	GGACGCAGGTAAGATTCTAT	YSBN6.OsTIR1w/oGFP.G4J gDNA
	Rev	CCTTGGAGCCGTACATGAA	
GCN5 Ver2	Fwd	GACAGTCACATCATGCC	
	Rev	CCTCTGGTGAAGAAAGACT	
Seq25	Fwd	GGATAACCGTATTACCGCCT	pG4J (This study)
Seq12	Rev	CCTGAAGTCTAGGTCCCTAT	
Seq 24	Rev	GGTCACAGCTTGTCTGTAA	
Seq 26	Rev	GGTGATACCTTCACGAAC	
Seq 103	Fwd	ACCAAGTCTAGATCCACG	pG25 (This study)
Seq 104	Rev	TACGACCTCGGTAAATACG	
Cdc14LinRFPex	Fwd	GTCGACGGTGCAGG	pG23ARFPex (Papagiannakis et al., 2017)
	Rev	TTTCTTGATGGAGCCACTT	
Seq 4	Fwd	AATTATCCTGGGCACGAG	pOsTIR1w/oGFP (Papagiannakis et al., 2017)
	Rev	ACTGTAAGATTCCGCCAC	

Supplemental References

Goldstein, A.L., McCusker, J.H., 1999. Three new dominant drug resistance cassettes for gene disruption in *Saccharomyces cerevisiae*. Yeast 15, 1541–53.

Huberts, D.H.E.W., Lee, S.S., González, J., Janssens, G.E., Vizcarra, I.A., Heinemann, M., 2013. Construction and use of a microfluidic dissection platform for long-term imaging of cellular processes in budding yeast. Nat. Protoc. 8, 1019–1027.

Kümmel, A., Ewald, J.C., Fendt, S.-M., Jol, S.J., Picotti, P., Aebersold, R., Sauer, U., Zamboni, N., Heinemann, M., 2010. Differential glucose repression in common yeast strains in response to HXK2 deletion. FEMS Yeast Res. 10, 322–32.

Morawska, M., Ulrich, H.D., 2013. An expanded tool kit for the auxin-inducible degron system in budding yeast. Yeast 30, 341–51.

Papagiannakis, A., Niebel, B., Wit, E.C., Heinemann, M., 2017. Autonomous metabolic oscillations robustly gate the early and the late cell cycle. Mol. Cell 65, 285–295.

Schmidt, A.M., 2014. Flux-Signaling and Flux-Dependent Regulation in Saccharomyces Cerevisae. PhD thesis, ETH Zurich 1–154.

Winzeler, E.A., Shoemaker, D.D., Astromoff, A., Liang, H., Anderson, K., Andre, B., Bangham, R., Benito, R., Boeke, J.D., Bussey, H., Chu, A.M., Connelly, C., Davis, K., Dietrich, F., Dow, S.W., El Bakkoury, M., Foury, F., Friend, S.H., Gentalen, E., Giaever, G., Hegemann, J.H., Jones, T., Laub, M., Liao, H., Liebundguth, N., Lockhart, D.J., Lucau-Danila, A., Lussier, M., ;Rabet, N., Menard, P., Mittmann, M., Pai, C., Rebischung, C., Revuelta, J.L., Riles, L., Roberts, C.J., Ross-MacDonald, P., Scherens, B., Snyder, M., Sookhai-Mahadeo, S., Storms, R.K., Véronneau, S., Voet, M., Volckaert, G., Ward, T.R., Wysocki, R., Yen, G.S., Yu, K., Zimmermann, K., Philippsen, P., Johnston, M., Davis, R.W., 1999. Functional Characterization of the *S. cerevisiae* Genome by Gene Deletion and Parallel Analysis. Science (80-.). 285, 901–906.

Chapter 4

CDK and cAMP/PKA signalling tune the amplitude of the metabolic oscillator, thereby controlling cell cycle initiation or arrest

Alexandros Papagiannakis, Vakil Takhaveev, Matthias Heinemann

Molecular Systems Biology, Groningen Biomolecular Sciences and Biotechnology Institute, University of Groningen, Nijenborgh 4, 9747 AG Groningen, The Netherlands

Summary

The cyclin/CDK machinery, the cAMP/PKA pathway and the metabolic oscillator are known to form an intertwined network for the robust coordination of metabolism with the cell cycle in response to nutrient availability. Here we perform a small-scale genetic screening, using constitutive and conditional genetic perturbations, to investigate the effects of cAMP/PKA- and CDK-signaling on the metabolic oscillator. We show the amplitudes of the metabolic oscillations to strongly correlate with the cell cycle, and constitute an accurate predictor of cell cycle initiation. The cAMP/PKA pathway is not necessary for metabolism to oscillate, but stabilizes the amplitude of the noisy metabolic oscillator above the required threshold for cell cycle initiation in nutrient rich conditions. Dampened metabolic dynamics, either the result of poor nutrient conditions or mating pheromone induced CDK inhibition, activate the metabolic attenuator Rim15 for the robust arrest of the cell cycle in G1. Our results point towards the metabolic oscillator and the correlated dynamics, as potential targets for cell cycle manipulation against proliferative disorders.

Highlights

- Metabolic oscillations persist upon inhibition of the cAMP/PKA and CDK signaling and thus are autonomous.
- In the absence of cAMP/PKA and CDK signaling, the amplitude of the metabolic oscillations is dampened.
- In nutrient rich conditions, a positive feedback loop via cAMP/PKA signaling stabilizes the metabolic dynamics above the threshold for cell cycle initiation.
- The amplitude of the metabolic oscillations strongly correlates with cell cycle progression, and can be used to predict cell cycle initiation or cell cycle arrest.

Introduction

Through the course of the cell cycle, eukaryotes are confronted with different metabolic demands, such as for DNA replication in the S phase, or for cell wall synthesis during mitosis. Additionally, the cell cycle and metabolic processes of DNA replication and respiration, have been conjectured to be incompatible due to the production of reactive oxygen species during respiration that could damage DNA (Tu et al., 2005). Thus, for a timely provision of resources, or for temporal separation of incompatible processes, coordination between metabolism and the cell cycle seems necessary

Cell cycle-driven coordination of metabolism has been revealed, partly through research done on nutrient-limited synchronized yeast populations (Cai and Tu, 2012; Lloyd and Murray, 2005; Müller et al., 2003; Slavov and Botstein, 2011; Tu et al., 2005). For instance, a periodic cAMP/PKA and CDK activity have been suggested to drive the liquidation of stored carbon, thereby fuelling glycolysis and triggering the G1/S transition (Ewald et al., 2016; Zhao et al., 2016). However, interactions in the opposite direction were also found. The glycolytic flux-dependent metabolite acetyl-CoA has been shown to activate the expression of cell cycle components (e.g. Cln3) and growth-related genes (e.g. ribosomal), via the Gcn5/SAGA complex and the acetylation of histones (Cai et al., 2011; Shi and Tu,

2013). Going one step further, we recently found autonomous metabolite oscillations in single yeast cells, which occur in synchrony with but also without cell cycle progression (Papagiannakis et al., 2017). These metabolic oscillations adjust their frequency to the available nutrients and gate the cell cycle phases, thus setting the rate of division and orchestrating the transition between the cell cycle phases. It is tempting to speculate that an autonomously oscillating metabolism exists, which provides periodic triggers for cell cycle progression.

However, with the intricate interactions between metabolism, nutrient-sensing pathways and the cyclin/CDK machinery, it is hard to pinpoint the driver(s) behind these oscillations and to establish causality. Such research is further complicated by the dynamic nature of the involved processes, with certain interactions being functional only at certain moments during cell division (Cornelia Amariei, 2014; Machné and Murray, 2012; Tu et al., 2005), as well as the wide range of unspecific effects of metabolic perturbations, either applied at the genetic level (Deutscher et al., 2008) or by nutrient changes (Papagiannakis et al., 2017). Thus, to find out the minimal functional ingredients of an autonomously oscillating metabolism, it is important to disentangle cross-influences and expose the redundancy in the network.

An example of a network that connects metabolism and the cell cycle machinery is the cAMP/PKA/Rim15 pathway, integrating metabolic signals to control metabolic fluxes and to determine cell fate (Thevelein and de Winde, 1999). The central enzyme of the pathway, adenylate cyclase (Cyr1), synthesizes cAMP, which activates protein kinase A (PKA). Elevated Cyr1 activity leads to liquidation of storage carbon into glycolysis, fermentation and growth (Lee et al., 2013; Reinders et al., 1998). Adversely, absence of Cyr1 activity correlates with the accumulation of storage carbohydrates, respiration and a stationary phase metabolism (Pedruzzi et al., 2000; Smith et al., 1998). Next to its metabolic targets, cAMP signalling is known to deactivate the cyclins Cln1/2 (Baroni et al., 1994), while inhibiting the binding of the Whi3 translational inhibitor to the Cln3 mRNA (Mizunuma et al., 2013), thus granting a Cln3- and size-dependent START (Ferrezuelo et al., 2012; Schmoller et al., 2015; Talia et al., 2007), while inhibiting the anaphase promoting complex (APC1/3) for a robust separation of the early and late cell cycle (Kotani et al., 2016). While a periodic cAMP/PKA activity during the course of cell division has previously been

suggested (Müller et al., 2003) on the basis of cAMP measurements in cell-cycle synchronized populations, it is not clear how such an oscillating activity could emerge solely from the cAMP/PKA components and their interactions. Eventually, an autonomous metabolic oscillator (Papagiannakis et al., 2017) manifested via the oscillating concentration of key metabolites (e.g. FBP - (Sasidharan et al., 2012)) could entrain the cAMP/PKA activity. In fact, PKA was found to receive input from oscillating metabolites such as glucose-6-phosphate, fructose-1,6-bisphosphate, dihydroxyacetone-phosphate and glyceraldehyde-3-phosophate, via Ras (Peters, 2013). Overall, the cAMP/PKA/Rim15 pathway is embedded in an intertwined network, receiving input from and at the same time targeting metabolism.

Here, we performed a small-scale genetic screen in budding yeast to quantify the influence of cAMP/PKA- and CDK-signalling on the metabolic oscillator and the cell cycle. We either dynamically or statically removed network components, and observed the respective phenotypes on the single-cell level, including the dynamics of the metabolic oscillations, cell cycle progression, as well as the cellular physiology assayed on the population level. We found that the cAMP/PKA pathway is not necessary for metabolism to oscillate but stabilizes its amplitude in the presence of the Rim15 metabolic attenuator, facilitating cell cycle initiation. The conditional depletion of the Cdc28, the only CDK in yeast cells and inhibition target of the mating pheromone, elicited a similar metabolic response, i.e. dampening of the amplitude of the metabolic oscillator. Our data indicate the existence of a metabolic oscillator, the amplitude of which is strengthened by nutrient and cell cycle signalling pathways. Further, we found that the amplitudes of the metabolic oscillations strongly correlate with cell cycle initiation or arrest. Thus, the signalling pathways as well as the metabolic oscillator may serve as potential targets for cell fate manipulation or against proliferative disorders.

Identification of perturbation targets

As outlined above, metabolism together with the cAMP/PKA/Rim15 nutrient signalling and the cyclin/CDK machinery form an intertwined and network of metabolic pathways, transcriptional regulators and phosphorylation cascades. In search of central nodes and

perturbation targets for the investigation of the effects of cAMP/PKA- and CDK-signalling on the metabolic oscillator and the cell cycle, we present an overview of the respective network topology (Figure 1).

The adenylate cyclase, Cyr1, is a central node in the cAMP/PKA/Rim15 pathway (Thevelein and de Winde, 1999), integrating extracellular and intracellular signals to a uniform response, that of cAMP production and PKA activation. Cyr1 deletion alone disrupts the cAMP/PKA signalling cascade and is known to be lethal (Peeters et al., 2006; Zimmermann et al., 1998). One downstream target of PKA is the Rim15 kinase. Rim15 activates transcription via the PDS (post-diauxic shift) elements (Pedruzzi et al., 2000) and STREs (stress responsive elements) (Smith et al., 1998) (Figure 1), suppressing glycolysis and ribosomal biosynthesis, thus facilitating entry into the stationary phase (G0). Rim15 deletion is known to rescue the lethal *Cyr1Δ* phenotype (Reinders et al., 1998). The cAMP/PKA and Rim15 together can be considered an inhibitor/activator pair, where elevated cAMP production suppresses the Rim15 stress response and post-diauxic shift metabolism, when intracellular and extracellular nutrients are available. To investigate the effect of this pathway on the metabolic oscillator and the cell cycle, Cyr1 and Rim15 can be targeted independently or combined.

Another downstream target of PKA and Cdc28 is the neutral trehalase (Nth1), liquidizing trehalose into glycolysis at the G1/S transition (Figure 1) (Ewald et al., 2016; Zhao et al., 2016). Although it has previously been conjectured that PKA/CDK-induced cycles of trehalose liquidation could explain the periodic entrainment of metabolism during cell division (Futcher, 2006; Müller et al., 2003), they cannot account for the oscillating metabolism for the following reasons: (i) trehalose accumulation and utilization occurs only on slow growth conditions (François and Parrou, 2001; Guillou et al., 2004), such as glucose-limited continuous cultures (Müller et al., 2003) or during growth on ethanol (Ewald et al., 2016; Zhao et al., 2016). However, we have previously shown that metabolism oscillates also during aerobic fermentation (Papagiannakis et al., 2017). (ii) Yeast mutants unable to store trehalose and glycogen do not exhibit any significant cell cycle or cell size phenotype during growth on ethanol or glycerol (Zhao et al., 2016). However, given the metabolic targets of cyclin-dependent kinases, such as the cyclinB1/CDK1-mediated activation of mitochondrial respiration during the G2/M

transition described in mammalian cells (Wang et al., 2014), the yeast cyclin dependent kinase Cdc28 still constitutes an interesting perturbation target towards unravelling the interplay between metabolism and the cell cycle.

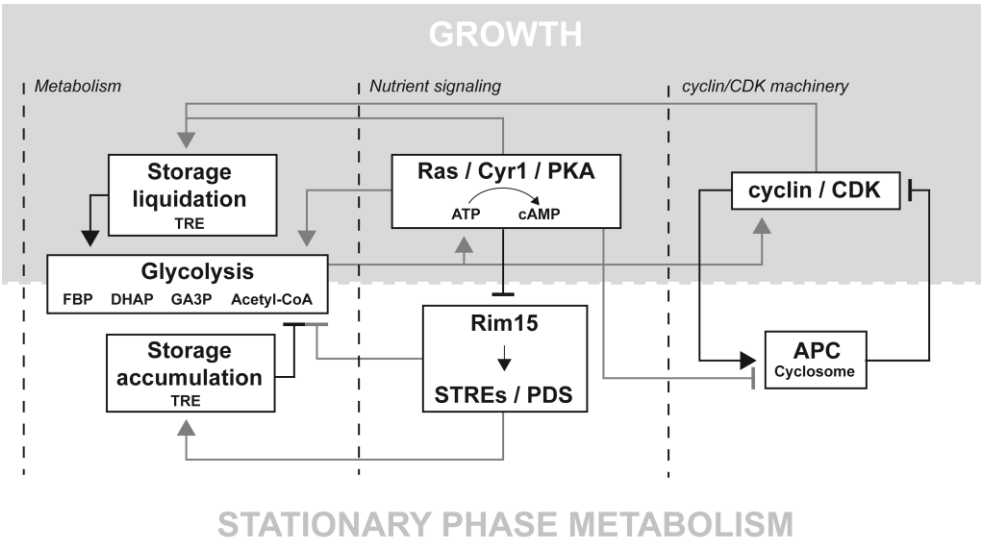

Figure 1: Metabolic pathways, nutrient signalling and the cyclin/CDK machinery form an intertwined network, for the robust coordination between the cell cycle and metabolism. According to the presented model, the cAMP/PKA pathway receives dynamic input from glycolytic intermediates (i.e. Fructose-1,6-bisphosphate - FBP, Dihydroxyacetone-phosphate - DHAP, Glyceraldehyde-3-phosphate - GA3P), the concentrations of which regulate the activity of Ras (Peters, 2013). Metabolism also provides input to the cyclin/CDK machinery, via the metabolite acetyl-CoA, which is known to epigenetically activate the expression of Cln3 at START (Cai et al., 2011; Shi and Tu, 2013). PKA and the CDK have been suggested to co-activate the enzyme neutral trehalase (Nth1), catalyzing the liquidation of trehalose (TRE) into glycolysis (Ewald et al., 2016; Zhao et al., 2016). Adversely, in the absence of cAMP signalling, Rim15 activates transcription via the stress responsive elements (STREs) and the post-diauxic shift (PDS) elements, suppressing glycolysis and activating trehalose accumulation (Pedruzzi et al., 2000; Smith et al., 1998). Finally, the anaphase promoting complex is known to be inhibited by high PKA activity (Kotani et al., 2016).

Means of perturbation and related experiments

In this study, we used different means of perturbation. Rim15 was deleted at the gene level. The auxin-inducible degron (AID) was used to conditionally and dynamically deplete essential proteins (Morawska and Ulrich, 2013; Nishimura et al., 2009). Cyr1 and Cdc28 were tagged with the auxin degron sequence at their C-terminal, for ubiquitination and proteasomal degradation upon the addition of the plant hormone auxin, in the presence of the plant F-box protein Os-TIR1. After the addition of auxin the targeted proteins were fully depleted within 25 min (Figure S1). Because the average doubling time of yeast during aerobic fermentation (10 gL^{-1} glucose) is 100 min, using the AID system we could generate deletion phenotypes within the duration of a single division cycle. Finally, the alpha factor was used as an additional way to perturb Cdc28 activity. The alpha factor is known to activate Far1, an inhibitor of the cyclin-dependent kinase, via the pheromone response pathway (Bardwell, 2004), a MAPK (Mitogen Activated Protein Kinase) phosphorylation cascade commencing from the pheromone receptor and its coupled G-proteins. Additionally, the alpha factor has been suggested to inhibit the adenylate cyclase (Cyr1) (Liao and Thorner, 1980; Valbuena and Moreno, 2010).

As a reporter of the oscillating metabolic activity we used the auto-fluorescence of the NAD(P)H, previously shown to oscillate in synchrony with, but also in the absence of cell division (Lloyd and Murray, 2005; Lloyd et al., 2002; Papagiannakis et al., 2017; Xu and Tsurugi, 2006). Fluorescently labelled Whi5 was used as a reporter of Cdc28 activity (Figure S2A-C) (Costanzo et al., 2004). Whi5 is an inhibitor of cell cycle transcription, which - in the absence of CDK activity – is sequestered in the nucleus during the G1 phase. At START, the active complex Cln3/Cdc28 phosphorylates Whi5 causing its sequestration into the cytoplasm, leading to cell cycle initiation (Figure S2A) (Ferrezuelo et al., 2012; Liu et al., 2015; Schmoller et al., 2015). NAD(P)H auto-fluorescence and Whi5 localization were measured in single yeast cells using epi-fluorescence microscopy (Figure S2B). A microfluidic dissection platform was used to cultivate single yeast cells (Huberts et al., 2013; Lee et al., 2012).

On the population level, we used flow cytometry to monitor the growth and morphological (cell size) effects of the applied perturbations. In addition, to determine changes in cell

physiology upon alpha factor addition, in the presence or absence of Rim15, the glucose uptake and ethanol production rates were determined from dynamic metabolite concentration measurements in the culture supernatant. Overall, combining different perturbation schemes, we screened for effects of cAMP/PKA- and CDK-signalling on the metabolic oscillator and the cell cycle.

Results

Results from perturbation experiments on the single cell and population level

In order to unravel the implications of cAMP signalling on the metabolic oscillator and the cell cycle we dynamically depleted the adenylate cyclase (Cyr1) using the AID system (Morawska and Ulrich, 2013; Nishimura et al., 2009). Upon Cyr1-AID depletion, all cells stopped dividing and were arrested in the G1 phase (Figures S3 & 2A), consistent with Cyr1 being essential (Peeters et al., 2006; Zimmermann et al., 1998) and with the presumed importance of cAMP signalling for the G1/S transition (Baroni et al., 1994; Futcher, 2006; Mizunuma et al., 2013; Müller et al., 2003). Focusing on the metabolic dynamics, we found that cells continued to exhibit metabolic oscillations even after Cyr1-AID depletion and cell cycle arrest, albeit with seemingly lower amplitudes (Figure 2A).

The downstream effector of the cAMP/PKA pathway, the Rim15 kinase, is known to suppress glycolysis and ribosomal biosynthesis in the absence of cAMP activity (Conrad et al., 2014; Pedruzzi et al., 2000; Smith et al., 1998). Consistent with the synthetic rescue of the *Cyr1Δ* lethal phenotype by deleting Rim15 (Reinders et al., 1998), in cells lacking Rim15 we found a significant fraction (40%) that continued budding upon Cyr1-AID depletion (Figure 2B). This fraction continued exhibiting metabolic oscillations with high amplitudes, contrary to the cells of the non-dividing fraction, which exhibited seemingly dampened metabolic dynamics (Figure 2B).

The experiments with the alpha factor (Figure 2C) yielded similar phenotypes as the experiments, in which we conditionally depleted Cyr1-AID (Figure 2A-B): Cells with Rim15 and exposed to alpha factor were arrested in the G1 phase (un-budded cells) and

exhibited dampened metabolic dynamics. In the absence of Rim15 (Figure 2C-top), two populations emerged after the addition of the mating pheromone. The dividing population exhibited high amplitude metabolic oscillations (Figure 2C-middle), in contrast to the arrested cells (Figure 2C-bottom) with seemingly dampened metabolic dynamics. Consistent with the pheromone induced CDK inhibition via the pheromone response pathway (Bardwell, 2004) and the here observed dampening of the metabolic dynamics after the addition of α-factor, also when we conditionally depleted the Cdc28 using the AID mechanism (Morawska and Ulrich, 2013; Nishimura et al., 2009), we found cells to exhibit dampened metabolic oscillations (Figure 2D).

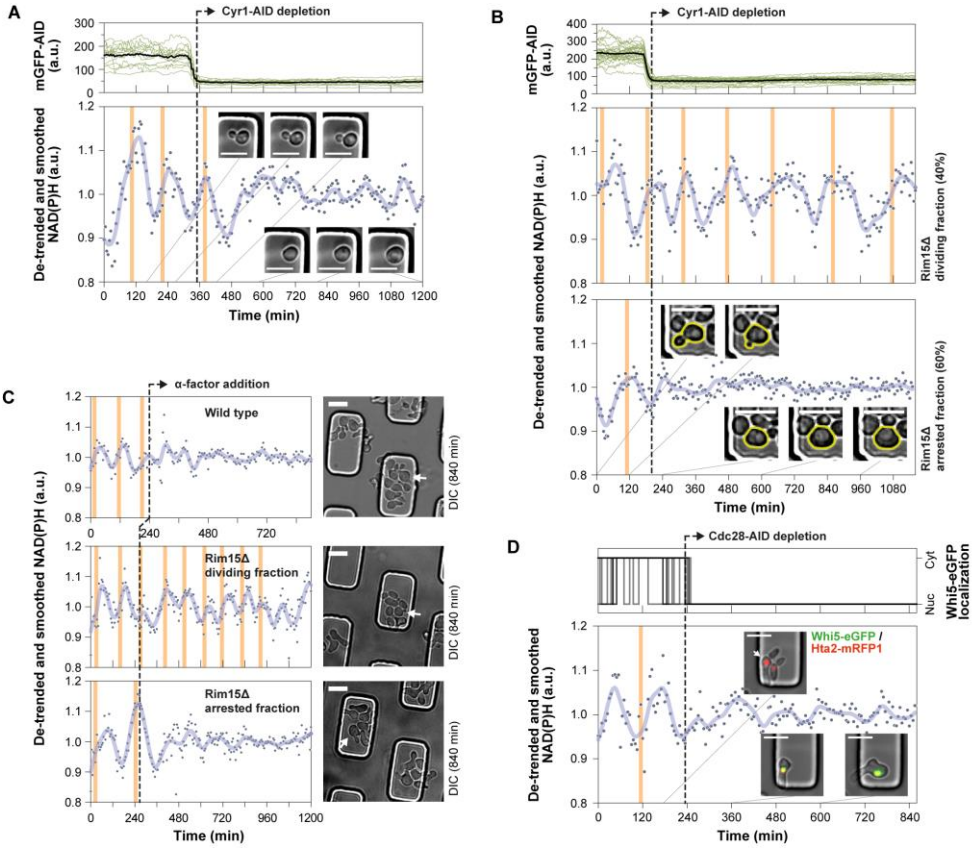

Figure 2: Results from the single cell perturbation experiments. Exemplary cells are presented for each perturbation experiment and subpopulation, including the metabolic (NAD(P)H) and cell cycle (budding, Whi5 localization) dynamics, as well as microscopy images (scale bars, 10 µm). All

experiments were performed with the microfluidic dissection platform for yeast. **(A)** Cyr1-AID was depleted using the auxin inducible degron. In order to determine the depletion dynamics of the adenylate cyclase, in the same experiment and the same microfluidic device we loaded control cells expressing mGFP tagged with the auxin degron sequence (mGFP-AID) and monitored their GFP dynamics. We have confirmed that the mGFP-AID can be used to estimate the Cyr1-AID depletion dynamics (Figure S1). Microscopy images confirm the cell cycle arrest in the G1 phase (cell without bud after Cyr1-AID depletion, see also Figure S2). Vertical orange lines correspond to budding. **(B)** As in Fig. 1A, also here we loaded mGFP-AID cells in the same microfluidic device to monitor the Cyr1-AID depletion dynamics in the *Rim15Δ* cells. Upon depletion of the adenylate cyclase and in the absence of Rim15 two populations emerge: a dividing population (approx. 40%) and a non-dividing population (approx. 60%). **(C)** Wild type (top) and *Rim15Δ* (middle and bottom) single cells before and after the addition of α-factor. Wild type cells (top) are arrested in the G1 phase after the addition of the mating pheromone adopting the shmoo phenotype (microscopy figure). In the *Rim15Δ*, we observe a dividing fraction of cells (middle), resembling exponentially growing unperturbed cells, and an arrested fraction (bottom) adopting the shmoo phenotype. **(D)** A single cell before and after the depletion of Cdc28-AID, signaled by the sequestration of Whi5-eGFP into the nucleus (as in Figure S2A-C). After the depletion of Cdc28-AID metabolic oscillations persist yet with seemingly lower amplitudes.

We confirmed the difference in the response of the wild type and the *Rim15Δ* cells to the addition of the mating pheromone also on the population level: First, analyzing the whole-population growth rates by flow cytometry after the addition of the mating pheromone, we found that in contrast to the wild type population which was almost completely growth arrested approaching a growth rate of 0 h^{-1}, in the absence of Rim15 cells achieved a higher population-averaged growth rate (approximately 0.1 h^{-1}) (Figure 3A), consistent with the incomplete cell cycle arrest in the *Rim15Δ* cells, and the existence of growing cell fractions that we found (Figure 2C).

Second, we focused on cell morphology. The α-factor induces the formation of mating projections upon cell cycle arrest, commonly known as the shmoo phenotype (Bardwell, 2004), resulting in bigger and polarized cells (cf. images in Figure 2C). Using flow-cytometry and the forward scatter as a proxy of cellular morphology we were able to discern between growing (mothers and daughters) and arrested (shmoo) cells (Figure 3B-C). Already 2.5 hours after the addition of the mating pheromone we could distinguish a growing fraction of dividing (non-shmooing and thus small) *Rim15Δ* cells (Figure 3C), in contrast to the wild type cells, which were all arrested (Figure 3B). By dividing the numbers of arrested cells prior and at different times after the addition of the mating

pheromone, we found a constantly increasing fraction of growing cells (after the α-factor addition) in the absence of Rim15, but not in the wild type cells (Figure 3D). These population level analyses based on a much larger number of cells confirmed the results on the two distinct phenotypes in the Rim15 deletion mutant as determined from the microfluidics experiments with much less analysed cells.

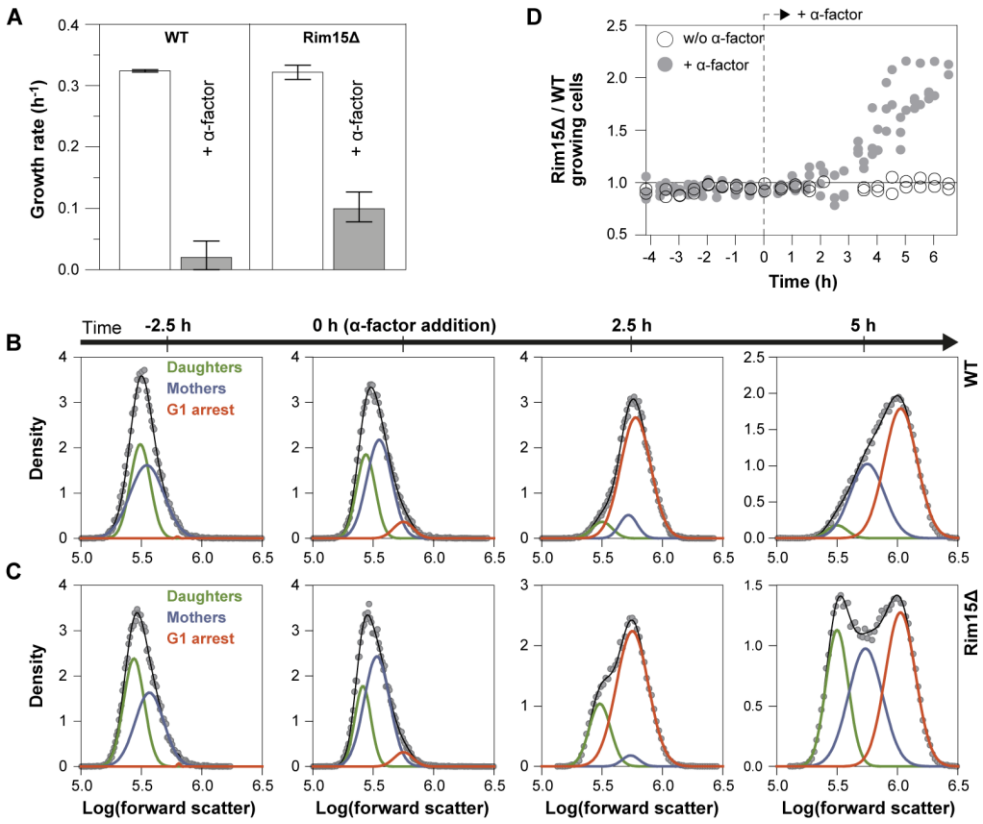

Figure 3: Phenotypic bistability, with dividing and G1-arrested population fractions, upon the addition of alpha factor in *Rim15*Δ cells. (A) The average growth rates (error bars: range of values) measured in wild type and *Rim15Δ* populations grown in the absence (2 biological replicates per strain) or in the presence of the mating pheromone (5 biological replicates per strain). **(B-C)** The Gaussian distributions of the daughter (green), mother (blue) and G1 arrested (red) cells, separated on the basis of their forwards scatter, prior and after the addition of α-factor (at 0 h), in wild type **(B)** or *Rim15Δ* **(C)** cells. A sum of three Gaussians (black line) was fitted to the entire population to determine the contribution of the three cell fractions. The mean logarithms of the forward scatter (fsc) of the daughter ($\log(fsc)_{daughters}$ = 5.45±0.05) and the mother ($\log(fsc)_{mothers}$ = 5.63±0.13) cells was

determined on the basis of exponentially growing unperturbed cultures and was fixed within the specified bounds during the fitting. The G1 arrested cells after the addition of the mating pheromone adopt the shmoo phenotype and are thus bigger than the corresponding mother cells ($\log(fsc)_{arrested} > 5.75$). **(D)** The number of dividing cells (daughters + mothers) in the *Rim15Δ* population, as determined from the fitted Gaussians, divided over the number of wild type growing cells, prior and after the addition of α-factor (grey markers), or during unperturbed growth in the absence of the mating pheromone (white markers).

Table 1: Overview of the applied perturbations and their effects on metabolism as well as the cell cycle. The auxin-inducible degron (AID) was used to conditionally deplete the essential adenylate cyclase (Cyr1) and cyclin dependent kinase (Cdc28). Rim15 was knocked out (KO) from the genome. The amplitudes of the metabolic oscillations were determined in single cells on the basis of the oscillating NAD(P)H signal. Metabolic oscillations were confirmed in all experiments by visual inspection. Budding was determined by microscopy or development of cell size and counts as determined by flow-cytometry were used to distinguish between growing and arrested cells.

Perturbation target(s)	Pathway(s)	Method(s)	NAD(P)H oscillations	Amplitude	Cell cycle
Cyr1	cAMP/PKA	AID	Yes	Dampened	Arrest
Cyr1 Rim15	cAMP/PKA	AID KO	Yes	Bistability Amp/Damp	Bistability Growth/Arrest
Cdc28 Cyr1	Cyclin/CDK cAMP/PKA	α-factor	Yes	Dampened	Arrest
Cdc28 Rim15	Cyclin/CDK cAMP/PKA	α-factor KO	Yes	Bistability Amp/Damp	Bistability Growth/Arrest
Cdc28	Cyclin/CDK	AID	Yes	Dampened	Arrest

The results from our perturbation experiments can be summarized into three main findings: (i) metabolic oscillations persisted even in the absence of cAMP and CDK signalling consistent with the previously conjectured autonomous nature of the metabolic oscillator, (ii) the metabolic dynamics were dampened in the absence of cAMP or CDK signalling, (iii) deletion of Rim15 generates phenotypic bistability in the absence of cAMP signalling or upon the addition of alpha factor, including a dividing cellular fraction with enhanced metabolic dynamics, and a G1-arrested cellular fraction with dampened metabolic oscillations. An overview of the applied perturbations and their observed effects on metabolism and the cell cycle is provided in Table 1.

The metabolic dynamics set a threshold between cell division and cell cycle arrest.

In our single cell perturbation experiments, we witnessed that every time the cell cycle was arrested, independently of the applied perturbation (Cyr1-AID depletion, Cdc28-AID depletion or α-factor addition), the metabolic oscillations as measured via NAD(P)H were dampened. To establish a correlation between the metabolic dynamics and the cell cycle, we needed to quantify the metabolic dynamics. For this purpose, we used the standard deviation of the NAD(P)H signals as an unbiased proxy of the amplitude of the metabolic oscillations. The standard deviation was estimated on the basis of single-cell NAD(P)H signals, after they were corrected for the low frequency noise by dividing over a fitted smoothing spline (p=1e-07, for all single cells).

Our results show a strong correlation between the metabolic dynamics and the cell cycle (division or arrest) (Figure 4A). The standard deviation of the single cell NAD(P)H signal sets a clear threshold between cell division and cell cycle arrest, independently of the applied perturbation. Enhanced NAD(P)H amplitudes (SD > 0.04) are predictive of cell cycle initiation, whereas attenuated metabolic amplitudes (SD < 0.04) are predictive of cell cycle arrest (Figure 4A). This is not the first time a metabolic threshold is identified between dividing and arrested cells. We have previously shown that the frequency of the metabolic oscillator is also a reliable predictor of cell cycle initiation (Papagiannakis et al., 2017), which can be used robustly distinguish between dividing and quiescent cells under nutrient limited conditions (0.01 gL^{-1} glucose). In fact, when found that the amplitude of the

metabolic oscillator can indeed also be used to distinguish between dividing and quiescent non-dividing cells, during respiratory growth on 0.01 gL^{-1} (Figure 4B).

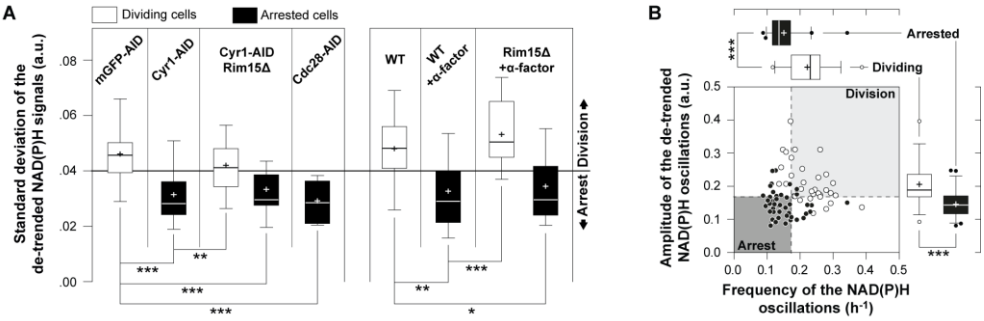

Figure 4: The frequency and the amplitude of the metabolic oscillations correlate with cell division or cell cycle arrest. (A) The standard deviation of the de-trended NAD(P)H signals was used as an unbiased proxy of the amplitude of the metabolic oscillator. The distribution of the standard deviations are presented (error bars 95% CI, + mean) from (left to right) 41 control cells (mGFP-AID depleted), 19 single cells after Cyr1-AID depletion in the presence of Rim15, 39 Rim15Δ single cells (18 dividing and 21 arrested) after Cyr1-AID depletion, 7 arrested cells after the conditional depletion of Cdc28-AID, 25 control cells (wild-type cells in the absence of α-factor), 24 arrested wild-type single cells after the addition of α-factor and 29 *Rim15Δ* cells after the addition of alpha factor (12 dividing and 17 arrested). Kruskal-Wallis significance test, Dunns post-test, * $p<0.05$, ** $p<0.01$, *** $p<0.001$. **(B)** The frequencies of 35 metabolic oscillations from an equal number of dividing cells (white markers), and the frequencies of 47 metabolic oscillations in the absence of cell division from 19 quiescent cells (black markers) of cells grown on 0.01 gL^{-1} glucose. Frequencies were estimated as the inverse of the time between consecutive troughs. The amplitudes of the oscillations were estimated by subtracting the average NAD(P)H level between two consecutive troughs from the NAD(P)H level at the intermediate peak. The distributions of the estimated frequencies and amplitudes are plotted in the corresponding box plots (whiskers: 5-95 percentile, cross: mean). The lower 25 percentiles of the measured amplitudes and frequencies in dividing cells were used to draw the respective thresholds (dotted lines) between cell division and cell cycle arrest (Mann-Whitney test, *** $p < 0.001$). All NAD(P)H signals were de-trended by dividing over fitted smoothing splines ($p = 1e\text{-}07$).

Here we show that cell cycle arrest requires the attenuation of the metabolic dynamics, which can be achieved via the inhibition of CDK or cAMP signalling (Figure 4A, Table 1). Our findings justify the interconnectivity between the metabolic oscillator, the cAMP/PKA pathway and the cyclin/CDK machinery, but also expose the redundancy in the network.

The cAMP/PKA pathway is not necessary for cell cycle initiation or pheromone mediated cell cycle arrest, but contributes to the robustness of both process, for a uniform metabolic and cell cycle response in the population.

The cAMP/PKA pathway establishes positive feedback to the metabolic dynamics and stabilizes the amplitude of the metabolic oscillations above the critical threshold for cell cycle initiation.

The cAMP/PKA pathway is thought to provide a molecular link between metabolism and the cell cycle. According to the "finishing kick to START" hypothesis (Futcher, 2006), developed on the basis of metabolite data from synchronized nutrient-limited cultures (Lloyd and Murray, 2005; Müller et al., 2003; Tu et al., 2005), elevated cAMP levels and PKA activity during the late G1 phase trigger the liquidation of trehalose into glycolysis, causing the onset of a fermentative metabolism and enhanced protein synthesis, until the trehalose reserves are depleted. As a result, the early cyclin production rates increase beyond their fast degradation, triggering cell cycle initiation and START.

However, our results contradict the "finishing kick to START" hypothesis" for two reasons: First, we found metabolism to continue to oscillate in Cyr1-AID depleted and cell cycle arrested cells, yet with lower amplitudes (Figures 2A & 4A). Second, when Cyr1-AID was conditionally depleted in the absence of the Rim15 kinase, i.e. the downstream target of PKA, we witnessed a significant fraction (40%) of normally dividing cells with normal metabolic dynamics (NAD(P)H SD > 0.04) (Figures 2B & 4A). Our results are consistent with the recent finding that yeast mutants, unable to synthesize storage carbohydrates, did not exhibit any growth defect or specific phenotype (Zhao et al., 2016). Thus, we show that the periodic entrainment of carbon storage metabolism by the cAMP/PKA pathway is not necessary for the metabolic oscillations or their coordination with the cell cycle.

Instead, the normal cell cycle progression and normal metabolic amplitudes (NAD(P)H SD > 0.04) that we observed in a significant fraction of the *Rim15Δ* cells, after the addition of α-factor and the conditional depletion of Cyr1-AID, suggests that Rim15 operates as a metabolic attenuator, robustly dampening the metabolic dynamics, which leads to cell cycle

arrest in the absence of cAMP signalling. In fact, confirming the metabolic role of Rim15, we found that the *Rim15Δ* cells yielded more ethanol per glucose molecule after the addition of alpha factor, as compared to wild type arrested cells (Figure 5A. Taking these observations together, we think that an oscillatory activity of cAMP/PKA – eventually induced by weak autonomous metabolic oscillations – dynamically activates Rim15 activity, which in turn dynamically impacts metabolism, thus together forming a positive feedback loop results in strengthened metabolic amplitudes (Figure 5B).

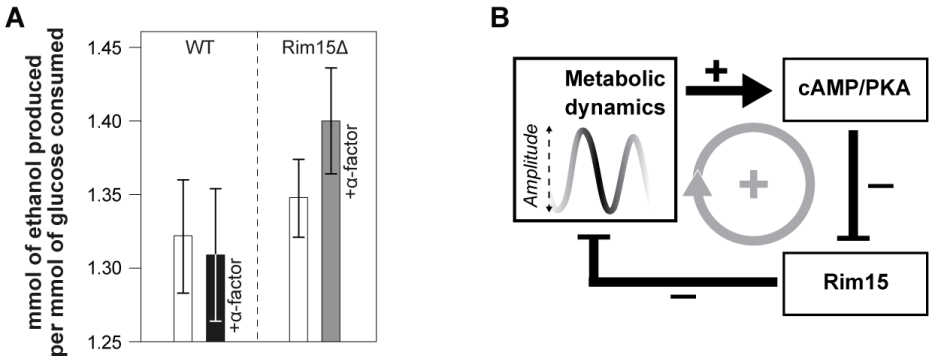

Figure 5: Rim15 is a metabolic attenuator, required for the robust pheromone induced cell cycle arrest. (A) The average ethanol yield measured in populations of wild type and *Rim15Δ* cells grown in the presence or the absence of the mating pheromone. Linear regression were fitted to data describing the amount of ethanol production per glucose production, both measured in the supernatant of the cultures. One linear regression was fitted to data from two biological replicates per strain and condition. The error bars represent the standard error of the slope of the fitted linear regression. **(B)** The cAMP/PKA/Rim15 pathway establishes a positive feedback loop on the metabolic dynamics. Metabolic dynamics activate cAMP signalling, thus strongly inhibiting the metabolic attenuator Rim15, and maintaining high amplitude oscillations. Reduced metabolic dynamics, insufficient to trigger cAMP signalling, activate the metabolic attenuator Rim15, which further dampens metabolism for a robust cell cycle arrest. The robust attenuation dynamics and cell cycle arrest is also be achieved by direct inhibition of the cAMP/PKA module, for instance by conditionally depleting Cyr1-AID.

The fact that we also observed strong metabolic oscillations in the absence of Cyr1 and Rim15 suggests that the positive feedback loop is not necessary to generate metabolic dynamics effective for cell cycle initiation (SD > 0.04). Adversely, our finding that a fraction of *Rim15Δ* cells was arrested in the absence of Cyr1, under rich nutrient conditions

($10gL^{-1}$ glucose), reveals stochasticity in the dynamics of the metabolic oscillator. In the absence of cAMP/PKA/Rim15 signaling this metabolic stochasticity is expressed as phenotypic bistability, due to the minimal metabolic threshold (SD = 0.04) required for cell cycle initiation. Overall we conclude that in nutrient rich conditions the cAMP/PKA/Rim15 positive feedback loop enhances and stabilizes the metabolic dynamics above the effective threshold for START, eliminating stochasticity in the metabolic and thus the cell cycle process.

The alpha factor arrests the cell cycle by dampening the metabolic dynamics

We have found that also the mating pheromone reduces the amplitude of the metabolic oscillator (Figure 6A) in a Rim15- and thus cAMP/PKA-dependent manner (Figure 2C), similarly to the conditional depletion of the adenylate cyclase (Figures 6A and 2A-B), leading to cell cycle arrest. Still, it remains unclear how the α-factor inhibits the cAMP/PKA pathway. Two models of mating pheromone-induced cAMP/PKA inhibition are possible: The "direct model of cAMP/PKA inhibition" (Figure 6B) is based on an old finding according to which the α-factor directly inhibits the adenylate cyclase (Liao and Thorner, 1980). Adversely, the mating pheromone could indirectly affect the cAMP/PKA activity, via the pheromone response pathway (Bardwell, 2004) and Cdc28 inhibition ("indirect model of cAMP/PKA inhibition" – Figure 6B). This could go as follow: the alpha factor inhibits CDK, which has also targets in metabolism (e.g. mitochondrial respiration), which in turn could affect cAMP/PKA through its input from metabolism, for instance through flux signalling metabolites (e.g. FBP). The thereby altered cAMP/PKA activity would lead to an activation of the Rim15 kinase, and would result in attenuation of metabolism.

The dampened metabolic oscillations in the Cdc28-AID depleted cells (Figure 4A & 6A), similarly to Cyr1-AID depletion or the addition of α-factor, confirm the metabolic function of CDK in yeast, and the support the "indirect model of cAMP/PKA inhibition" by the mating pheromone (Figure 6B). However, we cannot exclude the possibility that the mating pheromone targets the cAMP/PKA pathway both indirectly via Cdc28 and metabolism, as well as by directly inhibiting Cyr1 (Figure 6B).

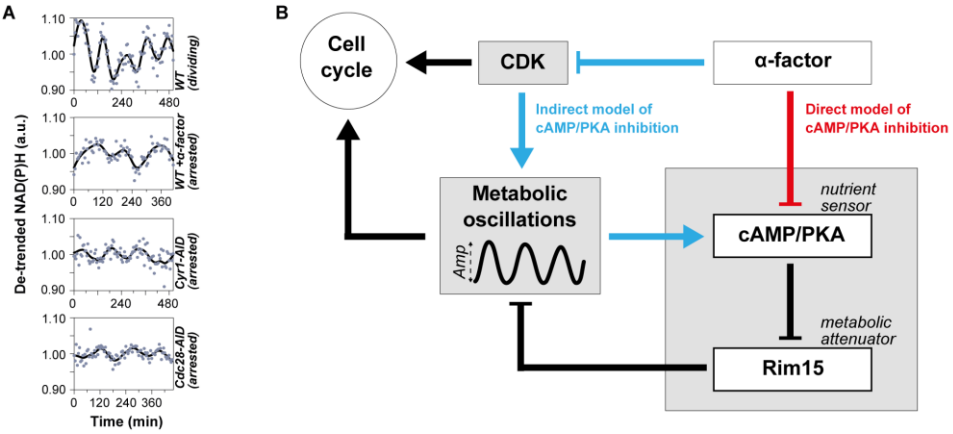

Figure 6: Reconstructed network topology derived from our single cell and population level perturbation experiments. (A) De-trended NAD(P)H oscillations from four exemplary single cells, including a control cell dividing normally on high glucose (top), a G1 arrested cell after the addition of α-factor, a G1 arrested cell after the conditional depletion of Cyr1-AID, and a cell cycle arrested cell after the conditional depletion of Cdc28-AID (bottom). **(B)** From our results we derive an interaction network topology between the metabolic oscillator, the cAMP/PKA/Rim15 pathway and the cyclin/CDK machinery, altogether contributing to cell cycle regulation. The cAMP/PKA/Rim15 pathway consists of (i) a sensory domain (cAMP/PKA) integrating signals from the autonomous (weak) metabolic oscillator and (ii) the attenuator module (Rim15) which reduces the metabolic dynamics in the absence of cAMP signalling. The mating pheromone inhibits the cAMP signalling indirectly (blue connections), via inhibiting Cdc28 consequently inhibiting metabolism, and possibly also directly (red connections) inhibiting Cyr1.

Discussion

In our small-scale genetic screening we have gained insight on the interactions between the metabolic oscillator, the cAMP/PKA pathway and cyclin/CDK machinery, as well as the emergent coordination between metabolism and the cell cycle. Here we show that the cAMP/PKA driven cycles of carbon storage accumulation/liquidation are not necessary for cell division or an oscillating metabolism. Our data expose the redundancy of the cAMP/PKA pathway, but most importantly suggest its role in removing noise from the metabolic dynamics. The adenylate cyclase (Cyr1) integrates signals from a periodic metabolism and the oscillating concentrations of glycolytic intermediates (e.g. FBP) via its

Ras activator (Peters, 2013), and thus functions as a sensor of the metabolic dynamics (Figure 6B). The Rim15 kinase constitutes the attenuation module (Figure 5B), which inhibits glycolysis and protein synthesis (Pedruzzi et al., 2000; Smith et al., 1998) when the sensory domain reports a "slow" metabolism (absence of PKA activity), either as a result if poor nutrient conditions, or after the addition of the mating pheromone, for the robust cell cycle arrest in G1. Adversely, in nutrient rich conditions, the cAMP/PKA pathway establishes a positive feedback to the metabolic dynamics (Figure 5B), stabilizing their amplitude above the effective threshold for cell cycle initiation, for a robust cell cycle initiation. If the metabolic sensor-attenuator pair (cAMP/PKA/Rim15) is removed altogether, then the cells are prone to the noise in the metabolic dynamics, occasionally escaping cell cycle arrest even upon the addition of the mating pheromone.

Here, we show a strong correlation between the amplitude of the metabolic oscillations and the cell cycle. Our findings are reminiscent of the previously conjectured metabolic checkpoint at START (Jones et al., 2016; Lee and Finkel, 2013; Schieke et al., 2008), controlling the G1/S transition in coordination with enhanced mitochondrial potential and bioenergetics, or the metabolic flux dependent expression of Cln3 triggering START (Cai et al., 2011; Shi and Tu, 2013). We identify this checkpoint as a threshold in the NAD(P)H dynamics, namely the frequency and the amplitude of the metabolic oscillations, which needs to be surpassed for cell cycle initiation. The same metabolic threshold is responsible for the emergence of two sub-populations, a dividing and a non-dividing one, during respiratory growth on low glucose (0.01 gL^{-1}) or upon the addition of alpha factor in the absence of the metabolic attenuator Rim15.

The metabolic oscillator constitutes a prime target for cell cycle regulation. Thus, it is not surprising that Cdc28 has an effect on the metabolic dynamics. In fact, metabolic functions have previously been attributed to the cyclin/CDK machinery. In mammalian cells, CDK1 has been shown to localize in mitochondria, phosphorylating components of the respiratory chain, enhancing mitochondrial respiration and accelerating the G2/M transition (Wang et al., 2014). The yeast CDK (Cdc28) has been suggested to co-activate the neutal trehalase together with the cAMP/PKA pathway (Ewald et al., 2016; Zhao et al., 2016), promoting the liquidation of trehalose into glycolysis at START. However, this has been identified as a secondary interaction. First, trehalose storages are almost empty during fermentative

growth on high ($10gL^{-1}$) glucose (François and Parrou, 2001; Guillou et al., 2004), whereas yeast mutants unable to store trehalose or glycogen did not exhibit any specific phenotype or growth defects during exponential growth on ethanol or glycerol (Zhao et al., 2016). It still remains unknown how the CDK activity stabilizes the amplitude of the metabolic oscillations during fermentative growth.

The Warburg effect provides a widely cited connection between metabolism and the cell cycle (Diaz-Ruiz et al., 2011; Vander Heiden et al., 2009). Cancer cells exhibit increased rates of glycolysis, secreting large amounts of fermentation products (e.g. lactate), even in the presence of oxygen. Adversely, somatic non-dividing cells reside solely on respiration to produce energy and biomass. Considering the here identified metabolic threshold separating cell division from cell cycle arrest, we envision that the metabolic oscillator and its correlated dynamics may constitute reliable diagnostic markers or therapeutic targets against cancer.

Experimental procedures

Chemicals

All regular chemicals were purchased from Sigma-Aldrich, Acros Organics, Formedium or Merck Milipore. Potassium phthalate monobasic and 3-indoleacetic acid sodium salt (auxin) were purchased from Sigma-Aldrich.

Strains and strain construction

The prototrophic YSBN6 strain, derived from S288c, and its HIS- variant (YSBN16) were used. For an overview on all strains refer to Table S1.

In order to dynamically deplete adenylate cyclase, the central node of the cAMP/PKA pathway, we tagged the respective protein (Cyr1), with the truncated degron sequence $AID^{71\text{-}114}$, previously tested and successfully applied in yeast cells (Morawska and Ulrich,

2013). Flanking sequences adjacent to the stop codon of Cyr1 were amplified using the primers CYR1-CDS and CYR-DOWN. The mCherry coding sequence, together with the truncated degron tag (AID^{71-114}) and the NatMX antibiotic resistance cassette, were amplified in a single piece from the pG23A plasmid (primers mCherry-IAA-Nat). The ampicillin resistance cassette and the ColE1 origin of replication, for selection and amplification into *Escherichia coli*, were amplified in one piece from the pG23A plasmid (primers Amp). The four pieces were assembled into the pG19A plasmid using Gibson assembly (Gibson et al., 2009). The pG19A assembly product was verified by sequencing (primers Seq102, G5NAT & CYR-DOWN Rev), linearized by PCR (primers CYR1Lin) and was used to transform YSBN6 wild type yeast cells, under the selection of ClonNAT. For all yeast transformations we used the lithium acetate high-efficiency protocol (Gietz and Schiestl, 2007). Correct integration into the YSBN6.G19A strain was confirmed using PCR (primers CYR1Lin).

For the deletion of the Rim15 metabolic attenuator, we substituted its coding sequence with the Ble gene, offering resistance to phleomycin. Flanking sequences upstream and downstream the Rim15 coding sequence were amplified using the primers RIM15-UP and RIM15-DOWN, respectively. The Ble antibiotic resistance cassette was amplified from the pG25 plasmid (primers Phleo). The ampicillin resistance cassette and the ColE1 origin of replication, for selection and amplification into *Escherichia coli*, were amplified in one piece from the pG23A plasmid (primers Amp). The four pieces were assembled into the pG27 plasmid using Gibson assembly. The pG27 assembly product was verified by sequencing (primers Phleo Fwd/Rev & Seq6Rev), linearized by PCR (primers RIM15Lin2) and was used to transform YSBN6 wild type and YSBN6.G19A yeast cells, under the selection of ClonNAT. Correct integration into the YSBN6.Rim15Δ and the YSBN6.G19A.Rim15Δ strains was confirmed using PCR (primers RIM15Lin2).

Cultivation

Single yeast colonies growing on YPD 20 gL^{-1} glucose agar plates were used to inoculate 10 mL minimal 10 gL^{-1} glucose medium (pH was adjusted with 10mM K-Phthalate-KOH to pH 5) (Verduyn et al., 1992) in 100 mL shake flasks, and grown (at 30°C, 300 rpm)

overnight. The overnight culture was used to inoculate fresh 10 gL^{-1} glucose medium to an OD of 0.1, which was grown to an OD between 1 and 1.5 (still exponential growth on 10 gL^{-1} glucose).

For microscopy experiments on 10 gL^{-1} glucose, the exponentially growing cells were again diluted to an OD of 0.05 in fresh 10 gL^{-1} glucose medium, and then used to load the microfluidic chip as described (Huberts et al., 2013; Lee et al., 2012). For microscopy experiments on 0.01 gL^{-1} glucose, the exponentially growing cells on 10 gL^{-1} glucose were used to inoculate a 0.01 gL^{-1} glucose medium to an OD of 0.05, and grown to an OD of 0.2 to 0.8. This exponentially growing culture was used to inoculate a fresh 0.01 gL^{-1} glucose medium to an OD of 0.05, where the cells were grown for 2 hours and then used to load the microfluidic chip. In the Cyr1 and Cdc28 depletion experiments, the Cyr1-mCherry-AID or Cdc28-AID expressing cells were always mixed with cells expressing mGFP-AID (YSBN6.G2J - Table S1) to determine the timing of protein depletion (Figures S1 & 2A-B). 0.1 mM of auxin were used in all perturbation experiments, where the auxin-inducible degron was used (AID). During cell culturing in the microfluidic chip, cells were fed at 4.8 μL min-1 with the same media as in the culture before loading. The provided media were pre-warmed to 30°C and saturated with atmospheric air by shaking at 300 rpm for at least two hours prior to use. In alpha factor perturbation experiments, the medium was switched to a medium supplemented with 5 μg mL-1 alpha factor, a previously specified concentration (Futcher, 1999).

For the flow-cytometry experiments, performed on the population level, exponentially growing cells were diluted in fresh, pre-warmed and oxygen saturated minimal medium containing 10gL^{-1} glucose, at an initial OD of 0.1.

Microscopic analyses

Image acquisition (Nikon Ti-E inverted microscopes with either an Andor 897 Ultra EX2 EM-CCD camera or 2x Andror LucaR EM-CCD dual camera system; CoolLed pE2 excitation system; Nikon PFS dynamic focusing system) took place every 5 min (for 10 gL^{-1}) and 10 min (for 0.01 gL^{-1} glucose), in the DIC, NAD(P)H, GFP and RFP channels using

a 40x Nikon Super Fluor Apochromat objective. For the observation of sustained metabolic oscillations in the absence of budding on low glucose, 20 minutes measurement intervals were applied. For NADH measurements, cells were excited at 365 nm with 15% excitation light intensity using a 350/50 nm bandpass filter. The NAD(P)H emission was recorded with no binning using a 409 nm beam-splitter and a 435/40 nm emission filter. For GFP measurements (mGFP-AID and Whi5-eGFP), cells were excited at 470 nm with 15% light intensity using a 470/40 nm bandpass filter. The GFP emission was recorded using a 495 nm beamsplitter and a 525/50 nm emission filter. For the mCherry (Cyr1, mCherry-AID) and mRFP1 (Hta2-mRFP1) measurements, cells were excited at 565 nm with 50% or 15% light intensity respectively, using a 560/40 nm bandpass filter. The mCherry/mRFP1 emission was recorded using a 585 nm beamsplitter and a 630/75 nm emission filter. 200 msec exposure time was applied for the NAD(P)H, GFP and mRFP1 channels, as well as during DIC imaging. 600 msec exposure time was applied for the mCherry channel. In the DIC channel, a halogen lamp was used as a light source, the light of which was filtered through an ultraviolet light filter (420 nm beamsplitter) to minimize cell damage during the long image acquisition. The NIS elements software (LIM) was used to control the microscope and image acquisition.

Image Analysis

For segmentation and tracking of single yeast cells, the BudJ plug-in (Ferrezuelo et al., 2012) for ImageJ (Schneider et al., 2012) was used. The plug-in was used to determine the background-corrected average cytoplasmic pixel fluorescence intensity from single cells, for the GFP (mGFP-AID) and NAD(P)H channels. Specifically, cells to be tracked over time were selected by clicking at the center of the desired cell and their boundaries were estimated by BudJ based on the pixel intensity change at the perimeter of the cell, as visualized in the DIC image. Because of the constitutive filamentation of the Cdc28-AID cells, they were manually segmented on the basis of the cellular borderline in the DIC channel, using ImageJ (Schneider et al., 2012).

The average fluorescence intensity of the pixels contained within the specified cell boundaries was determined for each cell by BudJ for the NAD(P)H channel, and the GFP

channel (mGFP-AID). The modal grey value of the whole image area in each fluorescent channel determined for each time-point was subtracted from the fluorescence of each monitored cell. A comparison of the automated background estimation (i.e. the modal grey value) with a manual background acquisition (average intensity of the pixels around the cell covering the pad area) showed no significant differences between the two methods. For the quantification of the Cyr1-mCherry-AID fluorescence, the cellular auto-fluorescence in the RFP channel was measured in the mGFP-AID cells, and subtracted from the Cyr1-mCherry-AID fluorescence.

The Whi5 nuclear or cytoplasmic localization was manually determined for each single cell. The time point of budding was also manually determined as the moment of first bud appearance on the cell surface, which we monitored in the DIC channel.

Flow cytometry

A BD Accuri flow-cytometer was used to measure the cell count and forward scatter of yeast cells upon the addition of auxin or the mating pheromone alpha factor. Cells were grown in 50 mL (500 mL flask) minimal medium supplemented with $10gL^{-1}$ glucose. At each time, point 25 µl of cell culture at appropriate dilutions to maintain the cell count below 200000 cells / 25 µl, were analyzed.

Ethanol yield estimation

To determine the ethanol yield in the presence or absence of alpha factor, in wild type or *Rim15Δ* cells, the ethanol production and glucose consumption rates were determined. Specifically, 300 µl of culture were sampled in 1.5 ml centrifuge tubes, at each time point. The cells were centrifuged at maximum speed (13000 rpm) for 1 minute and the supernatant was collected. To remove cell traces, the supernatant was additionally filtered through 0.22 µm filter spin-columns (SpinX).

The glucose and ethanol concentrations in the culture supernatant were determined using high performance liquid chromatography (Agilent, isocratic 1290 LC HPLC system) and the Hi-Plex H column, at 60 oC. A flow rate of 0.6 ml/min was applied, with a 5 mM H2SO4 eluent. Appropriate glucose and ethanol concentration standards were prepared and analyzed together with the samples, at the begging and the end of the experiment. The injection volume was set at 10 μl for both the samples and the standards. Substrate concentrations were detected with refractive index and UV (at 210 nm) detection. The chromatogram integration was done with Agilent Open Lab CDS.

Author contributions

AP conceived and designed the study, developed all strains, performed all experiments, and analyzed all data. VT Developed the Cyr1-AID strain. MH conceived and supervised the study. AP and MH wrote the manuscript.

Acknowledgments

Financial support is acknowledged from the EU ITN project ISOLATE. The authors thank the Molecular Systems Biology group for helpful discussion.

References

Bardwell, L. (2004). A walk-through of the yeast mating pheromone response pathway. Peptides 25, 1465–1476.

Baroni, M.D., Monti, P., and Alberghina, L. (1994). Repression of growth-regulated Gl cyclin expression by cyclic AMP in budding yeast. Nature 371, 339–342.

Cai, L., and Tu, B.P. (2012). Driving the cell cycle through metabolism. Annu. Rev. Cell Dev. Biol. 18, 59–87.

Cai, L., Sutter, B.M., Li, B., and Tu, B.P. (2011). Acetyl-CoA Induces Cell Growth and Proliferation by Promoting the Acetylation of Histones at Growth Genes. Mol. Cell 42, 426–437.

Conrad, M., Schothorst, J., Kankipati, H.N., Van Zeebroeck, G., Rubio-Texeira, M., and Thevelein, J.M. (2014). Nutrient sensing and signaling in the yeast *Saccharomyces cerevisiae*. FEMS Microbiol. Rev. 38, 254-299.

Cornelia Amariei, R.M.V.S.T.S.M.T. and D.B.M. (2014). Time resolved DNA occupancy dynamics during the respiratory oscillation uncover a global reset point in the yeast growth program. Microb. Cell 1, 279–288.

Costanzo, M., Nishikawa, J.L., Tang, X., Millman, J.S., Schub, O., Breitkreuz, K., Dewar, D., Rupes, I., Andrews, B., and Tyers, M. (2004). CDK activity antagonizes Whi5, an inhibitor of G1/S transcription in yeast. Cell 117, 899–913.

Deutscher, D., Meilijson, I., Schuster, S., and Ruppin, E. (2008). Can single knockouts accurately single out gene functions? BMC Syst. Biol. 2, 50.

Diaz-Ruiz, R., Rigoulet, M., and Devin, A. (2011). The Warburg and Crabtree effects: On the origin of cancer cell energy metabolism and of yeast glucose repression. Biochim. Biophys. Acta 1807, 568–576.

Ewald, J.C., Kuehne, A., Zamboni, N., and Skotheim, J.M. (2016). The Yeast Cyclin-Dependent Kinase Routes Carbon Fluxes to Fuel Cell Cycle Progression. Mol. Cell 62, 532–545.

Ferrezuelo, F., Colomina, N., Palmisano, A., Garí, E., Gallego, C., Csikász-Nagy, A., and Aldea, M. (2012). The critical size is set at a single-cell level by growth rate to attain homeostasis and adaptation. Nat. Commun. 3, 1–11.

François, J., and Parrou, J.L. (2001). Reserve carbohydrates metabolism in the yeast *Saccharomyces cerevisiae*. FEMS Microbiol. Rev. 25, 125-145.

Futcher, B. (1999). Cell cycle synchronization. Methods Cell Sci. 21, 79–86.

Futcher, B. (2006). Metabolic cycle, cell cycle, and the finishing kick to Start. Genome Biol. 7, 107.

Gibson, D.G., Young, L., Chuang, R.-Y., Venter, J.C., Hutchison, C.A., and Smith, H.O. (2009). Enzymatic assembly of DNA molecules up to several hundred kilobases. Nat Meth 6, 343–345.

Gietz, R.D., and Schiestl, R.H. (2007). High-efficiency yeast transformation using the LiAc/SS carrier DNA/PEG method. Nat. Protoc. 2, 31–34.

Guillou, V., Plourde-Owobi, L., Parrou, J.L., Goma, G., and François, J. (2004). Role of reserve carbohydrates in the growth dynamics of *Saccharomyces cerevisiae*. FEMS Yeast Res. 4, 773-787.

Vander Heiden, M.G., Cantley, L.C., and Thompson, C.B. (2009). Understanding the Warburg Effect: The Metabolic Requirements of Cell Proliferation. Science 324, 1029–1033.

Huberts, D.H.E.W., Lee, S.S., González, J., Janssens, G.E., Vizcarra, I.A., and Heinemann, M. (2013). Construction and use of a microfluidic dissection platform for long-term imaging of cellular processes in budding yeast. Nat. Protoc. 8, 1019–1027.

Jones, R.G., Plas, D.R., Kubek, S., Buzzai, M., Mu, J., Xu, Y., Birnbaum, M.J., and Thompson, C.B. (2016). AMP-Activated Protein Kinase Induces a p53-Dependent Metabolic Checkpoint. Mol. Cell 18, 283–293.

Kotani, S., Tugendreich, S., Fujii, M., Jorgensen, P.-M., Watanabe, N., Hoog, C., Hieter, P., and Todokoro, K. (2016). PKA and MPF-Activated Polo-like Kinase Regulate Anaphase-Promoting Complex Activity and Mitosis Progression. Mol. Cell 1, 371–380.

Lee, I.H., and Finkel, T. (2013). Metabolic regulation of the cell cycle. Curr. Opin. Cell Biol. 25, 724–729.

Lee, P., Kim, M.S., Paik, S.-M., Choi, S.-H., Cho, B.-R., and Hahn, J.-S. (2013). Rim15-dependent activation of Hsf1 and Msn2/4 transcription factors by direct phosphorylation in *Saccharomyces cerevisiae*. FEBS Lett. 587, 3648–3655.

Lee, S.S., Avalos, I., Huberts, D.H.E.W., Lee, L.P., and Heinemann, M. (2012). Whole lifespan microscopic observation of budding yeast aging through a microfluidic dissection platform. Proc. Natl. Acad. Sci. 109, 4916–4920.

Liao, H., and Thorner, J. (1980). Yeast mating pheromone a factor inhibits adenylate cyclase Biochemistry : 77, 1898–1902.

Liu, X., Wang, X., Yang, X., Liu, S., Jiang, L., Qu, Y., Hu, L., Ouyang, Q., and Tang, C. (2015). Reliable cell cycle commitment in budding yeast is ensured by signal integration. Elife 4, e03977.

Lloyd, D., and Murray, D.B. (2005). Ultradian metronome: timekeeper for orchestration of cellular coherence. Trends Biochem. Sci. 30, 373–377.

Lloyd, D., Salgado, L.E.J., Turner, M.P., Suller, M.T.E., and Murray, D. (2002). Cycles of mitochondrial energization driven by the ultradian clock in a continuous culture of *Saccharomyces cerevisiae*. Microbiology 148, 3715–3724.

Machné, R., and Murray, D.B. (2012). The yin and yang of yeast transcription: elements of a global feedback system between metabolism and chromatin. PLoS One 7, e37906.

Mizunuma, M., Tsubakiyama, R., Ogawa, T., Shitamukai, A., Kobayashi, Y., Inai, T., Kume, K., and Hirata, D. (2013). Ras/cAMP-dependent Protein Kinase (PKA) Regulates Multiple Aspects of Cellular Events by Phosphorylating the Whi3 Cell Cycle Regulator in Budding Yeast. J. Biol. Chem. 288, 10558–10566.

Morawska, M., and Ulrich, H.D. (2013). An expanded tool kit for the auxin-inducible degron system in budding yeast. Yeast 30, 341–351.

Müller, D., Exler, S., Aguilera-Vázquez, L., Guerrero-Martín, E., and Reuss, M. (2003). Cyclic AMP mediates the cell cycle dynamics of energy metabolism in *Saccharomyces cerevisiae*. Yeast 20, 351–367.

Nishimura, K., Fukagawa, T., Takisawa, H., Kakimoto, T., and Kanemaki, M. (2009). An auxin-based degron system for the rapid depletion of proteins in nonplant cells. Nat. Methods 6, 917–922.

Papagiannakis, A., Niebel, B., Wit, E.C., and Heinemann, M. (2017). Autonomous metabolic oscillations robustly gate the early and the late cell cycle. Mol. Cell 65, 285–295.

Pedruzzi, I., Bürckert, N., Egger, P., and De Virgilio, C. (2000). *Saccharomyces cerevisiae* Ras/cAMP pathway controls post-diauxic shift element-dependent transcription through the zinc finger protein Gis1. EMBO J. 19, 2569–2579.

Peeters, T., Louwet, W., Geladé, R., Nauwelaers, D., Thevelein, J.M., and Versele, M. (2006). Kelch-repeat proteins interacting with the G(α) protein Gpa2 bypass adenylate cyclase for direct regulation of protein kinase A in yeast. Proc. Natl. Acad. Sci. U. S. A. 103, 13034–13039.

Peters, K. (2013). Molecular mechanisms involved in activation of the Ras proteins by glycolytic flux. Katholieke Universiteit Leuven.

Reinders, A., Bürckert, N., Boller, T., Wiemken, A., and De Virgilio, C. (1998). *Saccharomyces cerevisiae* cAMP-dependent protein kinase controls entry into stationary phase through the Rim15p protein kinase. Genes Dev. 12, 2943–2955.

Sasidharan, K., Soga, T., Tomita, M., and Murray, D.B. (2012). A yeast metabolite extraction protocol optimised for time-series analyses. PLoS One 7, e44283.

Schieke, S.M., McCoy Jr., J.P., and Finkel, T. (2008). Coordination of mitochondrial bioenergetics with G1 phase cell cycle progression. Cell Cycle 7, 1782–1787.

Schmoller, K.M., Turner, J.J., Koivomagi, M., and Skotheim, J.M. (2015). Dilution of the cell cycle inhibitor Whi5 controls budding-yeast cell size. Nature 526, 268–272.

Schneider, C.A., Rasband, W.S., and Eliceiri, K.W. (2012). NIH Image to ImageJ: 25 years of image analysis. Nat Meth 9, 671–675.

Shi, L., and Tu, B.P. (2013). Acetyl-CoA induces transcription of the key G1 cyclin CLN3 to promote entry into the cell division cycle in Saccharomyces cerevisiae. Proc. Natl. Acad. Sci. 110, 7318–7323.

Slavov, N., and Botstein, D. (2011). Coupling among growth rate response, metabolic cycle, and cell division cycle in yeast. Mol. Biol. Cell 22, 1997–2009.

Smith, A., Ward, M.P., and Garrett, S. (1998). Yeast PKA represses Msn2p/Msn4p-dependent gene expression to regulate growth, stress response and glycogen accumulation. EMBO J. 17, 3556–3564.

Talia, S. Di, Skotheim, J.M., Bean, J.M., Siggia, E.D., and Cross, F.R. (2007). The effects of molecular noise and size control on variability in the budding yeast cell cycle. Nature 448, 947–951.

Thevelein, J.M., and de Winde, J.H. (1999). Novel sensing mechanisms and targets for the cAMP-protein kinase A pathway in the yeast Saccharomyces cerevisiae. Mol. Microbiol. 33, 904–918.

Tu, B.P., Kudlicki, A., Rowicka, M., and McKnight, S.L. (2005). Logic of the yeast metabolic cycle: temporal compartmentalization of cellular processes. Science 310, 1152–1158.

Valbuena, N., and Moreno, S. (2010). TOR and PKA Pathways Synergize at the Level of the Ste11 Transcription Factor to Prevent Mating and Meiosis in Fission Yeast. PLoS One 5, e11514.

Verduyn, C., Postma, E., Scheffers, A.W., and van Dijken, J. (1992). Effect of Benzoic Acid on Metabolic Fluxes in Yeasts: A Continuous-Culture Study on the Regulation of Respiration and Alcoholic Fermentation. Yeast 8, 501–517.

Wang, Z., Fan, M., Candas, D., Zhang, T.-Q., Eldridge, A., Wachsmann-Hogiu, S., Ahmed, K.M., Chromy, B.A., Nantajit, D., Duru, N., et al. (2014). CyclinB1/Cdk1 Coordinates Mitochondrial Respiration for Cell Cycle G2/M Progression. Dev. Cell 29, 217–232.

Xu, Z., and Tsurugi, K. (2006). A potential mechanism of energy-metabolism oscillation in an aerobic chemostat culture of the yeast Saccharomyces cerevisiae. FEBS J. 273, 1696–1709.

Zhao, G., Chen, Y., Carey, L., and Futcher, B. (2016). Cyclin-Dependent Kinase Co-Ordinates Carbohydrate Metabolism and Cell Cycle in S. cerevisiae. Mol. Cell 62, 546–557.

Zimmermann, G., Zhou, D., and Taussig, R. (1998). Genetic Selection of Mammalian Adenylyl Cyclases Insensitive to Stimulation by Gsα . J. Biol. Chem. 273, 6968–6975.

Supplemental Information for

CDK and cAMP/PKA signalling tune the amplitude of the metabolic oscillator, thereby controlling cell cycle initiation or arrest

Alexandros Papagiannakis, Vakil Takhaveev, Matthias Heinemann

Molecular Systems Biology, Groningen Biomolecular Sciences and Biotechnology Institute, University of Groningen, Nijenborgh 4, 9747 AG Groningen, The Netherlands;

Supplemental Figures

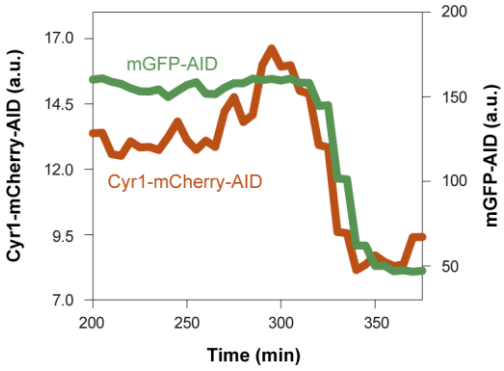

Figure S1: The mGFP-AID depletion dynamics can be used to estimate the timing of Cyr1-AID depletion in the same experiment. Two cell populations, one expressing mGFP-AID and a second population expressing Cyr1-mCherry-AID were loaded in the same microfluidic device and monitored in the same experiment upon the addition of 0.1 mM auxin. The average mGFP-AID depletion (from 13 single cells) was plotted against the average Cyr1-mCherry-AID depletion (from 4 single cells). The depletion dynamics of the two proteins are similar. Both mGFP-AID and Cyr1-mCherry-AID were fully depleted at 350 min. Because the Cyr1-mCherry-AID signal intensity is very low, we used mGFP-AID as reliable reporter for conditional protein depletion.

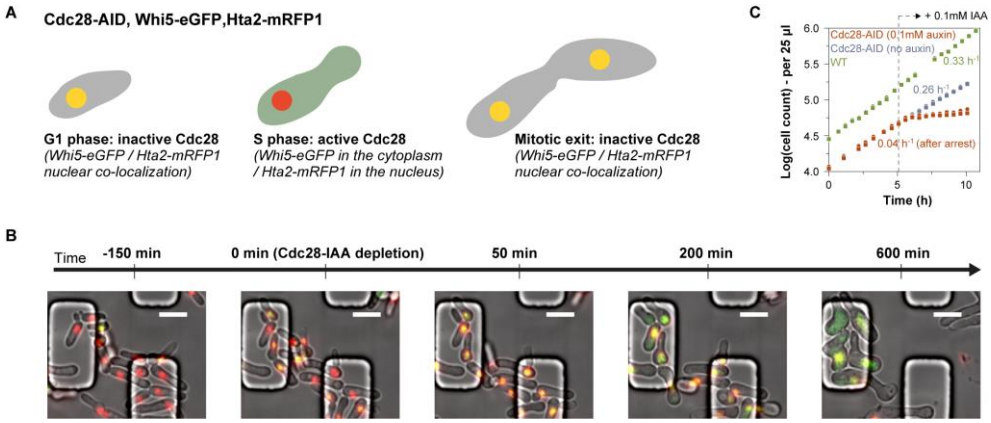

Figure S2: The localization of the transcriptional repressor Whi5 reports CDK activity in single yeast cells. (A) Whi5 is a repressor of cell cycle transcription and is sequestered in the nucleus during the G1 phase or when the cell cycle program is inactive. Whi5 is phosphorylated by Cdc28 and localizes into the cytoplasm at START signalling the initiation of the cell cycle program and reporting CDK activity. To follow the localization of Whi5-eGFP in single cells, we used the fluorescently labelled histone A2 (Hta2-mRFP1) as a nuclear marker. **(B)** Upon the conditional depletion of Cdc28-

AID, the Whi5 transcriptional repressor immediately enters the nucleus, reporting absence of CDK activity. Because yeast cells are not synchronized in the microfluidic device, at the time of Cdc28 depletion they are at different cell cycle phases. Thus we conclude that the cell cycle is arrested at any cell cycle phase. **(C)** The immediate arrest of the cell cycle and growth upon depletion of Cdc28-AID is also visible on the population level. Cell count was measured in batch cultures of wild type cells, and Cdc28-AID cells growing before and after the addition of auxin. The addition of 0.1 mM of auxin at 5.08 hours arrested the growth of Cdc28-AID cells. In the absence of auxin the Cdc28-AID cells grow exponentially, yet with lower growth rate as compared to wild type cells, where the Cdc28 is not tagged. Two biological replicates and their average growth rate are presented for each strain and condition (i.e. presence or absence of auxin). The Cdc28-AID cells exhibit a filamentous phenotype, which explains their slower growth as compared to wild type cells. It has previously been shown that the binding between Cdc28 and its regulatory subunit Cks1 is necessary to prevent filamentous growth of budding yeast. We conclude that the C-terminal tagging of Cdc28 with the auxin degron tag disturbs this interaction inducing constitutive filamentation. This filamentous phenotype we could not avoid even when we tagged the yeast CDK at its N-terminus (strain YSBN16.Whi5-eGFP.Hta2-mRFP1.OsTIR1w/oGFP.G28ARFPex – data not presented).

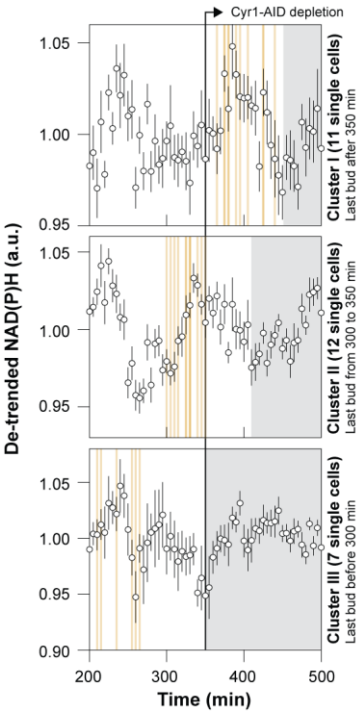

Figure S3: The conditional Cyr1 depletion arrests the cell cycle in G1. Single cells are clustered in 3 groups based on the timing of their last budding (orange vertical lines). The average NAD(P)H dynamics (error bars - SEM) are presented for each cluster. In all three clusters the cells were arrested after the following trough of the NAD(P)H oscillations (grey shaded area). We have previously

shown that the trough of the NAD(P)H oscillations coincide with mitotic exit independently of the nutrient conditions. Thus, upon Cyr1-AID depletion cells are arrested after mitotic exit, or in the G1 phase.

Supplemental Tables

Table S1: Yeast strains developed and/or used in this study.

Strain	Genotype	Source
YSBN6	YSBN6 wild type	Steve Oliver lab, Cambridge
YSBN6.Rim15Δ	YSBN6 Rim15::Ble (deletion)	This study
YSBN6.G19A	YSBN6 Cyr1::mCherry-AID -NatMX	This study
YSBN6.G19A.Rim15Δ	YSBN6 Cyr1::mCherry-AID -NatMX Rim15::Ble (deletion)	This study
YSBN6.G2J	YSBN6 ho::ADH1p-OsTIR1-mGFP-AID -KanMX4	(Papagiannakis et al., 2017)
YSBN6.OsTIR1w/oGFP	YSBN6 ho::ADH1p-OsTIR1-KanMX4	(Papagiannakis et al., 2017)
YSBN16.Whi5-eGFP.Hta2-mRFP1.OsTIR1w/oGFP.G23ARFPex	YSBN16 ho::ADH1p-OsTIR1-KanMX4 Whi5::eGFP-HIS3MX6 Hta2::mRFP1-Ble Cdc14::mCherry-AID$^{71-114}$-natMX	(Papagiannakis et al., 2017)
YSBN16.Whi5-eGFP.Hta2-mRFP1.OsTIR1w/oGFP.G25ARFPex	YSBN16 ho::ADH1p-OsTIR1-KanMX4 Whi5::eGFP-HIS3MX6 Hta2::mRFP1-Ble Cdc28::AID$^{71-114}$-natMX (C-terminal tagging)	(Chapter 3 of this Thesis)

YSBN16.Whi5-eGFP.Hta2-mRFP1.OsTIR1w/oGFP.G28ARFPex	YSBN16 ho::ADH1p-OsTIR1-KanMX4 Whi5::eGFP-HIS3MX6 Hta2::mRFP1-Ble Cdc28::AID$^{71-114}$-natMX (N terminal tagging)	This study

Table S2: Primer sequences used for the development of all recombinant strains.

The underlined sequences correspond to the overhangs designed for Gibson assembly. The term "gDNA" stands for purified genomic DNA.

Primer	Fwd/Rev	Sequence (5′ to 3′)	Templates
CYR1CDS	Fwd	TTATGCTTCCGCGGCTCGTATGTTGTGTGGGTATTGGTTGGGCATTTTTTGACTT	YSBN6 wild type gDNA
	Rev	CATGTTATCCTCCTCGCCCTTGCTCACCATAGTTGATAAATCCTTTGCGTTCTTAAC	
CYR1 DOWN	Fwd	CCGGGTGACCCGGCGGGGACAAGGCAAGCTGTTCTGTTCGTAAATTATGTACCACC	
	Rev	GTTCCAGTTTGGAACAAGAGTCCACTATTAGAGAGAGCTTAGAGACACCTTTT	
RIM15 UP	Fwd	TTATGCTTCCGCGGCTCGTATGTTGTGTGGCATTTCTCGAGTTGTCCATTGAG	
	Rev	GTCGAAAACGAGCTCTCGAGAACCCTTAATCTGTCTTCCTCTACTGGGC	
RIM15 DOWN	Fwd	CGAGGCAAGCTAAACAGATCTCTAGACCTAGCGATTCTGATGAAACGCAC	
	Rev	GTTCCAGTTTGGAACAAGAGTCCACTATTAGGAAGTGGAATCATCAAACGAC	
mCherry-IAA-Nat	Fwd	ATGGTGAGCAAGGGCGA	pG23A plasmid (Papagiannakis et
	Rev	AGCTTGCCTTGTCCCCG	

Amp	Fwd	TAATAGTGGACTCTTGTTCC	al., 2017)
	Rev	CCACACAACATACGAGC	
Phleo Phleo	Fwd	ATTAAGGGTTCTCGAGAGC	pG25 plasmid (Papagiannakis et al., 2017) pG27 plasmid (This study)
	Rev	TAGGTCTAGAGATCTGTTTAGC	
RIM15Lin	Fwd	CATTTCTCGAGTTGTCCATTGAG	pG27 plasmid (This study)
	Rev	GGAAGTGGAATCATCAAACGAC	
Seq102	Rev	CTTCAGGTTGTCTAACTCC	pG19A (This study)
G5NAT	For	GTCGACGGTGCAGG	
CYR1Lin	For	GTATTGGTTGGGCATTTTTTG	
	Rev	GAGAGAGCTTAGAGACACC	

Supplemental References

Papagiannakis, A., Niebel, B., Wit, E.C., and Heinemann, M. (2017). Autonomous metabolic oscillations robustly gate the early and the late cell cycle. Mol. Cell 65, 285–295.

Conclusions and outlook

Alexandros Papagiannakis

Molecular Systems Biology, Groningen Biomolecular Sciences and Biotechnology Institute, University of Groningen, Nijenborgh 4, 9747 AG Groningen, The Netherlands;

The cell cycle is a periodic process, a rhythmic switch between biomass (e.g. DNA and proteins) formation and segregation, in synchrony with cycles of chromatin activation, and mitochondrial energization. The CDK-centric model proposes the existence of a master oscillator, the cyclin/CDK machinery, as the driver of all periodic functions, from the cell cycle transcription to chromosome structure and dynamics. Another possibility is the existence of multiple biological oscillators, which synchronize to give rise to a higher order function, the cell division cycle. This model of coupled oscillators is supported by the late advent of the cyclin/CDK machinery (Krylov et al., 2003) in the evolution of eukaryotes, the previously reported global transcription (Orlando et al., 2008) and APC-activity oscillations in cell cycle arrested cells (Lu and Cross, 2010), or the metabolic oscillations previously reported in synchronized yeast populations (Lloyd and Murray, 2005; Slavov and Botstein, 2011; Tu et al., 2005).

The dynamic single cell metabolite (Chapter 2, Figures 1A-B, S2A-B & S3A-F, Movie S1) and cell cycle measurements (Chapter 2, Figures S5, 1C & S7), in the absence of synchronization or intercellular communication (Chapter 2, Figure S1C), performed in this thesis, show that metabolism is an autonomous oscillator, which orbits in synchrony (Chapter 2, Figures 1C, 4A-G but also without cell cycle, in cell cycle arrested (Chapter 2, Figures 2C & S6) or quiescent cells (Chapter 2, Figures 2A, 3B-C & S4C-D, Movie S2). The occurrence of metabolic oscillations across nutrient conditions and metabolic modes (respiration, fermentation and gluconeogenesis) (Chapter 2, Figures 1C & S3A-F) suggests that the metabolic oscillations are not due to the temporal activity of specific metabolic pathways but rather due to rhythmic behavior in the synthesis of biomass constituents, such as fatty acids, amino acids or nucleotide.

Consistently, the persistent metabolic oscillations in synchrony with waves of cell volume increase and DNA endo-replication in Cdc14-AID depleted cells (Chapter 2, Figure 6A-I, Movie S6), where the late cell cycle was inhibited, suggest a strong relation between the oscillating metabolism and biomass synthesis. With the protein and DNA synthesis being strongly dependent on ATP availability (Buttgereit and Brand, 1995; Wieser and Krumschnabel, 2001), and with the fatty acid synthesis requiring large amounts of redox equivalents (NADPH) (Halperin and Robinson, 1970), the metabolic

oscillations are well represented by the intracellular levels of the two metabolites, which we found to oscillate in single yeast cells oppositely in phase. However, up-to-date, the biochemical pathways which are responsible for the periodic metabolite dynamics remain unknown. Metabolic perturbation studies may help identify the functional constituents of the autonomous metabolic oscillator. Considering the strong connection between the metabolic oscillations and biomass synthesis, the deletion of any core component will possibly prove lethal. This signifies the use of novel methods for the conditional depletion (such as those used in Chapter 3) or ectopic expression of targeted proteins.

In our single cell NAD(P)H and ATP measurements we found metabolism to be a flexible oscillator, achieving periods between 1 and 24 hours depending on the available nutrients and the growth conditions (Chapter 2, Figures 1C & S4D). During fermentative growth on high glucose (10 gL^{-1}) yeast cells would exhibit metabolic oscillations with an average frequency of 0.6 h^{-1}, which corresponds to the maximum doubling time of yeast (approx. 100 min) (Chapter 2, Figure 1C). When we cultured yeast cells on low glucose (0.01 gL^{-1}) in the microfluidic device, we observed phenotypic bistability (Chapter 2, Figure 3B), and a clear metabolic threshold separating dividing from non-dividing cell fractions. Cells with metabolic frequencies above 0.15 h^{-1} would enter the cell division program, whereas single yeast cells with slower metabolism (frequency below 0.15 h^{-1}) would enter the circadian domain and quiescence. This metabolic threshold is reminiscent of the Warburg effect, and the distinct metabolic phenotype between cancer cells, fermenting even in the presence of oxygen, and non-dividing respiring cells. Consistent with the fact that the metabolic frequency sets a cell cycle threshold, it has previously been shown that somatic non-dividing cells exhibit metabolic oscillations in the circadian domain, whereas cancer (Sahar and Sassone-Corsi, 2009) or stem cells (Bessho et al., 2001, 2003; Isomura and Kageyama, 2014) exhibited ultradian oscillations with a frequency of 0.5 h^{-1}.

Next to the frequency of the metabolic oscillator, its amplitude also constitutes an accurate cell cycle predictor (Chapter 4, Figure 4A-B). Dividing cells exhibited enhanced amplitudes (NAD(P)H SD > 0.04), in contrast to the dampened metabolic oscillations (NAD(P)H SD < 0.04), which we measured in cell cycle arrested or quiescent cells. Consistently, the NADH concentration of cancer cells was found to be 1.8 times higher than normal cells (Yu and Heikal, 2009).

The autonomous metabolic oscillator may operate as a primitive timekeeper, setting the pace of global gene expression and cell division prior to the appearance of the cyclin/CDK machinery. Similarly to yeast (Causton et al., 2015), redox oscillations have been reported in different organisms across all domains of life, from archaea and cyanobacteria, to plants, insects and mammalian cells (Edgar et al., 2012). The conserved role of NAD^+ dependent deacetylases in epigenetic silencing (Vaquero, 2009), together with the A TP-dependent mechanisms of chromatin and DNA remodeling

(Gangaraju and Bartholomew, 2007), provide a link between energy (ATP and NADH) oscillations and global gene expression, which could function as a primitive cell cycle machinery. Additional cell cycle regulation might have been engrafted onto such primitive cell cycle regulation, to ensure the robust separation between cell cycle phases.

The cAMP/PKA pathway is an example of such added control. Using conditional (method presented and characterized in Chapter 3) or constitutive genetic perturbations we have exposed the redundancy of the cAMP/PKA pathway. The metabolic oscillations and their evident coordination with the cell cycle are not the result of periodic cAMP-signaling as previously conjectured (Ewald et al., 2016; Futcher, 2006; Zhao et al., 2016). Instead, the nutrient sensing pathway establishes a positive feedback loop on the metabolic dynamics (Chapter 4, Figure 5B), receiving input (Peters, 2013) from oscillating signaling metabolites (e.g. F1,6BP (Sasidharan et al., 2012)) and strengthening the amplitude of the metabolic oscillations above the minimal threshold (NAD(P)H SD > 0.04) for cell cycle initiation. Thus, the cAMP/PKA pathway ensures robust cell cycle initiation, under eventually nutritionally less optimal conditions. While the cAMP/PKA pathway is there to strengthen the metabolic oscillations, the cyclin/CDK machinery might have the function to eliminate noise in gene expression, via controlling the transcription of the early G1/S cluster (Swi6 dependent), and late G2/M cluster (Mcm1 dependent) (Haase and Wittenberg, 2014). Consistently, the existence of an autonomously oscillating transcription factor network entrained by the cyclin/CDK machinery was recently suggested (Hillenbrand et al., 2016).

In order to confirm the role of metabolism as a cell cycle regulator, it likely will be necessary to "reverse evolution" by identifying and removing the redundancy in the cell cycle control network, reproducing the primitive cell cycle engine. A cell lacking such redundant interactions would still be able to divide, but would be prone to the metabolic noise, as well as the noise in gene expression. This primitive cell would have to wait for the "right" metabolic oscillation (frequency above 0.15 h^{-1} and amplitude over 0.04 NAD(P)H SD – Chapter 4, Figure 4B) to trigger cell division. Stochasticity in gene expression would dominate the transitions between the cell cycle phases, eventually leading to DNA endo-replication and aneuploidy. Consistently, polyploidy is commonly observed in prokaryotes, and was possibly also present in amitotic proto-eukaryotes (Markov and Kaznacheev, 2016).

Next to the relevance of an autonomous metabolic oscillator in cell cycle control, a metabolic time-keeper might also be responsible for other rhythmic processes in the ultradian domain, such as the previously described periodic switch between the REM (rapid eye movement) and non-REM sleep, known as the rest-activity cycle (Kleitman, 1982; Lloyd and Murray, 2005), or the periodic secretion of growth hormone (Tannebaum and Martin, 1976). The flexible metabolic oscillator, which we have

shown to approach 24 h period during respiration on low glucose (0.01 gL^{-1} – Chapter 2, Figure 4C-D), may also constitute the basis for day-night rhythms. In fact, non- transcriptional redox circadian rhythms have been discovered in red blood cells, or in algae where RNA and protein synthesis were arrested (O'Neill et al., 2011), leading to the conclusion that metabolic circadian rhytms pre-existed the core clock components, namely transcriptional activators or inhibitors with interlocking feedback loops, traditionally thought to generate and regulate circadian rhythmicity (Takahashi, 2004).

Periodicity and synchrony is observed at all levels of biological organization, from genes, to pathways, organelles, cells, tissues, all the way up to multicellular organisms, ecosystems and human communities. Life is cycles within cycles: a higher order function emerging from the collective synchrony of coupled and mutually entrained oscillators.

References

Bessho, Y., Sakata, R., Komatsu, S., Shiota, K., Yamada, S., and Kageyama, R. (2001). Dynamic expression and essential functions of Hes7 in somite segmentation. Genes Dev. 15, 2642–2647.

Bessho, Y., Hirata, H., Masamizu, Y., and Kageyama, R. (2003) Periodic repression by the bHLH factor Hes7 is an essential mechanism for the somite segmentation clock. Genes Dev. 17, 1451–1456.

Buttgereit, F., and Brand, M.D. (1995). A hierarchy of ATP-consuming processes in mammalian cells. Biochem. J. 312, 163–167.

Causton, H.C., Feeney, K.A., Ziegler, C.A., and O'Neill, J.S. (2015). Metabolic Cycles in Yeast Share Features Conserved among Circadian Rhythms. Curr. Biol. 25, 1056–1062.

Edgar, R.S., Green, E.W., Zhao, Y., van Ooijen, G., Olmedo, M., Qin, X., Xu, Y., Pan, M., Valekunja, U.K., Feeney, K.A., et al. (2012). Peroxiredoxins are conserved markers of circadian rhythms. Nature 485, 459–464.

Ewald, J.C., Kuehne, A., Zamboni, N., and Skotheim, J.M. (2016). The Yeast Cyclin-Dependent Kinase Routes Carbon Fluxes to Fuel Cell Cycle Progression. Mol. Cell 62, 532–545.

Futcher, B. (2006). Metabolic cycle, cell cycle, and the finishing kick to Start. Genome Biol. 7, 107.

Gangaraju, V .K., and Bartholomew, B. (2007). Mechanisms of A TP Dependent Chromatin Remodeling. Mutat. Res. 618, 3–17.

Haase, S.B., and Wittenberg, C. (2014). Topology and control of the cell-cycle-regulated transcriptional circuitry. Genetics 196, 65–90.

Halperin, M.L., and Robinson, B.H. (1970). The role of the cytoplasmic redox potential in the control of fatty acid synthesis from glucose, pyruvate and lactate in white adipose tissue. Biochem. J. 116, 235–240.

Hillenbrand, P., Maier, K.C., Cramer, P., and Gerland, U. (2016). Inference of gene regulation functions from dynamic transcriptome data. Elife 5, e12188.

Isomura, A., and Kageyama, R. (2014). Ultradian oscillations and pulses: coordinating cellular responses and cell fate decisions. Development 141, 3627–3636.

Kleitman, N. (1982). Basic rest-activity cycle—22 years later. Sleep J. Sleep Res. Sleep Med. 5, 311–317.

Krylov, D.M., Nasmyth, K., and Koonin, E. V. (2003). Evolution of eukaryotic cell cycle regulation: stepwise addition of regulatory kinases and late advent of the CDKs. Curr. Biol. 13, 173–177.

Lloyd, D., and Murray, D.B. (2005). Ultradian metronome: timekeeper for orchestration of cellular coherence. Trends Biochem. Sci. 30, 373–377.

Lu, Y., and Cross, F.R. (2010). Periodic cyclin-Cdk activity entrains an autonomous Cdc14 release oscillator. Cell 141, 268–279.

Markov, A. V, and Kaznacheev, I.S. (2016). Evolutionary consequences of polyploidy in prokaryotes and the origin of mitosis and meiosis. Biol. Direct 11, 28.

O'Neill, J.S., van Ooijen, G., Dixon, L.E., Troein, C., Corellou, F., Bouget, F.-Y., Reddy, A.B., and Millar, A.J. (2011). Circadian rhythms persist without transcription in a eukaryote. Nature 469, 554–558.

Orlando, D.A., Lin, C.Y., Bernard, A., Wang, J.Y., Socolar, J.E.S., Iversen, E.S., Hartemink, A.J., and Haase, S.B. (2008). Global control of cell-cycle transcription by coupled CDK and network oscillators. Nature 453, 944–947.

Peters, K. (2013). Molecular mechanisms involved in activation of the Ras proteins by glycolytic flux. Katholieke Universiteit Leuven.

Sahar, S., and Sassone-Corsi, P. (2009). Metabolism and cancer: the circadian clock connection. Nat Rev Cancer 9, 886–896.

Sasidharan, K., Soga, T., Tomita, M., and Murray, D.B. (2012). A yeast metabolite extraction protocol optimised for time-series analyses. PLoS One 7, e44283.

Slavov, N., and Botstein, D. (2011). Coupling among growth rate response, metabolic cycle, and cell division cycle in yeast. Mol. Biol. Cell 22, 1997–2009.

Takahashi, J.S. (2004). Finding New Clock Components: Past and Future. J. Biol. Rhythm. 19, 339–347.

Tannebaum, G.S., and Martin, J.B. (1976). Evidence for an Endogenous Ultradian Rhythm Governing Growth Hormone Secretion in the Rat. Endocrinology 98, 562–570.

Tu, B.P., Kudlicki, A., Rowicka, M., and McKnight, S.L. (2005). Logic of the yeast metabolic cycle: temporal compartmentalization of cellular processes. Science 310, 1152–1158.

Vaquero, A. (2009). The conserved role of sirtuins in chromatin regulation. Int. J. Dev. Biol. 53, 303–322.

Wieser, W., and Krumschnabel, G. (2001). Hierarchies of ATP-consuming processes: direct compared with indirect measurements, and comparative aspects. Biochem. J. 355, 389–395.

Yu, Q., and Heikal, A.A. (2009). Two-photon autofluorescence dynamics imaging reveals sensitivity of intracellular NADH concentration and conformation to cell physiology at the single-cell level. J. Photochem. Photobiol. B. 95, 46–57.

Zhao, G., Chen, Y., Carey, L., and Futcher, B. (2016). Cyclin-Dependent Kinase Co-Ordinates Carbohydrate Metabolism and Cell Cycle in S. cerevisiae. Mol. Cell 62, 546–557.

Academic summary

The cell cycle is the periodic alteration between biomass production and segregation. According to the traditional view on cell cycle regulation, waves of cyclins, in strict temporal order, control the cyclin dependent kinase (CDK), which orchestrates the different processes of the cell division cycle. However, there are cues pointing towards cell cycle regulators external to the cyclin/CDK machinery. First, the cell cycle can commence even in the absence of all early cyclins. Second, global transcription and late cell cycle oscillations persist even in the absence of periodic cyclin/CDK activity. Third, a phylogenetic analysis of cell cycle control kinases, indicates that CDKs appeared late in the evolution of eukaryotes, and thus early eukaryotes must have a employed other means to regulate the cell cycle.

The starting point of this thesis was the hypothesis that a metabolic oscillator exists, and acts as a cell cycle regulator. A metabolic oscillator could exert cell cycle control via the oscillating concentration of metabolites, known to interact with the cyclin/CDK machinery and also regulate biomass formation via the epigenetic activation or silencing of growth related genes. In order to test our hypothesis, we first investigated if a metabolic oscillator exists. Using metabolite sensors and cell cycle reporters, combined with microfluidics and epi-fluorescence time-lapse microscopy, we found metabolic oscillations in ATP and NAD(P)H levels in single *Saccharomyces cerevisiae* cells, in the absence of synchronization and intercellular communication. The oscillating metabolism maintains frequency synchrony with the cell cycle across metabolic modes (fermentation, respiration, gluconeogenesis) and growth rates, but also orbits in the absence of cell division, in G1-arrested cells, treated with the mating pheromone alpha factor, cells stochastically skipping cell division on high glucose, or G0 cells occurring under glucose-limited conditions. Based on these findings we concluded that the yeast metabolism is a cell cycle-autonomous oscillator.

The strict synchrony between the oscillating metabolites and the cyclin/CDK machinery in dividing cells, suggests a system of coupled oscillators, consisting of the metabolic oscillator, the early and the late cell cycle. We found metabolism and the cell cycle to exhibit a number of characteristics, representative for systems of coupled oscillators, similarly to what otherwise is found in nature (e.g. neuronal networks or the synchronized discharge of cells in the sinoatrial node). First, we witnessed the proportionality between the compromise and the natural metabolic frequencies. The cell cycle, possibly due to its biosynthetic demands, slows down the metabolic oscillator upon coupling. Second, coupling between metabolism and the cell cycle is achieved only when their frequencies are proximal. When metabolism orbits too slow or too fast, it cannot compromise with the cell cycle to a common frequency and thus cells are unable to divide. We found a clear metabolic frequency threshold robustly separating dividing from non-dividing cells. Third, we found the metabolic oscillator to

robustly gate the phase of the early and the late cell cycle during steady or perturbed growth. The synchrony between the metabolic oscillator and the early cell cycle (biomass formation and DNA replication) persisted even when we halted the late cell cycle, suggesting a direct coupling between metabolism and the early cell cycle.

In this thesis, perturbations served as necessary tools to investigate the interactions between periodic processes, such as the metabolic oscillator and its coupled cell cycle. Nutrient switches were used to perturb the frequency and phase of the metabolic oscillator, and the auxin-inducible degron was used for the conditional and dynamic depletion of cell cycle proteins. Before we could use the auxin-inducible degron system, we had to establish and to thoroughly characterized it on the single cell level. We measured the depletion and recovery dynamics of the targeted proteins for a wide range of auxin concentrations in microfluidics experiments. Although, the auxin-inducible degron exhibits fast protein depletion dynamics (approx. 20 minutes for complete protein depletion), the full recovery of the targeted proteins after removal of the plant hormone auxin requires several generations. This time is crucial for the cells to achieve an equilibrium between protein synthesis and dilution. Here, we also raise awareness on the growth defects caused by the plant hormone auxin, especially when combined with blue light illumination and GFP measurements. With microfluidics becoming largely accessible and the development of novel single cell reporters, we anticipate that our work will facilitate single cell perturbations, exploiting their unprecedented potential in studying dynamic processes.

Investigating the mechanisms responsible for cell-cycle autonomous metabolic oscillations, we studied the role of the cAMP/PKA pathway on the metabolic dynamics, using conditional protein depletion, together with gene knock-outs. . We found Rim15, the activator of stress response and inhibition target of cAMP/PKA signaling, to operate as a metabolic attenuator, dampening the amplitude of the metabolic oscillations, in the absence of cAMP signaling. Such a metabolic attenuation is necessary for the robust cell cycle arrest upon the addition of the mating pheromone alpha factor. Our results indicate that the cAMP/PKA pathway, known to be activated by flux-dependent metabolite signals, provides positive feedback to the metabolic dynamics, via the inhibition of stress response and possibly also via the liquidation of carbon storage.

Overall, this work establishes yeast metabolism as a cell-cycle autonomous oscillator and provides evidence that cell cycle control is a higher order function emerging from the collective synchrony between coupled oscillators, including the metabolic and the cyclin/CDK oscillator. Because central metabolic pathways are conserved across all taxa of life, the metabolic oscillator may constitute a primitive cell cycle regulator, also present in early eukaryotes prior to the appearance of the cyclin/CDK machinery. Additional control, such as the early cyclins and the onset of CDK activity or nutrient signaling, was possibly engrafted on the metabolic oscillator, entraining the metabolic

dynamics for the robust separation of the cell cycle phases, or the robust cell cycle initiation when nutrients are abundant. If a similar metabolic oscillator also exists in mammalian cells, then it may provide novel therapeutic targets against proliferative disorders.

Nederlandse samenvatting

De celcyclus is een periodieke afwisseling tussen de productie van biomassa en afscheiding. Traditioneel wordt de regulatie van de celcyclus gezien als golven van cyclines. Deze volgen elkaar in temporeel opzicht strak op en reguleren zo de cycline-afhankelijke kinase (CDK), die de verschillende processen van de celdelingscyclus aanstuurt. Er zijn echter aanwijzingen die duiden op regulatoren van de celcyclus buiten de cycline/CDK machinerie om. Allereerst kan de celcyclus ook beginnen in afwezigheid van alle vroege cyclines. Ten tweede houden oscillaties in globale transcriptieniveaus en tijdens de late celcyclus aan, ook zonder periodieke cycline/CDK activiteit. En tot slot wijst een fylogenetische analyse van de celcycluskinases erop dat CDK's pas laat in de evolutie van eukaryoten zijn ontstaan, en dus moeten vroege eukaryoten andere manieren gehad hebben om de celcyclus te reguleren.

Het beginpunt van dit proefschrift was de hypothese dat er een metabole oscillator bestaat, en dat deze als regulator van de celcyclus fungeert. Metabole oscillatoren zouden controle kunnen uitoefenen op de celcyclus door oscillerende metabolietconcentraties, waarvan bekend is dat deze met de cycline/CDK machinerie interactie aangaan en bovendien de formatie van biomassa reguleren door epigenetische activatie of het silencen van genen die gerelateerd zijn aan groei. Om onze hypothese te testen hebben we eerst uitgezocht of een metabole oscillator bestaat. Door sensors voor metabolieten en reporters voor de celcyclus te combineren met microfluidics en epifluorescence time-lapse microscopie, hebben we metabole oscillaties in ATP en NAD(P)H niveaus gevonden in *Saccharomyces cerevisiae* op cellulaire schaal, in afwezigheid van synchronisatie en intercellulaire communicatie. Oscillerend metabolisme houdt zijn frequentie synchroon met de celcyclus in verschillende metabole modi (fermentatie, respiratie of gluconeogenese) en groeisnelheden, maar gaat ook door zonder celdeling. Bij cellen die vastgezet zijn in G1 door behandelding met paarferomoon alpha factor, zijn er cellen die stochastisch de celdeling overslaan bij hoge glucose concentraties, terwijl G0 cellen voorkomen tijdens glucose-gelimiteerde condities. Gebaseerd op wat we gevonden hebben, concluderen we dat metabolisme in gist een oscillator is die autonoom van celcyclus opereert.

De strakke synchronie tussen oscillerende metabolieten en de cycline/CDK machinerie in delende cellen suggereert dat er een systeem van gekoppelde oscillatoren is, bestaande uit de metabole oscillator, de vroege en de late celcyclus. We hebben gevonden dat metabolisme en de celcyclus een aantal eigenschappen vertonen, die representatief zijn voor systemen van gekoppelde oscillatoren, en bovendien lijken op wat verder gevonden is in de natuur (bijv. neurale netwerken of gesynchroniseerde ontlading van cellen in de sinusknoop). Eerst waren we getuige van de proportionaliteit tussen de compromis en natuurlijke metabole frequenties. De celcyclus vertraagt de

metabole oscillator na koppeling, mogelijk door zijn biosynthetische behoeftes. Verder vonden we dat koppeling tussen metabolisme en de celcyclus alleen bereikt kan worden als de frequenties dicht bij elkaar liggen. Als metabolisme te snel of te langzaam gaat, kan het geen compromisfrequentie vinden met de celcyclus, en dus zijn deze cellen niet in staat te delen. We hebben een duidelijke drempelwaarde gevonden voor metabole frequenties om robuust delende van niet-delende cellen te kunnen scheiden. Als laatste hebben we gevonden dat de metabole oscillator robuust de fase van de vroege en de late celcyclus bewaakt tijdens stabiele of verstoorde groei. De synchronie tussen de metabole oscillator en de vroege celcyclus (biomassa formatie en DNA replicatie) hield zelfs aan als we de late celcyclus stopzetten, wat suggereert dat er een directe koppeling is tussen metabolisme en de vroege celcyclus.

In dit proefschrift dienden perturbaties als het gereedschap om de interacties tussen periodieke processen te onderzoeken, zoals de metabole oscillator en de hieraan gekoppelde celcyclus. Wisselingen in nutriënten werden gebruikt om de frequentie en de fase van de metabole oscillator te verstoren, en de auxine-induceerbare degron voor de conditionele en dynamische afbraak van celcycluseiwitten. Voordat we het auxine-induceerbare degron systeem konden gebruiken, moesten we het tot stand brengen en grondig karakteriseren op cellulair niveau. We maten de afbraak- en opbouwdynamica van de doeleiwitten voor een breed scala aan auxineconcentraties in microfluidics experimenten. Hoewel de auxine-induceerbare degron snelle eiwitafbraak induceert (ongeveer 20 minuten voor complete eiwitafbraak), duurde het volledige herstel van de doeleiwitten na verwijdering van het planthormoon auxine ten minste enkele generaties. Deze tijd is cruciaal voor de cellen om een evenwicht te bereiken tussen eiwitsynthese en verdunning. We wijzen hier ook op de groeidefecten ten gevolge van de het planthormoon auxine, vooral als het gecombineerd wordt met belichting van blauw licht en GFP metingen. Doordat microfluidics steeds toegankelijker worden en met de ontwikkeling van nieuwe cellulaire reporters, anticiperen we erop dat ons werk zal faciliteren in perturbaties op cellulair niveau, waarbij hun onovertroffen potentiaal in het bestuderen van dynamische processen benut wordt.

Om de mechanismen verantwoordelijk voor metabole oscillaties die autonoom zijn van de celcyclus te onderzoeken, bestudeerden we de rol van de cAMP/PKA pathway op de metabole dynamica met conditionele eiwitafbraak, tezamen met gen knockouts. We vonden dat Rim15, activator van stressrespons en negatief gereguleerd door de cAMP/PKA pathway, als metabole demper fungeert door het afzwakken van de metabole oscillaties in afwezigheid van cAMP signaling. Zo'n metabole demping is nodig voor het robuust tot stilstand brengen van de celcyclus na toevoeging van paarferomoon alpha factor. Onze resultaten duiden erop dat de cAMP/PKA pathway, waarvan bekend is dat deze geactiveerd wordt door flux-afhankelijke metabolietsignalen, positieve terugkoppeling

verschaft aan de metabole dynamica door de inhibitie van stressrespons en mogelijk ook door de afbraak van opgeslagen koolhydraten.

Samenvattend constateert dit werk dat gistmetabolisme autonoom is van de celcyclus en verschaft bovendien bewijs dat controle op celcyclus van een hogere orde is, die pas ontstaat vanuit de collectieve synchronie tussen gekoppelde oscillatoren, waaronder de metabole en cycline/CDK oscillator. Omdat centrale metabole pathways geconserveerd zijn over alle taxa van het leven, zou de metabole oscillator een primitieve regulator voor de celcyclus kunnen vormen, ook aanwezig in de vroege eukaryoten voor de verschijning van de cycline/CDK machinerie. Extra controle, zoals de vroege cyclines en de start van CDK activiteit of signaling van nutriënten, is mogelijk geënt op de metabole oscillator, en nam zo de metabole dynamica mee voor de robuuste scheiding van de fases van de celcyclus, of robuuste initiatie van celcyclus wanneer nutriënten overvloedig aanwezig zijn. Als een soortgelijke metabole oscillator ook bestaat in zoogdiercellen, dan zou het kunnen voorzien in nieuwe therapeutische doelen tegen proliferatieve aandoeningen.

Akcnowledgements

Matthias, I am honestly grateful for your mentoring and patience during the four years of my PhD research, as well as your guidance and care thereafter .

Prof. Benjamin Tu, Prof. Bert Poolman and Prof. Peter van Haastert thank you for taking the time to read my thesis and provide useful and insightful comments.

Dr. James Murray, Prof. Margarita Chatzopoulou-Cladaras, Prof. Anastasia Kouvatsi, Prof. Theodore Abatzopoulos, Dr. Triantafyllidis Alexandros, thank you for your support during my trembling first steps into the academia.

Pieter Blom and Milou Hoving, thank you for translating the extended and the lay summary. Despite my four and a half years in The Netherlands your help was indispensable.

To my family: I am grateful for your discreet, substantial and unconditional support throughout my life, and especially during those obscure, incomprehensible moments of PhD research.